NEUROCARDIAC OSCILLATION IN REPOLARIZATION AND CARDIAC ARRHYTHMIAS

EDITED BY: Peter Taggart and George E. Billman
PUBLISHED IN: Frontiers in Physiology

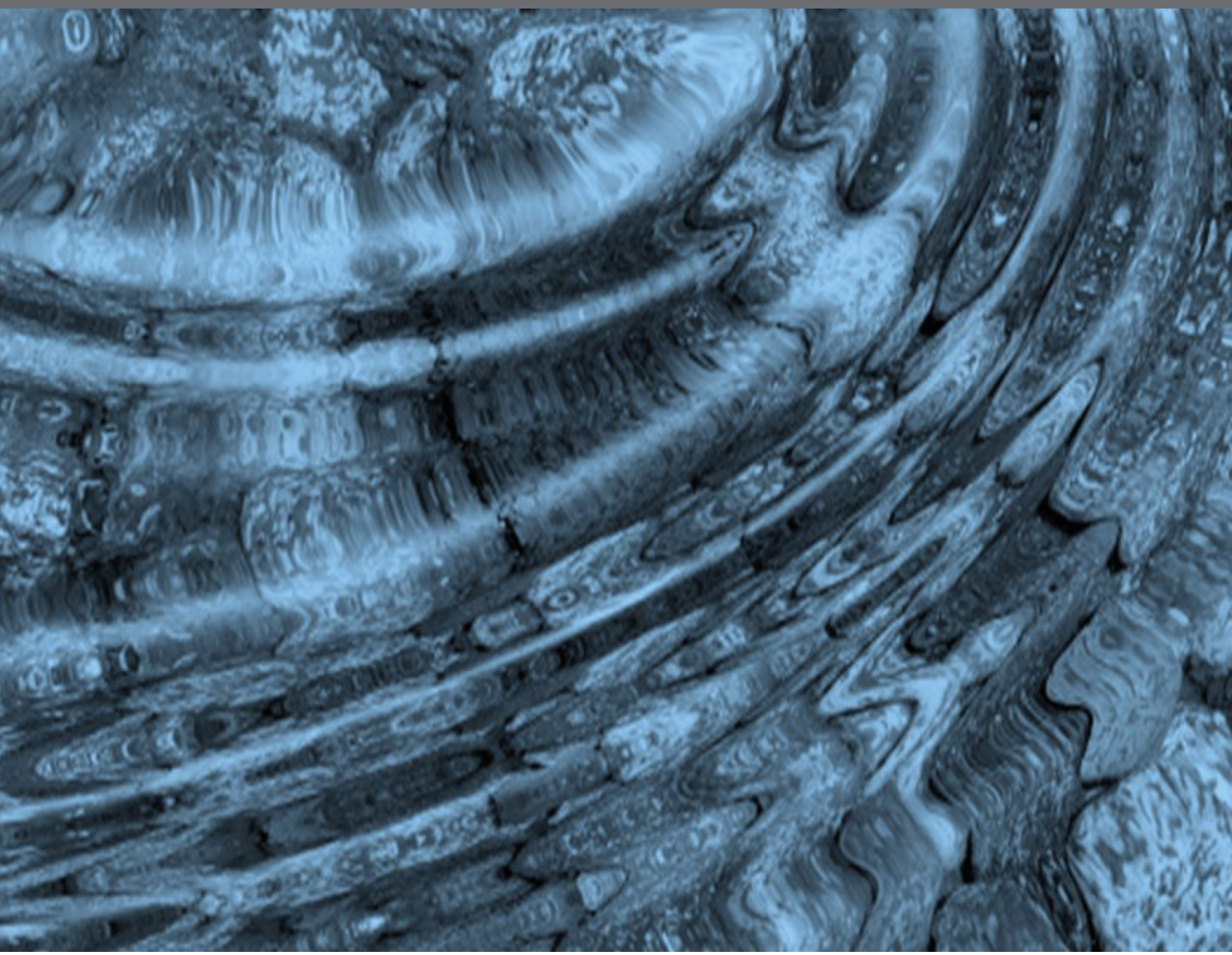

frontiers Research Topics

frontiers

ISSN 1664-8714
ISBN 978-2-88966-216-6
DOI 10.3389/978-2-88966-216-6

About Frontiers

Frontiers is more than just an open-access publisher of scholarly articles: it is a pioneering approach to the world of academia, radically improving the way scholarly research is managed. The grand vision of Frontiers is a world where all people have an equal opportunity to seek, share and generate knowledge. Frontiers provides immediate and permanent online open access to all its publications, but this alone is not enough to realize our grand goals.

Frontiers Journal Series

The Frontiers Journal Series is a multi-tier and interdisciplinary set of open-access, online journals, promising a paradigm shift from the current review, selection and dissemination processes in academic publishing. All Frontiers journals are driven by researchers for researchers; therefore, they constitute a service to the scholarly community. At the same time, the Frontiers Journal Series operates on a revolutionary invention, the tiered publishing system, initially addressing specific communities of scholars, and gradually climbing up to broader public understanding, thus serving the interests of the lay society, too.

Dedication to Quality

Each Frontiers article is a landmark of the highest quality, thanks to genuinely collaborative interactions between authors and review editors, who include some of the world's best academicians. Research must be certified by peers before entering a stream of knowledge that may eventually reach the public - and shape society; therefore, Frontiers only applies the most rigorous and unbiased reviews.
Frontiers revolutionizes research publishing by freely delivering the most outstanding research, evaluated with no bias from both the academic and social point of view. By applying the most advanced information technologies, Frontiers is catapulting scholarly publishing into a new generation.

What are Frontiers Research Topics?

Frontiers Research Topics are very popular trademarks of the Frontiers Journals Series: they are collections of at least ten articles, all centered on a particular subject. With their unique mix of varied contributions from Original Research to Review Articles, Frontiers Research Topics unify the most influential researchers, the latest key findings and historical advances in a hot research area! Find out more on how to host your own Frontiers Research Topic or contribute to one as an author by contacting the Frontiers Editorial Office: researchtopics@frontiersin.org

NEUROCARDIAC OSCILLATION IN REPOLARIZATION AND CARDIAC ARRHYTHMIAS

Topic Editors:
Peter Taggart, University College London, United Kingdom
George E. Billman, The Ohio State University Columbus, United States

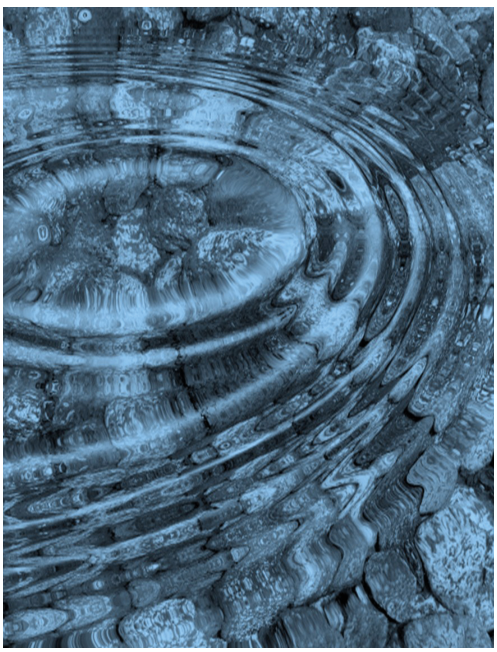

Image: Linnaea Mallette CC0 Public Domain.

Citation: Taggart, P., Billman, G. E., eds. (2020). Neurocardiac Oscillation in Repolarization and Cardiac Arrhythmias. Lausanne: Frontiers Media SA.
doi: 10.3389/978-2-88966-216-6

Table of Contents

frontiers in Physiology

EDITORIAL
published: 27 October 2020
doi: 10.3389/fphys.2020.604950

Editorial: Neurocardiac Oscillation in Repolarization and Cardiac Arrhythmias

Peter Taggart[1] *and George E. Billman*[2]*

[1] Department of Cardiovascular Sciences, University College London, London, United Kingdom, [2] Department of Physiology and Cell Biology, The Ohio State University, Columbus, OH, United States

Keywords: autonomic nervous system, cardiac arrhythmias, ventricular repolarization, heart rate variability, action potential duration

Editorial on the Research Topic

Neurocardiac Oscillation in Repolarization and Cardiac Arrhythmias

INTRODUCTION

Oscillations are a ubiquitous property throughout many biological systems. In the heart, beat to beat variability of heart rate (heart rate variability, HRV) and the ECG QT interval (QT variability, QTV) fluctuate over time at specific frequencies in particular, at a high frequency of about 0.25 Hz and at a lower frequency of about 0.1 Hz in humans (Task Force of the European Society of Cardiology North American Society of Pacing Electrophysiology, 1996; Billman, 2011; Baumert et al., 2016) These oscillations are related to the effect of the autonomic nervous system on the sinus node. High frequency (HF) oscillations of HRV occur at the respiratory frequency and are generally considered to reflect vagal activity and are widely used as a measure of parasympathetic activity. The physiological basis of low frequency oscillations (LF) of HRV is less clear cut but thought to reflect a combination of sympathetic and parasympathetic influence. The QT interval is a global representation of a combination of activation times and action potential duration (APD). As APD is strongly cycle length dependent, QTV is influenced by RR interval fluctuations as well as APD fluctuations particularly at faster heart rates when the APD falls on the steep part of its restitution curve. LF QTV has been shown to be increased by manoeuvers known to enhance sympathetic activity (Baumert et al., 2016) suggesting that at least a substantial part of the LF component of QTV may relate to sympathetic activity.

Both HRV and QTV have been shown to provide prognostic information in cardiac patients. Recently low frequency oscillations of ventricular repolarization measured from the ECG T wave vector, referred to as periodic repolarization dynamics, have been identified as one of the strongest predictors of sudden cardiac death (Rizas et al., 2014). These findings were confirmed and established for ventricular arrhythmia as well as sudden cardiac death in a large multicentre clinical trial (Bauer et al., 2019). These oscillations which are independent of respiration and enhanced during increased sympathetic activity have been proposed to relate to the effect of the intrinsic oscillation of sympathetic nerve activity on ventricular APD. In support of this contention, ventricular APD has recently been shown to exhibit oscillations at a low frequency in humans *in vivo* and these oscillations are enhanced by sympathetic provocation (Hanson et al., 2014; Porter et al., 2018). Potential cellular mechanisms underlying sympathetically mediated oscillations of ventricular APD have recently been identified (Pueyo et al., 2016).

Given the importance of oscillatory behavior in the clinical setting for both risk stratification and the identification of mechanisms for arrhythmogenesis, it is purpose of the present book to

OPEN ACCESS

Edited and reviewed by:
Ruben Coronel,
University of Amsterdam, Netherlands

***Correspondence:**
George E. Billman
george.billman@frontiersin.org

Specialty section:
This article was submitted to Cardiac Electrophysiology, a section of the journal Frontiers in Physiology

Received: *10 September 2020*
Accepted: *14 September 2020*
Published: *27 October 2020*

Citation:
Taggart P and Billman GE (2020) Editorial: Neurocardiac Oscillation in Repolarization and Cardiac Arrhythmias. Front. Physiol. 11:604950. doi: 10.3389/fphys.2020.604950

evaluate the physiology and electrophysiology of oscillatory behavior in the heart, particularly in the low frequency range. A particular focus has been placed on the oscillatory properties of ventricular repolarization and related aspects as briefly summarized as follows.

In chapter 1, Sprenkeler et al. using monophasic action potentials in a canine model showed that ventricular APD oscillated in both the HF and LF ranges. These oscillations were increased following remodeling induced by A-V block. LF power was greater in dogs in which Torsades de Pointes could be induced following dofetilide compared to non-inducible dogs. HF power was not related to inducibility (Sprenkeler et al.). In chapter 2, Palacios et al. describe novel methods to measure oscillations of ventricular repolarization from the ECG T-wave vector using continuous wavelet transform and phase rectified signal averaging. Microgravity was simulated by head down bed rest. Sympathetic stimulation using head up tilt increased oscillations before microgravity and more so following microgravity (Palacios et al.). In chapter 3, Van Duijvenboden et al. report the results of studies in patients showing that ß-adrenergic receptor blockade reduced LF APD oscillations and beat-to-beat APD variability. The two effects were correlated suggesting an interaction between the two. In chapter 4, computational modeling studies by Sampedro-Puente et al. revealed a time delay in the development of LF oscillations of APD following sympathetic stimulation. The mechanism was related to the slow phosphorylation kinetics of the slow component of the delayed rectifier current (Iks). In chapter 5, Orini et al. evaluated the effect of emotion (the response to pleasant or unpleasant music) on QT interval variability. These authors report that QT variability increased and was highly correlated with RR variability (Orini et al.). Since changes in RR interval elicit corresponding changes in QT interval, these results further confirm that QT variability should be measured during a constant RR interval (i.e., during atrial pacing, in order to obtain an accurate assessment of oscillations in ventricular repolarization independent of changes in RR interval). Chapter 6, reports the results of studies of HRV using a range of analytical methods showed a unique non-linear pattern in dogs compared to humans. These authors suggest that linearity was related to sympathetic dominance and non-linearity to parasympathetic dominance (Moïse et al.). In chapter 7, De Maria et al. addressed the much debated issue of the relative contributions of sympathetic and parasympathetic activity to the HF and LF components of HRV. They tested the combination of HF HRV in combination with LF QT variability as a measure of parasympathetic and sympathetic activity, respectively (De Maria et al.). They report that QT variability (SD) at rest identified the elderly patients with aortic stenosis who were at a greater risk of ventricular arrhythmia. In chapter 8, the effect of mental stress on the RR interval spectral power are discussed. Specifically these authors report that both LF and LF/HF spectral power increase in response to mental stress (Piccirillo et al.). In chapter 9, Ang and Marina evaluate the scientific evidence to identify neuronal networks responsible for generating LF rhythms along the neurocardiac axis. The functional significance of rhythmic sympathetic activity on neurotransmission efficiency and its role in the pathogenesis of repolarization instability is discussed. Finally in chapter 10, Schwartz and colleagues provide a personal overview of specific aspects of autonomic nervous system based on many years of their own pioneering research. These include the role of the baroreceptors, risk stratification, interventions to reduce sympathetic or enhance vagal nerve activity, RR and QT intervals (La Rovere et al.).

AUTHOR CONTRIBUTIONS

PT and GB jointly wrote the article, and proofread and approved submission of the article. All authors contributed to the article and approved the submitted version.

REFERENCES

Bauer, A., Klemm, M., Rizas, K. D., Hamm, W., von Stülpnagel, L., and Dommasch, M. (2019). Prediction of mortality benefit based on periodic repolarisation dynamics in patients undergoing prophylactic implantation of a defibrillator: a prospective, controlled, multicentre cohort study. *Lancet* 394, 1344–1351. doi: 10.1016/S0140-6736(19)31996-8

Baumert, M., Porta, A., Vos, M. A., Malik, M., Couderc, J. P., and Laguna, P. (2016). QT interval variability in body surface ECG: measurement, physiological basis, and clinical value: position statement and consensus guidance endorsed by the European heart rhythm association jointly with the ESC working group on cardiac cellular electrophysiology. *Europace* 18, 925–944. doi: 10.1093/europace/euv405

Billman, G. E. (2011). Heart rate variability: a historical perspective. *Front. Physiol.* 2:86. doi: 10.3389/fphys.2011.00086

Hanson, B., Child, N., Van Duijvenboden, S., Orini, M., Chen, Z., and Coronel, R., et al. (2014). Oscillatory behaviour of ventricular action potential duration in heart failure patients at respiratory rate and low frequency. *Front. Physiol.* 5:414. doi: 10.3389/fphys.2014.00414

Porter, B., Van Duijvenboden, S., Bishop, M. J., Orini, M., Claridge, S., Gould, J., et al. (2018). Beat-to-Beat variability of ventricular action potential duration oscillates at low frequency during sympathetic provocation in humans. *Front. Physiol.* 9:147. doi: 10.3389/fphys.2018.00147

Pueyo, E., Orini, M., Rodríguez, J. F., and Taggart, P. (2016). Interactive effect of beta-adrenergic stimulation and mechanical stretch on low-frequency oscillations of ventricular action potential duration in humans. *J. Mol. Cell. Cardiol.* 97, 93–105. doi: 10.1016/j.yjmcc.2016.05.003

Rizas, K. D., Nieminen, T., Barthel, P., Zürn, C. S., Kähönen, M., Viik, J., et al. (2014). Sympathetic activity – associated periodic repolarization dynamics predict mortality following myocardial infarction. *J. Clin. Invest.* 124, 1770–1780. doi: 10.1172/JCI70085

Task Force of the European Society of Cardiology and North American Society of Pacing and Electrophysiology (1996). Heart rate variability: standards of measurement, physiological interpretation and clinical use. *Circulation* 93, 1043–165.

Conflict of Interest: The authors declare that the research was conducted in the absence of any commercial or financial relationships that could be construed as a potential conflict of interest.

frontiers in Physiology

ORIGINAL RESEARCH
published: 06 August 2019
doi: 10.3389/fphys.2019.00991

Arrhythmic Risk in Elderly Patients Candidates to Transcatheter Aortic Valve Replacement: Predictive Role of Repolarization Temporal Dispersion

Gianfranco Piccirillo[1], Federica Moscucci[1], Marcella Fabietti[1], Ilaria Parrotta[1], Fabiola Mastropietri[1], Claudia Di Iorio[1], Teresa Sabatino[1], Davide Crapanzano[1], Giulia Vespignani[1], Marco Valerio Mariani[1], Nicolò Salvi[1] and Damiano Magrì[2]*

[1] *Dipartimento di Scienze Cardiovascolari, Respiratorie, Geriatriche, Anestesiologiche e Nefrologiche, Policlinico Umberto I, "La Sapienza" University of Rome, Rome, Italy,* [2] *Dipartimento di Medicina Clinica e Molecolare, S. Andrea Hospital, "Sapienza" University of Rome, Rome, Italy*

OPEN ACCESS

Edited by:
Peter Taggart, University College London, United Kingdom

Reviewed by:
Gary Tse, Xiamen Cardiovascular Hospital Xiamen University, China
Tong Liu, Tianjin Medical University, China

***Correspondence:**
Federica Moscucci
federica.moscucci@uniroma1.it

Specialty section:
This article was submitted to Cardiac Electrophysiology, a section of the journal Frontiers in Physiology

Received: *06 May 2019*
Accepted: *18 July 2019*
Published: *06 August 2019*

Citation:
Piccirillo G, Moscucci F, Fabietti M, Parrotta I, Mastropietri F, Di Iorio C, Sabatino T, Crapanzano D, Vespignani G, Mariani MV, Salvi N and Magrì D (2019) Arrhythmic Risk in Elderly Patients Candidates to Transcatheter Aortic Valve Replacement: Predictive Role of Repolarization Temporal Dispersion. Front. Physiol. 10:991. doi: 10.3389/fphys.2019.00991

Background/Aim: Degenerative aortic valve stenosis (AS) is associated to ventricular arrhythmias and sudden cardiac death, as well as mental stress in specific patients. In such a context, substrate, autonomic imbalance as well as repolarization dispersion abnormalities play an undoubted role. Aim of the study was to evaluate the increase of premature ventricular contractions (PVC) and complex ventricular arrhythmias during mental stress in elderly patients candidate to the transcatheter aortic valve replacement (TAVR).

Methods: In eighty-one elderly patients with AS we calculated several short-period RR- and QT-derived variables at rest, during controlled breathing and during mild mental stress, the latter being represented by a mini-mental state evaluation (MMSE).

Results: All the myocardial repolarization dispersion markers worsened during mental stress ($p < 0.05$). Furthermore, during MMSE, low frequency component of the RR variability increased significantly both as absolute power (LF_{RR}) and normalized units (LF_{RRNU}) ($p < 0.05$) as well as the low-high frequency ratio (LF_{RR}/HF_{RR}) ($p < 0.05$). Eventually, twenty-four (30%) and twelve (15%) patients increased significantly PVC and, respectively, complex ventricular arrhythmias during the MMSE administration. At multivariate logistic regression analysis, the standard deviation of QTend (QTe_{sd}), obtained at rest, was predictive of increased PVC (odd ratio: 1.54, 95% CI 1.14–2.08; $p = 0.005$) and complex ventricular arrhythmias (odd ratio: 2.31, 95% CI 1.40–3.83; $p = 0.001$) during MMSE. The QTe_{sd} showed the widest sensitive-specificity area under the curve for the increase of PVC (AUC: 0.699, 95% CI: 0.576–0.822, $p < 0.05$) and complex ventricular arrhythmias (AUC: 0.801, 95% CI: 0.648–0.954, $p < 0.05$).

Conclusion: In elderly with AS ventricular arrhythmias worsened during a simple cognitive assessment, this events being a possible further burden on the outcome of TAVR. QTe_{sd} might be useful to identify those patients with the highest risk of ventricular arrhythmias. Whether the TAVR could led to a QTe_{sd} reduction and, hence, to a reduction of the arrhythmic burden in this setting of patients is worthy to be investigated.

Keywords: aortic stenosis, TAVR, QT, QT standard deviation, T peak-T end, QTc, QT variability

INTRODUCTION

Senile degenerative aortic valve stenosis (AS) represents the most relevant valvular heart disease both in terms of prevalence and of prognostic implications in Western countries. Indeed, about 3.4% of over 75 years subjects suffers from this valvulopathy (Osnabrugge et al., 2013) and, after the beginning of symptoms, in absence of surgical or transcatheter replacement, the survival is less than half at 2 years (Lindman et al., 2014; Afilalo et al., 2017). Obviously, the poor prognosis in this setting of patients is strongly influenced by a number of possible comorbidities over the AS. However, a mainly neglected factor possibly impacting the AS patients prognosis is represented by their propensity to the malignant arrhythmias. Myocardial hypertrophy, fibers disarray, fibrosis, necrosis and calcification are all features constituting an optimum structural substrate for arrhythmic sudden cardiac death. Furthermore, sympathetic over-activity, typical in chronic heart failure, could also play an important role as malignant ventricular arrhythmias' trigger. In such a context, there are two previous observations corroborating these claims: it was recently confirmed that the sudden cardiac death during AS remains statistically important (Minamino-Muta et al., 2017) and, some non-invasive electrocardiographic (ECG) markers were found significantly associated to a poor outcome in elderly patients with AS after the transcatheter aortic valve replacement (TAVR) (Piccirillo et al., 2018).

Therefore, the present study evaluated a number of non-invasive markers of myocardial electrical instability in a cohort of elderly patients with AS candidate to the TAVR procedure. Particularly, we analyzed the short period RR- and QT-interval variables (Baumert et al., 2016) at rest, during controlled breathing and during mild mental stress, the latter being represented by a mini-mental state evaluation (MMSE). Thereafter we evaluated a possible MMSE-induced increase in premature ventricular contraction (PVC) or complex ventricular arrhythmias (bigeminy, trigeminy, couplets episodes, R on T phenomena, sustained or non-sustained ventricular tachycardia) (Zanobetti et al., 2017). Eventually, we sought to assess a possible relationship between the abovementioned ECG derived markers obtained during rest and the arrhythmic risk in terms of complex ventricular arrhythmias increase during MMSE.

The major part of these repolarization markers are normalized for RR variability (Baumert Europace 2016; 18, 925–944) (Baumert et al., 2016) and for this reason the patients with frequent premature contractions or atrial fibrillation are frequently excluded from these kind of studies. Notwithstanding, the elderly with AS presented a very high level of supra- or ventricular arrhythmias, consequently we decided to use repolarization indexes only, without RR variability normalization; in this way, we were able to include even patients with atrial fibrillation or with frequent premature atrial or ventricular contractions.

MATERIALS AND METHODS

Participants and Protocol

A total of 92 consecutive symptomatic (NYHA III class) elderly patients who underwent evaluation for TAVR HCM were recruited between September 2017 and July 2018 at Policlinico Umberto I University Hospital in Rome. Patients' characteristics, preoperative echocardiographic issues, a complete functional assessment and ECG-derived data were recorded at time of enrollment.

The functional assessment included the following: Mini-Mental State Examination (MMSE), Activity of Daily Living (ADL), Instrumental Activities of Daily Living (IADL), and Mini-Nutritional Assessment (MNA). Furthermore the Clinical Frailty Scale (Rockwood et al., 2005) and the Essential Frailty Toolset (Afilalo et al., 2017) have been administered.

The ECG study included, for each patients, three distinct and consecutive sessions with a short-period single lead (II) ECG acquired in supine position: the first session during rest (REST); the second session during controlled breathing (15 breaths per minute) (RESP) and the third one during MMSE (MENTAL STRESS). Both the REST and RESP recordings lasted 5 min while the MENTAL STRESS session lasted averagely 10 min (11.5 ± 3.9 min), being the sum of the three recordings equal to 22.1 ± 3.9 min. Contextually, a non-invasive beat-to-beat blood pressure wave recordings (Finometer MIDI, FMS B.V., Amsterdam, Netherlands) has been recorded.

No patient has been excluded from the ECG analysis, being included also those with atrial and ventricular arrhythmias (premature ventricular or atrial contractions, atrial fibrillation, etc.) or pacemaker. Concerning the latter category, the pacing setting during the study was VDD with lower rate well below the patient's lowest intrinsic heart rate so that the physiological atrial tracking under study conditions has been preserved. In patients with bundle branch block, J-T interval was considered in place of QT.

The study was approved by the Ethical Committee of Azienda Universitaria Policlinico Umberto I. Each patients signed an appropriate informed consent. Trial was registered on ClinicalTrial.gov database with number NCT03145376.

Off-Line Data Analysis

To acquire and digitalize the ECG and pressure signals, we used a custom-designed card (National Instruments USB-6008; National Instruments, Austin, TX, United States) with a sampling frequency equal to 500 Hz. The software for data acquisition, storage, and analysis with the LabView program (National Instruments), designed and produced from our research team, follows the technical recommendation of consensus guidance endorsed by European Heart Rhythm Association jointly with the European Society of Cardiology Working Group on cardiac cellular electrophysiology (Baumert et al., 2016). With respect the QT-derived measurements, they were obtained with the template method proposed by Berger et al. (1997).

Each ECG recording undergoes three consecutive processes: rhythm analysis; elimination of ventricular and atrial premature contraction (PVC ad sPVC) from ECG traces; RR and QT interval analysis. During the rhythm analysis, a quantitative evaluation of PVC has been made by dividing the number of PVC every 3 min of each single examined recording thus disclosing the patients with the increase of PVC per minutes during the MENTAL STRESS session. If during the MENTAL STRESS session only, patients showed bigeminy, trigeminy, couplets episodes, R on T phenomenon, sustained or non-sustained ventricular tachycardia, we considered this fact as an increase of arrhythmias (Zanobetti et al., 2017). Secondly, we identified the PVC and sPVC on the traces and we eliminated manually their QRS-T data and also the corresponding following beat (**Figure 1**), as recommended in previous consensus guidance (Baumert et al., 2016). After this preliminary phase, we used three time-series of "cleaned" 256 consecutive QRS-T (REST, RESP, and MENTAL STRESS) to study the repolarization variables. With respect the MENTAL STRESS recording, we focused on the period with the higher sympathetic activity (i.e., the QRS-T data series with lower RR cycle length and then higher heart rate). Short-term myocardial temporal repolarization dispersion measurements were obtained on three different intervals: the interval from Q to end of T wave (QTe); the interval between and the Q and the peak of T wave (QTp); the interval between peak and end of T wave (Te) (**Figure 2**). We then calculated the following QT-derived data: mean and standard deviation of QTe, QTp and Te (QTe_m, QTe_{sd}, QTp_m, QTp_{sd}, Te_m, and Te_{sd}), Te_m and QTe_m ratio (Te_m/QTe_m). We also calculated normalized QTe (QTeVN), QTp (QTpVN) and Te (TeVN) interval variances (Baumert et al., 2016) according to the formulas:

$$QTeVN = QTe_{sd}{}^2/QeT_m{}^2;$$

$$QTpVN = QTp_{sd}{}^2/QTp_m{}^2;$$

$$TeVN = Te_{sd}{}^2/Te_m{}^2.$$

Short term variability of QTe (QTe_{STV}), QTp (QTp_{STV}) and Te (Te_{STV}) (Baumert et al., 2016) was also obtained according to the formulas:

$$QTe_{STV} = \Sigma[QT_{n+1} - QT_n]\,(256 \times \sqrt{2});$$

$$QTp_{STV} = p\Sigma[QTp_{n+1} - QTp_n]\,(256 \times \sqrt{2});$$

$$Te_{STV} = [Te_{n+1} - Te_n]\,(256 \times \sqrt{2}).$$

Furthermore, we calculated the spectral coherence between the QTp and Te (Piccirillo et al., 2014b) on the 256 beats in the three different study sessions according to the formula (Baumert et al., 2016):

$$\text{Coherence}^2_{(QTp-Te)}(f);$$

$$\frac{\text{Cross spectral power density}^2_{(QTp-Te)}(f)}{\text{Spectral density}_{Te}(f)\ \text{Spectral density}_{QTp}(f)} = |\ \text{Coherence}_{(QTp-Te)}(f)^2$$

where f was the spectral frequency.

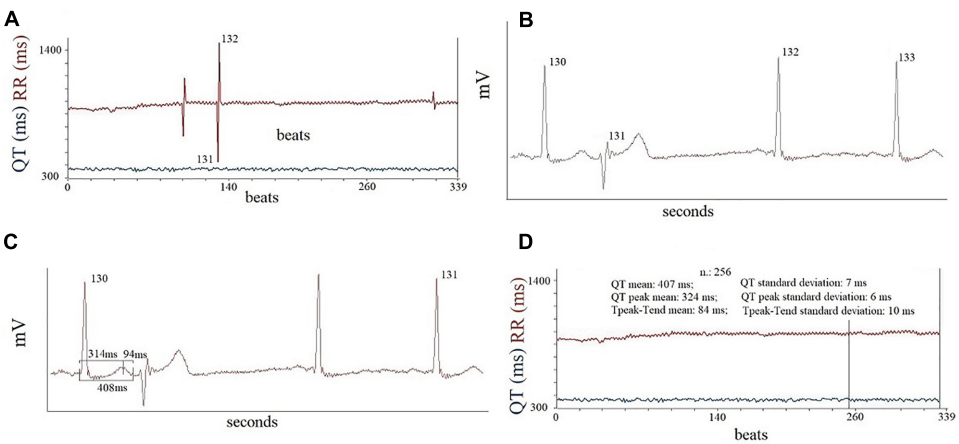

FIGURE 1 | An example of RR and QTe recordings at rest **(A)**, it is possible to observe three PVC in picture, the second PVC is the beat number 131. In the second phase of off-line analysis **(B)**, the computer eliminated the data of PVC (131) and of following beats number 132. Note, the complete flattening of T wave of beat number 132. Therefore, this beats was eliminated from final analysis of data **(C)**. Finally, it was reported the some final analyses in the 256 window data recordings **(D)**.

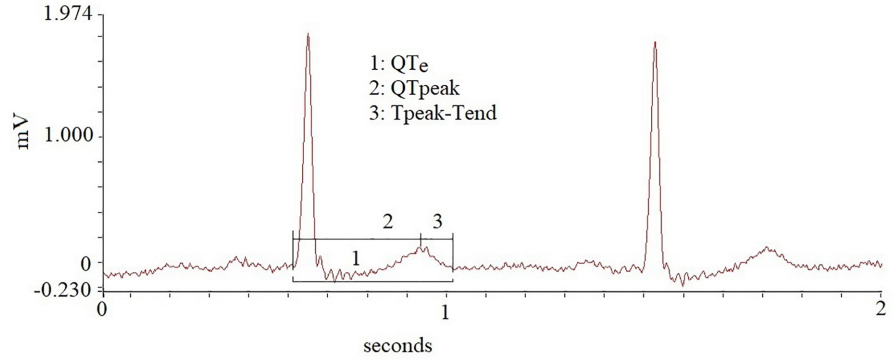

FIGURE 2 | Different repolarization intervals obtained in the study.

The spectral coherence value ranges between 0 and 1 with the high level of coherence being closer to 1 and it indicates the temporal relation between two signals (QTp and Te).

We also measured manually, by means an electronic caliper and applying the tangent method on three consecutive cycles (II lead), the following intervals: QT (from q to end T wave); QRS (from q to end S wave); JT (from J point to end of T wave); Te (from the peak to the end of T wave) and we corrected them on three preceding RR interval with Bazett method (QT_{Bazett}: $QT/RR^{0.5}$; QRS_{Bazett}: $QRS/RR^{0.5}$; JT_{Bazett}: $JT/RR^{0.5}$; $Te_{Bazett}/RR^{0.5}$) (Crow et al., 2003; Rautaharju et al., 2004, 2009).

Eventually, only in those patients with sinus rhythm, excluding those with higher than one PVC per minute, we obtained the spectral and cross-spectral analysis, using the autoregressive method (Task Force of the European Society of Cardiology, and the North American Society of Pacing, and Electrophysiology, 1996; Berger et al., 1997; Baumert et al., 2016) and we reported the following RR and systolic blood pressure (SBP) variables: the total power (TP_{RR}, TP_{SBP}), resulted from the spectral densities included between the 0 and 0.40 Hz; the high-frequency (HF_{RR}, HF_{SBP}) component (from 0.15 to 0.40 Hz); the low-frequency (LF_{RR}, LF_{SBP}) component (from 0.04 to 0.15 Hz Eq); the very-low frequency (VLF_{RR}, VLF_{SBP}) component (below 0.04 Hz Eq) (Task Force of the European Society of Cardiology, and the North American Society of Pacing, and Electrophysiology, 1996; Piccirillo et al., 2009b, 2016). We also calculated the LF (LF_{NU}) and HF (HF_{NU}) normalized units according the following formulas:

$$LF_{NU} = LF_{RR}/(TP_{RR} - VLF_{RR}) \times 100;$$

$$HF_{NU} = HF_{RR}/(TP_{RR} - VLF_{RR}) \times 100.$$

We also measured LF and HF central frequencies and the α index was calculated according to the formulas: (Robbe et al., 1987; Pagani et al., 1988; Piccirillo et al., 2000a,b, 2004b, 2013, 2016).

$$\alpha LF = \sqrt{LF_{RR}}/\sqrt{LF_{SBP}};$$

$$\alpha HF = \sqrt{HF_{RR}}/\sqrt{HF_{SBP}}.$$

Absolute power, LF/HF, α LF and α HF were converted in natural logarithm (ln) (Task Force of the European Society of Cardiology, and the North American Society of Pacing, and Electrophysiology, 1996; Piccirillo et al., 2009b, 2016).

Statistical Analysis

All data with normal distribution were expressed as means ± standard deviation; non-normally distributed variables were expressed as median and inter-quartile range (iqr); categorical variables are presented as frequencies and percentage (%). In normal distributed data one-way repeated-measures ANOVA test has been used to compare the same variable in the three different study session (REST, RESP, and MENTAL STRESS); the variables with non-normal distribution were compared using Friedman test.

Then, we grouped patients in two categories according to the presence or the absence of complex ventricular arrhythmias recorded during the MENTAL STRESS session. The criteria to include a patient in the complex ventricular arrhythmia group were the following rhythm disturbs during the MENTAL STRESS session: bigeminy, trigeminy or couplet episodes, R on T phenomenon, sustained or non-sustained ventricular tachycardia (Zanobetti et al., 2017). Thereafter we also grouped the patients in two other categories according the presence or the absence of an increase PVC per minute during the MENTAL STRESS session. The values of repolarization obtained during REST of these study groups were compared using Student's T and Mann-Whitney U tests, respectively for normal and non-normal distribution data.

Uni- and multivariable forward (A. Wald) stepwise logistic regression analysis were used to determine the association between the increase of the number or the complex ventricular arrhythmias during the MENTAL STRESS session and clinical, hemodynamic, repolarization and spectral data during the REST session. Particularly, we considered covariates the following repolarization data: QTe_m, QTe_{sd}, QTp_m, QTp_{sd}, Te_m, Te_{sd}, Te_m/QTe_m, QTe_{STV}, QTp_{STV}, Te_{STV}, $Coherence_{(QTp-Te)}$,QRS, QT, JT, Te, QRS_{Bazett}, QT_{Bazett}, JT_{Bazett}, Te_{Bazett}, Te/QTe, Te_{Bazett}/QTe_{Bazett}. QTeVN, QTpVN, TeVN were excluded from the present analysis because of their non-normal distribution.

Receiver operating characteristic (ROC) curves were used to determine the sensitivity and specificity of studied parameters predictive of complex ventricular arrhythmias and areas under ROC curves and 95% confidence intervals (CI) were calculated to compare the diagnostic efficiencies. All data were evaluated by use of database SPSS-PC + (SPSS-PC + Inc., Chicago, IL, United States).

RESULTS

From the initial 92 patients' study sample, 11 patients were excluded because the ECG traces' poor quality (No. 4 patients) or because they did not complete the protocols (No. 6 patients). **Table 1** summarized clinical, echocardiographic, cognitive, nutritional and functional data for a total of 81 elderly patients effectively enrolled in the present study.

TABLE 1 | General characteristic of the degenerative aortic valve stenosis.

	N: 81
Age, years	81 ± 7
M/F,	36/45
BMI, kg/m^2	26.7 ± 4.5
Complete right bundle branch block	6(7)
Complete left bundle branch block	10(12)
Aortic peak gradient, mm Hg	73 ± 23
Aortic mean gradient, mm Hg	45 ± 15
Aortic valve area, cm^2/m^2	0.46 ± 0.14
Aortic peak velocity, m/s	4.2 ± 0.8
Ejection fraction,%	51 ± 9
Stroke volume index, ml/m^2	41 ± 17
Left ventricular mass index, g/m^2	143 ± 39
Mini-mental state evaluation	26.3 ± 3.9
Activity of day living	5 ± 1
Instrumental activities of day living	5 ± 2
Clinical frailty scale	4 ± 1
Essential frailty toolset	2 ± 1
Mini-nutritional assessment	23 ± 4
β-blockers, n (%)	43(53)
Verapamil/Diltiazem, n (%)	4(5)
Amiodarone, n (%)	4(5)
Flecainide, n (%)	2(2)
Propafenone, n (%)	1(1)
Ivabradine, n (%)	2(2)
Digoxin, n (%)	4(5)
ACE/sartan, n (%)	47(58)
Dihydropyridine calcium channel blockers, n (%)	26(32)
Furosemide, n (%)	46(57)
Nitrate, n (%)	7(9)
Ranolazine, n (%)	6(7)
Statine, n (%)	37(46)
Antiplatelet therapy, (%)	39(48)
Oral anticoagulants, (%)	26 (32)
Pacemaker, n (%)	5(6)

Data are expressed as mean ± SD or number (n) of patients (%).

The arrhythmic characteristics obtained during the three sessions (REST, RESP, MENTAL STRESS) were reported in the **Table 2**. During the MENTAL STRESS session, an increase of PVC and of arrhythmic ventricular complexity were found in 24 (from 0.3 [2.1] to 0.8 [3.9], $p < 0.001$) and, respectively, in 12 patients (from 0 [0] to 7 ventricular bigeminy or trigemini – 8 ventricular couplets episodes; 3 non-sustained ventricular tachycardia; 3 R on T phenomenon). Remarkably, two patients with an increased complexity of ventricular arrhythmias during MENTAL STRESS did not report any isolated PVC during REST (both of them showed a ventricular couplet episode and, only one of them, an R on T phenomenon, too). Three subjects showed premature ventricular couplets during the RESP session, these type of arrhythmic episodes interesting a total of 11 patients. No significant difference was found between those patients with increased PVC's number or complexity of ventricular arrhythmias and all the other AS patients with respect clinical, cognitive, nutritional, functional and echocardiographic data.

Hemodynamic and Repolarization Data

During MENTAL STRESS, all patients reported a significant increase of heart rate ($p < 0.01$) and, at the same time, they significantly reduced the non-invasively measured stroke volume ($p < 0.001$) and cardiac output ($p < 0.05$) (**Table 3**).

The QTe mean and QTp_m values were steady between REST and MENTAL STRESS session while Te_m significantly increased ($p < 0.05$) (**Table 3**). Moreover the Te_m value increased significantly during the RESP session in comparison to the REST one, too. All markers of myocardial ventricular temporal dispersion, excepted the Te_m/QTe_m, were significantly higher during the MENTAL STRESS in comparison to the REST ($p < 0.05$) and RESP ($p < 0.05$) (**Table 3**). Instead, the $Coherence_{(QTp-Te)2}$ showed a mirrored trend, this variable decreasing during MENTAL STRESS and RESP in comparison to the REST session ($p < 0.05$) (**Table 3**). Eventually, during the RESP session, in all study patients a significant increase of QTe ($p < 0.001$), Te_m/QTe_m ($p < 0.05$) and QTeVN ($p < 0.05$) in comparison to the REST session have been observed (**Table 3**).

TABLE 2 | Arrhythmic characteristic of study subjects during short term ECG monitoring.

	N: 81
Sinus rhythm	59(73)
Permanent atrial fibrillation	22(27)
Premature supraventricular contraction	17(21)
Premature ventricular contraction	50(62)
>1 Premature ventricular contraction/minute	19(23)
<1 Premature ventricular contraction/minute	31(38)
Complex ventricular arrhythmias	15(19)
Ventricular bigeminy or trigeminy	7(9)
Premature ventricular couplets	11(14)
Non-sustained ventricular tachycardia	3(4)
R on T phenomenon	3(4)
Increasing premature ventricular contractions during mental stress	24(30)
Increasing ventricular arrhythmic complexity during mental stress	12(15)

TABLE 3 | Hemodynamic (Fenometer) and short period repolarization variability data obtained on 256 beats in all study subjects.

	Rest N:81	Controlled breathing N:81	Mental challenge N:81	*P ANOVA*
Variables				
Heart rate, b/m	69 ± 11**	69 ± 11**	72 ± 12	<0.001
Systolic blood pressure, mm Hg	119 ± 23	118 ± 24	116 ± 41	Ns
Diastolic blood pressure, mm Hg	62 ± 11	61 ± 12	62 ± 20	Ns
Stroke volume, ml	39 ± 13**	39 ± 14**	35 ± 18	<0.001
Cardiac output, l/m	2.72 ± 0.94	2.71 ± 0.98*	2.48 ± 1.20	0.032
Peripheral resistance, a.u.	3853 ± 2316	3925 ± 2431	4425 ± 3342	Ns
QTe mean, ms	408 ± 53	412 ± 53	407 ± 50	ns
QTe standard deviation, ms	7 ± 2§§*	8 ± 2*	11 ± 2	<0.001
QTp mean, ms	328 ± 45	326 ± 48	322 ± 45	Ns
QTp standard deviation, ms	7 ± 2*	7 ± 2*	9 ± 5	0.002
Te mean, ms	80 ± 24§*	86 ± 24	85 ± 24	0.026
Te standard deviation, ms	10 ± 2*	10 ± 2*	13 ± 9	<0.001
Te mean/QTe mean	0.22 ± 0.06§*	0.24 ± 0.06	0.24 ± 0.06	0.005
QTeVN	0.28[0.21]§§**	0.33[0.33]**	0.46[0.29]	<0.001
QTpVN	0.56[0.49]**	0.58[0.51]**	0.97[2.00]	<0.001
TeVI	14[21.33]**	14[15]*	21[20]	<0.001
$Coherence_{(QTp-Te)}{}^2$	0.600 ± 0.139§*	0.555 ± 0.122	0.552 ± 0.115	0.002
QTe_{STV}	14 ± 4§§**	15 ± 4*	19 ± 13	<0.001
QTp_{STV}	14 ± 5*	15 ± 6*	16 ± 6	0.023
Te_{STV}	20 ± 6*	21 ± 8	25 ± 13	0.010

*Values are expressed as mean ± SD or median [interquartile range 75th percentile – 25th percentile]. **$p < 0.001$ REST or RESP vs. MENTAL STRESS; *$p < 0.05$ REST or RESP vs. MENTAL STRESS; §§$p < 0.001$ REST vs. RESP; §$p < 0.05$ REST vs. RESP.*

During MENTAL STRESS, the repolarization data manually obtained were almost steady (**Table 4**) when corrected for the heart rate (Bazett). Only the Te_{Bazett} value decreased significantly during the MENTAL STRESS with respect the REST and RESP sessions ($p < 0.001$).

RR Spectra Analysis Data

RR and SBP power and cross spectral analysis were obtained in only 59 patients on sinus rhythm. LF, expressed in absolute and normalized power, and LF/HF were significantly higher during MENTAL STRESS (ln LF_{RR}: 4.44 ± 1.35 ms^2; LF NU: 48 ± 17; ln LF/HF; 0.76 ± 1.13) in comparison to REST (ln LF_{RR}: 3.66 ± 1.42, $p < 0.05$; LF_{NU}: 39 ± 20, $p < 0.05$; ln LF/HF; 0.22 ± 1.1.52, $p < 0.05$) and RESP (ln LF_{RR}: 3.63 ± 1.46, $p < 0.001$; LF_{NU}: 34 ± 22, $p < 0.001$; ln LF/HF: -0.14 ± 1.17, $p < 0.001$).

HF_{NU} was significantly lower in REST (HF_{NU}: 35 ± 25, $p < 0.05$) and RESP (HF_{NU}: 39 ± 22, $p < 0.001$) than during MENTAL STRESS (HF_{NU}: 26 ± 18).

TABLE 4 | Manual repolarization data obtained on 3 QRS-T cycles.

	Rest N:81	Controlled breathing N:81	Mental challenge N:81	*P ANOVA*
Variables				
RR, ms	881 ± 150*	873 ± 134*	853 ± 133	0.017
QT, ms	425 ± 54*	424 ± 53*	414 ± 49	0.003
QRS, ms	91 ± 23	91 ± 24	93 ± 40	Ns
JT, ms	334 ± 55*	333 ± 54*	321 ± 64	0.006
Te, ms	92 ± 25*	88 ± 20	86 ± 20	0.034
QT_{Bazett}, ms	455 ± 48	455 ± 51	450 ± 41	Ns
QRS_{Bazett}, ms	98 ± 28	99 ± 29	102 ± 47	Ns
JT_{Bazett}, ms	357 ± 49	356 ± 50	348 ± 61	Ns
Te_{Bazett}, ms	98 ± 28**	95 ± 21*	94 ± 23	<0.001
Te/QTe,	0.21 ± 0.5	0.21 ± 0.5	0.21 ± 0.5	Ns
Te_{Bazett}/QTe_{Bazett}	0.21 ± 0.5	0.21 ± 0.4	0.21 ± 0.4	Ns

*Values are expressed as mean ± SD or median [interquartile range 75th percentile – 25th percentile]. **$p < 0.001$ REST or RESP vs. MENTAL STRESS; *$p < 0.05$ REST or RESP vs. MENTAL STRESS.*

Both the α indexes, marker of baroreflex sensitivity, were lower during MENTAL STRESS (α LF: 0.80 ± 0.90; α HF: 0.77 ± 0.91) than REST (α LF: 1.32 ± 0.96, $p < 0.001$; α HF: 1.41 ± 0.96, $p < 0.001$) and RESP (α LF: 1.42 ± 0.79, $p < 0.001$; α HF: 1.44 ± 0.95, $p < 0.001$).

No statistically significant difference have been found between RR variability data obtained at REST and RESP.

Category With PCVs' Increase During the MENTAL STRESS Session

At REST, the 24 patients with an increase of PVC during MENTAL STRESS showed the following repolarization markers significantly higher than other 57 patients: QTe_{SD} (8 ± 2 vs. 7 ± 2 ms^2, $p < 0.05$), QTeVN (0.37[0.22] vs. 0.25 [0.20], $p < 0.05$), QTe_{STV} (15 ± 3 vs. 13 ± 5, $p < 0.05$) (**Figures 3A,C,E**), QRS (102 ± 27 vs. 87 ± 20 ms, $p < 0.05$), QRS_{Bazett} (111 ± 32 vs. 93 ± 25 ms, $p < 0.05$). No other significant differences were observed between these two study groups.

Category With Complex Ventricular Arrhythmias' Increase During the MENTAL STRESS Session

At REST, the 12 patients with an increased complexity of ventricular arrhythmias during MENTAL STRESS showed the following markers significantly higher than other 69 patients: QTe_{sd} (9 ± 2 vs. 7 ± 2 ms^2, $p < 0.001$), Te_m SD (12 ± 3 vs. 10 ± 2 ms^2, $p < 0.05$), QTeVN (0.43[0.49] vs. 0.25 [0.20], $p < 0.001$), QTpVN (0.52[0.56] vs. 0.41 [0.31], $p < 0.05$) and QTe_{STV} (17 ± 5 vs. 13 ± 4, $p < 0.05$) (**Figures 3B,D,F**). Instead $Coherence_{(QTp-Te)2}$ was lower in the arrhythmic patients' group in comparison with the counterpart (0.524 ± 0.119 vs. 0.613, $p < 0.05$). Eventually, excepted the Te/QTe (0.242 ± 0.049 vs. 0.210 ± 0.046 ms, $p < 0.05$) and Te_{Bazett}/QTe_{Bazett} (0.241 ± 0.051 vs. 0.210 ± 0.046, $p < 0.05$), most of the manual repolarization indexes were not significantly different between the study groups.

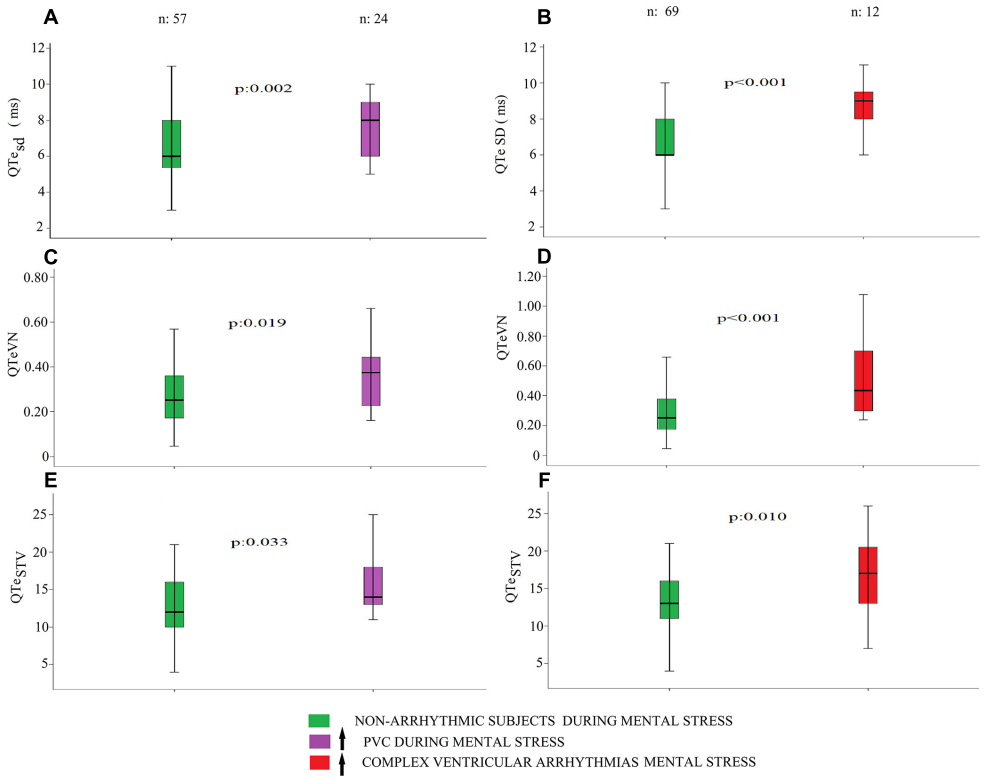

FIGURE 3 | QTe standard deviation QTe_{sd}, QTeVN and QTe_{STV}, obtained at rest, in subjects with an increase of PVC (purple) and complex ventricular arrhythmias (red) during mental stress. At REST, the 24 patients with an increase of PVC during MENTAL STRESS showed the following repolarization markers significantly higher than other 57 patients: QTe_{SD} ($p < 0.05$), QTeVN ($p < 0.05$), QTe_{STV} ($p < 0.05$) (panel **A**, **C**, and **E**). At REST, the 12 patients with an increased complexity of ventricular arrhythmias during MENTAL STRESS showed the following markers significantly higher than other 69 patients: QTe_{sd} ($p < 0.001$), Te_m SD ($p < 0.05$), QTeVN ($p < 0.001$), QTpVN ($p < 0.05$) and QTe_{STV} ($p < 0.05$) (panel **B**, **D**, and **F**).

Relationship Between Ventricular Arrhythmic Risk and Clinical, Hemodynamic and Repolarization Data

Uni- and multivariable logistic regression analysis reported only statistically significant associations between increase of PVC or complex ventricular arrhythmias during MENTAL STRESS and repolarization data at REST (**Table 5**). None of clinical, echocardiographic, non-invasive hemodynamic spectral data showed a significant relationship with the ventricular arrhythmic risk during the MENTAL STRESS session.

The univariable logistic analysis identified the following repolarization variables obtained at REST and the risk factors of PVC increase: QTe_{sd} ($p < 0.05$), QTe_{STV} ($p < 0.05$), QRS ($p < 0.05$), QRS_{Bazett} ($p < 0.05$) (**Table 5**). On the contrary, the same statistical approach detected the following repolarization variables obtained at REST as predictors of complex ventricular arrhythmias during MENTAL STRESS: QTe_{sd} ($p < 0.05$); Te SD ($p < 0.05$); $Coherence_{(QTp-Te)2}$ ($p < 0.05$); QTe_{STV} ($p < 0.05$); Te/QTe; Te_{Bazett}/QTe_{Bazett} (**Table 5**).

Multivariable logistic analysis identified only the QTe_{SD} as risk factor of the increase of PVC (odd ratio: 1.54, 95% CI 1.14–2.08; $p = 0.005$) and complex ventricular arrhythmias (odd ratio: 2.31, 95% CI 1.40–3.83; $p = 0.001$).

Short Period Analysis Versus Manual Measurements: Comparative Study in the Ventricular Arrhythmic Risk Prediction

Although several short period and manual repolarization markers reached a sufficient statistical significance only QTe_{sd} showed the widest sensitivity-specificity area under curve (AUC) for predicting both the increase of PVC (AUC: 0.699, 95% CI: 0.576–0.822, $p < 0.05$) and complex ventricular arrhythmias (AUC: 0.801, 95% CI: 0.648–0.954, $p < 0.05$) during the MENTAL STRESS session (**Figure 4**). Particularly, the other markers with significant area under the curve were: QTeVN (AUC: 0.685, 95% CI 0.565–0.805, $p < 0.05$); QRS (AUC: 0.682, 95% CI 0.556–0.809, $p < 0.05$); QRS_{Bazett} (AUC: 0.673, 95% CI 0.545–0.800, $p < 0.05$); and QTe_{STV} (AUC: 0.664, 95% CI 0.545–0.780, $p < 0.05$) for an increase of PVC during the MENTAL STRESS session (**Figure 4A**). On the contrary, the other variable with statistically significant area under the curve were: QTeVN (AUC: 0.781, 95% CI 0.655–0.908, $p < 0.05$); QTpVN (AUC: 0.694, 95% CI 0.530–0.859, $p < 0.05$),; Te/QTe (AUC: 0.692, 95% CI 0.525–0.859, $p < 0.05$), QTe_{STV} (AUC: 0.688, 95% CI 0.501–0.875, $p < 0.05$), and $Coherence_{(QTp-Te)2}$ (AUC: 0.303, 95% CI 0.154–0.451, $p < 0.05$) (**Figure 4B**).

TABLE 5 | Univariable logistic regression analysis data.

	↑ PVC during mental stress	↑ Complex ventricular arrhythmias during mental stress
	Odds ratio (95% CI) *P*-value	**Odds ratio (95% CI) *P*-value**
QTe standard deviation, ms	1.540(1.114–2.080) $p = 0.005$	2.153(1.338–3.465) $p = 0.002$
Te standard deviation, ms	p = ns	1.353(1.061–1.726) $p = 0.015$
$Coherence_{(QTp-Te)}{}^2$	p = ns	0.009(0–0.930) $p = 0.047$
QTe_{STV}	1.131(1.007–1.270) $p = 0.038$	1.207(1.036–1.405) $p = 0.016$
QRS	1.030(1.007–1.053) $p = 0.010$	p = ns
QRS_{Bazett}	1.022(1.004–1.041) $p = 0.016$	p = ns
Te/QTe	p = ns	1.143(1.007–1.297) $p = 0.039$
Te_{Bazett}/QTe_{Bazett}	p = ns	1.136(1.002–1.289) $p = 0.047$

Effects of Possible Confounders (β-Blocker Therapy, Atrial Fibrillation)

A concomitant therapy with β-blocker was present in 43 patients (53%) but this group did not any differences with respect the increase PVC or complex ventricular arrhythmias. The others repolarization markers, as well as clinical and hemodynamic data, did not even change in relation to the β-blocker therapy.

Multivariable logistic analysis confirmed QTe_{sd} as predictive of the complex ventricular arrhythmias' increase also considering sinus rhythm patients alone (odd ratio: 3.17, 95% CI 1.37–7.35; $p = 0.007$), thus excluding from those with atrial fibrillation (odd ratio: 2.92, 95% CI 1.23–6.93; $p = 0.015$). On the contrary, excluding the patients on atrial fibrillation, the same statistical analysis confirmed QTe_{sd} (odd ratio: 1.84, 95% CI 1.59–2.92; $p = 0.01$) predicative only for an increase of PVC during the MENTAL STRESS session.

DISCUSSION

The main finding of the present study was that a non-negligible percentage of elderly patients with degenerative AS group increased the PVC and complex ventricular arrhythmias during a mild mental stress, such as the one represented by a simple MMSE and, notably, it happens regardless a concomitant beta-blockers therapy. The MMSE is usually needed to assess possible cognitive impairment in elderly candidates to a TAVR procedure (Lindman et al., 2014; Otto et al., 2017). It is highly conceivable that this simple standard test might lead, through a mental arithmetical exercise and several other cognitive tests (orientation, registration recall, language, repetition and complex tasks) (Folstein et al., 1975), to an increase of ventricular arrhythmias due to an increase of sympathetic activity and a reduced vagal tone. Supporting the abovementioned hypothesis, we found a significant increase in the explored sympathetic markers at RR power spectral analysis (ln LF_{RR}; LF NU; ln LF/HF) (Task Force of the European Society of Cardiology, and the North American Society of Pacing, and Electrophysiology, 1996; Piccirillo et al., 2009b, 2016) as well a significant reduction in two well-known vagal markers (ln HF_{RR} and ln α HF) (Robbe et al., 1987; Pagani et al., 1988; Piccirillo et al., 2000a,b, 2004b, 2013, 2016).

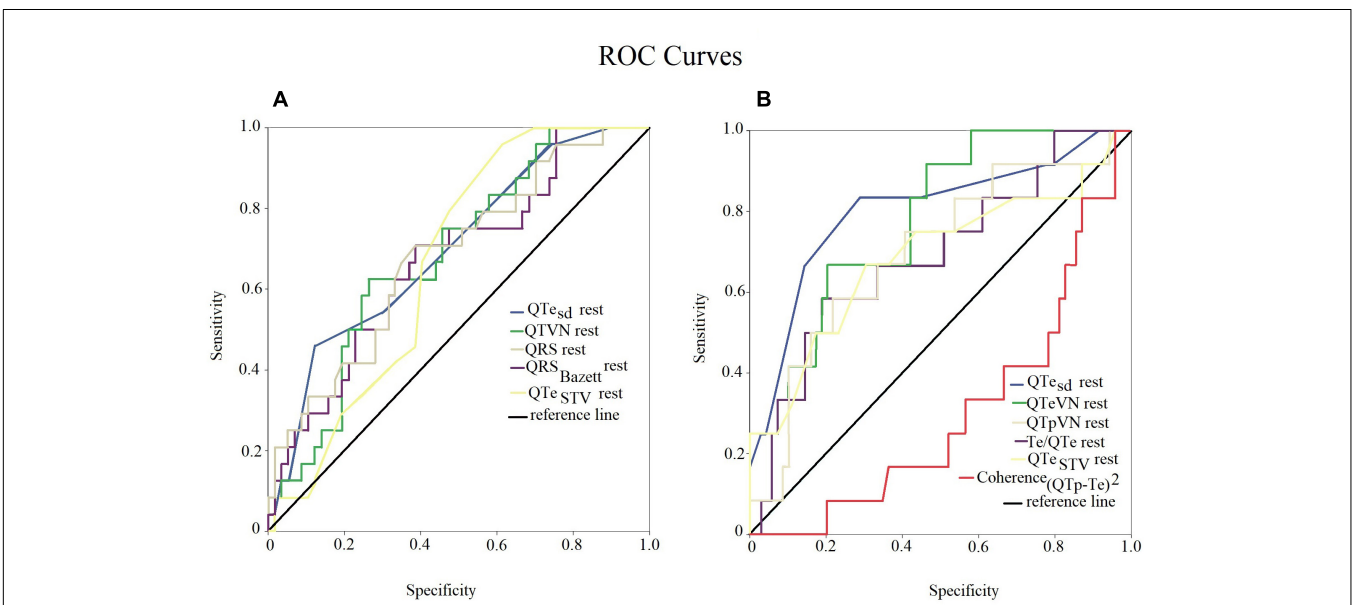

FIGURE 4 | ROC curve of statistical significant examined variables. Sensitivity-specificity of different variables, obtained at rest, to individuate patients with increase of PVC **(A)** and complex ventricular arrhythmias **(B)** during mental stress. QTe standard deviation (QTe_{sd}) had the widest area under the curve in both the diagrams (blue lines).

Another, possibly clinical relevant, finding of the present study was that a simple non-invasive short period myocardial repolarization index, such as the QTe_{sd} obtained at rest, seems to be able to identify those patients with the highest probability to increase ventricular arrhythmias (PVC or complex ventricular arrhythmias) during the MMSE administration. Thus, albeit highly speculative, the QTe_{sd} obtained at rest could be potentially useful in disclosing a general arrhythmias propensity and, accordingly, an increased risk of sudden cardiac death in elderly patients with AS candidate to a TAVR procedure (Massing et al., 2006; Cheriyath et al., 2011; Ataklte et al., 2013; Agarwal et al., 2015; Zanobetti et al., 2017). This clinical feature could frustrate the TAVR's outcomes and, accordingly, should be worthy to be weighted during the screening procedures. Indeed, although the TAVR improves undoubtedly the hemodynamic patient's conditions, the myocardial arrhythmic substrate of AS (hypertrophy, disarray, calcifications, ischemia, fibrosis, necrosis, etc.) remains theoretically and practically still able to induce malignant reentrant ventricular arrhythmias also after the AS resolution. In such a context, we also compared the predicative power of conventional QTe and Te measurements with novel short period repolarization variability markers and we found that the QTe_{sd} demonstrated the best accuracy in disclosing those patients more susceptible to increase ventricular arrhythmias during MMSE. Thus, an easy-to-obtain surface ECG-derived parameter, that is the QTe_{sd} obtained at rest, might be considered in guiding at least a more aggressive treatment in these specific category (i.e., high dosage of β-blockers or amiodarone therapy).

Mental Stress and Sudden Cardiac Death

Emotions are able to trigger malignant ventricular arrhythmias and sudden cardiac death in subjects with known or unknown heart disease and this aspect is particularly relevant in elderly patients. In such a context, retrospective studies highlighted an increase of sudden cardiac death during natural or unnatural thrilling events such as earthquakes (Trichopoulos et al., 1981; Leor et al., 1996; Kario et al., 1997; Kitamura et al., 2013; Kiyohara et al., 2015) bombings (Meisel et al., 1991), terrorist attack (Steinberg et al., 2004) and also football matches (Wilbert-Lampen et al., 2008) or other positive (Phillips et al., 2004) or negative emotional events (Cannon, 2002; Lampert et al., 2002; Williams et al., 2011).

Although no specific data on elderly patients with AS are present in literature, it is easily supposable from a pathophysiologic viewpoint that the simultaneous joint of degenerative valve disease with chronic heart failure and mental stress can exacerbated a tendency for life-threatening arrhythmias. The myocardial hypertrophy and reentrant circuits provide the substratum and electrophysiologic mechanism; the resulting simpato-vagal imbalance, induced by the chronic heart failure, constitutes the "milieu ideal"; and, finally, the sudden sympathetic stimulus, emotion mediated, can easily trigger a fatal arrhythmias. Noteworthy two patients of our study reported ventricular couplets during mental stress without preexistent PVC at rest and one of them reported a R on T phenomenon. Thus it might be hypothesized that the MMSE alone was able to induce a sympathetic overstimulation leading a complex ventricular arrhythmias. Therefore, in these two elderly patients an episode of malignant ventricular arrhythmias could be triggered "like a bolt from the blue" during a high emotional level event. This clinical feature might be clinically relevant in defining the therapeutic strategy: i.e., the elderly patient with AS candidate to a TAVR procedure who shows ventricular complex arrhythmias just during mental stress without any PVC at rest should be aggressively beta-blocked or should receive amiodarone. Clearly, in light of our present data, we strongly recommend the ECG monitoring during MMSE in such patient's category.

Sympatho-Vagal Imbalance, Abnormal Repolarization and Ventricular Malignant Arrhythmias

Myocardial repolarization phase is abnormal in patients with myocardial hypertrophy and it might be non-invasively evaluated by analyzing the QT interval prolongation and its dispersion. The molecular basis of these ECG features are complex (Abriel et al., 2015; Rahm et al., 2018). Briefly, in chronic heart failure the potassium channels (I_{to}, I_{Ks}, I_{Kr} and I_{K1}) are downregulated, sodium channel (I_{Na}) shows a delayed inactivation, finally, calcium handling is deeply altered. Then, chronic heart failure is able to induce a prolonged and inhomogeneous action potential duration both in the time and spatial domain, detectable on ECG as a prolonged and temporal dispersed QT interval. This condition constitutes an optimum "pabulum" for reentry arrhythmias. Several experimental and clinical studies, mostly by our research group reported that the sympathetic stimulation was able to exacerbate the QT temporal dispersion in different clinical setting all characterized by myocardial structural abnormalities (Piccirillo et al., 2009a, 2012, 2013, 2014a; Baumert et al., 2016). However, up to now, specific data in elderly patients with AS were not present. Originally we now supplied data with respect a worsening of all markers of myocardial temporal dispersion of repolarization phases during a mild mental stress. In sush a context, between several conventional manually measurements of myocardial repolarization, only Te and Te_{Bazett} were increased during mental stress. Obviously, the temporal dispersion markers were more sensitive to detect the sympathetic-dependent changes, probably because they were obtained on a longer period (256 cycles) in comparison with the manual measurement (3 cycles). These two ECG parameters followed the trend of all short period markers of QT most likely because the Te interval represents the QT interval subsegment more susceptible to the sympathetic variations (Shimizu and Antzelevitch, 2000; Shimizu et al., 2003; Piccirillo et al., 2012, 2013, 2014a). Indeed, in this last part of repolarization phase, I_{Ks} is capable to modulate the QT duration to RR cycle length and, in chronic heart failure, these channels are downregulated. Thus, a mental stress could be sufficient to trigger this alteration also with conventional QT measurement (Aro et al., 2017; Tse et al., 2017; Piccirillo et al., 2018; Yu et al., 2018).

Autonomic cardiovascular regulation is deeply involved in the pathophysiology of the AS, too. The sympathetic drive's increase and the vagal control alterations are typical of all

different stages of this syndrome, together with the baroreflex sensitivity depression. Therefore, RR power spectral analysis shows different spectral pattern according the class impairment and the related therapy. In the first two NYHA classes, the LF spectral component tend to increase (Guzzetti et al., 1995; Yaniv et al., 2014) whereas the most advanced stages are usually associated to a reduction of LF spectral power (Mortara et al., 1994; Guzzetti et al., 1995; Piccirillo et al., 2006, 2009b; Yaniv et al., 2014). The latter changes are also usually observed as quite physiological aging-related changes (Piccirillo et al., 1995, 1998) our sample with symptomatic AS showed a low short period heart rate variability and, consequently LF, in normalize and absolute power, but the patients were still able to increase LF during mental stress; probably this ability could be impaired in comparison with normal age-matched subjects (Piccirillo et al., 1995, 1998). Therefore, the β-blocker treatment can modify all spectral components and LF in particular (Piccirillo et al., 2000a). Nevertheless, chronic heart failure and aging are capable to reduce contextually the HF spectral component (Pagani et al., 1986; Piccirillo et al., 2004a). Eventually, during mental stress, our patients showed a decrease of baroreflex sensitivity indexes (α-index), this behavior mirroring a sympathetic activation and parasympathetic deactivation (Piccirillo et al., 2001a,b; Pinna et al., 2015).

Temporal Repolarization Variability as Markers of Sudden Cardiac Death

Probably the most dreadful AS complication is sudden cardiac death induced by reentrant ventricular arrhythmias.

CONCLUSION

In elderly with AS, ventricular arrhythmias worsened during a simple cognitive assessment, this events could be a further burden on the outcome of TAVR. Although, the TAVR reduces the morbidity and mortality, in some subjects sudden death's risk remains high. Therefore, it could come in handy to stratify the ventricular malignant arrhythmias risk using a non-invasive, not expensive, repeatable and simple test. In such a context, our data enlightened that QTe_{sd}, obtained at rest on 256 consecutive cycles, shows the best accuracy in identifying those patients with AS more prone to develop ventricular arrhythmias. Obviously, in the present study we evaluated the predictive repolarization markers in stratifying the increase of number and complexity of ventricular arrhythmias as a surrogate of major arrhythmic risk (i.e., sudden cardiac death). Then we could reasonably hypothesize that these two markers of electrical ventricular instability could represent the first point of reference waiting more specific data. However, it is reasonable to suggest a more aggressive antiarrhythmic therapy in those patients with AS candidates to TAVR procedures and high QTe_{sd} value at rest.

DATA AVAILABILITY

The datasets analyzed in this manuscript are not publicly available. Requests to access the datasets should be directed to gianfranco.piccirillo@uniroma1.it.

ETHICS STATEMENT

This study was approved by the Ethical Committee of Azienda Universitaria Policlinico Umberto I. Each patient signed an appropriate informed consent. Trial was registered on ClinicalTrial.gov database with number NCT03145376.

AUTHOR CONTRIBUTIONS

GP: conceptualization, data curation, formal analysis, and writing. FeM: writing – review and editing. MF, CDI, FaM, TS, DC, MM, NS, and GV: investigation, methodology, and data curation. IP: data curation. DM: supervision, validation, visualization, review, and editing.

FUNDING

This study was funded by the University "La Sapienza" research funding 2017.

REFERENCES

Abriel, H., Rougier, J. S., and Jalife, J. (2015). Ion channel macromolecular complexes in cardiomyocytes: roles in sudden cardiac death. *Circ. Res.* 116, 1971–1988. doi: 10.1161/CIRCRESAHA.116.305017

Afilalo, J., Lauck, S., Kim, D. H., Lefèvre, T., Piazza, N., Lachapelle, K., et al. (2017). Frailty in older adults undergoing aortic valve replacement: the FRAILTY-AVR study. *J. Am. Coll. Cardiol.* 70, 689–700. doi: 10.1016/j.jacc.2017.06.024

Agarwal, S. K., Chao, J., Peace, F., Judd, S. E., Kissela, B., Kleindorfer, D., et al. (2015). Premature ventricular complexes on screening electrocardiogram and risk of ischemic stroke. *Stroke* 46, 1365–1367. doi: 10.1161/strokeaha.114.008447

Aro, A. L., Reinier, K., Rusinaru, C., Uy-Evanado, A., Darouian, N., Phan, D., et al. (2017). Electrical risk score beyond the left ventricular ejection fraction: prediction of sudden cardiac death in the oregon sudden unexpected death study and the atherosclerosis risk in communities study. *Eur. Heart J.* 38, 3017–3025. doi: 10.1093/eurheartj/ehx331

Ataklte, F., Erqou, S., Laukkanen, J., and Kaptoge, S. (2013). Meta-analysis of ventricular premature complexes and their relation to cardiac mortality in general populations. *Am. J. Cardiol.* 112, 1263–1270. doi: 10.1016/j.amjcard.2013.05.065

Baumert, M., Porta, A., Vos, M. A., Malik, M., Couderc, J. P., Laguna, P., et al. (2016). QT interval variability in body surface ECG: measurement, physiological basis, and clinical value: position statement and consensus guidance endorsed by the European Heart Rhythm Association jointly with the ESC working group on cardiac cellular electrophysiology. *Europace* 18, 925–944. doi: 10.1093/europace/euv405

Berger, R. D., Kasper, E. K., Baughman, K. L., Marban, E., Calkins, H., and Tomaselli, G. F. (1997). Beat-to-beat QT interval variability: novel evidence for repolarization lability in ischemic and nonischemic dilated cardiomyopathy. *Circulation* 96, 1557–1565. doi: 10.1161/01.cir.96.5.1557

Cannon, W. B. (2002). "Voodoo" death. American anthropologist, 1942;44(new series):169-181. *Am. J. Public Health* 92, 1593–1596; discussion 1594–1595.

Cheriyath, P., He, F., Peters, I., Li, X., Alagona, P. Jr., Wu, C., et al. (2011). Relation of atrial and/or ventricular premature complexes on a two-minute rhythm strip to the risk of sudden cardiac death (the Atherosclerosis Risk in Communities [ARIC] study). *Am. J. Cardiol.* 107, 151–155. doi: 10.1016/j.amjcard.2010.09.002

Crow, R. S., Hannan, P. J., and Folsom, A. R. (2003). Prognostic significance of corrected QT and corrected JT interval for incident coronary heart disease in a general population sample stratified by presence or absence of wide QRS complex: the ARIC Study with 13 years of follow-up. *Circulation* 108, 1985–1989. doi: 10.1161/01.cir.0000095027.28753.9d

Folstein, M. F., Folstein, S. E., and McHugh, P. R. (1975). "Mini-mental state". A practical method for grading the cognitive state of patients for the clinician. *Psychiatr. Res.* 12, 189–198.

Guzzetti, S., Cogliati, C., Turiel, M., Crema, C., Lombardi, F., and Malliani, A. (1995). Sympathetic predominance followed by functional denervation in the progression of chronic heart failure. *Eur. Heart J.* 16, 1100–1107. doi: 10.1093/oxfordjournals.eurheartj.a061053

Kario, K., Matsuo, T., Kobayashi, H., Yamamoto, K., and Shimada, K. (1997). Earthquake-induced potentiation of acute risk factors in hypertensive elderly patients: possible triggering of cardiovascular events after a major earthquake. *J. Am. Coll. Cardiol.* 29, 926–933. doi: 10.1016/s0735-1097(97)00002-8

Kitamura, T., Kiyohara, K., and Iwami, T. (2013). The great east Japan earthquake and out-of-hospital cardiac arrest. *N. Engl. J. Med.* 369, 2165–2167.

Kiyohara, K., Kitamura, T., Iwami, T., Nishiyama, C., and Kawamura, T. (2015). Impact of the Great East Japan earthquake on out-of-hospital cardiac arrest with cardiac origin in non-disaster areas [corrected]. *J. Epidemiol. Commun. Health* 69, 185–188. doi: 10.1136/jech-2014-204380

Lampert, R., Joska, T., Burg, M. M., Batsford, W. P., McPherson, C. A., and Jain, D. (2002). Emotional and physical precipitants of ventricular arrhythmia. *Circulation* 106, 1800–1805. doi: 10.1161/01.cir.0000031733.51374.c1

Leor, J., Poole, W. K., and Kloner, R. A. (1996). Sudden cardiac death triggered by an earthquake. *N. Engl. J. Med.* 334, 413–419. doi: 10.1056/nejm199602153340701

Lindman, B. R., Alexander, K. P., O'Gara, P. T., and Afilalo, J. (2014). Futility, benefit, and transcatheter aortic valve replacement. *JACC Cardiovasc. Interv.* 7, 707–716. doi: 10.1016/j.jcin.2014.01.167

Massing, M. W., Simpson, R. J. Jr., Rautaharju, P. M., Schreiner, P. J., Crow, R., and Heiss, G. (2006). Usefulness of ventricular premature complexes to predict coronary heart disease events and mortality (from the atherosclerosis risk in communities cohort). *Am. J. Cardiol.* 98, 1609–1612. doi: 10.1016/j.amjcard.2006.06.061

Meisel, S. R., Kutz, I., Dayan, K. I., Pauzner, H., Chetboun, I., Arbel, Y., et al. (1991). Effect of Iraqi missile war on incidence of acute myocardial infarction and sudden death in Israeli civilians. *Lancet* 338, 660–661. doi: 10.1016/0140-6736(91)91234-l

Minamino-Muta, E., Kato, T., Morimoto, T., Taniguchi, T., Shiomi, H., Nakatsuma, K., et al. (2017). Causes of death in patients with severe aortic stenosis: an observational study. *Sci. Rep.* 7:14723. doi: 10.1038/s41598-017-15316-6

Mortara, A., La Rovere, M. T., Signorini, M. G., Pantaleo, P., Pinna, G., Martinelli, L., et al. (1994). Can power spectral analysis of heart rate variability identify a high risk subgroup of congestive heart failure patients with excessive sympathetic activation? A pilot study before and after heart transplantation. *Br. Heart J.* 71, 422–430. doi: 10.1136/hrt.71.5.422

Osnabrugge, R. L., Mylotte, D., Head, S. J., Van Mieghem, N. M., Nkomo, V. T., LeReun, C. M., et al. (2013). Aortic stenosis in the elderly: disease prevalence and number of candidates for transcatheter aortic valve replacement: a meta-analysis and modeling study. *J. Am. Coll. Cardiol.* 62, 1002–1012. doi: 10.1016/j.jacc.2013.05.015

Otto, C. M., Kumbhani, D. J., Alexander, K. P., Calhoon, J. H., Desai, M. Y., Kaul, S., et al. (2017). ACC expert consensus decision pathway for transcatheter aortic valve replacement in the management of adults with aortic stenosis: a report of the american college of cardiology task force on clinical expert consensus documents. *J. Am. Coll. Cardiol.* 69, 1313–1346. doi: 10.1016/j.jacc.2016.12.006

Pagani, M., Lombardi, F., Guzzetti, S., Rimoldi, O., Furlan, R., Pizzinelli, P., et al. (1986). Power spectral analysis of heart rate and arterial pressure variabilities as a marker of sympatho-vagal interaction in man and conscious dog. *Circ. Res.* 59, 178–193. doi: 10.1161/01.res.59.2.178

Pagani, M., Somers, V., Furlan, R., Dell'Orto, S., Conway, J., Baselli, G., et al. (1988). Changes in autonomic regulation induced by physical training in mild hypertension. *Hypertension* 12, 600–610. doi: 10.1161/01.hyp.12.6.600

Phillips, D. P., Jarvinen, J. R., Abramson, I. S., and Phillips, R. R. (2004). Cardiac mortality is higher around Christmas and New Year's than at any other time: the holidays as a risk factor for death. *Circulation* 110, 3781–3788. doi: 10.1161/01.cir.0000151424.02045.f7

Piccirillo, G., Bucca, C., Bauco, C., Cinti, A. M., Michele, D., Fimognari, F. L., et al. (1998). Power spectral analysis of heart rate in subjects over a hundred years old. *Int. J. Cardiol.* 63, 53–61. doi: 10.1016/s0167-5273(97)00282-9

Piccirillo, G., Cacciafesta, M., Viola, E., Santagada, E., Nocco, M., Lionetti, M., et al. (2001a). Influence of aging on cardiac baroreflex sensitivity determined non-invasively by power spectral analysis. *Clin. Sci.* 100, 267–274. doi: 10.1042/cs1000267

Piccirillo, G., Di Giuseppe, V., Nocco, M., Lionetti, M., Moisè, A., Naso, C., et al. (2001b). Influence of aging and other cardiovascular risk factors on baroreflex sensitivity. *J. Am. Geriatr. Soc.* 49, 1059–1065. doi: 10.1046/j.1532-5415.2001.49209.x

Piccirillo, G., Fimognari, F. L., Viola, E., and Marigliano, V. (1995). Age-adjusted normal confidence intervals for heart rate variability in healthy subjects during head-up tilt. *Int. J. Cardiol.* 50, 117–124. doi: 10.1016/0167-5273(95)93680-q

Piccirillo, G., Luparini, R. L., Celli, V., Moisè, A., Lionetti, M., Marigliano, V., et al. (2000a). Effects of carvedilol on heart rate and blood pressure variability in subjects with chronic heart failure. *Am. J. Cardiol.* 86, 1392–1395, A6.

Piccirillo, G., Viola, E., Nocco, M., Durante, M., Tarantini, S., and Marigliano, V. (2000b). Autonomic modulation of heart rate and blood pressure in normotensive offspring of hypertensive subjects. *J. Lab. Clin. Med.* 135, 145–152. doi: 10.1067/mlc.2000.103428

Piccirillo, G., Magrì, D., di Carlo, S., De Laurentis, T., Torrini, A., Matera, S., et al. (2006). Influence of cardiac-resynchronization therapy on heart rate and blood pressure variability: 1-year follow-up. *Eur. J. Heart Fail.* 8, 716–722. doi: 10.1016/j.ejheart.2006.01.008

Piccirillo, G., Magrì, D., Naso, C., di Carlo, S., MoisE, A., De Laurentis, T., et al. (2004a). Factors influencing heart rate variability power spectral analysis during controlled breathing in patients with chronic heart failure or hypertension and in healthy normotensive subjects. *Clin. Sci.* 107, 183–190. doi: 10.1042/cs20030401

Piccirillo, G., Naso, C., Moisè, A., Lionetti, M., Nocco, M., Di Carlo, S., et al. (2004b). Heart rate and blood pressure variability in subjects with vasovagal syncope. *Clin. Sci.* 107, 55–61. doi: 10.1042/cs20030327

Piccirillo, G., Magrì, D., Ogawa, M., Song, J., Chong, V. J., Han, S., et al. (2009a). Autonomic nervous system activity measured directly and QT interval variability in normal and pacing-induced tachycardia heart failure dogs. *J. Am. Coll. Cardiol.* 54, 840–850. doi: 10.1016/j.jacc.2009.06.008

Piccirillo, G., Ogawa, M., Song, J., Chong, V. J., Joung, B., Han, S., et al. (2009b). Power spectral analysis of heart rate variability and autonomic nervous system activity measured directly in healthy dogs and dogs with tachycardia-induced heart failure. *Heart Rhythm.* 6, 546–552. doi: 10.1016/j.hrthm.2009.01.006

Piccirillo, G., Magrì, D., Pappadà, M. A., Maruotti, A., Ogawa, M., Han, S., et al. (2012). Autonomic nerve activity and the short-term variability of the Tpeak-Tend interval in dogs with pacing-induced heart failure. *Heart Rhythm.* 9, 2044–2050. doi: 10.1016/j.hrthm.2012.08.030

Piccirillo, G., Moscucci, F., D'Alessandro, G., Pascucci, M., Rossi, P., Han, S., et al. (2014a). Myocardial repolarization dispersion and autonomic nerve activity in a canine experimental acute myocardial infarction model. *Heart Rhythm.* 11, 110–118. doi: 10.1016/j.hrthm.2013.10.022

Piccirillo, G., Moscucci, F., Persi, A., Di Barba, D., Pappadà, M. A., Rossi, P., et al. (2014b). Intra-QT spectral coherence as a possible noninvasive marker of sustained ventricular tachycardia. *Biomed. Res. Int.* 2014:583035. doi: 10.1155/2014/583035

Piccirillo, G., Moscucci, F., Mastropietri, F., Di Iorio, C., Mariani, M. V., Fabietti, M., et al. (2018). Possible predictive role of electrical risk score on transcatheter aortic valve replacement outcomes in older patients: preliminary data. *Clin. Interv. Aging* 13, 1657–1667. doi: 10.2147/CIA.S170226

Piccirillo, G., Ottaviani, C., Fiorucci, C., Petrocchi, N., Moscucci, F., Di Iorio, C., et al. (2016). Transcranial direct current stimulation improves the QT

variability index and autonomic cardiac control in healthy subjects older than 60 years. *Clin. Interv. Aging* 11, 1687–1695. doi: 10.2147/cia.s116194

Piccirillo, G., Rossi, P., Mitra, M., Quaglione, R., Dell'Armi, A., Di Barba, D., et al. (2013). Indexes of temporal myocardial repolarization dispersion and sudden cardiac death in heart failure: any difference? *Ann. Noninvasive Electrocardiol.* 18, 130–139. doi: 10.1111/anec.12005

Pinna, G. D., Maestri, R., and La Rovere, M. T. (2015). Assessment of baroreflex sensitivity from spontaneous oscillations of blood pressure and heart rate: proven clinical value? *Physiol. Meas.* 36, 741–753. doi: 10.1088/0967-3334/36/4/741

Rahm, A. K., Lugenbiel, P., Schweizer, P. A., Katus, H. A., and Thomas, D. (2018). Role of ion channels in heart failure and channelopathies. *Biophys. Rev.* 10, 1097–1106. doi: 10.1007/s12551-018-0442-3

Rautaharju, P. M., Surawicz, B., Gettes, L. S., Bailey, J. J., Childers, R., Deal, B. J., et al. (2009). AHA/ACCF/HRS recommendations for the standardization and interpretation of the electrocardiogram: part IV: the ST segment, T and U waves, and the QT interval: a scientific statement from the American Heart Association Electrocardiography and Arrhythmias Committee, Council on Clinical Cardiology; the American College of Cardiology Foundation; and the Heart Rhythm Society. Endorsed by the International Society for Computerized Electrocardiology. *J. Am. Coll. Cardiol.* 53, 982–991. doi: 10.1016/j.jacc.2008.12.014

Rautaharju, P. M., Zhang, Z. M., Prineas, R., and Heiss, G. (2004). Assessment of prolonged QT and JT intervals in ventricular conduction defects. *Am. J. Cardiol.* 93, 1017–1021. doi: 10.1016/j.amjcard.2003.12.055

Robbe, H. W., Mulder, L. J., Rüddel, H., Langewitz, W. A., Veldman, J. B., and Mulder, G. (1987). Assessment of baroreceptor reflex sensitivity by means of spectral analysis. *Hypertension* 10, 538–543. doi: 10.1161/01.hyp.10.5.538

Rockwood, K., Song, X., MacKnight, C., Bergman, H., Hogan, D. B., McDowell, I., et al. (2005). A global clinical measure of fitness and frailty in elderly people. *CMAJ* 173, 489–495. doi: 10.1503/cmaj.050051

Shimizu, W., and Antzelevitch, C. (2000). Differential effects of beta-adrenergic agonists and antagonists in LQT1, LQT2 and LQT3 models of the long QT syndrome. *J. Am. Coll. Cardiol.* 35, 778–786. doi: 10.1016/s0735-1097(99)00582-3

Shimizu, W., Noda, T., Takaki, H., Kurita, T., Nagaya, N., Satomi, K., et al. (2003). Epinephrine unmasks latent mutation carriers with LQT1 form of congenital long-QT syndrome. *J. Am. Coll. Cardiol.* 41, 633–642. doi: 10.1016/s0735-1097(02)02850-4

Steinberg, J. S., Arshad, A., Kowalski, M., Kukar, A., Suma, V., Vloka, M., et al. (2004). Increased incidence of life-threatening ventricular arrhythmias in implantable defibrillator patients after the World Trade Center attack. *J. Am. Coll. Cardiol.* 44, 1261–1264. doi: 10.1016/j.jacc.2004.06.032

Task Force of the European Society of Cardiology, and the North American Society of Pacing, and Electrophysiology (1996). Heart rate variability Standards of measurement, physiological interpretation, and clinical use. *Eur. Heart J.* 17, 354–381. doi: 10.1093/oxfordjournals.eurheartj.a014868

Trichopoulos, D., Katsouyanni, K., Zavitsanos, X., Tzonou, A., and Dalla-Vorgia, P. (1981). Psychological stress and fatal heart attack: the Athens earthquake natural experiment. *Lancet* 1, 441–444. doi: 10.1016/s0140-6736(83)91439-3

Tse, G., Gong, M., Wong, W. T., Georgopoulos, S., Letsas, K. P., Vassiliou, V. S., et al. (2017). The Tpeak - Tend interval as an electrocardiographic risk marker of arrhythmic and mortality outcomes: a systematic review and meta-analysis. *Heart Rhythm.* 14, 1131–1137. doi: 10.1016/j.hrthm.2017.05.031

Wilbert-Lampen, U., Leistner, D., Greven, S., Pohl, T., Sper, S., Völker, C., et al. (2008). Cardiovascular events during World Cup soccer. *N. Engl. J. Med.* 358, 475–483. doi: 10.1056/NEJMoa0707427

Williams, B. R., Zhang, Y., Sawyer, P., Mujib, M., Jones, L. G., Feller, M. A., et al. (2011). Intrinsic association of widowhood with mortality in community-dwelling older women and men: findings from a prospective propensity-matched population study. *J. Gerontol. A Biol. Sci. Med. Sci.* 66, 1360–1368. doi: 10.1093/gerona/glr144

Yaniv, Y., Lyashkov, A. E., and Lakatta, E. G. (2014). Impaired signaling intrinsic to sinoatrial node pacemaker cells affects heart rate variability during cardiac disease. *J. Clin. Trials* 4:152.

Yu, Z., Chen, Z., Wu, Y., Chen, R., Li, M., Chen, X., et al. (2018). Electrocardiographic parameters effectively predict ventricular tachycardia/fibrillation in acute phase and abnormal cardiac function in chronic phase of ST-segment elevation myocardial infarction. *J. Cardiovasc. Electrophysiol.* 29, 756–766. doi: 10.1111/jce.13453

Zanobetti, A., Coull, B. A., Kloog, I., Sparrow, D., Vokonas, P. S., Gold, D. R., et al. (2017). Fine-scale spatial and temporal variation in temperature and arrhythmia episodes in the VA Normative aging study. *J. Air Waste Manag. Assoc.* 67, 96–104. doi: 10.1080/10962247.2016.1252808

Conflict of Interest Statement: The authors declare that the research was conducted in the absence of any commercial or financial relationships that could be construed as a potential conflict of interest.

frontiers in Physiology

ORIGINAL RESEARCH
published: 23 August 2019
doi: 10.3389/fphys.2019.01095

Pro-Arrhythmic Ventricular Remodeling Is Associated With Increased Respiratory and Low-Frequency Oscillations of Monophasic Action Potential Duration in the Chronic Atrioventricular Block Dog Model

David Jaap Sprenkeler, Jet D. M. Beekman, Alexandre Bossu, Albert Dunnink and Marc A. Vos*

Department of Medical Physiology, Division of Heart and Lungs, University Medical Center Utrecht, Utrecht, Netherlands

OPEN ACCESS

Edited by:
Peter Taggart, University College London, United Kingdom

Reviewed by:
Daniel M. Johnson, University of Birmingham, United Kingdom
Gudrun Antoons, Maastricht University, Netherlands

***Correspondence:**
David Jaap Sprenkeler
d.j.sprenkeler@umcutrecht.nl

Specialty section:
This article was submitted to Cardiac Electrophysiology, a section of the journal Frontiers in Physiology

Received: *04 June 2019*
Accepted: *08 August 2019*
Published: *23 August 2019*

Citation:
Sprenkeler DJ, Beekman JDM, Bossu A, Dunnink A and Vos MA (2019) Pro-Arrhythmic Ventricular Remodeling Is Associated With Increased Respiratory and Low-Frequency Oscillations of Monophasic Action Potential Duration in the Chronic Atrioventricular Block Dog Model. Front. Physiol. 10:1095. doi: 10.3389/fphys.2019.01095

In addition to beat-to-beat fluctuations, action potential duration (APD) oscillates at (1) a respiratory frequency and (2) a low frequency (LF) (<0.1 Hz), probably caused by bursts of sympathetic nervous system discharge. This study investigates whether ventricular remodeling in the chronic AV block (CAVB) dog alters these oscillations of APD and whether this has consequences for arrhythmogenesis. We performed a retrospective analysis of 39 dog experiments in sinus rhythm (SR), acute AV block (AAVB), and after 2 weeks of chronic AV block. Spectral analysis of left ventricular monophasic action potential duration (LV MAPD) was done to quantify respiratory frequency (RF) power and LF power. Dofetilide (0.025 mg/kg in 5 min) was infused to test for inducibility of Torsade de Pointes (TdP) arrhythmias. RF power was significantly increased at CAVB compared to AAVB and SR (log[RF] of −1.13 ± 1.62 at CAVB vs. log[RF] of −2.82 ± 1.24 and −3.29 ± 1.29 at SR and AAVB, respectively, $p < 0.001$). LF power was already significantly increased at AAVB and increased even further at CAVB (−3.91 ± 0.70 at SR vs. −2.52 ± 0.85 at AAVB and −1.14 ± 1.62 at CAVB, $p < 0.001$). In addition, LF power was significantly larger in inducible CAVB dogs (log[LF] −0.6 ± 1.54 in inducible dogs vs. −2.56 ± 0.43 in non-inducible dogs, $p < 0.001$). In conclusion, ventricular remodeling in the CAVB dog results in augmentation of respiratory and low-frequency (LF) oscillations of LV MAPD. Furthermore, TdP-inducible CAVB dogs show increased LF power.

Keywords: chronic AV block dog, electrical remodeling, respiration, action potential duration, low-frequency oscillations

INTRODUCTION

Repolarization lability, quantified as beat-to-beat fluctuations in action potential duration (APD), is known to contribute to arrhythmogenesis (Thomsen et al., 2004, 2007). An increased beat-to-beat repolarization variability has been found in patients with a high risk of ventricular arrhythmias, such as patients with heart failure (Berger et al., 1997; Hinterseer et al., 2010),

ischemia (Murabayashi et al., 2002), long QT-syndrome (Hinterseer et al., 2008, 2009), hypertrophic cardiomyopathy (Atiga et al., 2000), or hypertension with left ventricular hypertrophy (Piccirillo et al., 2002). In these patients, adverse cardiac remodeling has led to heterogeneous downregulation of repolarizing ionic currents and a disruption of normal Ca^{2+} handling (Armoundas et al., 2001). As a result, the so called "repolarization reserve" is reduced, making the process of repolarization unstable and prone to arrhythmogenic challenges (Roden, 1998).

In addition to beat-to-beat variations in repolarization, the APD also oscillates at a broader range of frequencies. First, APD fluctuates with respiration, which appears to be independent of the respiratory effects on heart rate (Hanson et al., 2012). Second, APD oscillates at a LF of around 0.1 Hz, which has been attributed to LF bursts of sympathetic nerve terminals on the ventricular myocardium (Hanson et al., 2014). While a sympathetically mediated LF pattern of arterial blood pressure (known as Mayer waves) is well-known (Malpas, 2002), oscillations at 0.1 Hz have only recently been found in APD as well (Hanson et al., 2014; Porter et al., 2018). Moreover, these fluctuations have also been identified on the surface ECG as changes in T wave vector angle between consecutive beats, referred to as "periodic repolarization dynamics" (PRD; Rizas et al., 2014).

However, it is unknown whether APD oscillations at these frequency bands (i.e., respiratory and LF) reflect normal physiology or whether they are linked to the occurrence of ventricular arrhythmias. In this regard, a computational modeling study showed that during Ca^{2+} overload and reduction of repolarizing currents, APD oscillations could become arrhythmogenic and elicit afterdepolarizations (Pueyo et al., 2016). Furthermore, in clinical studies of post-myocardial infarction patients, PRD appears to be a strong independent predictor of all-cause mortality (Hamm et al., 2017; Rizas et al., 2017). Therefore, we could hypothesize that these oscillations are altered by ventricular remodeling, thereby further destabilizing repolarization and contributing to arrhythmogenesis.

In the present study, we evaluated both respiratory and low-frequency (LF) oscillations of APD in the chronic complete AV block dog model. In this arrhythmogenic animal model, creation of complete AV block results in cardiac remodeling and reduction of repolarization reserve. Administration of anesthesia and a pro-arrhythmic drug, i.e., the I_{Kr} blocker dofetilide, will act as the final "hit" on repolarization, resulting in electrical storm with multiple episodes of Torsades de Pointes arrhythmias (TdP) in approximately 75% of the dogs (Oros et al., 2008). This model has been widely used in our laboratory and by others to investigate the mechanisms of arrhythmogenesis in the remodeled heart (Thomsen et al., 2007; Zhou et al., 2008; Oosterhoff et al., 2010; Dunnink et al., 2012). Therefore, we could use this model to investigate whether ventricular remodeling alters respiratory and LF oscillations of APD.

The current study is a retrospective analysis of previously performed experiments in which we analyzed respiratory and LF oscillations under different conditions of remodeling, i.e., during sinus rhythm (SR), acutely after creation of AV block (AAVB) and after (at least 2 weeks) of remodeling at chronic AV block (CAVB). In addition, we compared inducible with non-inducible CAVB dogs, to evaluate the relevance of these oscillations for arrhythmogenesis.

MATERIALS AND METHODS

Animal handling was in accordance with the "Directive 2010/63/EU of the European Parliament and of the Council of 22 September 2010 on the protection of animals used for scientific purposes" and the Dutch law, laid down in the Experiments on Animals Act. All experiments were performed with approval of the Central Authority for Scientific Procedures on Animals (CCD).

We did a retrospective analysis on electrophysiological data in our database of dog experiments executed between 2014 and 2017, which were done to study the mechanisms of TdP arrhythmias or to test new anti-arrhythmic agents or interventions. In order to maintain a homogenous population, only dogs remodeled on their own idioventricular rhythm (IVR) were included, thereby excluding dogs that were chronically paced from the right ventricular apex (RVA), which has shown to influence the remodeling process. Furthermore, only baseline recordings before the administration of any anti-arrhythmic drugs were used for the analysis to exclude the effect of these interventions on the oscillatory pattern of APD. In addition, we excluded experiments that had a baseline recording shorter than 5 min or recordings that had too much ectopy or noise (approximately more than 10% of the recording).

Animal Experiments

Detailed description of the experimental set-up has been reported previously (Dunnink et al., 2010, 2012). In brief, all experiments were performed under general anesthesia with induction *via* pentobarbital sodium 25 mg/kg i.v. and maintained by isoflurane 1.5% in O_2 and N_2O, 1:2. Animals were ventilated with positive pressure ventilation at a rate of 12 breaths/min. Next, monophasic action potential catheters (Hugo Sachs Elektronik, March, Germany) were introduced *via* the femoral artery and vein into the heart to measure the left ventricular and right ventricular monophasic action potential duration (LV and RV MAPD). In the initial experiment, complete atrioventricular (AV) block was created by radiofrequency ablation of the proximal His bundle. Subsequently, the dogs remodeled for at least 2 up to 5 weeks on IVR.

In all experiments, after a baseline measurement of at least 5 min, inducibility of TdP arrhythmias was tested by infusing the I_{Kr} blocker dofetilide (0.025 mg/kg in 5 min or before the first TdP). TdP was defined as a run of five or more short-coupled (occurring before the end of the T wave) ectopic beats, with polymorphic twisting of the QRS-axis. When ≥3 TdP arrhythmias occurred in the first 10 min after the start of infusion, the dog was considered inducible. During baseline and dofetilide challenge, all subjects were paced from the RV-apex at 60 beats per minute.

Data Analysis

For this retrospective analysis, we used LV MAPD recordings at SR, AAVB, and CAVB conditions. The monophasic action potential was recorded with EP Tracer (Cardiotek, Maastricht,

The Netherlands) at a sampling frequency of 1,000 Hz. LV MAPD was measured offline semi-automatically from the initial peak to 80% of repolarization using custom-made software in MATLAB (MathWorks, Natick, USA). In addition, for analysis of LF oscillations, the absolute difference in LV MAPD between two consecutive beats was calculated. Any extrasystolic beats and the subsequent post-extrasystolic beats were removed. The 5-min time series of MAPD or MAPD difference was detrended and interpolated at 4 Hz *via* cubic spline interpolation to get evenly spaced samples. Data series were split into epochs of 512 samples with 50% overlap. Spectral analysis was performed in MATLAB with Welch's periodogram and a Hanning window to derive the power spectral density (PSD). The power of the frequency bands was calculated by integrating the area under the PSD plot for bandwidths of different frequencies. For the respiratory frequency (RF), we selected a frequency band between 0.19 and 0.21 Hz, since all dogs were ventilated at 12 breaths per minute (every 5 s, 0.2 Hz). For the LF oscillations, we used a frequency band between 0.04 and 0.15 Hz as has been used in previous studies (Hanson et al., 2014; Porter et al., 2018), since the frequency of sympathetic bursts can differ between individual subjects.

Measurement of RR-interval and QT-interval was performed in lead II of the surface ECG. QT-interval was corrected for heart rate (QT_c) with the van der Water formula (Van de Water et al., 1989). Short-term variability (STV) of LV MAPD was calculated over 31 consecutive beats using the formula: $STV = \sum |D_{n+1} - D_n| / 30 \times \sqrt{2}$, where D represents LV MAPD.

Statistical Analysis

Numerical values are expressed as mean ± standard deviation (SD). Logarithmic transformation of both RF and LF was used to correct for skewness of the data. Normality of the transformed data was checked with the Shapiro-Wilk test. Group comparison was done with an unpaired Students *t*-test. Group comparison of more than two groups was performed with a one-way analysis of variance (ANOVA) with Tukey's correction for multiple comparisons. p equal to or smaller than 0.05 was considered significant. GraphPad Prism 6 (GraphPad Software, Inc., La Jolla, CA, USA) was used for the statistical analysis.

RESULTS

A total of 39 experiments in 29 adult mongrel dogs (13 males, 16 females, weight 25 ± 2.5 kg) were used for the analysis. We included 10 dogs in SR, 10 dogs in AAVB, and 19 dogs in CAVB (14 inducible, 5 non-inducible). Of three dogs, data of both AAVB and CAVB experiment were used.

Baseline Electrophysiological Parameters

Baseline electrophysiological data at the three conditions (SR, AAVB, and CAVB) are depicted in **Table 1**. As expected, QT-interval increased acutely after the creation of AV block, due to the sudden drop in heart rate. In CAVB, electrical remodeling has occurred as seen by a significant increase in QT, QTc, and LV MAPD. Furthermore, STV is significantly increased, reflecting a reduced repolarization reserve. **Table 2** shows electrophysiological parameters separately for the non-inducible and inducible CAVB dogs. Only STV appears to be higher in the inducible dogs; however, this did not reach statistical significance (p = 0.08).

Respiratory Oscillations

Figure 1 shows an example of the respiratory fluctuations in MAPD of dogs in SR, AAVB, and CAVB in both, time domain and frequency domain. At SR and AAVB, low amplitude respiratory oscillations of LV MAPD were present, while at CAVB, larger oscillations are seen around the respiratory frequency. **Figure 2** displays the quantified logarithmic RF power (log[RF]) of the analyzed dogs. The remodeling process (**Figure 2A**) resulted in augmentation of the variability at the respiratory frequency, as seen by a significant increase in a log[RF] of −2.55 ± 1.48 and −2.99 ± 1.20 at SR and AAVB, respectively, to a log[RF] of −0.82 ± 1.53 ($p < 0.001$) at CAVB. When comparing inducible with non-inducible dogs, no significant difference could be found in RF power (**Figure 2B**).

Low-Frequency Oscillations

Next, we examined LF oscillations in MAPD difference in SR, AAVB, and CAVB. As depicted in **Figure 3A**, already a significant rise in LF power can be seen at AAVB compared to SR, which further increased after 2 weeks of remodeling (log[LF] of −3.91 ± 0.70 at SR, vs. −2.52 ± 0.85 at AAVB, and −1.14 ± 1.62 at CAVB, $p < 0.001$). Finally, we looked for differences of these oscillations between inducible and non-inducible CAVB dogs. A representative example of the MAPD during the 5-min recording of an inducible and a non-inducible dog is shown in **Figure 4A**. A clear oscillation can be observed in the

TABLE 1 | Baseline electrophysiological parameters.

	SR (n = 10)	AAVB (n = 10)	CAVB (n = 19)
RR (ms)	557 ± 32	1,000*	1,000
QT (ms)	267 ± 15	357 ± 19*	407 ± 56§
QTc (ms)	305 ± 15	357 ± 19	407 ± 56§
LV $MAPD_{80}$ (ms)	200 ± 11	243 ± 14*	275 ± 36§
STV LV $MAPD_{80}$ (ms)	0.31 ± 0.06	0.54 ± 0.30	1.20 ± 0.80§

*$p < 0.05$ vs. SR.
§$p < 0.05$ vs. AAVB.

TABLE 2 | Baseline electrophysiological parameters of inducible and non-inducible dogs.

	Inducible (n = 14)	Non-inducible (n = 5)
RR (ms)	1,000	1,000
QT (ms)	414 ± 60	388 ± 43
QTc (ms)	414 ± 60	388 ± 43
LV $MAPD_{80}$ (ms)	283 ± 34	260 ± 34
STV LV $MAPD_{80}$ (ms)	1.39 ± 0.83	0.64 ± 0.40

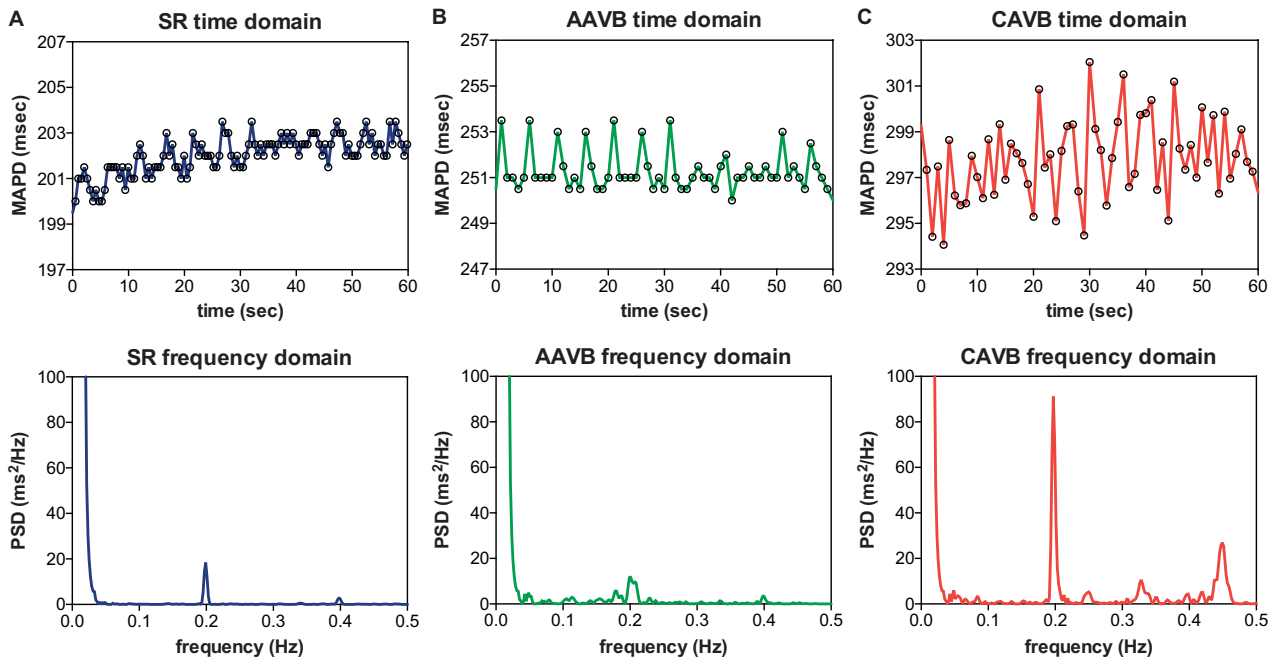

FIGURE 1 | Respiratory frequency oscillations in time and frequency domain. Representative examples of oscillations in monophasic action potential duration (MAPD) in the time domain (top) and frequency domain (bottom) during **(A)** sinus rhythm (SR), **(B)** acutely after creation of AV block (AAVB), and **(C)** after remodeling at chronic AV block (CAVB). A clear increase in a 0.2 Hz oscillation is seen at CAVB.

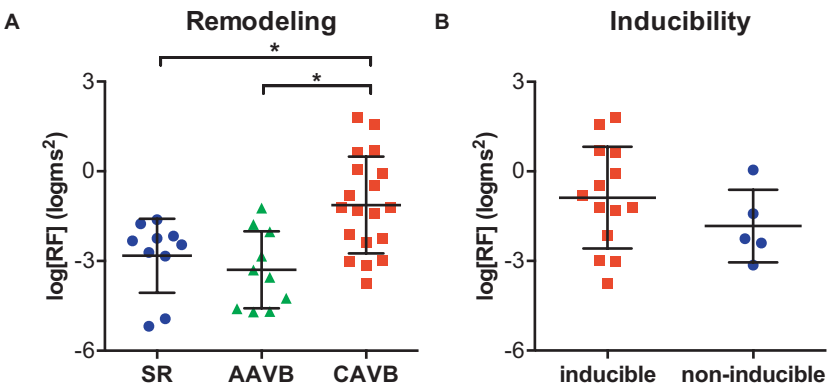

FIGURE 2 | Respiratory oscillations of monophasic action potential duration. **(A)** The logarithmic transformed power of respiratory oscillations of APD (log[RF]) at sinus rhythm (SR), acutely after AV block (AAVB), and at chronic AV block (CAVB). **(B)** log[RF] of the inducible vs. the non-inducible CAVB dogs. *$p < 0.05$.

inducible subject, with a rhythmic fluctuation in MAPD. This oscillatory behavior of MAPD can more clearly be discerned when the difference between consecutive beats is plotted against time (**Figure 4B**): approximately every 10–15 s, a clear increase in the variability between successive beats is seen. When this MAPD variability is visualized in the frequency domain by spectral analysis (**Figure 4C**), a prominent peak appears in the LF band (0.04–0.15 Hz). As depicted in **Figure 3B**, the inducible dogs demonstrated a significant higher LF power of MAPD difference when compared to non-inducible dogs (log[LF] −0.6 ± 1.54 vs. −2.56 ± 0.43, $p < 0.001$).

DISCUSSION

In this retrospective analysis of previously performed animal experiments, we demonstrated that (1) respiratory frequency oscillations of MAPD are increased after electrical remodeling, but they do not differ between inducible and non-inducible dogs and (2) LF oscillations of MAPD difference are already increased at AAVB and rise even further at CAVB. Furthermore, these 0.1 Hz oscillations are more pronounced in CAVB dogs that are susceptible to dofetilide-induced TdP arrhythmias.

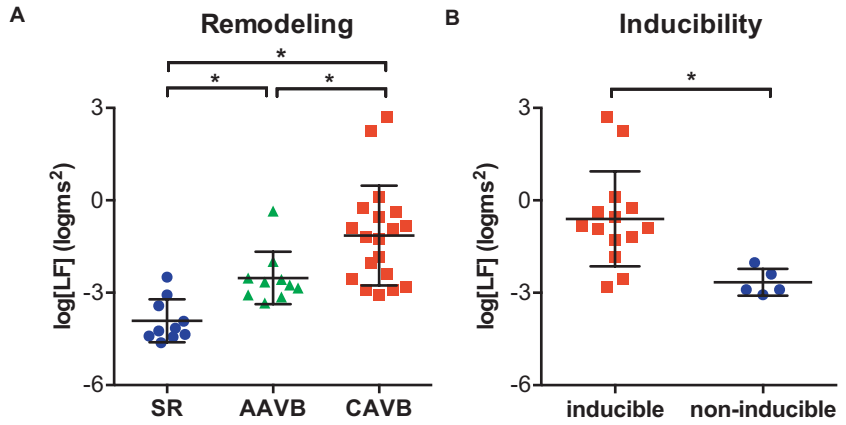

FIGURE 3 | Low-frequency (LF) oscillations of monophasic action potential duration. **(A)** The logarithmic transformed power of LF oscillations of APD (log[LF]) at sinus rhythm (SR), acutely after AV block (AAVB), and at chronic AV block (CAVB). **(B)** log[LF] of the inducible vs. the non-inducible CAVB dogs. *$p < 0.05$.

The Chronic Atrioventricular Block Dog Model to Study the Effects of Electrical Remodeling on Arrhythmogenesis

A variety of structural heart diseases (e.g., myocardial infarction, pressure overload due to hypertension or aortic stenosis, volume overload as seen in valvular regurgitation) can lead to pathological cardiac remodeling, causing downregulation of potassium currents (I_{to}, I_{Ks}, I_{Kr}, and I_{K1}) (Long et al., 2015), enhanced late Na^+-current ($I_{Na\text{-}L}$) (Antzelevitch et al., 2014), and Ca^{2+} handling abnormalities (Sipido et al., 2002). As a result, repolarization reserve is reduced, making the heart prone to repolarization-dependent ventricular arrhythmias. The CAVB dog model, as used in this study, is a model of ventricular remodeling and reduced repolarization reserve that reflects the vulnerable patient at risk for these arrhythmias. In this model, it has been shown that beat-to-beat variability of APD, quantified as STV, is a better marker of reduced repolarization reserve and pro-arrhythmia than APD prolongation itself (Thomsen et al., 2004). STV is significantly increased at CAVB compared to AAVB and dogs susceptible to dofetilide-induced TdP arrhythmias show a further rise in STV prior to occurrence of arrhythmias (Thomsen et al., 2007).

In the current study, we have shown that not only successive beat-to-beat fluctuations of APD exists in the CAVB dog, but also that the APD oscillates at other frequency bands. This is in line with previous studies that have demonstrated important contributions of variation in heart rate (Hnatkova et al., 2013), respiration (Hanson et al., 2012), and autonomic nervous system activity (Baumert et al., 2011) on APD variability. Concerning heart rate, a complex and dynamic APD to heart rate relation exists that is highly individual-specific and contains significant hysteresis effects (Malik et al., 2008). In this study, we have eliminated important heart rate effects on APD by including only dogs that were paced during the experiments. Therefore, we could focus solely on the respiratory and autonomic influences on APD.

Respiratory Oscillations of Action Potential Duration in the Chronic Atrioventricular Block Dog

While heart rate is well-known to fluctuate with respiration, it was recently shown by Hanson et al. that APD, measured as activation recovery interval (ARI) from the intracardiac electrogram, also displays rhythmic fluctuations in synchrony with respiration, even when heart rate was controlled by pacing. The authors suggested multiple mechanisms for the respiratory oscillations of APD. One of these, mechano-electrical feedback, relates to the modulation of electrophysiology by changes in ventricular loading conditions. Both in animal models as in patient studies, a direct effect of altered mechanical load on APD have been found; increased ventricular load resulted in shortening of the APD, while reduction in load was associated with prolongation of the APD (Levine et al., 1988; Zabel et al., 1996). Stretch-activated ion-channels or alterations in Ca^{2+} handling have been suggested as the underlying molecular mechanism of load-dependent APD changes (Eckardt et al., 2001). Stretch-activated ion channels are non-specific cation (Na^+, K^+, and Ca^{2+}) channels that open in respond to changes in stretch instead of voltage (Zeng et al., 2000). In addition, mechanical stretch increases Ca^{2+} release from the sarcoplasmic reticulum, which can alter action potential duration *via* negative feedback on the L-type Ca^{2+}-channel or by exchange of Ca^{2+} for Na^+ *via* the Na^{2+}-Ca^{2+}-exchanger (Iribe et al., 2009). One important physiological mechanism that can alter ventricular loading conditions is the change in intrathoracic pressure difference during respiration. During spontaneous inspiration, intrathoracic pressure drops, causing an increased systemic venous return to the RV, which will shift the interventricular septum into the LV. As a result, left ventricular end-diastolic volume and left ventricular preload will decrease. The opposite will occur during positive pressure ventilation: in that situation, an increase in left ventricular preload will be seen during inspiration (Mitchell et al., 2005). Nevertheless, in either case,

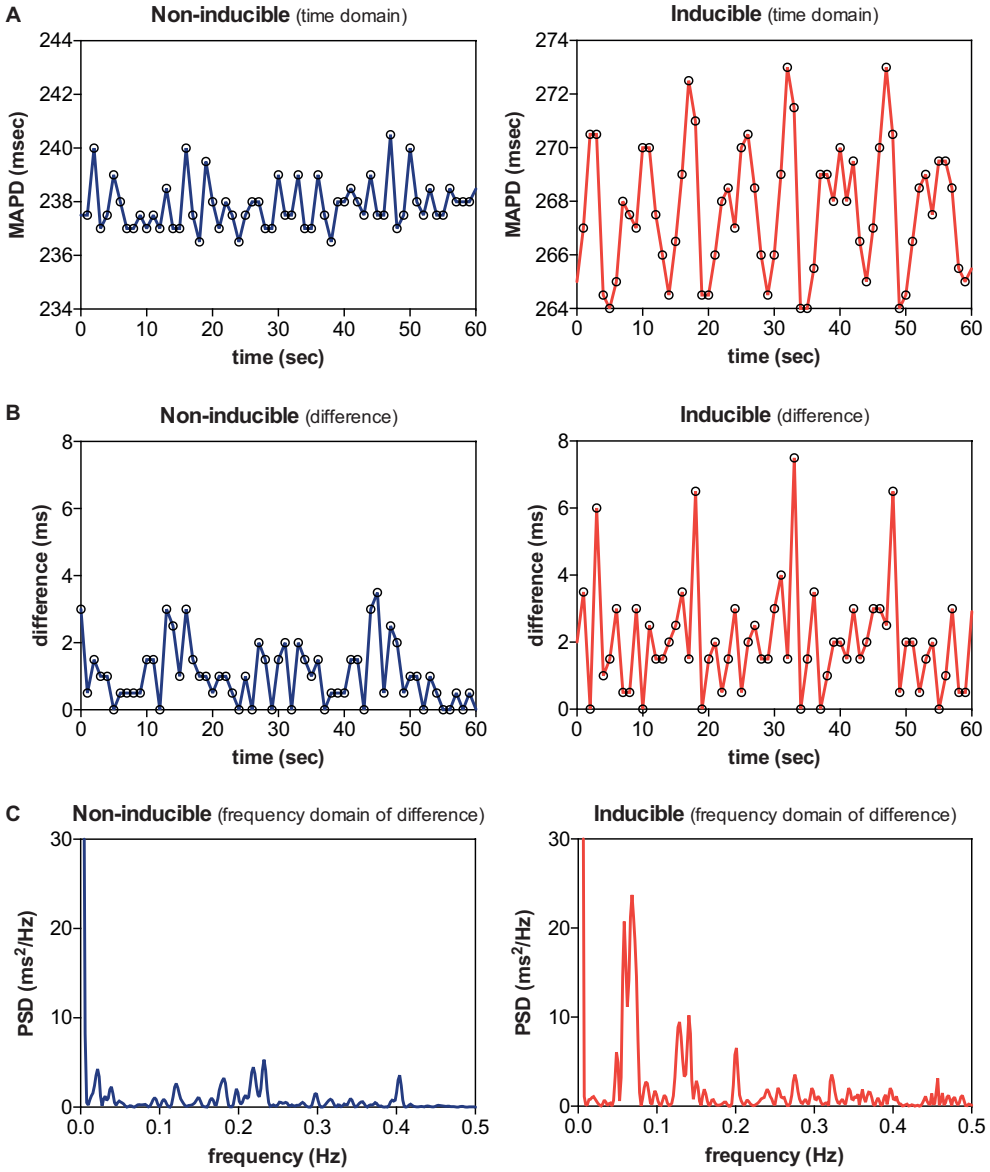

FIGURE 4 | Low-frequency (LF) oscillations in a non-inducible dog vs. an inducible dog. A representative example of MAPD **(A)**, MAPD difference in the time domain **(B)**, and MAPD difference in the frequency domain **(C)** of a non-inducible dog (left) and an inducible dog (right). A clear LF pattern in MAPD difference can be discerned in the inducible dog.

a respiratory oscillatory behavior of ventricular loading is present, which could therefore alter APD in a cyclical pattern.

In the present study, we showed that the modulating effect of respiration on APD is enhanced after cardiac remodeling. A possible explanation could be that alternating changes in ventricular loading have greater impact on repolarization, when repolarization reserve is already reduced. This is consistent with a study by Stams et al. in which the effect of preload changes on beat-to-beat variability of APD was studied in the CAVB dog (Stams et al., 2016). The authors used a pacing protocol with either a constant or alternating PQ interval to artificially control preload conditions. They observed that in AAVB, alternating preload had no effect on APD or STV. In contrast, in CAVB dogs pacing with an alternating PQ interval resulted in APD variability and a significantly higher STV compared to conditions of constant preload. Furthermore, blockade of stretch-activated ion current (I_{SAC}) by streptomycine prevented the increase of $STV_{LV\ MAPD}$ during alternating preload. Although streptomycine is not a selective (I_{SAC})-blocker and has affinity for other ion channels that could affect STV (like L-type Ca^{2+} channels), these results suggest that mechano-electrical feedback *via* specialized stretch-activated ion channels could have profound influence on repolarization during reduced repolarization reserve. This is further supported by a study of Kamkin et al., which showed that isolated cardiomyocytes from hypertrophied ventricles were more sensitive to stretch than

control cardiomyocytes, resulting in prolongation of APD at smaller mechanical stimuli (Kamkin et al., 2000). Thus, we may hypothesize that after remodeling and downregulation of repolarizing K^+-currents, the relative contribution of I_{SAC} to the repolarization process is increased; therefore, we observed an augmentation of APD variability caused by changes in respiration-mediated loading conditions.

Interestingly, we did not find a difference in respiratory oscillations between inducible and non-inducible CAVB dogs. In both groups, electrical remodeling reduced repolarization reserve, as we observed by enhanced respiratory fluctuation of APD. A similar finding was reported by the study of Stams et al.: alternating preload, which led to an increase in APD variability, did not result in more TdP arrhythmias compared to conditions of constant preload. Thus, we could assume that an additional trigger is required to create the optimal environment for dofetilide-induced TdP arrhythmias.

Low-Frequency Oscillations of Action Potential Duration Difference in the Chronic Atrioventricular Block Dog

LF oscillations in the range from 0.04 to 0.15 Hz that are unrelated to respiration have long been observed in both heart rate and arterial blood pressure, and are referred to as Mayer waves (Julien, 2006). These oscillations have been linked to rhythmic bursts of sympathetic nervous system activity; however, the precise mechanism remains controversial. Two theories exist: (1) these oscillations are the effect of a central autonomous oscillator within the central nervous system that fires at a certain frequency and (2) they are the result of a time delay in the baroreflex loop, causing resonance in the feedback system (Malpas, 2002). Either way, states of increased sympathetic activation, such as during tilt test or when blood pressure was artificially lowered, resulted in an increase in the magnitude of Mayer waves (Pagani et al., 1997; Furlan et al., 2000). In addition, blockade of sympathetic drive resulted in a reduction of LF components of both RR interval and blood pressure (Pagani et al., 1997).

In addition to respiratory fluctuations, Hanson et al. also showed that APD displays an oscillatory pattern at Mayer wave frequency (Hanson et al., 2014). Moreover, these LF oscillations increased during autonomic challenge with Valsalva maneuver (Porter et al., 2018). A similar LF oscillatory pattern was found by Rizas et al. in T wave vector changes on the surface-ECG, called periodic repolarization dynamics (PRD; Rizas et al., 2014). These variations in T wave vector could also be increased with exercise and reduced by β-adrenergic blockade, suggesting a role for sympathetic input on the myocardium in the pathogenesis of these oscillations. Furthermore, increased PRD appeared to be a strong predictor of all-cause mortality in a cohort of more than 900 post-MI patients. Combined with a marker of vagal activity (i.e. deceleration capacity), PRD was able to accurately stratify mortality risk in these patients (Hamm et al., 2017). Nevertheless, the cause of death, whether arrhythmic or due to pump failure, was not further specified.

In this regard, the findings of the current study could be of great interest. In this study, we evaluated the effect of ventricular remodeling on LF oscillations, but, more importantly, whether these oscillations were different in dogs susceptible to arrhythmias. For this analysis, the MAPD difference between two consecutive beats was used, instead of MAPD itself. The reason for this is that in the previous study by Rizas et al., PRD was also measured on differences in T wave vector between beats. They observed that approximately every 10 s, the T wave vector changed markedly, while in the intermittent periods T wave vector remained relatively stable. We hypothesized that 0.1 Hz bursts of sympathetic discharge could also result in sudden changes in MAPD, which are more clearly visualized when spectral analysis is done of MAPD difference instead of MAPD.

Consequently, we could show that acutely after creation of AV block, LF power of APD difference is already significantly increased. The sudden drop in cardiac output and blood pressure that occur after creation of AV block will be sensed by baroreceptors in the aortic arch and carotid sinus, which will increase efferent sympathetic input on the heart, while simultaneously reducing parasympathetic firing. We observed this baroreflex-mediated increase in sympathetic tone by augmentation of LF APD oscillations acutely after AV block. More importantly, cardiac remodeling further increased the LF oscillatory behavior of APD difference, predominantly in CAVB dogs susceptible to drug-induced TdP arrhythmias. From the existing literature, it becomes clear that increased sympathetic nervous system activity is an important contributor to repolarization variability and arrhythmogenesis. A study by Johnson et al. in isolated cardiomyocytes showed that the addition of β-adrenergic stimulation to a state of reduced repolarization reserve (by blockade of I_{Ks}) led to a dramatically increase in beat-to-beat variability of repolarization (BVR; Johnson et al., 2010). In addition, sympathetic stimulation promoted Ca^{2+} overload, spontaneous Ca^{2+}-release and the formation of early and delayed afterdepolarizations (EADs/DADs; Johnson et al., 2013). Gallagher et al. found similar results in an *in vivo* canine model of drug-induced LQTS-1. Infusion of HMR1556, an I_{Ks} blocker, in combination with isoproterenol resulted in paradoxically increased APD, increased spatial and temporal dispersion of repolarization and reproducible TdP arrhythmias (Gallacher et al., 2007). The same was found in a study of Ter Bekke et al., who used direct left stellate ganglion stimulation instead of pharmacological adrenergic stimulation, combined with Iks blockade (Ter Bekke et al., 2019). A simulation study by Pueyo et al. evaluated the effect of phasic β-adrenergic stimulation on APD dynamics (Pueyo et al., 2016). They observed a LF oscillatory pattern of APD, whose magnitude increased with higher β-adrenergic strength. Interestingly, simulated pathological conditions of Ca^{2+}-overload and reduced repolarization reserve (comparable to the CAVB dog model) enhanced the APD oscillations caused by adrenergic stimulation. Therefore, the authors suggested an important role of these oscillations in arrhythmogenesis. In the present study, we could confirm these *in silico* results experimentally in an arrhythmogenic *in vivo* model.

The reason for the clear difference in LF oscillations of APD difference between inducible and non-inducible dogs remains speculative. Two mechanisms can be proposed: either repolarization reserve is even more reduced in the inducible dogs, therefore making the effect of β-adrenergic stimulation on repolarization more prominent and repolarization more vulnerable to arrhythmogenic challenges, or sympathetic output itself (either systematically or due to increased local density of sympathetic neurons) is further enhanced in the inducible dogs, causing increased repolarization instability, Ca^{2+} overload, and triggered activity. Concerning the latter, studies in dogs with chronic AV block and MI have shown that in addition to electrical remodeling, also neural remodeling takes place, as seen by denervation, hyperinnervation, and nerve sprouting (Cao et al., 2000a,b). Regional hyperinnervation, where some regions are more densely innervated than others, combined with heterogeneous electrical remodeling, further enhances spatial dispersion of repolarization; thereby, facilitating the initiation and perpetuation of ventricular arrhythmias.

Implications

In addition to beat-to-beat variation in APD or QT-interval, we have shown that fluctuations in other frequency bands are altered in subjects with pro-arrhythmic ventricular remodeling and an increased risk of ventricular arrhythmias. Therefore, these oscillations might eventually be used in risk stratification of patients at high risk of sudden cardiac death, who might benefit from implantation of an implantable cardioverter-defibrillator (ICD). While in the current study, MAP-catheters were used, Hanson et al. showed that respiratory and LF oscillations are also measurable on the ARI of intracardiac EGM, which could be obtained from implantable devices. Furthermore, PRD is a non-invasive parameter that can be measured from a converted 12-lead surface ECG, which would make it more suitable for risk stratification prior to ICD implantation. In this regard, PRD is currently being studied as a predictive marker in the multicentre, observational EU-CERT-ICD study (NCT02064192), which evaluates new risk stratification methods that could identify subgroups of patients with low or high risk of ICD-shocks or mortality.

Study Limitations

Since the CAVB dog is a specific model of ventricular remodeling caused by volume overload, extrapolation of these results to patients with other causes of remodeling (ischemia, infarction, and pressure overload) should be done with caution. Second, an important limitation of the study is its retrospective nature, which made it impossible to control for all, possible confounding, variables. By selecting only dogs remodeled on IVR without control of activation pattern, we tried to keep the analyzed group of dogs as homogeneous as possible. Third, all dogs were mechanically ventilated with positive pressures, which has an opposite effect on loading conditions of the heart compared to spontaneous breathing. Nevertheless, both ventilation techniques result in an oscillatory pattern, albeit with a shift in phase. Next, all experiments were done under general anesthesia, which has profound effects on the autonomic nervous system. In addition, no direct measurements of neural activity were done to confirm that the LF oscillations of APD we found were also caused by sympathetic discharge. Yet, preliminary data of our group shows that stellectomy results in significant reduction in TdP inducibility in the CAVB dog, which implies that, even under anesthetic conditions, the sympathetic nervous system contributes for a great part to arrhythmogenesis in this model [abstract presented at AHA 2017 (van Weperen et al., 2017, unpublished data)]. Finally, it would have been of great interest to measure PRD in the CAVB dog, so we could evaluate if the intracardiac MAP oscillations correlate with PRD on the surface ECG. Unfortunately, PRD measurement requires transformation of the ECG to Frank leads with either Kors or inverse Dower's matrix, which are not validated for the canine ECG. Furthermore, because of the complete AV-block, the T waves are often distorted by the interference of P waves, which impedes accurate measurement of beat-to-beat T wave changes.

CONCLUSION

In the chronic AV block dog model, we observed oscillations of LV MAPD at respiratory frequency, which are augmented after remodeling compared to non-remodeled conditions. In addition, LF oscillations of MAPD difference were already altered acutely after creation of AV block and increased even further at chronic AV block conditions. Furthermore, CAVB dogs, that are susceptible to drug-induced TdP, show increased LF oscillations compared to their non-inducible counterparts.

DATA AVAILABILITY

The datasets generated for this study are available on request to the corresponding author.

ETHICS STATEMENT

The animal study was reviewed and approved by Centrale Commissie Dierproeven (Central Committee of Animal Experiments), The Hague, the Netherlands.

AUTHOR CONTRIBUTIONS

DS contributed in writing, data collection, and analysis. JB contributed in technical support. AB and AD conducted animal experiments. MV helped in supervision and review of manuscript.

FUNDING

This research was performed with support of the EU-CERT-ICD study, which has received funding from the European Community's Seventh Framework Programme FP7/2007-2013 under grant agreement no. 602299.

REFERENCES

Antzelevitch, C., Nesterenko, V., Shryock, J. C., Rajamani, S., Song, Y., and Belardinelli, L. (2014). The role of late I Na in development of cardiac arrhythmias. *Handb. Exp. Pharmacol.* 221, 137–168. doi: 10.1007/978-3-642-41588-3_7

Armoundas, A. A., Wu, R., Juang, G., Marbán, E., and Tomaselli, G. F. (2001). Electrical and structural remodeling of the failing ventricle. *Pharmacol. Ther.* 92, 213–230. doi: 10.1016/S0163-7258(01)00171-1

Atiga, W. L., Fananapazir, L., McAreavey, D., Calkins, H., and Berger, R. D. (2000). Temporal repolarization lability in hypertrophic cardiomyopathy caused by beta-myosin heavy-chain gene mutations. *Circulation* 101, 1237–1242. doi: 10.1161/01.CIR.101.11.1237

Baumert, M., Schlaich, M. P., Nalivaiko, E., Lambert, E., Sari, C. I., Kaye, D. M., et al. (2011). Relation between QT interval variability and cardiac sympathetic activity in hypertension. *Am. J. Physiol. Circ. Physiol.* 300, H1412–H1417. doi: 10.1152/ajpheart.01184.2010

Berger, R. D., Kasper, E. K., Baughman, K. L., Marban, E., Calkins, H., and Tomaselli, G. F. (1997). Beat-to-beat QT interval variability: novel evidence for repolarization lability in ischemic and nonischemic dilated cardiomyopathy. *Circulation* 96, 1557–1565. doi: 10.1161/01.CIR.96.5.1557

Cao, J. M., Chen, L. S., Ken Knight, B. H., Ohara, T., Lee, M. H., Tsai, J., et al. (2000a). Nerve sprouting and sudden cardiac death. *Circ. Res.* 86, 816–821. doi: 10.1161/01.res.86.7.816

Cao, J. M., Fishbein, M. C., Han, J. B., Lai, W. W., Lai, A. C., Wu, T. J., et al. (2000b). Relationship between regional cardiac hyperinnervation and ventricular arrhythmia. *Circulation* 101, 1960–1969. doi: 10.1161/01.cir.101.16.1960

Dunnink, A., Sharif, S., Oosterhoff, P., Winckels, S., Montagne, D., Beekman, J., et al. (2010). Anesthesia and arrhythmogenesis in the chronic atrioventricular block dog model. *J. Cardiovasc. Pharmacol.* 55, 601–608. doi: 10.1097/FJC.0b013e3181da7768

Dunnink, A., van Opstal, J. M., Oosterhoff, P., Winckels, S. K. G., Beekman, J. D. M., van der Nagel, R., et al. (2012). Ventricular remodelling is a prerequisite for the induction of dofetilide-induced torsade de pointes arrhythmias in the anaesthetized, complete atrio-ventricular-block dog. *Europace* 14, 431–436. doi: 10.1093/europace/eur311

Eckardt, L., Kirchhof, P., Breithardt, G., and Haverkamp, W. (2001). Load-induced changes in repolarization: evidence from experimental and clinical data. *Basic Res. Cardiol.* 96, 369–380. doi: 10.1007/s003950170045

Furlan, R., Porta, A., Costa, F., Tank, J., Baker, L., Schiavi, R., et al. (2000). Oscillatory patterns in sympathetic neural discharge and cardiovascular variables during orthostatic stimulus. *Circulation* 101, 886–892. doi: 10.1161/01.CIR.101.8.886

Gallacher, D. J., Van de Water, A., van der Linde, H., Hermans, A. N., Lu, H. R., Towart, R., et al. (2007). In vivo mechanisms precipitating torsades de pointes in a canine model of drug-induced long-QT1 syndrome. *Cardiovasc. Res.* 76, 247–256. doi: 10.1016/j.cardiores.2007.06.019

Hamm, W., Stülpnagel, L., Vdovin, N., Schmidt, G., Rizas, K. D., and Bauer, A. (2017). Risk prediction in post-infarction patients with moderately reduced left ventricular ejection fraction by combined assessment of the sympathetic and vagal cardiac autonomic nervous system. *Int. J. Cardiol.* 249, 1–5. doi: 10.1016/j.ijcard.2017.06.091

Hanson, B., Gill, J., Western, D., Gilbey, M. P., Bostock, J., Boyett, M. R., et al. (2012). Cyclical modulation of human ventricular repolarization by respiration. *Front. Physiol.* 3:379. doi: 10.3389/fphys.2012.00379

Hanson, B., Child, N., Van Duijvenboden, S., Orini, M., Chen, Z., Coronel, R., et al. (2014). Oscillatory behavior of ventricular action potential duration in heart failure patients at respiratory rate and low frequency. *Front. Physiol.* 5:414. doi: 10.3389/fphys.2014.00414

Hinterseer, M., Thomsen, M. B., Beckmann, B.-M., Pfeufer, A., Schimpf, R., Wichmann, H.-E., et al. (2008). Beat-to-beat variability of QT intervals is increased in patients with drug-induced long-QT syndrome: a case control pilot study. *Eur. Heart J.* 29, 185–190. doi: 10.1093/eurheartj/ehm586

Hinterseer, M., Beckmann, B.-M., Thomsen, M. B., Pfeufer, A., Dalla Pozza, R., Loeff, M., et al. (2009). Relation of increased short-term variability of QT interval to congenital long-QT syndrome. *Am. J. Cardiol.* 103, 1244–1248. doi: 10.1016/j.amjcard.2009.01.011

Hinterseer, M., Beckmann, B.-M., Thomsen, M. B., Pfeufer, A., Ulbrich, M., Sinner, M. F., et al. (2010). Usefulness of short-term variability of QT intervals as a predictor for electrical remodeling and proarrhythmia in patients with nonischemic heart failure. *Am. J. Cardiol.* 106, 216–220. doi: 10.1016/j.amjcard.2010.02.033

Hnatkova, K., Kowalski, D., Keirns, J. J., van Gelderen, E. M., and Malik, M. (2013). Relationship of QT interval variability to heart rate and RR interval variability. *J. Electrocardiol.* 46, 591–596. doi: 10.1016/j.jelectrocard.2013.07.007

Iribe, G., Ward, C. W., Camelliti, P., Bollensdorff, C., Mason, F., Burton, R. A. B., et al. (2009). Axial stretch of rat single ventricular cardiomyocytes causes an acute and transient increase in Ca^{2+} spark rate. *Circ. Res.* 104, 787–795. doi: 10.1161/CIRCRESAHA.108.193334

Johnson, D. M., Heijman, J., Pollard, C. E., Valentin, J.-P., Crijns, H. J. G. M., Abi-Gerges, N., et al. (2010). IKs restricts excessive beat-to-beat variability of repolarization during beta-adrenergic receptor stimulation. *J. Mol. Cell. Cardiol.* 48, 122–130. doi: 10.1016/j.yjmcc.2009.08.033

Johnson, D. M., Heijman, J., Bode, E. F., Greensmith, D. J., van der Linde, H., Abi-Gerges, N., et al. (2013). Diastolic spontaneous calcium release from the sarcoplasmic reticulum increases beat-to-beat variability of repolarization in canine ventricular myocytes after β-adrenergic stimulation. *Circ. Res.* 112, 246–256. doi: 10.1161/CIRCRESAHA.112.275735

Julien, C. (2006). The enigma of Mayer waves: facts and models. *Cardiovasc. Res.* 70, 12–21. doi: 10.1016/j.cardiores.2005.11.008

Kamkin, A., Kiseleva, I., and Isenberg, G. (2000). Stretch-activated currents in ventricular myocytes: amplitude and arrhythmogenic effects increase with hypertrophy. *Cardiovasc. Res.* 48, 409–420. doi: 10.1016/S0008-6363(00)00208-X

Levine, J. H., Guarnieri, T., Kadish, A. H., White, R. I., Calkins, H., and Kan, J. S. (1988). Changes in myocardial repolarization in patients undergoing balloon valvuloplasty for congenital pulmonary stenosis: evidence for contraction-excitation feedback in humans. *Circulation* 77, 70–77. doi: 10.1161/01.CIR.77.1.70

Long, V. P., Bonilla, I. M., Vargas-Pinto, P., Nishijima, Y., Sridhar, A., Li, C., et al. (2015). Heart failure duration progressively modulates the arrhythmia substrate through structural and electrical remodeling. *Life Sci.* 123, 61–71. doi: 10.1016/j.lfs.2014.12.024

Malik, M., Hnatkova, K., Novotny, T., and Schmidt, G. (2008). Subject-specific profiles of QT/RR hysteresis. *Am. J. Physiol. Circ. Physiol.* 295, H2356–H2363. doi: 10.1152/ajpheart.00625.2008

Malpas, S. C. (2002). Neural influences on cardiovascular variability: possibilities and pitfalls. *Am. J. Physiol. Heart Circ. Physiol.* 282, H6–H20. doi: 10.1152/ajpheart.2002.282.1.H6

Mitchell, J. R., Whitelaw, W. A., Sas, R., Smith, E. R., Tyberg, J. V., and Belenkie, I. (2005). RV filling modulates LV function by direct ventricular interaction during mechanical ventilation. *Am. J. Physiol. Circ. Physiol.* 289, H549–H557. doi: 10.1152/ajpheart.01180.2004

Murabayashi, T., Fetics, B., Kass, D., Nevo, E., Gramatikov, B., and Berger, R. D. (2002). Beat-to-beat QT interval variability associated with acute myocardial ischemia. *J. Electrocardiol.* 35, 19–25. Available at: http://www.ncbi.nlm.nih.gov/pubmed/11786943 (Accessed December 29, 2017)

Oosterhoff, P., Thomsen, M. B., Maas, J. N., Atteveld, N. J. M., Beekman, J. D. M., VAN Rijen, H. V. M., et al. (2010). High-rate pacing reduces variability of repolarization and prevents repolarization-dependent arrhythmias in dogs with chronic AV block. *J. Cardiovasc. Electrophysiol.* 21, 1384–1391. doi: 10.1111/j.1540-8167.2010.01824.x

Oros, A., Beekman, J. D. M., and Vos, M. A. (2008). The canine model with chronic, complete atrio-ventricular block. *Pharmacol. Ther.* 119, 168–178. doi: 10.1016/j.pharmthera.2008.03.006

Pagani, M., Montano, N., Porta, A., Malliani, A., Abboud, F. M., Birkett, C., et al. (1997). Relationship between spectral components of cardiovascular variabilities and direct measures of muscle sympathetic nerve activity in humans. *Circulation* 95, 1441–1448. doi: 10.1161/01.CIR.95.6.1441

Piccirillo, G., Germanò, G., Quaglione, R., Nocco, M., Lintas, F., Lionetti, M., et al. (2002). QT-interval variability and autonomic control in hypertensive subjects with left ventricular hypertrophy. *Clin. Sci.* 102, 363–371. doi: 10.1042/cs1020363

Porter, B., van Duijvenboden, S., Bishop, M. J., Orini, M., Claridge, S., Gould, J., et al. (2018). Beat-to-beat variability of ventricular action potential duration oscillates at low frequency during sympathetic provocation in humans. *Front. Physiol.* 9:47. doi: 10.3389/fphys.2018.00147

Pueyo, E., Orini, M., Rodríguez, J. F., and Taggart, P. (2016). Interactive effect of beta-adrenergic stimulation and mechanical stretch on low-frequency oscillations of ventricular action potential duration in humans. *J. Mol. Cell. Cardiol.* 97, 93–105. doi: 10.1016/j.yjmcc.2016.05.003

Rizas, K. D., Nieminen, T., Barthel, P., Zürn, C. S., Kähönen, M., Viik, J., et al. (2014). Sympathetic activity-associated periodic repolarization dynamics predict mortality following myocardial infarction. *J. Clin. Invest.* 124, 1770–1780. doi: 10.1172/JCI70085

Rizas, K. D., McNitt, S., Hamm, W., Massberg, S., Kääb, S., Zareba, W., et al. (2017). Prediction of sudden and non-sudden cardiac death in post-infarction patients with reduced left ventricular ejection fraction by periodic repolarization dynamics: MADIT-II substudy. *Eur. Heart J.* 38, 2110–2118. doi: 10.1093/eurheartj/ehx161

Roden, D. M. (1998). Taking the "idio" out of "idiosyncratic": predicting torsades de pointes. *Pacing Clin. Electrophysiol.* 21, 1029–1034. doi: 10.1111/j.1540-8159.1998.tb00148.x

Sipido, K. R., Volders, P. G. A., Schoenmakers, M., De Groot, S. H. M., Verdonck, F., and Vos, M. A. (2002). Role of the Na/Ca exchanger in arrhythmias in compensated hypertrophy. *Ann. N. Y. Acad. Sci.* 976, 438–445. doi: 10.1111/j.1749-6632.2002.tb04773.x

Stams, T. R., Oosterhoff, P., Heijdel, A., Dunnink, A., Beekman, J. D., van der Nagel, R., et al. (2016). Beat-to-beat variability in preload unmasks latent risk of torsade de pointes in anesthetized chronic atrioventricular block dogs. *Circ. J.* 80, 1336–1345. doi: 10.1253/circj.CJ-15-1335

Ter Bekke, R. M. A., Moers, A. M. E., de Jong, M. M. J., Johnson, D. M., Schwartz, P. J., Vanoli, E., et al. (2019). Proarrhythmic proclivity of left-stellate ganglion stimulation in a canine model of drug-induced long-QT syndrome type 1. *Int. J. Cardiol.* 286, 66–72. doi: 10.1016/j.ijcard.2019.01.098

Thomsen, M., Oros, A., Schoenmakers, M., van Opstal, J., Maas, J., Beekman, J., et al. (2007). Proarrhythmic electrical remodelling is associated with increased beat-to-beat variability of repolarisation. *Cardiovasc. Res.* 73, 521–530. doi: 10.1016/j.cardiores.2006.11.025

Thomsen, M. B., Verduyn, S. C., Stengl, M., Beekman, J. D. M., de Pater, G., van Opstal, J., et al. (2004). Increased short-term variability of repolarization predicts d-sotalol-induced torsades de pointes in dogs. *Circulation* 110, 2453–2459. doi: 10.1161/01.CIR.0000145162.64183.C8

Van de Water, A., Verheyen, J., Xhonneux, R., and Reneman, R. S. (1989). An improved method to correct the QT interval of the electrocardiogram for changes in heart rate. *J. Pharmacol. Methods* 22, 207–217. Available at: http://www.ncbi.nlm.nih.gov/pubmed/2586115 (Accessed August 30, 2016)

Zabel, M., Portnoy, S., and Franz, M. R. (1996). Effect of sustained load on dispersion of ventricular repolarization and conduction time in the isolated intact rabbit heart. *J. Cardiovasc. Electrophysiol.* 7, 9–16. doi: 10.1111/j.1540-8167.1996.tb00455.x

Zeng, T., Bett, G. C. L., and Sachs, F. (2000). Stretch-activated whole cell currents in adult rat cardiac myocytes. *Am. J. Physiol. Circ. Physiol.* 278, H548–H557. doi: 10.1152/ajpheart.2000.278.2.H548

Zhou, S., Jung, B.-C., Tan, A. Y., Trang, V. Q., Gholmieh, G., Han, S.-W., et al. (2008). Spontaneous stellate ganglion nerve activity and ventricular arrhythmia in a canine model of sudden death. *Heart Rhythm.* 5, 131–139. doi: 10.1016/j.hrthm.2007.09.007

Conflict of Interest Statement: The authors declare that the research was conducted in the absence of any commercial or financial relationships that could be construed as a potential conflict of interest.

frontiers in Physiology

ORIGINAL RESEARCH
published: 29 November 2019
doi: 10.3389/fphys.2019.01478

Concomitant Evaluation of Heart Period and QT Interval Variability Spectral Markers to Typify Cardiac Control in Humans and Rats

*Beatrice De Maria[1], Vlasta Bari[2], Andrea Sgoifo[3,4], Luca Carnevali[3,4], Beatrice Cairo[5], Emanuele Vaini[2], Aparecida Maria Catai[6], Anielle Cristhine de Medeiros Takahashi[6], Laura Adelaide Dalla Vecchia[1] and Alberto Porta[2,5]**

[1] IRCCS Istituti Clinici Scientifici Maugeri, Milan, Italy, [2] Department of Cardiothoracic, Vascular Anesthesia and Intensive Care, IRCCS Policlinico San Donato, Milan, Italy, [3] Stress Physiology Laboratory, Department of Chemistry, Life Sciences and Environmental Sustainability, University of Parma, Parma, Italy, [4] Microbiome Research Hub, University of Parma, Parma, Italy, [5] Department of Biomedical Sciences for Health, University of Milan, Milan, Italy, [6] Department of Physiotherapy, Federal University of São Carlos, São Carlos, Brazil

OPEN ACCESS

Edited by:
George E. Billman,
The Ohio State University,
United States

Reviewed by:
Veronique Meijborg,
Academic Medical Center (AMC),
Netherlands
Jerzy Sacha,
Opole University of Technology,
Poland

***Correspondence:**
Alberto Porta
alberto.porta@unimi.it

Specialty section:
This article was submitted to Cardiac Electrophysiology, a section of the journal Frontiers in Physiology

Received: 09 July 2019
Accepted: 18 November 2019
Published: 29 November 2019

Citation:
De Maria B, Bari V, Sgoifo A, Carnevali L, Cairo B, Vaini E, Catai AM, de Medeiros Takahashi AC, Dalla Vecchia LA and Porta A (2019) Concomitant Evaluation of Heart Period and QT Interval Variability Spectral Markers to Typify Cardiac Control in Humans and Rats. Front. Physiol. 10:1478. doi: 10.3389/fphys.2019.01478

The variability of heart period, measured as the time distance between two consecutive QRS complexes from the electrocardiogram (RR), was exploited to infer cardiac vagal control, while the variability of the duration of the electrical activity of the heart, measured as the time interval from Q-wave onset to T-wave end (QT), was proposed as an indirect index of cardiac sympathetic modulation. This study tests the utility of the concomitant evaluation of RR variability (RRV) and QT variability (QTV) markers in typifying cardiac autonomic control of humans under different experimental conditions and of rat groups featuring documented differences in resting sympatho-vagal balance. We considered: (i) 23 healthy young subjects in resting supine position (REST) undergoing head-up tilt at 45° (T45) and 90° (T90) followed by recovery to the supine position; (ii) 9 Wistar (WI) and 14 wild-type Groningen (WT) rats in unstressed conditions, where the WT animals were classified as non-aggressive (non-AGG, $n = 9$) and aggressive (AGG, $n = 5$) according to the resident intruder test. In humans, spectral analysis of RRV and QTV was performed over a single stationary sequence of 250 consecutive values. In rats, spectral analysis was iterated over 10-min recordings with a frame length of 250 beats with 80% overlap and the median of the distribution of the spectral markers was extracted. Over RRV and QTV we computed the power in the low frequency (LF, from 0.04 to 0.15 Hz in humans and from 0.2 to 0.75 Hz in rats) band (LF_{RR} and LF_{QT}) and the power in the high frequency (HF, from 0.15 to 0.5 Hz in humans and from 0.75 to 2.5 Hz in rats) band (HF_{RR} and HF_{QT}). In humans the HF_{RR} power was lower during T90 and higher during recovery compared to REST, while the LF_{QT} power was higher during T90. In rats the HF_{RR} power was lower in WT rats compared to WI rats and the LF_{QT} power was higher in AGG than in non-AGG animals. We concluded that RRV and QTV provide complementary information in describing the functioning of vagal and sympathetic limbs of the autonomic nervous system in humans and rats.

Keywords: power spectral analysis, heart rate variability, QTV, ventricular repolarization, autonomic nervous system, wild-type rat, Wistar, head-up tilt

INTRODUCTION

Heart period, measured as the time distance between two consecutive QRS complexes from the electrocardiogram (RR), exhibits spontaneous fluctuations usually referred to as RR variability (RRV). The analysis of RRV provides some markers that have been found useful to infer the state of the cardiac autonomic control (Task Force of the European Society of Cardiology and the North American Society of Pacing and Electrophysiology,, 1996). Short-term RRV markers in humans are mainly associated with vagal modulation given that the magnitude of RR changes is dramatically reduced by full vagal blockade (Pomeranz et al., 1985). This consideration holds not only in humans but also in rats (Japundzic et al., 1990; Cerutti et al., 1991; Silva et al., 2017) and this analogy strengthened the use of rats as an animal model of human autonomic cardiac control. The amplitude of the respiratory sinus arrhythmia is one of the most utilized RRV indexes to typify cardiac vagal control (Hirsch and Bishop, 1981): it is frequently estimated via spectral analysis as the power of RRV in the high frequency (HF) band in both humans and rats, even though the definition of the HF band was adapted to account for the differences between the respiratory rates in the two species, namely from 0.15 to 0.5 Hz in humans and from 0.75 to 2.5 Hz in rats (Japundzic et al., 1990; Cerutti et al., 1991; Rubini et al., 1993). In particular, in humans the HF power of RRV is known to decrease during physiological conditions characterized by sympathetic activation and vagal withdrawal, such as during graded orthostatic challenge (Montano et al., 1994; Cooke et al., 1999; Porta et al., 2011; Marchi et al., 2016) or physical exercise (Shin et al., 1995a,b; Brenner et al., 1997; Porta et al., 2018). Similarly, in rats the HF power of RRV was utilized to typify the autonomic response to several types of stressors either pharmacological, interventional, or social (Akselrod et al., 1987; Japundzic et al., 1990; Cerutti et al., 1991; Rubini et al., 1993; Stauss et al., 1997; Sgoifo et al., 1998, 1999; Jaenisch et al., 2011; Carnevali et al., 2013; Carnevali and Sgoifo, 2014; Silva et al., 2016, 2017).

More recently, in parallel with the more traditional RRV analysis, the variability of the overall duration of the electrical activity of the heart, comprising depolarization and repolarization periods, usually quantified as the time interval from Q-wave onset to T-wave end (QT) from the electrocardiogram, has been proposed and validated as a marker of cardiac sympathetic control in humans (Berger, 2009; Malik, 2009; Porta et al., 2010; Baumert et al., 2016). QT variability (QTV) markers computed in the low frequency (LF) band (i.e., from 0.04 to 0.15 Hz in humans) have been found to increase in situations where sympatho-vagal balance is shifted toward sympathetic activation and vagal withdrawal, especially when the sympathetic drive is particularly high (Lombardi et al., 1996; Porta et al., 1998a, 2010, 2011; Yeragani et al., 2000a,b; Piccirillo et al., 2001, 2006; Bar et al., 2007; Baumert et al., 2008, 2011; El-Hamad et al., 2015), with relevant clinical consequences in risk stratification (Berger et al., 1997; Atiga et al., 1998; Porta et al., 2015). Conversely, no information was provided about the possibility to use QTV in rats, mainly because of the technical difficulties in reliably assessing QT fluctuations due to the very limited signal-to-noise ratio of QTV (Laguna et al., 1990; Speranza et al., 1993; Lombardi et al., 1996; Porta et al., 1998b) and the peculiarities of cardiac repolarization in rodents (Conrath and Opthof, 2006; Fabritz et al., 2010; Speerschneider and Thomsen, 2013; Boukens et al., 2014).

The aim of the present study is to propose the concomitant evaluation of RRV and QTV to provide a more complete view on cardiac autonomic control and to test whether this strategy could be fruitfully exploited in both humans and rats. The hypothesis of the study is that the concomitant evaluation of RRV and QTV markers can describe simultaneously cardiac vagal control via the analysis of the RRV and cardiac sympathetic regulation via the analysis of the QTV in both humans and rats. In humans we evaluated two situations of sympathetic activation and vagal withdrawal of different intensities, namely head-up tilt at 45° and 90° (Montano et al., 1994), and the following recovery to supine position during which a progressive decline of sympathetic control and a gradual vagal rebound are expected. In rats, we considered two strains with documented differences in resting cardiac sympatho-vagal balance, namely the Wistar (WI) and wild-type Groningen (WT) rats (Carnevali and Sgoifo, 2014), and, within the WT population, two subgroups featuring opposite levels of aggressiveness that have been linked to different states of the cardiac autonomic control (Carnevali et al., 2013).

MATERIALS AND METHODS

Experimental Protocol on Humans

We studied 23 young healthy volunteers (11 males, age: 26.3 ± 5.6 years). A detailed medical history and examination excluded the evidence of any disease. The subjects did not take any medication and consume any caffeine or alcohol-containing beverages in the 24 h before the recording session. Each subject underwent two consecutive head-up tilt tests with different table inclination angles, namely 45° (T45) and 90° (T90). T45 and T90 sessions were carried out in a random order, lasted 10 min and were followed by 40 min of recovery (R45 and R90, respectively) starting when the tilt table was moved back to the horizontal position. The first tilt session was preceded by a 10-min recording period in supine position (REST). Subjects lay on the tilt table supported by two belts at the level of the thigh and waist, respectively, and with both feet touching the footrest of the tilt table. During the recording sessions, subjects breathed spontaneously but were not allowed to talk. The electrocardiographic activity from a modified lead II was recorded (Biosignal Conditioning Device, Marazza, Monza, Italy) throughout all the experimental sessions and sampled at 1000 Hz. Attention was paid during the positioning of the electrodes to prevent flat or biphasic T-waves. All subjects were able to complete the protocol without experiencing any sign of presyncope. The duration of the phases was never varied.

Informed consent was obtained from all subjects before taking part in the study. The study adheres to the principles of the Declaration of Helsinki for medical research involving human subjects. The Human Research and Ethical Review Board of the L. Sacco Hospital, Milan, Italy, approved the protocol.

Experimental Protocol on Rats

We studied two different strains of rats: 9 male WI rats (age: 5.5 ± 0.5 months; weight: 436 ± 34 g) and 14 male WT rats (age: 4.4 ± 0.5 months; weight: 395 ± 40 g). Initially WT rats were classified into non-aggressive (non-AGG, n = 5) and aggressive (AGG, n = 9) WT rats, according to the resident intruder test described in Carnevali et al. (2013).

After the preliminary behavioral tests in WT rats, all rats were implanted, under tiletamine hydrochloride plus zolazepam hydrochloride anesthesia (Zoletil Virbac, France, 20 mg kg^{-1}), with radiotelemetric transmitters (TA11CTA-F40, Data Sciences International, St. Paul, MN, United States) for the recording of the cardiac electrical activity. Electrocardiograms were picked up by platform receivers (RPC-1, Data Sciences Int., St. Paul, MN, United States) located under the animal's cage and acquired via ART-Gold 4.2 data acquisition system (Data Sciences International, St. Paul, MN, United States) at a sampling rate of 1000 Hz. Animals were individually housed and kept in rooms with controlled temperature (22 ± 2°C) and lighting (lights on from 7:00 P.M. to 7:00 A.M.). After a 14-day recovery period from surgery, electrocardiograms were recorded in all rats for 1 h during the dark (active) phase of the light–dark cycle (i.e., between 10:00 A.M. and 11:00 A.M.) on different days.

The experimental protocol was approved by the Veterinarian Animal Care and Use Committee of the University of Parma, Parma, Italy, and the animals were cared in accordance with the European Community Council Directives of 22 September 2010 (2010/63/UE).

Extraction of the Beat-to-Beat RRV and QTV Series

The electrocardiographic traces recorded in both healthy humans and rats were processed with a software, developed in house, automatically measuring RR and QT (Porta et al., 1998b). The peak of the QRS complex (i.e., the R-wave) was automatically located via a method based on a threshold on the first derivative of the electrocardiogram. The peak of the QRS complex was fixed via parabolic interpolation. The RR was measured as the time distance between two consecutive QRS complex peaks. The QT was approximated as the time interval between the peak of the QRS complex and the T-wave offset (RTend) (Porta et al., 2010, 2011). The end of the T-wave was automatically delineated where the absolute value of the first derivative calculated on T-wave downslope became smaller than 30% of the absolute value of the steepest slope of the T-wave. **Figure 1** shows an example of the automatic detection of the T-wave end in a healthy subject (top panel), a WI rat (middle panel), and a WT rat (bottom panel). The detections of the QRS complex were visually checked and corrected in case of identification errors and in this case the T-wave offset delineation procedure was run again starting from the new position of the QRS complex. T-wave end detections were checked to assure the quality of the T-wave delineation. Problematic T-wave morphologies such as biphasic shapes were not observed and the first return to the isoelectric line after the onset of the T-wave always denotes the offset of the repolarization period in both humans and rats. The effects of isolated ectopic beats on RR and QT beat-to-beat series were corrected by means of cubic spline interpolation starting from the RR and QT measures unaffected by non-sinus cardiac beats. Corrections never exceeded the 5% of the total beats. Within each experimental session of the human protocol (i.e., REST, T45, R45, T90, and R90) segments of 250 consecutive RR and QT measures were selected. Stationarity of the selected sequences was tested according to Magagnin et al. (2011). The first stationary sequence found 3 min after the onset of posture changes was taken as the representative segment during T45 and T90 sessions and the first stationary sequence 10 min after returning to the supine position after head-up tilt was taken as the representative segment during R45 and R90 sessions. As to the animal protocol, a 10-min segment was selected in a random position within the overall recording session. The analysis was carried out over the 10-min segments divided into adjacent windows of 250 consecutive RR and QT measures with 80% overlap. The median

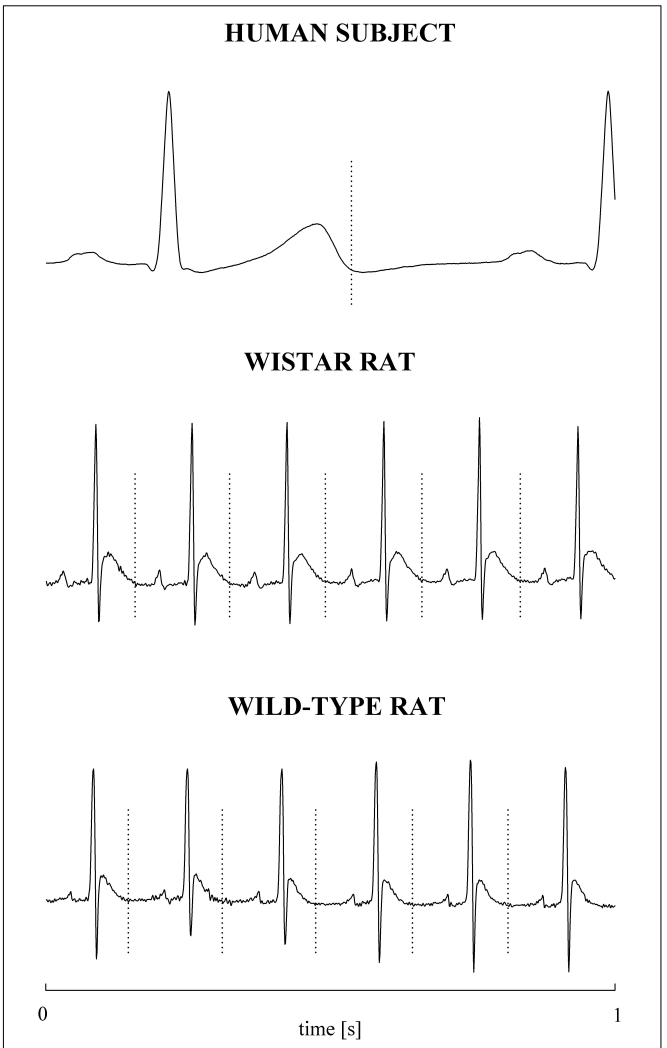

FIGURE 1 | Examples of T-wave end delineation in ECG signals of a healthy young human subject **(top)**, WI rat **(middle)**, and WT rat **(bottom)** in basal condition. T-wave end is marked with a vertical dotted line.

of the distribution was chosen as the representative value of the whole series. **Figure 2** shows some examples of beat-to-beat RRV and QTV series derived from a human subject at REST (**Figures 2A,D**), from a WI rat (**Figures 2B,E**) and a WT rat (**Figures 2C,F**) in unstressed conditions.

Time and Frequency Domain RRV and QTV Analyses

In the time domain, we computed the mean of RR and QT beat-to-beat series (μ_{RR} and μ_{QT}, respectively). μ_{RR} and μ_{QT} were expressed in ms. Linear detrending procedure, subtracting from the original series the best fit linear trend, was exploited to prevent the drift of the mean and favor stationarity. After linear detrending of the series, the variances of RR and QT beat-to-beat series (σ^2_{RR} and σ^2_{QT}, respectively) were calculated and expressed in ms^2. Parametric power spectral analysis was performed. RRV and QTV series were modeled as realizations of an autoregressive process. The coefficients of the autoregressive process and the variance of the white noise corrupting the determinist part of the process were estimated via least squares method solved via the Levinson–Durbin recursion (Kay and Marple, 1981). The number of coefficients was optimized via Akaike's (1974) criterion within the range from 10 to 16. Power spectral density was decomposed into power spectral components (Baselli et al., 1997), classified as LF or HF component, according to their central frequency. The LF band range was 0.04–0.15 Hz for humans (Task Force of the European Society of Cardiology and the North American Society of Pacing and Electrophysiology,, 1996) and 0.2–0.75 Hz for rats (Carnevali et al., 2013), while the HF band range was 0.15–0.5 Hz for humans (Task Force of the European Society of Cardiology and the North American Society of Pacing and Electrophysiology,, 1996) and 0.75–2.5 Hz for rats (Carnevali et al., 2013). The sum of the absolute power of all HF components of the RR series was termed as HF_{RR} and considered to be an index of vagal modulation directed to the sinus node (Pomeranz et al., 1985), whereas the sum of the absolute power of all LF components of the QT series was labeled LF_{QT} and considered to be an index of sympathetic modulation directed to the heart (Porta et al., 2010, 2011; Baumert et al., 2011; El-Hamad et al., 2015). The power of RRV in the LF band, indicated as LF_{RR}, and the power of the QTV in the HF band, labeled as HF_{QT}, were computed as well. LF_{RR}, HF_{RR}, LF_{QT}, and HF_{QT} indexes were given in absolute units and expressed in ms^2. Spectral analysis was carried out over the linearly detrended RRV and QTV series.

Statistical Analysis

In the human protocol one-way repeated measures analysis of variance (Dunnett's test for multiple comparisons) was performed to check the significance of the differences of T45, R45, T90, and R90 versus REST. If the Kolmogorov–Smirnov normality test was not passed, Friedman one-way repeated measures analysis of variance on ranks (Dunnett's test for multiple comparisons) was carried out. In the animal protocol unpaired *t*-test was performed to assess the significance of the differences between the strains (WI versus WT) and subgroups (AGG versus non-AGG). If the Kolmogorov–Smirnov normality test was not passed, Mann–Whitney rank sum test was carried out. Statistical analysis was carried out using a commercial statistical program (Sigmaplot, Systat Software, Inc., Chicago, IL, United States, version 11.0). A $p < 0.05$ was always considered as significant.

RESULTS

Box-and-whisker plots of **Figure 3** show the results of RRV (**Figures 3A–C**) and QTV (**Figures 3D–F**) analyses performed on human data as a function of the experimental condition (i.e., REST, T45, R45, T90, and R90). Compared to REST, μ_{RR} decreased during both T45 and T90, while it was unchanged during R45 and R90 (**Figure 3A**). σ^2_{RR} was significantly higher during both R45 and R90 and was not affected by the orthostatic challenge (**Figure 3B**). HF_{RR} power significantly decreased during T90 and increased during R90 compared to REST (**Figure 3C**). μ_{QT} was significantly reduced during both T45 and T90 and did not vary during R45 and R90 (**Figure 3D**). σ^2_{QT} did not change with the experimental condition (**Figure 3E**). LF_{QT} power increased during T90 and remained stable in all the other experimental conditions (**Figure 3F**). Results relevant to time and frequency domain RRV and QTV markers derived from the experimental protocol on humans are summarized in **Table 1**. The same table reports the LF_{RR} and HF_{QT} powers as well. Both these latter markers did not vary with the experimental condition.

Box-and-whisker plots of **Figure 4** show the results of RRV (**Figures 4A–C**) and QTV (**Figures 4D–F**) analyses performed on data derived from WI and WT rats. μ_{RR} (**Figure 4A**) and σ^2_{RR} (**Figure 4B**) were similar between the two strains, while the HF_{RR} power (**Figure 4C**) was higher in WI compared to WT rats. μ_{QT} (**Figure 4D**) was longer in WI rats, while no strain differences in σ^2_{QT} (**Figure 4E**) and LF_{QT} power (**Figure 4F**) were observed. **Figure 5** has the same structure as **Figure 4** but it shows the results of RRV (**Figures 5A–C**) and QTV (**Figures 5D–F**) analyses performed on data obtained from WT rats that were classified as non-AGG and AGG. μ_{RR} (**Figure 5A**), σ^2_{RR} (**Figure 5B**), HF_{RR} (**Figure 5C**), and μ_{QT} (**Figure 5D**) did not differentiate the two subgroups. On the contrary, σ^2_{QT} (**Figure 5E**) and LF_{QT} (**Figure 5F**) were able to separate the two groups of WT rats, being both σ^2_{QT} and LF_{QT} power higher in AGG than in non-AGG animals. RRV and QTV markers derived from the experimental protocol on rats are summarized in **Tables 2**, **3**. These tables reported LF_{RR} and HF_{QT} powers as well. Both these markers were similar in WI and WT animals (**Table 2**) and they were not able to distinguish non-AGG from AGG animals (**Table 3**).

DISCUSSION

To the best of our knowledge this is the first study in which QTV parameters were evaluated in rats concomitantly with traditional RRV measures for the assessment of cardiac autonomic control and a parallel between human and rat RRV and QTV markers was drawn. The most important findings of this study can be

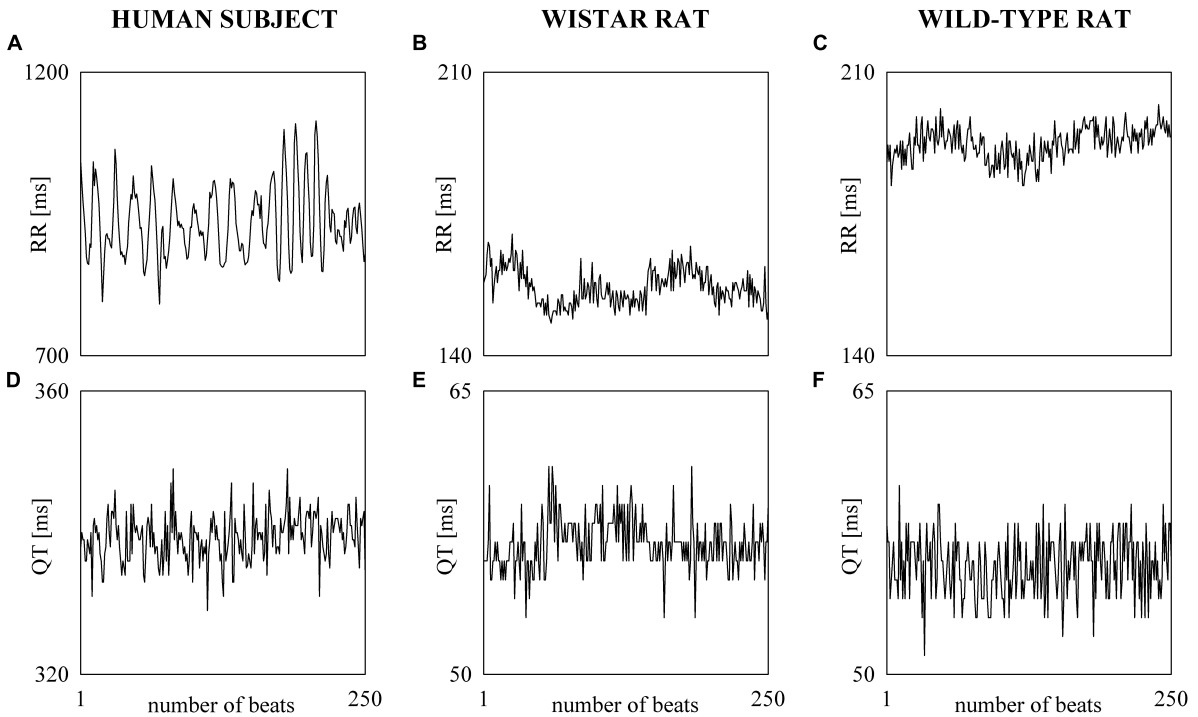

FIGURE 2 | The line plots show examples of beat-to-beat RRV **(A–C)** and QTV **(D–F)** series undergoing power spectral analysis recorded in a healthy young human subject **(A,D)**, WI rat **(B,E)**, and WT rat **(C,F)**.

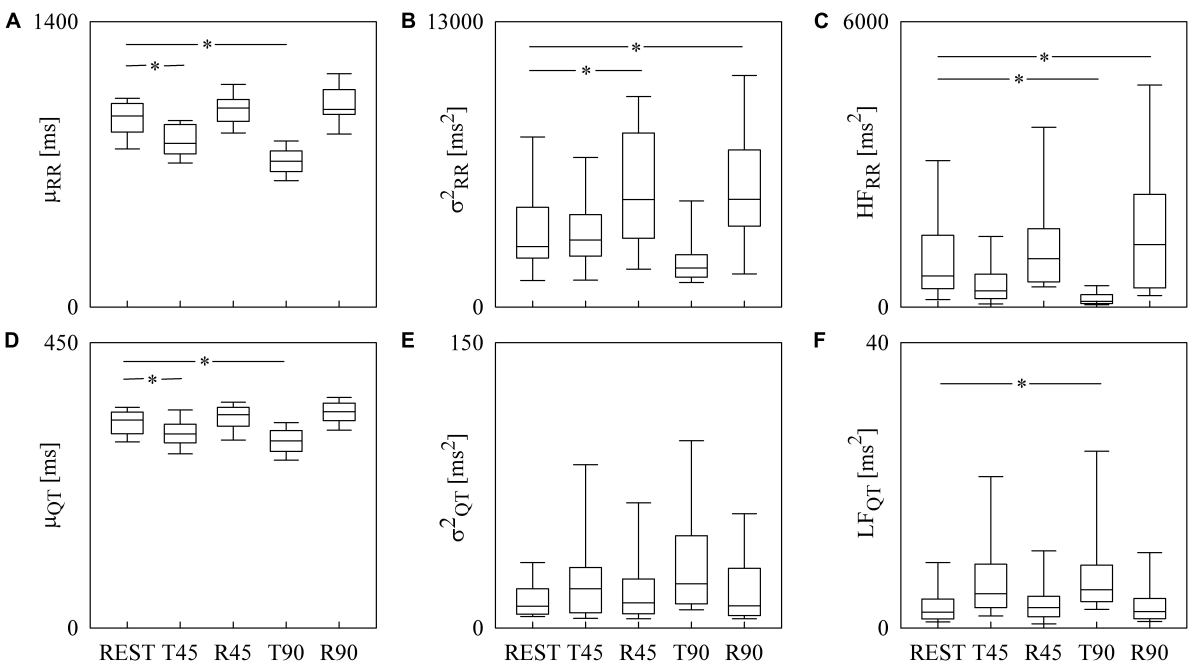

FIGURE 3 | The box-and-whisker graphs show the results of the time and frequency domain analyses of RRV and QTV in healthy young humans. The μ_{RR} **(A)**, σ^2_{RR} **(B)**, HF_{RR} **(C)**, μ_{QT} **(D)**, σ^2_{QT} **(E)**, and LF_{QT} **(F)** are given as a function of the experimental condition (i.e., REST, T45, R45, T90, and R90). Box height represents the interquartile range, median is marked with a horizontal solid segment, and whiskers denote the 10th and 90th percentile. The symbol * indicates a $p < 0.05$ versus REST.

TABLE 1 | Results of the time and frequency domain analyses of RRV and QTV in healthy young subjects.

Index	REST	T45	R45	T90	R90
μ_{RR} (ms)	937.18 (135.11)	802.56 (142.08)*	975.94 (97.25)	715.18 (96.47)*	969.17 (117.36)
σ^2_{RR} (ms^2)	2755.2 (2083.51)	3049.86 (1596.87)	4894.99 (4585.21)*	1773.36 (940.24)	4904.22 (3447.03)*
LF_{RR} (ms^2)	952.56 (1219.09)	1180.74 (1161.83)	1694.45 (1840.67)	890.56 (766.05)	1372.49 (1741.51)
HF_{RR} (ms^2)	651.6 (1095.69)	342.08 (479.25)	1016.27 (1040.69)	117.27 (182.51)*	1312.98 (1651.28)*
μ_{QT} (ms)	327.91 (33.6)	306.05 (26.65)*	336.25 (27.46)	295.09 (30.19)*	341.03 (26.73)
σ^2_{QT} (ms^2)	11.43 (12.29)	20.67 (23.11)	13.13 (16.72)	23.21 (33.49)	11.59 (23.18)
LF_{QT} (ms^2)	2.2 (3.98)	4.8 (5.71)	2.86 (2.76)	5.36 (4.78)*	2.29 (2.5)
HF_{QT} (ms^2)	4.45 (5.91)	7.43 (12.09)	3.34 (9.89)	8.62 (11.9)	4.09 (11.28)

*REST, supine position; T45, head-up tilt at 45°; R45, recovery in supine position after T45; T90, head-up tilt at 90°; R90, recovery in supine position after T90; LF, low frequency; HF, high frequency; RR, time interval between two consecutive QRS complexes; QT, time interval between the peak of the QRS complex and the T-wave offset; RRV, RR variability; QTV, QT variability; LF_{RR}, RRV power in the LF band expressed in absolute units; HF_{RR}, RRV power in the HF band expressed in absolute units; LF_{QT}, QTV power in the LF band expressed in absolute units; HF_{QT}, QTV power in the HF band expressed in absolute units. Results are presented as median with the interquartile range in round brackets. The symbol * indicates a $p < 0.05$ versus REST.*

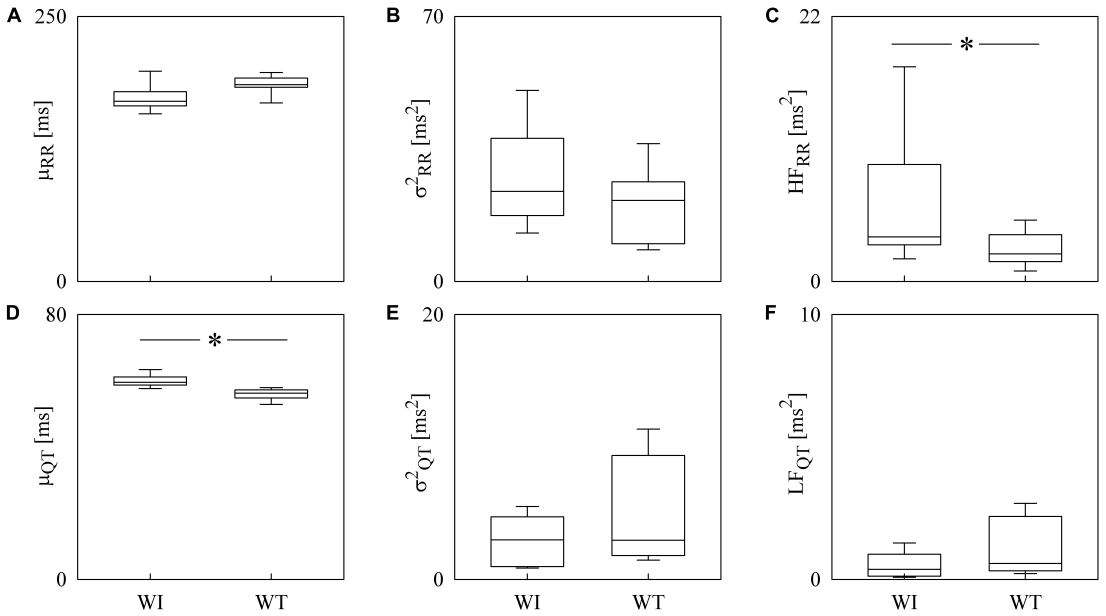

FIGURE 4 | The box-and-whisker graphs show the results of the time and frequency domain analyses of RRV and QTV in rats. The μ_{RR} **(A)**, σ^2_{RR} **(B)**, HF_{RR} **(C)**, μ_{QT} **(D)**, σ^2_{QT} **(E)**, and LF_{QT} **(F)** are given as a function of the strain (i.e., WI and WT). Box height represents the interquartile range, median is marked with a horizontal solid segment, and whiskers denote the 10th and 90th percentile. The symbol * indicates a $p < 0.05$ versus WI rats.

summarized as follows: (i) RRV is descriptive of the cardiac vagal regulation in both humans and rats; (ii) QTV is representative of cardiac sympathetic control in both humans and rats; (iii) results of RRV and QTV should be simultaneously considered to more deeply describe cardiac autonomic control in both humans and rats.

RRV and QTV Provide Complementary Information About Cardiac Autonomic Control in Humans and Rats

One of the major difficulties in exploiting RRV and spectral markers derived from RRV analysis to comprehensively characterize cardiac autonomic control is the strong link of RRV with the variation of vagal autonomic outflow, while its sensitivity to changes of the activity of the sympathetic autonomic limb is more limited. Indeed, since the initial studies on RRV (Akselrod et al., 1981; Pomeranz et al., 1985) it is well-known that the HF_{RR} power is completely abolished by full vagal blockade carried out via a high dose of atropine and that the same pharmacological challenge affects remarkably the LF_{RR} power as well. This observation suggested that the HF_{RR} power is a genuine marker of vagal modulation directed to the sinus node, while the LF_{RR} power results from the changes of the activity of both sympathetic and vagal limbs of the autonomic nervous system (Akselrod et al., 1981; Pomeranz et al., 1985). Normalization strategies attempted to limit the dependence of the LF_{RR} power on cardiac vagal control. For example, the ratio of the LF_{RR} power to σ^2_{RR} minus the RRV power in the very LF band, known as LF_{RR} power expressed

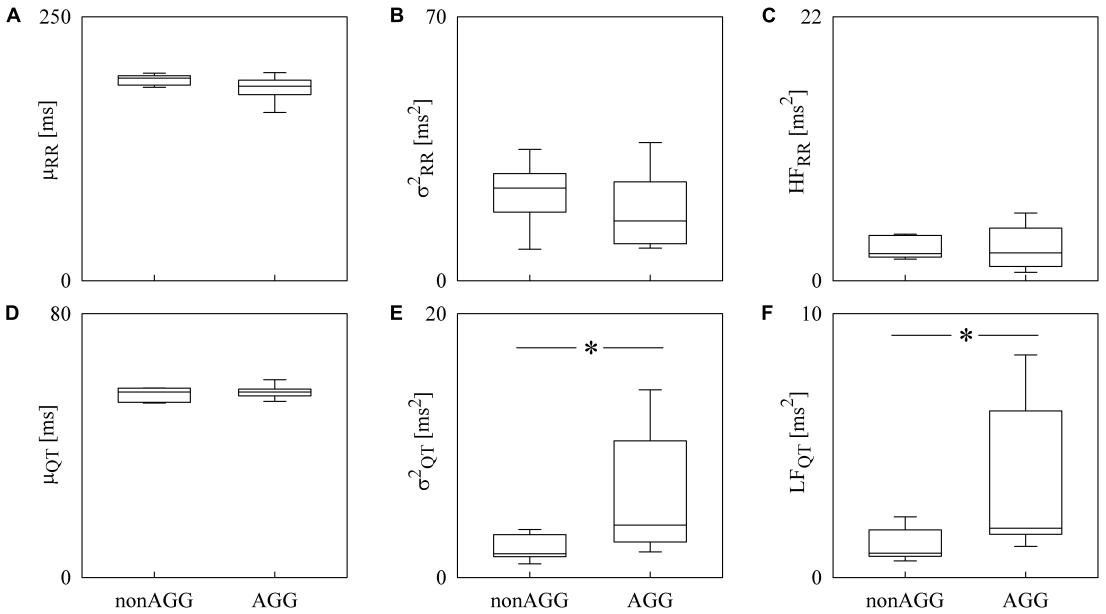

FIGURE 5 | The box-and-whisker graphs show the results of the time and frequency domain analyses of RRV and QTV in WT rats classified into non-AGG and AGG animals. The μ_{RR} **(A)**, σ^2_{RR} **(B)**, HF_{RR} **(C)**, μ_{QT} **(D)**, σ^2_{QT} **(E)**, and LF_{QT} **(F)** are given as a function of the WT subcategory (i.e., non-AGG and AGG). Box height represents the interquartile range, median is marked with a horizontal solid segment, and whiskers denote the 10th and 90th percentile. The symbol * indicates a $p < 0.05$ versus non-AGG animals.

TABLE 2 | Results of time and frequency domain analyses of RRV and QTV in WI and WT rats.

Index	WI	WT
μ_{RR} (ms)	169.99 (7.37)	185.6 (8.31)
σ^2_{RR} (ms^2)	23.76 (19.62)	21.38 (15.5)
LF_{RR} (ms^2)	1.22 (1.4)	0.58 (0.37)
HF_{RR} (ms^2)	3.69 (4.63)	2.29 (2.16)*
μ_{QT} (ms)	59.54 (2.21)	56.23 (2.32)*
σ^2_{QT} (ms^2)	2.98 (3.49)	2.95 (6.01)
LF_{QT} (ms^2)	0.38 (0.78)	0.6 (1.63)
HF_{QT} (ms^2)	1.36 (1.93)	1.68 (3.76)

*WI, Wistar rats; WT, wild-type Groningen rats; LF, low frequency; HF, high frequency; RR, time interval between two consecutive QRS complexes; QT, time interval between the peak of the QRS complex and the T-wave offset; RRV, RR variability; QTV, QT variability; LF_{RR}, RRV power in the LF band expressed in absolute units; HF_{RR}, RRV power in the HF band expressed in absolute units; LF_{QT}, QTV power in the LF band expressed in absolute units; HF_{QT}, QTV power in the HF band expressed in absolute units. Results are presented as median with the interquartile range in round brackets. The symbol * indicates a $p < 0.05$ versus WI.*

TABLE 3 | Results of time and frequency domain analyses of RRV and QTV in WT rats classified as non-AGG and AGG animals.

Index	non-AGG	AGG
μ_{RR} (ms)	191.9 (7.27)	184.22 (11.4)
σ^2_{RR} (ms^2)	24.57 (4.83)	15.86 (12.84)
LF_{RR} (ms^2)	0.66 (0.24)	0.53 (0.45)
HF_{RR} (ms^2)	2.26 (1.71)	2.32 (2.89)
μ_{QT} (ms)	56.21 (4.2)	56.25 (1.9)
σ^2_{QT} (ms^2)	1.8 (1.37)	3.98 (7.5)*
LF_{QT} (ms^2)	0.3 (0.54)	0.67 (1.96)*
HF_{QT} (ms^2)	0.92 (0.78)	1.87 (4.59)

*WT, wild-type Groningen rats; non-AGG, non-aggressive WT rats; AGG, aggressive WT rats; LF, low frequency; HF, high frequency; RR, time interval between two consecutive QRS complexes; QT, time interval between the peak of the QRS complex and the T-wave offset; RRV, RR variability; QTV, QT variability; LF_{RR}, RRV power in the LF band expressed in absolute units; HF_{RR}, RRV power in the HF band expressed in absolute units; LF_{QT}, QTV power in the LF band expressed in absolute units; HF_{QT}, QTV power in the HF band expressed in absolute units. Results are presented as median with the interquartile range in round brackets. The symbol * indicates a $p < 0.05$ versus non-AGG.*

in normalized units (Pagani et al., 1986), is one of the most frequently exploited normalized RRV indexes. The attempts of normalizing frequency domain markers of RRV to achieve a more genuine marker of sympathetic control generated some controversies (Eckberg, 1997; Pagani et al., 1997; Billman, 2013; Reyes del Paso et al., 2013). Among the most controversial issues there is the non-zero value of normalized LF_{RR} power after full vagal blockade in presence of null RR changes and the strict link between normalized LF_{RR} and normalized HF_{RR} powers given that their sum is 100 (Eckberg, 1997). The final result is that no normalization procedure solved the original problem due to the inherent contribution of vagal limb to RRV in the LF band (Akselrod et al., 1981; Pomeranz et al., 1985). More recently, some studies on QTV have suggested the possibility of monitoring cardiac sympathetic control via markers extracted from QTV (Porta et al., 1998a, 2010; Berger, 2009; Malik, 2009; El-Hamad et al., 2015; Baumert et al., 2016) and have outlined the clinical relevance of this approach in pathological populations and risk stratification (Berger et al., 1997; Atiga et al., 1998; Baumert et al., 2008, 2011; Bari et al., 2014; Porta et al., 2015).

A pragmatic route to face the issue generated by the debate on the use of RRV markers in the frequency domain was made operational in Porta et al. (2015) who proposed the simultaneous exploitation of RRV and QTV to derive a frequency domain description of the cardiac vagal control via the HF_{RR} power and of the cardiac sympathetic control via the LF_{QT} power. The strategy proposed in Porta et al. (2015) was tested in this study in humans during an experimental protocol evoking sympathetic activation and vagal withdrawal (i.e., head-up tilt) and the progressive sympathetic regulation departure and vagal control rebound during recovery after the postural challenge (Montano et al., 1994; Cooke et al., 1999; Porta et al., 2011; Marchi et al., 2016) and in rats featuring documented differences in cardiac sympatho-vagal balance at baseline (Carnevali et al., 2013; Carnevali and Sgoifo, 2014). The present study outlines the ability of the simultaneous exploitation of the HF_{RR} and LF_{QT} markers in typifying state- and trait-related modifications of the cardiac autonomic regulation in human and animal experiments. In the human protocol the significant decrease of the HF_{RR} marker during T90 and the concomitant increase of LF_{QT} power suggest, respectively, a reduced vagal and an augmented sympathetic controls as it is expected in response to the postural challenge (Montano et al., 1994; Cooke et al., 1999; Porta et al., 2011; Marchi et al., 2016). The specific ability of the HF_{RR} marker in tracking the cardiac vagal control was emphasized by the particular design of the experimental protocol in humans considering the period of recovery after the postural challenge. Indeed, the greater cardiac vagal regulation regaining after T90 was stressed by the increase of the HF_{RR} power above the levels observed at REST. The independence of the LF_{QT} power from the level of cardiac vagal control was supported by the stable values of this index during recovery compared to REST, thus stressing the complementary information that can be derived from the joint use of HF_{RR} and LF_{QT} markers. The strategy proposing the concomitant use of HF_{RR} and LF_{QT} powers excludes the utilization of the LF_{RR} power due to its mixed nature and that of the HF_{QT} power due to its non-autonomic origin. The mixed origin of the LF_{RR} power is supported by the present study as well: indeed, the constancy of the LF_{RR} power as a function of the experimental condition in the head-up tilt protocol and the inability of the LF_{RR} power to distinguish non-AGG from AGG rats is in agreement with a simultaneous increase of sympathetic modulation and a decrease of the vagal one (Porta et al., 2011). The non-autonomic origin of the HF_{QT} power results from the observation that it is likely to be the consequence of the projection of cardiac axis movements due to respiration over a single lead given that it increased when assessed over Z lead compared to X and Y ones (Porta et al., 1998b) and it is present in subjects under cardiac pacing (Lombardi et al., 1996). The non-autonomic nature of the HF_{QT} power was supported by the present study as well: indeed, it is invariable in both human and animal protocols.

The proposed strategy has the inherent limitation of disregarding the dependence of QTV on RRV due to the well-known relation linking QT to the preceding RR (Bazett, 1929). However, the selection of spectral indexes computed in different frequency bands (i.e., HF_{RR} and LF_{QT} powers) should mitigate the effects of this dependence. Our result corroborates this observation given that in humans during R90 the HF_{RR} power increased compared to REST, while the LF_{QT} marker remained stable, and in rats only the LF_{QT} power was greater in the AGG group compared to the non-AGG one while the HF_{RR} power was unvaried. However, models of the dynamical dependence of QTV on RRV should be tested (Porta et al., 1998a, 2010) in future to understand whether some normalization procedure should be applied to better represent the genuine contribution of the sympathetic drive directed to the ventricles.

RRV and QTV Can Be Fruitfully Exploited for Cardiac Autonomic Characterization in Rats

To the best of our knowledge, this is the first study in which QTV analysis was carried out on rats with the aim at assessing cardiac autonomic control and QTV markers were discussed along with those derived from RRV analysis. This approach was successfully applied with the aim at differentiating WI and WT rats and divergent subpopulations within the WT strain. WI rats are highly domesticated, docile, and placid, while WT rats exhibit a more aggressive behavior during a social conflict (Buwalda et al., 2011) than WI rats. These differences in trait aggressiveness between the two strains are mirrored by a different state of the sympatho-vagal balance in unstressed conditions, with WT rats generally showing lower indexes of cardiac vagal modulation than WI counterparts (Carnevali and Sgoifo, 2014). Our results are in agreement with Carnevali and Sgoifo (2014) given that we found a lower HF_{RR} power in WT rats than in WI rats. The expected increase of the LF_{QT} marker, suggesting a higher sympathetic control in WT rats than in WI animals, was not found even though a tendency toward an increase of the LF_{QT} power was evident. Since in presence of an active sympatho-vagal balance it is expected that a significant increase of HF_{RR} power is associated to a significant decrease of the LF_{QT} one, the decrease of HF_{RR} power in WT animals in association with an unvaried LF_{QT} index might suggest a greater complexity of the interactions between vagal and sympathetic branches of the autonomic nervous system. Complex interactions between the two branches of the autonomic nervous system are known to lead to imbalanced situations in which a vagal withdrawal is not linked to a simultaneous and proportional sympathetic activation or *vice versa* (Porta et al., 2007) or situations featuring co-activation or co-inhibition of both the autonomic nervous system limbs (Kollai and Koizumi, 1979; Paton et al., 2005). These situations might lead to non-reciprocal trends in cardiac vagal and sympathetic controls (Kollai and Koizumi, 1979). The complexity of the sympatho-vagal interactions requires a more flexible tool that does not pretend to quantify cardiac autonomic control from a unique variability series like RRV-based analysis, but considers the joint observation of RRV and QTV as a mandatory standpoint for the reliable inference of autonomic nervous system state.

The relevance of the simultaneous assessment of RRV and QTV is even more evident when the WT rats were subdivided into non-AGG and AGG animals (de Boer et al., 2003). In previous studies, AGG rats were found to be characterized

by lower RRV markers in unstressed conditions compared to non-AGG rats, thus suggesting that the aggressive behavior is associated with a lower vagal control (Carnevali et al., 2013; Carnevali and Sgoifo, 2014). Such a low cardiac vagal modulation was associated with a higher arrhythmia susceptibility and a greater vulnerability to cardiac morbidity in the AGG group (Carnevali et al., 2013). Differences in resting autonomic modulation between AGG and non-AGG rats were not evident in the current study using the RRV markers given that the HF_{RR} power was similar, but they were unveiled by the QTV markers given that the LF_{QT} power was greater in AGG than in non-AGG rats. Therefore, our results suggest that the AGG rats are characterized by a higher resting sympathetic modulation that is not accompanied by a concomitant reduction of vagal modulation. This finding might be another evidence of the complexity of the cardiac control in rats where a high sympathetic drive does not imply by necessity a vagal withdrawal and further corroborates the need of an approach to the study of the cardiac autonomic control integrating different signals and not necessarily based on the concept of sympatho-vagal balance.

Time Domain RRV and QTV Parameters Versus Spectral RRV and QTV Markers

Time domain markers were commonly shown to provide the representation of the effect of a physiological challenge or an experimental maneuver on the cardiovascular system. For example, in our human protocol, the trend of the μ_{RR} suggests that the orthostatic challenge was effective because the reduction of the venous return due to posture modification provokes a tachycardic response in the attempt to prevent the arterial pressure drop (Montano et al., 1994; Cooke et al., 1999; Porta et al., 2011; Marchi et al., 2016). For example, in the same protocol the evolution of μ_{QT} suggests that the QT measures are reliable given that it is well-known that in humans μ_{QT} is shorter when μ_{RR} is reduced (Bazett, 1929). However, the limits of time domain measures in providing a complete picture appear evidently as well. For example, σ^2_{QT} was less powerful than the LF_{QT} power in describing the effect of the orthostatic challenge likely because non-autonomic effects resulting from cardiac axis movements synchronous with respiration (Porta et al., 1998b) are likely to influence more remarkably σ^2_{QT} than its portion in the LF band. For example, in non-AGG and AGG rats the μ_{RR} and μ_{QT} were similar, while the LF_{QT} power increased in the AGG group, thus stressing the non-redundant nature of time and frequency domain markers.

On the Use of Rats as an Animal Model of Human Cardiac Autonomic Control Explored via RRV and QTV Analyses

Rats are considered animals exhibiting a sympathetic dominance given that their intrinsic heart rate (i.e., the cardiac frequency under complete pharmacological autonomic blockade) is lower than the resting heart rate (Opthof, 2000). However, this observation does not imply that vagal control is absent. Indeed, the full muscarinic receptor blockade induced via a high dose of atropine dramatically reduced RRV (Japundzic et al., 1990; Cerutti et al., 1991; Silva et al., 2017), thus supporting the observation that changes of vagal activity contribute importantly to σ^2_{RR} and corroborating the use of these animals in translational studies on cardiac autonomic control. More importantly for the present study, rats respond differently to sympathetic stimulation: indeed, they show a QT prolongation, while in humans a QT shortening is observed (Conrath and Opthof, 2006; Speerschneider and Thomsen, 2013). The parallel changes of μ_{RR} and μ_{QT} reported in the present study in the human protocol and the opposite trends of μ_{RR} and μ_{QT} in WI and WT groups are in agreement with the diverse effect of an augmented sympathetic drive on μ_{RR} and μ_{QT} in humans and rats. In spite of this peculiarity, the RRV and QTV markers seem to maintain similar interpretation in both species. However, the lack of application of a stressor inducing a sympathetic activation in both WI and WT rats prevents us to deepen this issue.

Limitations of the Study and Future Developments

While our data support the association between QTV magnitude and sympathetic control, they are less informative about the shape of the relation between them. It is likely that the QTV could reflect mean sympathetic activity and its modifications about the mean when sympathetic drive is sufficiently high, while below a certain mean neural activity value QTV could be useless. We advocate pharmacological studies that could graduate the challenge in a finer manner and the contemporaneous direct recording of sympathetic activity to provide insight on the shape of this relation.

There is an open debate on the dependency of the magnitude of RRV and QTV on their means and on the need of some normalization (Sacha and Pluta, 2008; Sacha, 2013; Boyett et al., 2019; Malik et al., 2019). In the present study we tested the redundancy between QTV and μ_{QT} by calculating the normalized QT variance (QTVN), namely the ratio of the square QT standard deviation to the square μ_{QT} (Baumert et al., 2016). No difference was found either among experimental conditions in the human protocol or between groups in the animal protocol. This result might suggest a certain degree of dependency between QTV and μ_{QT}. However, the lack of significant differences is due to the enormous standard deviation of QTVN, sometimes close to two times the QTVN mean. This observation suggests some caution in using QTVN given that normalization procedure might behave differently at diverse values of μ_{QT} and the need of more deeply exploring the relation between QTV and μ_{QT}.

Since in rats the T-wave morphology is different from that in humans, due to the different shapes of the ventricular action potentials (Fabritz et al., 2010; Boukens et al., 2014), future studies should be focused on the comparison of methods based on a threshold on the first derivative (Laguna et al., 1990; Nollo et al., 1992; Porta et al., 1998b), on the tangent method taking the interception between the straight line at the steepest point of the T-wave downslope and the isoelectric line (Lepeschkin and Surawicz, 1952; Yamada et al., 1993; Porta et al., 1998b) and on template matching approach (Berger et al., 1997; Baumert et al., 2012).

CONCLUSION

In the present study, we computed frequency domain markers concurrently derived from RRV and QTV for a deeper characterization of the cardiac autonomic control. The power of RRV in the HF band and the power of QTV in the LF band were exploited to typify state- and trait-related modifications of the cardiac autonomic regulation in humans and rats. We found that the information derived from RRV and QTV spectral markers is not redundant given that trends of the HF power of RRV cannot be inferred from those of the LF power of QTV and vice versa. The complementary information was interpreted in relation to the inherent ability of RRV and QTV spectral markers to describe, respectively, cardiac vagal and sympathetic controls. Therefore, we conclude that the concomitant evaluation of RRV and QTV frequency domain markers can provide a more insightful view on cardiac autonomic function in both humans and rats than the sole exploitation of RRV indexes.

DATA AVAILABILITY STATEMENT

The datasets generated for this study are available on request to the corresponding author.

ETHICS STATEMENT

The studies involving human participants were reviewed and approved by the Human Research and Ethical Review Board of the L. Sacco Hospital, Milan, Italy. The patients/participants provided their written informed consent to participate in this study. The animal study was reviewed and approved by the Veterinarian Animal Care and Use Committee of the University of Parma, Parma, Italy.

AUTHOR CONTRIBUTIONS

AP conceived and designed the study. AS, LC, AMT, and AC performed the experiments. BM analyzed the data. BM and AP drafted the manuscript and prepared the figures. BM, VB, AS, LC, BC, EV, AMT, AC, LDV, and AP interpreted the results, edited and revised the manuscript, and approved the final version of the manuscript.

FUNDING

This work was partially supported by the Ricerca Corrente from the Ministry of Health, Italy.

REFERENCES

Akaike, H. (1974). A new look at the statistical novel identification. *IEEE Trans. Autom. Control* 19, 716–723. doi: 10.1109/tac.1974.1100705

Akselrod, S., Eliash, S., Oz, O., and Cohen, S. (1987). Hemodynamic regulation in SHR: investigation by spectral analysis. *Am. J. Physiol.* 253, H176–H183.

Akselrod, S., Gordon, D., Ubel, F. A., Shannon, D. C., Berger, A. C., and Cohen, R. J. (1981). Power spectrum analysis of heart rate fluctuation: a quantitative probe of beat-to-beat cardiovascular control. *Science* 213, 220–222. doi: 10.1126/science.6166045

Atiga, W. L., Calkins, H., Lawrence, J. H., Tomaselli, G. F., Smith, J. M., and Berger, R. D. (1998). Beat-to-beat repolarization lability identifies patients at risk for sudden cardiac death. *J. Cardiovasc. Electrophysiol.* 9:908.

Bar, K. J., Koschke, M., Boettger, M. K., Berger, S., Kabisch, A., Sauer, H., et al. (2007). Acute psychosis leads to increased QT variability in patients suffering from schizophrenia. *Schizophr. Res.* 95, 115–123. doi: 10.1016/j.schres.2007.05.034

Bari, V., Valencia, J. F., Vallverdú, M., Girardengo, G., Marchi, A., Bassani, T., et al. (2014). Multiscale complexity analysis of the cardiac control identifies asymptomatic and symptomatic patients in long QT syndrome type 1. *PLoS One* 9:e93808. doi: 10.1371/journal.pone.0093808

Baselli, G., Porta, A., Rimoldi, O., Pagani, M., and Cerutti, S. (1997). Spectral decomposition in multichannel recordings based on multi-variate parametric identification. *IEEE Trans. Biomed. Eng.* 44, 1092–1101. doi: 10.1109/10.641336

Baumert, M., Porta, A., Vos, M. A., Malik, M., Couderc, J. P., Laguna, P., et al. (2016). QT interval variability in body surface ECG: measurement, physiological basis, and clinical value: position statement and consensus guidance endorsed by the european heart rhythm association jointly with the esc working group on cardiac cellular electrophysiology. *Europace* 186, 925–944. doi: 10.1093/europace/euv405

Baumert, M., Lambert, G. W., Dawood, T., Lambert, E. A., Esler, M. D., McGrane, M., et al. (2008). QT interval variability and cardiac norepinephrine spillover in patients with depression and panic disorder. *Am. J. Physiol.* 295, H962–H968. doi: 10.1152/ajpheart.00301.2008

Baumert, M., Schlaich, M. P., Nalivaiko, E., Lambert, E., Sari, C. I., Kaye, D. M., et al. (2011). Relation between QT interval variability and cardiac sympathetic activity in hypertension. *Am. J. Physiol.* 300, H1412–H1417.

Baumert, M., Starc, V., and Porta, A. (2012). Conventional QT variability measurement vs. template matching techniques: comparison of performance using simulated and real ECG. *PLoS One* 7:e41920. doi: 10.1371/journal.pone.0041920

Bazett, H. C. (1929). An analysis of the time-relations of electrocardiograms. *Heart* 7, 353–370.

Berger, R. D. (2009). QT Interval variability: is it a measure of autonomic activity? *J. Am. Coll. Cardiol.* 54, 821–852.

Berger, R. D., Kasper, E. K., Baughman, K. L., Marban, E., Calkins, H., and Tomaselli, G. F. (1997). Beat-to-beat QT interval variability: novel evidence for repolarization lability in ischemic and nonischemic dilated cardiomyopathy. *Circulation* 96, 1557–1565. doi: 10.1161/01.cir.96.5.1557

Billman, G. E. (2013). The LF/HF ratio does not accurately measure cardiac sympatho-vagal balance. *Front. Physiol.* 4:26. doi: 10.3389/fphys.2013.00026

Boukens, B. J., Rivaud, M. R., Rentschler, S., and Coronel, R. (2014). Misinterpretation of the mouse ECG: 'musing the waves of Mus musculus'. *J. Physiol.* 592, 4613–4626. doi: 10.1113/jphysiol.2014.279380

Boyett, M., Wang, Y., and D'Souza, A. (2019). CrossTalk opposing view: heart rate variability as a measure of cardiac autonomic responsiveness is fundamentally flawed. *J. Physiol.* 597, 2599–2601. doi: 10.1113/jp277501

Malik, M., Hnatkova, K., Huikuri, H. V., Lombardi, F., Schmidt, G., and Zabel, M. (2019). CrossTalk proposal: heart rate variability is a valid measure of cardiac autonomic responsiveness. *J. Physiol.* 597, 2595–2598. doi: 10.1113/jp277500

Brenner, I. K., Thomas, S., and Shephard, R. J. (1997). Spectral analysis of heart rate variability during heat exposure and repeated exercise. *Eur. J. Appl. Physiol. Occup. Physiol.* 76, 145–156. doi: 10.1007/s004210050227

Buwalda, B., Geerdink, M., Vidal, J., and Koolhaas, J. M. (2011). Social behavior and social stress in adolescence: a focus on animal models. *Neurosci. Biobehav. Rev.* 35, 1713–1721. doi: 10.1016/j.neubiorev.2010.10.004

Carnevali, L., and Sgoifo, A. (2014). Vagal modulation of resting heart rate in rats: the role of stress, psychosocial factors, and physical exercise. *Front. Physiol.* 5:118. doi: 10.3389/fphys.2014.00118

Carnevali, L., Trombini, M., Porta, A., Montano, N., de Boer, S. F., and Sgoifo, A. (2013). Vagal withdrawal and susceptibility to cardiac arrhythmias in rats with high trait aggressiveness. *PLoS One* 87:e68316. doi: 10.1371/journal.pone.0068316

Cerutti, C., Gustin, M. P., Paultre, C. Z., Lo, M., Julien, C., Vincent, M., et al. (1991). Autonomic nervous system and cardiovascular variability in rats: a spectral analysis approach. *Am. J. Physiol.* 261, H1292–H1299.

Conrath, C. E., and Opthof, T. (2006). Ventricular repolarization: an overview of (patho)physiology, sympathetic effects and genetic aspects. *Prog. Biophys. Mol. Biol.* 92, 269–307. doi: 10.1016/j.pbiomolbio.2005.05.009

Cooke, W. H., Hoag, J. B., Crossman, A. A., Kuusela, T. A., Tahvanainen, K. U. O., and Eckberg, D. L. (1999). Human responses to upright tilt: a window on central autonomic integration. *J. Physiol.* 517, 617–628. doi: 10.1111/j.1469-7793.1999.0617t.x

de Boer, S. F., van der Vegt, B. J., and Koolhaas, J. M. (2003). Individual variation in aggression of feral rodent strains: a standard for the genetics of aggression and violence? *Behav. Genet.* 33, 485–501.

Eckberg, D. L. (1997). Sympathovagal balance: a critical appraisal. *Circulation* 96, 3224–3232. doi: 10.1161/01.cir.96.9.3224

El-Hamad, F., Lambert, E., Abbott, D., and Baumert, M. (2015). Relation between QT interval variability and muscle sympathetic nerve activity in normal subjects. *Am. J. Physiol.* 309, H1218–H1224. doi: 10.1152/ajpheart.00230.2015

Fabritz, L., Damke, D., Emmerich, M., Kaufmann, S. G., Theis, K., Blana, A., et al. (2010). Autonomic modulation and antiarrhythmic therapy in a model of long QT syndrome type 3. *Cardiovasc. Res.* 87, 60–72. doi: 10.1093/cvr/cvq029

Hirsch, J. A., and Bishop, B. (1981). Respiratory sinus arrhythmia in humans: how breathing pattern modulates heart rate. *Am. J. Physiol.* 241, H620–H629.

Jaenisch, R. B., Hentschke, V. S., Quagliotto, E., Cavinato, P. R., Schmeing, L., Xavier, L. L., et al. (2011). Respiratory muscle training improves hemodynamics, autonomic function, baroreceptor sensitivity, and respiratory mechanics in rats with heart failure. *J. Appl. Physiol.* 111, 1664–1670. doi: 10.1152/japplphysiol.01245.2010

Japundzic, N., Grichois, M. L., Zitoun, P., Laude, D., and Elghozi, J. L. (1990). Spectral analysis of blood pressure and heart rate in conscious rats: effects of autonomic blockers. *J. Auton. Nerv. Syst.* 30, 91–100. doi: 10.1016/0165-1838(90)90132-3

Kay, S. M., and Marple, S. L. (1981). Spectrum analysis: a modern perspective. *Proc. IEEE* 69, 1380–1418.

Kollai, M., and Koizumi, K. (1979). Reciprocal and non-reciprocal action of the vagal and sympathetic nerves innervating the heart. *J. Auton. Nerv. Syst.* 1, 33–52. doi: 10.1016/0165-1838(79)90004-3

Laguna, P., Thakor, N. V., Caminal, P., Jane, R., Yoon, H. R., Bayes de Luna, A., et al. (1990). New algorithm for QT interval analysis in 24-hour Holter ECG: performance and applications. *Med. Biol. Eng. Comput.* 281, 67–73. doi: 10.1007/bf02441680

Lepeschkin, E., and Surawicz, B. (1952). The measurement of the Q-T interval of the electrocardiogram. *Circulation* 6, 378–388. doi: 10.1161/01.cir.6.3.378

Lombardi, F., Sandrone, G., Porta, A., Torzillo, D., Terranova, G., Baselli, G., et al. (1996). Spectral analysis of short term R-Tapex interval variability during sinus rhythm and fixed atrial rate. *Eur. Heart J.* 17, 769–778. doi: 10.1093/oxfordjournals.eurheartj.a014945

Magagnin, V., Bassani, T., Bari, V., Turiel, M., Maestri, R., Pinna, G. D., et al. (2011). Non-stationarities significantly distort short-term spectral, symbolic and entropy heart rate variability indexes. *Physiol. Meas.* 32, 1775–1786. doi: 10.1088/0967-3334/32/11/s05

Malik, M. (2009). Beat-to-beat QT variability and cardiac autonomic regulation. *Am. J. Physiol.* 295, H923–H925.

Marchi, A., Bari, V., De Maria, B., Esler, M., Lambert, E., Baumert, M., et al. (2016). Calibrated variability of muscle sympathetic nerve activity during graded head-up tilt in humans and its link with noradrenaline data and cardiovascular rhythms. *Am J. Physiol.* 310, R1134–R1143. doi: 10.1152/ajpregu.00541.2015

Montano, N., Gnecchi-Ruscone, T., Porta, A., Lombardi, F., Pagani, M., and Malliani, A. (1994). Power spectrum analysis of heart rate variability to assess changes in sympatho-vagal balance during graded orthostatic tilt. *Circulation* 90, 1826–1831. doi: 10.1161/01.cir.90.4.1826

Nollo, G., Speranza, G., Grasso, R., Bonamini, R., Mangiardi, L., and Antolini, R. (1992). Spontaneous beat-to-beat variability of the ventricular repolarisation duration. *J. Electrocardiol.* 25, 9–17. doi: 10.1016/0022-0736(92)90124-i

Opthof, T. (2000). The normal range and determinants of the intrinsic heart rate in man. *Cardiovasc. Res.* 45, 177–184. doi: 10.1016/s0008-6363(99)00322-3

Pagani, M., Lombardi, F., Guzzetti, S., Rimoldi, O., Furlan, R., Pizzinelli, P., et al. (1986). Power spectral analysis of heart rate and arterial pressure variabilities as a marker of sympatho-vagal interaction in man and conscious dog. *Circ. Res.* 59, 178–193. doi: 10.1161/01.res.59.2.178

Pagani, M., Montano, N., Porta, A., Malliani, A., Abboud, F. M., Birkett, C., et al. (1997). Relationship between spectral components of cardiovascular variabilities and direct measures of muscle sympathetic nerve activity in humans. *Circulation* 95, 1441–1448. doi: 10.1161/01.cir.95.6.1441

Paton, J. F., Boscan, P., Pickering, A. E., and Nalivaiko, E. (2005). The yin and yang of cardiac autonomic control: vago-sympathetic interactions revisited. *Brain Res. Rev.* 49, 555–565. doi: 10.1016/j.brainresrev.2005.02.005

Piccirillo, G., Cacciafesta, M., Lionetti, M., Nocco, M., Di Giuseppe, V., Moisé, A., et al. (2001). Influence of age, the autonomic nervous system and anxiety on QT-interval variability. *Clin. Sci.* 101, 429–438. doi: 10.1042/cs10010429

Piccirillo, G., Magnanti, M., Matera, S., Di Carlo, S., De Laurentis, T., Torrini, A., et al. (2006). Age and QT variability index during free breathing, controlled breathing and tilt in patients with chronic heart failure and healthy control subjects. *Transl. Res.* 142, 72–78. doi: 10.1016/j.trsl.2006.02.001

Pomeranz, B., Macaulay, R. J. B., Caudill, M. A., Kutz, I., Adam, D., Gordon, D., et al. (1985). Assessment of autonomic function in humans by heart-rate spectral-analysis. *Am. J. Physiol.* 248, H151–H153.

Porta, A., Bari, V., Badilini, F., Tobaldini, E., Gnecchi-Ruscone, T., and Montano, N. (2011). Frequency domain assessment of the coupling strength between ventricular repolarization duration and heart period during graded head-up tilt. *J. Electrocardiol.* 44, 662–668. doi: 10.1016/j.jelectrocard.2011.08.002

Porta, A., Bari, V., De Maria, B., Cairo, B., Vaini, E., Malacarne, M., et al. (2018). Peripheral resistance baroreflex during incremental bicycle ergometer exercise: characterization and correlation with cardiac baroreflex. *Front. Physiol.* 9:688. doi: 10.3389/fphys.2018.00688

Porta, A., Baselli, G., Caiani, E., Malliani, A., Lombardi, F., and Cerutti, S. (1998a). Quantifying electrocardiogram RT-RR variability interactions. *Med. Biol. Eng. Comput.* 36, 27–34. doi: 10.1007/bf02522854

Porta, A., Baselli, G., Lombardi, F., Cerutti, S., Antolini, R., Del Greco, M., et al. (1998b). Performance assessment of standard algorithms for dynamic R-T interval measurement: comparison between R-Tapex and R-Tend approach. *Med. Biol. Eng. Comput.* 36, 35–42. doi: 10.1007/bf02522855

Porta, A., Girardengo, G., Bari, V., George, A. L. Jr., Brink, P. A., Goosen, A., et al. (2015). Autonomic control of heart rate and QT interval variability influences arrhythmic risk in long QT syndrome type I. *J. Am. Coll. Cardiol.* 65, 367–374. doi: 10.1016/j.jacc.2014.11.015

Porta, A., Tobaldini, E., Gnecchi-Ruscone, T., and Montano, N. (2010). RT variability unrelated to heart period and respiration progressively increases during graded head-up tilt. *Am. J. Physiol.* 298, H1406–H1414. doi: 10.1152/ajpheart.01206.2009

Porta, A., Tobaldini, E., Guzzetti, S., Furlan, R., Montano, N., and Gnecchi-Ruscone, T. (2007). Assessment of cardiac autonomic modulation during graded head-up tilt by symbolic analysis of heart rate variability. *Am. J. Physiol.* 293, H702–H708.

Reyes del Paso, G. A., Langewitz, W., Mulder, L. J., van Roon, A., and Duschek, S. (2013). The utility of low frequency heart rate variability as an index of sympathetic cardiac tone: a review with emphasis on a reanalysis of previous studies. *Psychophysiology* 50, 477–487. doi: 10.1111/psyp.12027

Rubini, R., Porta, A., Baselli, G., Cerutti, S., and Paro, M. (1993). Power spectrum analysis of cardiovascular variability monitored by telemetry in conscious unrestrained rats. *J. Auton. Nerv. Syst.* 45, 181–190. doi: 10.1016/0165-1838(93)90050-5

Sacha, J. (2013). Why should one normalize heart rate variability with respect to average heart rate. *Front. Physiol.* 4:306. doi: 10.3389/fphys.2013.00306

Sacha, J., and Pluta, W. (2008). Alterations of an average heart rate change heart rate variability due to mathematical reasons. *Int. J. Cardiol.* 128, 444–447. doi: 10.1016/j.ijcard.2007.06.047

Sgoifo, A., De Boer, S. F., Buwalda, B., Korte-Bouws, G., Tuma, J., Bohus, B., et al. (1998). Vulnerability to arrhythmias during social stress in rats with different

sympathovagal balance. *Am. J. Physiol.* 275, H460–H466. doi: 10.1152/ajpheart.1998.275.2.H460

Sgoifo, A., Koolhaas, J., De Boer, S., Musso, E., Stilli, D., Buwalda, B., et al. (1999). Social stress, autonomic neural activation, and cardiac activity in rats. *Neurosci. Biobehav. Rev.* 237, 915–923. doi: 10.1016/s0149-7634(99)00025-1

Shin, K., Minamitani, H., Onishi, S., Yamazaki, H., and Lee, M. (1995a). The power spectral analysis of heart rate variability in athletes during dynamic exercise - Part I. *Clin. Cardiol.* 18, 583–586. doi: 10.1002/clc.4960181011

Shin, K., Minamitani, H., Onishi, S., Yamazaki, H., and Lee, M. (1995b). The power spectral analysis of heart rate variability in athletes during dynamic exercise - Part II. *Clin. Cardiol.* 18, 664–668. doi: 10.1002/clc.4960181114

Silva, L. E. V., Lataro, R. M., Castania, J. A., da Silva, C. A. A., Valencia, J. F., Murta, L. O. Jr., et al. (2016). Multiscale entropy analysis of heart rate variability in heart failure, hypertensive and sinoaortic-denervated rats: classical and refined approaches. *Am. J. Physiol.* 310, R150–R156. doi: 10.1152/ajpregu.00076.2016

Silva, L. E. V., Rezende Geraldini, V., Potratz de Oliveira, B., Aguiar Silva, C. A., Porta, A., and Fazan, R. (2017). Comparison between spectral analysis and symbolic dynamics for heart rate variability analysis in the rat. *Sci. Rep.* 7:8428. doi: 10.1038/s41598-017-08888-w

Speerschneider, T., and Thomsen, M. B. (2013). Physiology and analysis of the electrocardiographic T wave in mice. *Acta Physiol.* 209, 262–271. doi: 10.1111/apha.12172

Speranza, G., Nollo, G., Ravelli, F., and Antolini, R. (1993). Beat-to-beat measurement and analysis of the R-T interval in 24 h ECG Holter recordings. *Med. Biol. Eng. Comput.* 315, 487–494. doi: 10.1007/bf02441984

Stauss, H. M., Persson, P. B., Johnson, A. K., and Kregel, K. C. (1997). Frequency response characteristics of autonomic nervous system function in conscious rats. *Am. J. Physiol.* 273, H786–H795.

Task Force of the European Society of Cardiology and the North American Society of Pacing and Electrophysiology, (1996). Heart rate variability. Standards of measurement, physiological interpretation, and clinical use. *Eur. Heart. J.* 17, 354–381. doi: 10.1093/oxfordjournals.eurheartj.a014868

Yamada, A., Hayano, J., Horie, K., Ieda, K., Mukai, S., Yamada, M., et al. (1993). Regulation of QT interval during postural transitory changes in heart rate in normal subjects. *Am. J. Cardiol.* 71, 996–998. doi: 10.1016/0002-9149(93)90922-y

Yeragani, V. K., Pohl, R., Jampala, V. C., Balon, R., Kay, J., and Igel, G. (2000a). Effect of posture and isoproterenol on beat-to-beat heart rate and QT variability. *Neuropsychobiology* 41, 113–123. doi: 10.1159/000026642

Yeragani, V. K., Pohl, R., Jampala, V. C., Balon, R., Ramesh, C., and Srinivasan, K. (2000b). Increased QT variability in patients with panic disorder and depression. *Psychiatry Res.* 93, 225–235. doi: 10.1016/s0165-1781(00)00119-0

Conflict of Interest: The authors declare that the research was conducted in the absence of any commercial or financial relationships that could be construed as a potential conflict of interest.

frontiers in Physiology

ORIGINAL RESEARCH
published: 29 November 2019
doi: 10.3389/fphys.2019.01465

The Effect of Emotional Valence on Ventricular Repolarization Dynamics Is Mediated by Heart Rate Variability: A Study of QT Variability and Music-Induced Emotions

Michele Orini[1,2], Faez Al-Amodi[1], Stefan Koelsch[3] and Raquel Bailón[4,5]*

[1] *Institute of Cardiovascular Sciences, University College London, London, United Kingdom,* [2] *The William Harvey Research Institute, Queen Mary University of London, London, United Kingdom,* [3] *Department of Biological and Medical Psychology, University of Bergen, Bergen, Norway,* [4] *Aragon Institute for Engineering Research, University of Zaragoza, Zaragoza, Spain,* [5] *Center for Biomedical Research in the Network in Bioengineering, Biomaterials and Nanomedicine (CIBER-BBN), Madrid, Spain*

OPEN ACCESS

Edited by:
Ademuyiwa S. Aromolaran, Masonic Medical Research Institute, United States

Reviewed by:
Leonardo Roever, Federal University of Uberlândia, Brazil
John Pearce Morrow, Columbia University, United States

***Correspondence:**
Michele Orini
m.orini@ucl.ac.uk;
michele.orini.maculotti@gmail.com

Specialty section:
This article was submitted to Cardiac Electrophysiology, a section of the journal Frontiers in Physiology

Received: *19 September 2019*
Accepted: *14 November 2019*
Published: *29 November 2019*

Citation:
Orini M, Al-Amodi F, Koelsch S and Bailón R (2019) The Effect of Emotional Valence on Ventricular Repolarization Dynamics Is Mediated by Heart Rate Variability: A Study of QT Variability and Music-Induced Emotions. Front. Physiol. 10:1465. doi: 10.3389/fphys.2019.01465

Background: Emotions can affect cardiac activity, but their impact on ventricular repolarization variability, an important parameter providing information about cardiac risk and autonomic nervous system activity, is unknown. The beat-to-beat variability of the QT interval (QTV) from the body surface ECG is a non-invasive marker of repolarization variability, which can be decomposed into QTV related to RR variability (QTVrRRV) and QTV unrelated to RRV (QTVuRRV), with the latter thought to be a marker of intrinsic repolarization variability.

Aim: To determine the effect of emotional valence (pleasant and unpleasant) on repolarization variability in healthy volunteers by means of QTV analysis.

Methods: 75 individuals (24.5 ± 3.2 years, 36 females) without a history of cardiovascular disease listened to music-excerpts that were either felt as pleasant (n = 6) or unpleasant (n = 6). Excerpts lasted about 90 s and were presented in a random order along with silent intervals (n = 6). QTV and RRV were derived from the ECG and the time-frequency spectrum of RRV, QTV, QTVuRRV and QTVrRRV as well as time-frequency coherence between QTV and RRV were estimated. Analysis was performed in low-frequency (LF), high frequency (HF) and total spectral bands.

Results: The heart rate-corrected QTV showed a small but significant increase from silence (median 347/interquartile range 31 ms) to listening to music felt as unpleasant (351/30 ms) and pleasant (355/32 ms). The dynamic response of QTV to emotional valence showed a transient phase lasting about 20 s after the onset of each musical excerpt. QTV and RRV were highly correlated in both HF and LF (mean coherence ranging 0.76–0.85). QTV and QTVrRRV decreased during listening to music felt as pleasant and unpleasant with respect to silence and further decreased during listening to music felt as pleasant. QTVuRRV was small and not affected by emotional valence.

Conclusion: Emotional valence, as evoked by music, has a small but significant effect on QTV and QTVrRRV, but not on QTVuRRV. This suggests that the interaction between emotional valence and ventricular repolarization variability is mediated by cycle length dynamics and not due to intrinsic repolarization variability.

Keywords: QT variability, heart rate variability, repolarization, music-induced emotions, emotional valence, time-frequency

INTRODUCTION

The beat to beat variability of the QT interval (QTV) of the electrocardiogram is an established measure of ventricular repolarization dynamics and a marker of both cardiovascular risk and cardiac autonomic modulation (Baumert et al., 2016). Since the QTV correlates with the cardiac cycle length through cardiac restitution properties (Orini et al., 2016), QTV is largely affected by RR variability (RRV), which reflects supra-ventricular as opposed to ventricular dynamics. A methodology that separates QTV into two components, one related to RRV and the other unrelated to RRV and thought to represent intrinsic repolarization variability, has been recently proposed (Orini et al., 2018).

Emotions are known to be associated with changes in cardiac function, mediated by the autonomic nervous system. These changes include parameters such as heart rate, heart rate variability and respiration (Steptoe and Brydon, 2009; Steptoe and Kivimäki, 2012). In some studies, emotions have been linked to increased risk of malignant arrhythmias and cardiovascular diseases (Taggart et al., 2011a,b), in particular when related to stress (Steptoe and Kivimäki, 2012). Emotions can be measured along two dimensions: intensity (arousal) and valence (attractiveness versus averseness), with the former exerting a stronger effect on physiological parameters (Hilz et al., 2014). The impact of emotional valence on cardiac repolarization is unknown.

This study investigates for the first time the dynamic interactions between emotional valence and QTV in healthy volunteers, and sought to determine whether the QTV response reflects intrinsic ventricular repolarization dynamics or is mediated by RRV. As in previous studies (Orini et al., 2010; Krabs et al., 2015), emotional states with opposite valence (pleasantness and unpleasantness) were induced by listening to pleasant or noise-like unpleasant music, while silence was used as a baseline control.

MATERIALS AND METHODS

Experimental Set-Up

The experimental set-up was described in details in previous studies (Orini et al., 2010; Krabs et al., 2015) and examples of the acoustic stimuli can be found in Krabs et al. (2015). Briefly, 75 volunteers (age 24.5 $\pm$ 3.2 years, 36 female) listened to acoustic stimuli through headphones at a comfortable loudness of around 60 dB in supine position with closed eyes. Participants were exposed to: (1) Six excerpts of pleasant joyful instrumental music (pleasant condition). (2) Six excerpts of isochronous Shepard tones. (3) Six excerpts of isochronous Shepard tones overlaid with unpleasant dissonant music-like noise (unpleasant condition). These were electronically created by recording backward a modified version of the pleasant excerpts, previously simultaneously recorded one semitone above and a tritone below the original pitch. (4) Six intervals of silence (resting condition). All excerpts and intervals of silence lasted about 90 s and were presented in the same randomized order (an example will be described in the "Results" section). All excerpts were matched by tempo and volume in an attempt to control for emotional arousal. Successive excerpts were separated by a 20 s pause during which participants were requested to rate how they felt by pressing response buttons (participants were asked to rate their own emotional state on a six point scale from 1, "very pleasant" to 6, "very unpleasant"). To ensure that participants paid equal attention to all excerpts, they were instructed to listen carefully and to tap the meter of the stimuli with their right index finger. No tapping was required during the resting condition. The study was approved by the ethics committee of the University of Leipzig. Written informed consent was obtained from all participants.

ECG Analysis

Standard 12 lead electrocardiograms were measured using a 32 MREFA amplifier (Twente Medical Systems, Enschede, Netherlands) and digitized with a sampling rate of 1000 Hz. For the sake of this study, lead V4 was analyzed to derive the main results while lead II was used to assess intra-lead reproducibility. This was chosen because lead V4 usually shows tall R- and T-waves and was therefore assumed to be characterized by high signal-to-noise ratio (Baumert et al., 2016), whereas lead II is one of the most clinically relevant and most widely used lead. The data were analyzed off-line using MATLAB, MathWorks. The peak of the R-wave and the end of the T-wave were detected, with the latter measured using the tangent method (**Figure 1**). The RT interval was used as a robust estimate of the QTV, which is particularly suitable for analysis of beat to beat variability. In fact, QT and RT variabilities are expected to be very similar, because the beat-to-beat variability of the QRS duration in sinus rhythm in healthy volunteers is negligible, and RT measurement is more robust than QT measurement as the identification of the R-wave peak is easier than the identification of QRS onset. All recordings were revised. Artifacts and ectopic beats were rare and were corrected using a bespoke graphical user interface as in previous studies (Orini et al., 2016, 2017b).

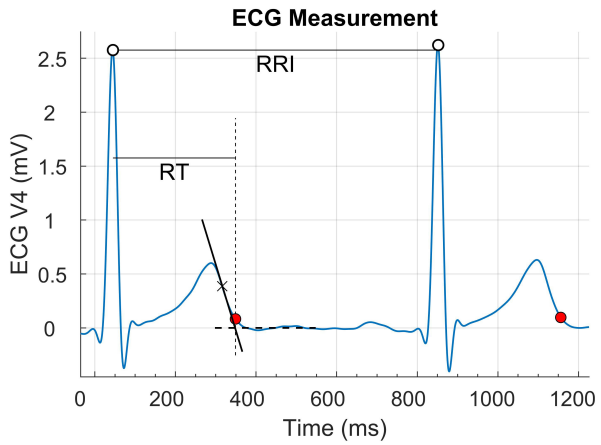

FIGURE 1 | Measurement of RR and QT intervals. White and red circles identify the R-wave and the end of the T-wave, respectively. The RT interval variability was used as robust surrogate for QT variability.

QTV and HRV Analysis

Time series were evenly resampled at 4 Hz. Time-frequency distributions were used to study the time course of the signals' spectral components and overcome the limitations of traditional spectral analysis in non-stationary conditions (Cohen, 1989; Hlawatsch and Boudreaux-Bartels, 1992). The Wigner-Ville distribution of RRV and QTV signals were filtered using a kernel designed to provide the minimum amount of time-frequency smoothing while achieving complete elimination of crossterms and time-frequency coherence bounded between zero and one (Orini et al., 2012c,d). Temporal and spectral resolutions were 12.5 s and 0.039 Hz, respectively. The time-frequency coherence between QTV and RRV was computed using previously described algorithms (Orini et al., 2012c). This time-frequency representation provides an assessment of the local linear coupling between the signals' spectral components in both time and frequency. It ranges from zero to one, and it is equal to one for a given time, t_0, and frequency, f_0, if at time t_0 the two signals show an oscillation with same instantaneous frequency f_0. The time-frequency spectrum of QTV was separated into two components, one representing QTV related to RRV (QTVrRRV) and the other representing QTV unrelated to RRV (QTVuRRV). This was achieved by modulating the time-frequency spectrum of QTV, $S_{QT}(t,f)$, by the time-frequency coherence between QTV and RRV, $\gamma_{QTV,RV}(t,f)$ as demonstrated in Orini et al. (2018):

$$S_{QTVuRR}(t,f) = S_{QTV}(t,f) - S_{QTVrRRV}(t,f) = \left(1 - \left|\gamma_{QTV,RRV}(t,f)\right|^2\right) S_{QTV}(t,f)$$

The time course of the magnitude of low frequency (LF) and high frequency (HF) oscillations were obtained by averaging the time-frequency distributions in the LF (0.04–0.15 Hz) and HF (0.15–0.4) spectral bands. The time course of the total signals' magnitude was obtained by averaging the time-frequency distributions in the spectral band (0.04–0.4 Hz).

Statistical Analysis

ECG recordings from five individuals were discarded due to insufficient signal quality.

To assess physiological changes between different conditions, pair-wise comparisons were performed using the Wilcoxon signed-rank test for related samples. 18 physiological indices were considered (see **Table 1**). For each one of them, the temporal mean was obtained in 50 s long temporal windows starting 20 s after the onset of a given condition to exclude the transient occurring immediately after the condition's onset (Orini et al., 2010). This provided a single value for each one of the 24 epochs (6 different excerpts × 4 conditions). Values corresponding to the same condition (i.e., pleasant, unpleasant, rest, and Shepard tones) were grouped and averaged to provide a single value per condition per individual. Mathematically, this is described as:

$$X_i^C = \frac{1}{T \times R} \sum_{j=1}^{6} \overline{X_i^{C,j}}$$

where X_i^C is a scalar representing a given physiological index X for the individual $i = \{1 : N\}$ during condition $C = \{Pleasant, Unpleasant, Rest, Shepard\}$ obtained by averaging the tempotal mean $\overline{X_i^{C,j}}$ across epochs j.

For the sake of this study, the condition characterized by Shepard tones was not considered and comparisons were performed between pleasant, unpleasant and resting conditions. In total, 54 pairwise tests were performed (5 time-frequency indices × 3 spectral bands × 3 comparisons + 3 time invariant indices × 3 comparisons). Threshold for significance was set at $P < 9.26 \times 10^{-4}$ after Bonferroni correction.

RESULTS

There was agreement between the participants' ratings, with all participants rating the consonant excerpts as more pleasant than the dissonant ones (see **Supplementary Figure S1**). On a scale from 1 (very pleasant) to 6 (very unpleasant), ratings were equal to (median, 1st–3rd quartiles): 2.4, 1.9–2.9 for silence, 1.8, 1.7–2.2 for pleasant music, 4.7, 4.2–5.2 for noise-like unpleasant music and 4.1, 3.54.5 for Shepard's tones. All comparisons were highly significant after Bonferroni correction ($P < 5 \times 10^{-6}$, Wilcoxon signed-rank test).

A representative example of temporal fluctuations in QT and RR intervals during the entire procedure is shown in **Figure 2**, where vertical dashed lines represent different epochs. As shown in the inset at the bottom of the figure, QT and RR exhibit similar oscillations and they were therefore characterized by a high level of time-frequency coherence.

Detailed results, including median and interquartile range of all physiological parameters as well as P-values for all 54 pair-wise comparisons, are shown in **Table 1**.

TABLE 1 | Median (interquartile range) of cardiac parameters during rest, pleasant, and unpleasant conditions evaluated within the stable phase (20–70 s after the onset of excerpts) are shown on the left.

	Rest	Pleasant	Unpleasant	Rest vs. pleasant	Rest vs. unpleasant	Pleasant vs. unpleasant
RR	878 (163)	835 (182)	864 (179)	**2.11E-10**	**8.00E-10**	**3.62E-04**
QT	333 (37)	328 (36)	329 (35)	**5.30E-08**	**4.31E-09**	9.80E-01
QTc	347 (31)	355 (32)	351 (30)	**9.02E-11**	**8.76E-10**	**5.24E-07**
QTV-LF	0.73 (0.62)	0.56 (0.50)	0.56 (0.47)	**1.28E-05**	6.28E-03	6.28E-03
QTV-HF	0.95 (1.04)	0.67 (0.87)	0.74 (0.89)	**9.27E-08**	**3.80E-06**	**8.92E-05**
QTV-TOT	1.88 (1.72)	1.31 (1.20)	1.45 (1.28)	**2.98E-07**	**2.02E-05**	**1.80E-04**
RRV-LF	577 (583)	289 (371)	363 (357)	**3.99E-08**	**4.36E-06**	**2.22E-05**
RRV-HF	558 (684)	224 (326)	345 (419)	**3.45E-11**	**8.76E-10**	**5.08E-10**
RRV-TOT	1226 (1235)	518 (801)	763 (842)	**2.01E-10**	**1.75E-08**	**1.31E-08**
QTVuRRV-LF	0.11 (0.08)	0.10 (0.10)	0.11 (0.09)	4.78E-02	1.95E-01	9.63E-02
QTVuRRV-HF	0.17 (0.14)	0.17 (0.17)	0.17 (0.17)	3.09E-01	2.70E-01	9.97E-01
QTVuRRV-TOT	0.31 (0.20)	0.28 (0.25)	0.27 (0.25)	7.17E-01	7.11E-01	5.98E-01
QTVrRRV-LF	0.59 (0.50)	0.42 (0.32)	0.48 (0.36)	**9.13E-07**	1.07E-02	3.05E-03
QTVrRRV-HF	0.68 (0.97)	0.46 (0.61)	0.58 (0.67)	**5.08E-10**	**1.13E-07**	**2.50E-06**
QTVrRRV-TOT	1.54 (1.49)	1.04 (0.94)	1.16 (1.11)	**6.35E-09**	**6.35E-06**	**2.22E-05**
Cohe-LF	0.87 (0.10)	0.84 (0.11)	0.85 (0.07)	9.82E-03	4.84E-01	3.82E-02
Cohe-HF	0.80 (0.13)	0.76 (0.17)	0.77 (0.14)	**1.61E-07**	**2.19E-04**	**1.65E-04**
Cohe-TOT	0.81 (0.11)	0.78 (0.14)	0.79 (0.11)	**3.60E-07**	1.07E-03	**1.70E-04**

P-values of pairwise tests (signed rank Wilcoxon test) are shown on the right, with P-values lower than the Bonferroni-corrected threshold reported in bold. RR: R-R interval; QT: QT interval; QTc: heart rate corrected QT; LF, HF, and TOT: low-frequency, high-frequency, and total spectral bands; QTV and RRV: QT and RR variability, respectively; QTVrRRV and QTVuRRV: QTV related and unrelated to RRV, respectively. Cohe: time-frequency coherence.

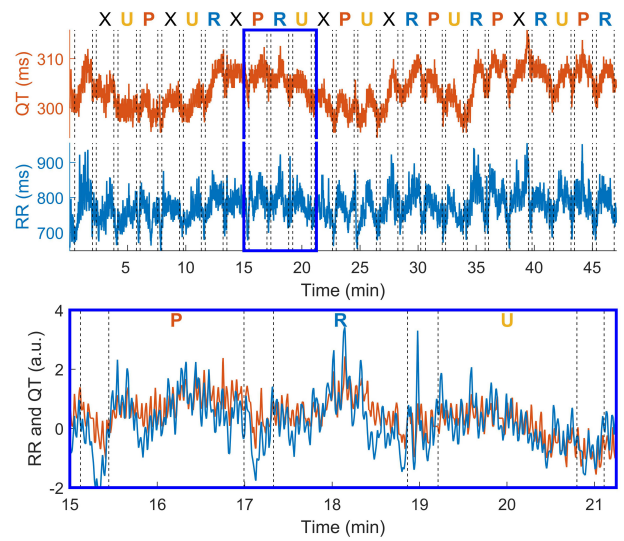

FIGURE 2 | QT and RR interval oscillations in one individual during the entire recording **(top)** and during three consecutive conditions **(bottom)**. Dashed vertical lines represent the beginning and the end of each condition, which are separated by about 20 s pause. The type of condition is reported above the **top panel**. R: rest; P: pleasant music; U: unpleasant music; X: sequence of Shepard tones (not considered in statistical analysis).

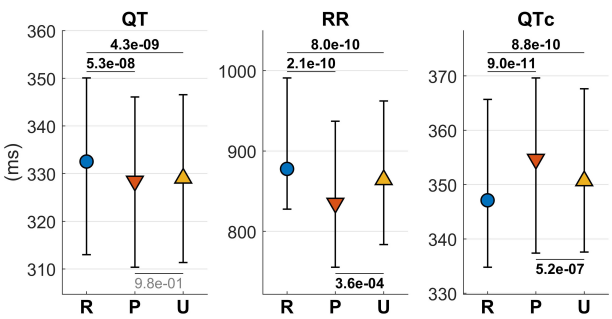

FIGURE 3 | QT, RR, and QTc (QT corrected for heart rate) during listening to pleasant music (P), unpleasant music (U), and rest (R). Markers represent the median values and bars span from the first to the third quartile. *P*-values measuring pair-wise differences are reported in bold if significant and in light gray if not significant.

QT Interval

Changes in the QTV during different conditions are shown in **Figure 3**. The QTV was significantly shorter during both unpleasant (329/35 ms, median/interquartile range) and pleasant (328/36 ms) than during resting (333/37 ms) condition ($P < 5.3 \times 10^{-8}$). After correcting for heart rate using the Bazett's formula, this pattern changed, with corrected QTV increasing from resting (347/41 ms) to unpleasant (351/30 ms) to pleasant (355/32 ms) ($P < 5 \times 10^{-7}$) (**Figure 3**).

QTV Related and Unrelated to RRV

A representative example of time-frequency representations during three consecutive epochs (resting, pleasant and unpleasant) is shown in **Figure 4**. These include the time-frequency spectra of QTV and RRV, $S_{QT}(t,f)$ and $S_{RRV}(t,f)$ respectively, the time-frequency coherence between QTV

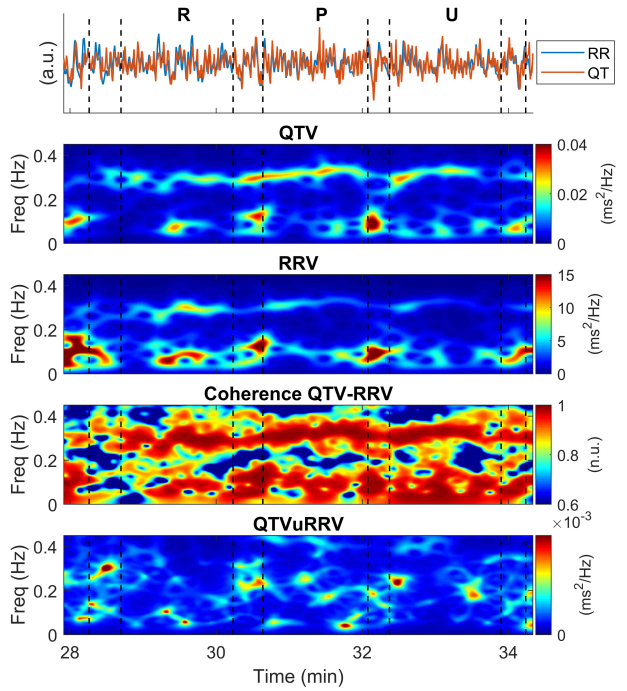

FIGURE 4 | Example of time-frequency representations in a representative individual. The same interval including three consecutive epochs (resting, pleasant and unpleasant conditions) shown in **Figure 2** is analyzed. From **top** to **bottom**: QTV and RRV superimposed and normalized to show same amplitude, QTV and RRV time-frequency spectra, time-frequency coherence between QTV and RRV and time-frequency spectrum of QTV unrelated to RRV. R: Rest; P: Pleasant condition; U: Unpleasant condition.

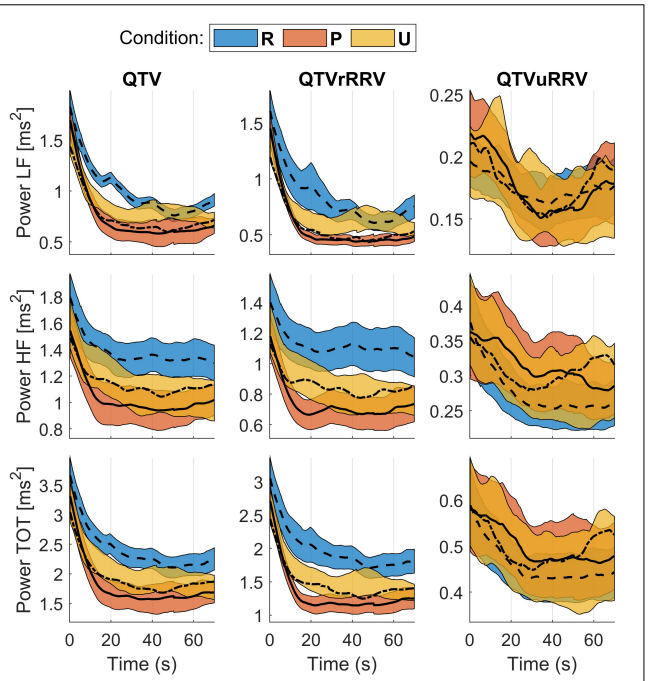

FIGURE 5 | QTV trends. From **left** to **right**: QTV, QTV related to RRV (QTVrRRV), and QTV unrelated to RRV (QTVrRRV). From **top** to **bottom**: instantaneous power of LF, HF, and total spectral band. Solid lines represent the mean trend across all individuals and shaded areas represent standard error. R: rest; P: pleasant condition; U: unpleasant condition.

and RRV, $\gamma_{QTV,RV}(t,f)$and the time-frequency spectrum of QTVuRRV, $S_{QTVuRRV}(t,f)$ Changes in the patterns of color in these time-frequency representations indicate changes in the magnitude and frequency of the signals' spectral components typical of non-stationary conditions. QTV and RRV showed similar time-frequency structures and high coherence. This implies that most of the spectral content of QTV was related to RRV and QTVuRRV was much smaller than QTV (note the different scale of the color bars in **Figure 4**).

The time course of the QTV's spectral components (instantaneous power) presented two phases (**Figure 5**): A sharp decrease with respect to the preceding interval (the pause between two consecutive epochs during which the individuals were asked to rate how they felt) during the first 20 s with subsequent stabilization during the remaining 50–60 s until the end of the epoch. QTVrRRV showed the biggest intra-condition changes (**Figure 5**, middle panel) whereas QTVuRRV showed little intra-condition changes as demonstrated by overlapping trends in the right hand side of **Figure 5**.

Figure 6 shows the distribution of mean QTV, QTV related and unrelated to RRV during the stable phase of the recordings (from 20 to 50 s after the onset of each epoch). QTV and QTVrRRV show similar patterns, with oscillations of higher magnitude in all spectral band during rest than during pleasant and unpleasant conditions, and with lower magnitude for HF oscillations and total power during pleasant than unpleasant condition. The time-frequency coherence between QTV and RRV was high (0.76–0.85) in all spectral bands for all conditions. In HF, a small but significant decrease in coherence was observed from rest (0.80/0.13) to unpleasant (0.77/0.14) to pleasant (0.76/0.17) conditions (**Table 1**). QTVuRRV was much smaller than QTVrRRV and did not show any significant change in any spectral band (**Table 1**).

Intra-Lead Reproducibility

The entire analysis was repeated using beat to beat QTVs obtained from lead II for assessment of intra-lead reproducibility. Correlation between the time series of QTVs from lead V4 and lead II was high, with Spearman's correlation coefficient equal to 0.95/0.09. However, the correlation between QTV was lower at 0.59/0.26. A lower intra-lead correlation for QTV than for the QTV is expected as QTV has a much lower magnitude than the QTV series, which show very slow oscillations (i.e., very low frequency components with frequency <0.03 Hz) that are removed from QTV. The standard deviation of the QTV signals (entire recording) across all patients was slightly higher in lead II than V4

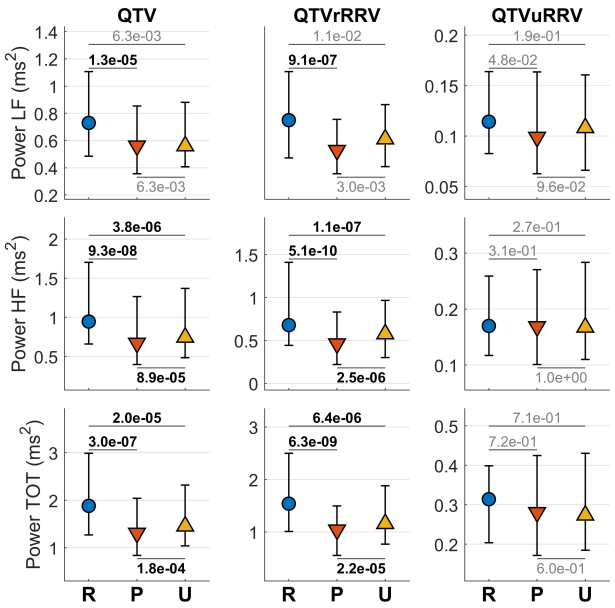

FIGURE 6 | QTV and QTV related and unrelated to RRV during listening to pleasant music (P), unpleasant music (U), and rest (R). From **left** to **right**: QTV, QTV related to RRV (QTVrRRV), and QTV unrelated to RRV (QTVrRRV). From **top** to **bottom**: mean power of LF, HF and total spectral band. Markers represent the median values and bars span from the first to the third quartile. *P*-values measuring pair-wise differences are reported in bold if significant and in light gray if not significant.

at 1.8/0.7 ms versus 1.7/0.6 ms, $P < 0.001$, and their correlation was equal to $cc = 0.78$. There was no difference in the SNR of the leads V4 and II ($P = 0.60$). The correlation coefficient between the standard deviation of QTV and SNR was equal to -0.49 ($P = 8.1 \times 10^{-5}$) in lead V4 and -0.60 in lead II ($P = 3.6 \times 10^{-7}$). This suggests that QTV in lead V4 was less affected by noise than QTV in lead II.

During the different conditions (silence, pleasant and unpleasant), changes in the QTV and QTc from lead II (**Supplementary Figure S2**) mirrored those from lead V4. Changes in QTV, QTVrRRV, and QTVuRRV followed a similar pattern in both leads. However, in lead II some differences were no longer significant after Bonferroni's correction (**Supplementary Figure S3**).

DISCUSSION

This study investigated the effect of emotional valence on cardiac repolarization and repolarization dynamics by analyzing the QTV response to music. The main findings are: (1) The QTV decreases during both unpleasant and pleasant emotional states, mirroring similar changes in the RR interval. This pattern is reversed after correction for heart rate, with QTc showing small but significant increase during listening to both pleasant and unpleasant music compared to silence, and during pleasant compared to unpleasant music. (2) The dynamic response of QTV to emotional valence showed a transient phase of about 20 s. (3) Because of the strong coupling between QTV and RRV, both QTV and QTVrRRV followed a similar pattern showing a decrease in variability during both pleasant and unpleasant conditions with respect to the resting condition and a further decrease during pleasant condition with respect to unpleasant condition in HF and in the total spectral components. (4) QTVuRRV was small and not affected by emotional valence.

The existence of a link between emotions or psychological stress and cardiovascular mortality has been demonstrated by many studies (Steptoe and Brydon, 2009). Strong emotions, i.e., characterized by a high level of arousal, have an acute impact on the cardiovascular function and can serve as triggers for arrhythmias and cardiovascular disease, mainly through a complex interaction with the autonomic nervous system (Kreibig, 2010; Taggart et al., 2011b). While it is accepted that emotional arousal (activating versus deactivating) has a stronger effect on human physiology than emotional valence (positive versus negative feeling), the latter has been less investigated and its effect on cardiac repolarization remained undetermined. This is the first study to investigate the simultaneous interaction between emotional valence and QT dynamics. A unique feature of this study is that the experimental set-up was designed to control for arousal by matching excerpts by tempo and volume with the intent of focusing on the effect of felt pleasantness with respect to unpleasantness.

Previous studies have demonstrated a link between intense emotions and potentially pro-arrhythmic repolarization changes (Ziegelstein, 2007; Lampert, 2016). In patients with a history of ventricular arrhythmia, psychological stress induces autonomically mediated repolarization changes (Lampert et al., 2005), while anger-induced T-wave alternans, a marker of repolarization variability (Orini et al., 2019), predicts future ventricular arrhythmias (Lampert et al., 2009). In patients with structurally normal hearts, mental stress altered repolarization inhomogeneity balance (Taggart et al., 2005) and dispersion of repolarization (Child et al., 2014; Finlay et al., 2016). A recent study has shown that not only acute and strong emotions, but also subtle everyday fluctuations in emotional arousal can affect repolarization, with a more noticeable impact in patients with Long QT syndrome and ischemic heart disease (Lane et al., 2018). In the same study, similar QT changes were observed as a response of emotions characterized by both positive and negative valence, which may suggest that the effect of everyday emotions could be primarily a function of arousal.

Music-induced emotions affect several cerebrovascular and cardiovascular parameters, especially heart rate and heart rate variability (Koelsch and Jancke, 2015). Although music-induced emotions may have a smaller impact on cardiac activity as compared to other types of emotions, evidence shows that music can reduce pain and anxiety, and that relaxing music is associated with lower heart rate and blood pressure (Koelsch and Jancke, 2015), which could be beneficial in particular in patients with cardiovascular disease.

The interest in the QTV response to music-induced emotions is motivated by the fact that QTV, and in particular QTVuRRV, provides an indirect assessment of ventricular repolarization variability, which is believed to be modulated by sympathetic drive directed to the ventricles (Porta et al., 2010; El-Hamad et al., 2015). Recent studies have demonstrated the existence of respiratory and LF oscillations in the ventricular action potential of the intact human heart during steady state ventricular pacing and therefore unrelated to cycle length variations (Hanson et al., 2014; Van Duijvenboden et al., 2016; Porter et al., 2019). Several studies have shown that indices of ventricular repolarization, mainly based on QTV, are associated with cardiac risk (Tereshchenko et al., 2009; Oosterhoff et al., 2011; Baumert et al., 2016), with periodic repolarization dynamics being affected by music (Cerruto et al., 2017). The mechanisms promoting intrinsic ventricular repolarization variability are still under investigation, but may imply both the autonomic nervous system (adrenergic stimulation) and mechano-electric feedback (Pueyo et al., 2016; Orini et al., 2017a).

One of the main results of this study is that in young healthy individuals listening to pleasant and unpleasant music, QTV dynamics are largely determined by RRV, whereas QTVuRRV remains stable. This highlights the importance of separating RRV-related and unrelated components to reveal intrinsic repolarization variability (Orini et al., 2018).

In this cohort of young healthy volunteers, the effect of emotional valence on QT and QTV was significant but relatively small, whereas its effect on QTVuRRV was not significant. Although these findings may not have an immediate impact on clinical practice, they provide valuable information to advance our understanding of the interplay between emotions and cardiac disease. Further research is needed to test the effect of emotional valence in the context of preexisting cardiac disorders and to better understand how to translate these findings in strategies that can impact patients' health. The observation that valance and not only arousal affects the QTV is interesting, because it suggests that potentially clinically relevant changes in arrhythmogenic substrates may be triggered by emotions unrelated to dramatic events. For instance, a small but significant increase in QTc associated with pleasant emotions may be relevant for arrhythmogenesis in the context of repolarization disorders such as long QT syndrome. A recent study analyzing the effect of everyday emotions on the QTV has suggested that in patients with heart conditions (long QT syndrome and ischemic heart disease), but not in healthy individuals, these can affect arrhythmia susceptibility (Lane et al., 2018). Interestingly, although the authors concluded that emotional arousal had a predominant effect with respect to valance, they observed a prolongation of QTc with positive and low-arousal emotions, which, despite important methodological differences between the two studies, is in agreement with our findings. Of note, silence has been previously reported to have a strong relaxing effect on the respiratory rate, heart rate and blood pressure (Bernardi et al., 2006; Orini et al., 2010). The finding that QTc decreases while QTV increases during silence provides further support to the protective effect of relaxation that could be used in specific cohorts to reduce cardiovascular risk (Schneider et al., 2005).

Limitations and Future Directions

Although this study is based on a relatively large cohort, it only includes young healthy individuals. The presentence of heart disease may amplify the effect of emotions (Lampert, 2016; Lane et al., 2018) and future studies should include patients with a pre-existing arrhythmogenic substrate. Emotions were induced using musical excerpts. Functional neuroimaging studies using similar stimuli have demonstrated that music can modulate activity in brain structures that are known to be crucially involved in emotion (Koelsch et al., 2006; Koelsch, 2014). Future studies are needed to determine if the effect of music-induced emotions can be generalized to other types of emotions and psychological stress. Inter-subject variability in the emotional predisposition to and elaboration of the stimuli were not controlled during the study and may have played a role in the physiological response. For instance, interoceptive awareness has been shown to modulate the heart rate response to emotional pictures (Pollatos et al., 2007) and may also play a role in the modulation cardiac repolarization. This may be assessed in future studies. Although the tangent method is a standard method for identifying the end of the T-wave, it has some limitations (Baumert et al., 2016). Although results obtained from the analysis of lead V4 (main text) generally correlated with those obtained from lead II (**Supplementary Material**), the statistical significance of some differences differ, especially in the LF band of QTV. Intra-lead differences in QTV have been previously reported and linked to T-wave amplitude, with QTV increasing in leads showing smaller T-waves (Hasan et al., 2012). This is in agreement with our finding that QTV in lead V4, which shows taller T-waves than lead II, was less affected by noise than QTV in lead II. Thus, results obtained from the analysis of V4 are more robust. Although these intra-lead differences are partially due to the technical challenge of measuring small amplitude oscillations of the order of few ms, ECG leads capture repolarization dynamics of different cardiac segments (Srinivasan et al., 2019) and small intra-leads differences may also partially reflect a spatially heterogeneous response of ventricular repolarization.

Finally, although the time-frequency approach implemented in this study is built upon a robust framework that has been tested in several studies (Orini et al., 2012a,b,c,d, 2018), other approaches to decompose QT variability in its different component exist (Porta et al., 2010, 2017; El-Hamad et al., 2015) and future studies may investigate the reproducibility of these findings.

CONCLUSION

Emotional valence, as evoked by music, has a small but significant effect on beat-to-beat repolarization variability and this effect is principally mediated by heart rate variability.

DATA AVAILABILITY STATEMENT

All datasets generated for this study are included in the article/**Supplementary Material**.

ETHICS STATEMENT

The studies involving human participants were reviewed and approved by the Max Plank Institute, Leipzig, Germany. The patients/participants provided their written informed consent to participate in this study.

AUTHOR CONTRIBUTIONS

MO contributed to the design of the analysis. MO and FA-A contributed to the data and statistical analysis. MO and RB contributed to the methodological development. SK contributed to the experimental set-up. MO contributed to the drafting of the work. MO, FA-A, SK, and RB contributed to the critical revision and proofreading.

FUNDING

RB was supported by the AEI and FEDER under the project RTI2018-097723-B-I00, CIBER-BBN through Instituto de Salud Carlos III, and Gobierno de Aragón under projects LMP44-18 and T39-17R.

SUPPLEMENTARY MATERIAL

The Supplementary Material for this article can be found online at: https://www.frontiersin.org/articles/10.3389/fphys.2019.01465/full#supplementary-material

REFERENCES

Baumert, M., Porta, A., Vos, M. A., Malik, M., Couderc, J. P., Laguna, P., et al. (2016). QT interval variability in body surface ECG: measurement, physiological basis, and clinical value: position statement and consensus guidance endorsed by the European Heart Rhythm Association jointly with the ESC Working Group on cardiac cellular electroph. *Europace* 18, 925–944. doi: 10.1093/europace/euv405

Bernardi, L., Porta, C., and Sleight, P. (2006). Cardiovascular, cerebrovascular, and respiratory changes induced by different types of music in musicians and non-musicians: the importance of silence. *Heart* 92, 445–452. doi: 10.1136/hrt.2005.064600

Cerruto, G., Mainardi, L., Koelsch, S., and Orini, M. (2017). The periodic repolarization dynamics index identifies changes in ventricular repolarization oscillations associated with musicinduced emotions. *Comput. Cardiol.* 44, 2–5. doi: 10.22489/CinC.2017.259-372

Child, N., Hanson, B., Bishop, M., Rinaldi, C. A., Bostock, J., Western, D., et al. (2014). Effect of mental challenge induced by movie clips on action potential duration in normal human subjects independent of heart rate. *Circ. Arrhythmia Electrophysiol.* 7, 518–523. doi: 10.1161/CIRCEP.113.000909

Cohen, L. (1989). Time-frequency distributions-a review. *Proc. IEEE* 77, 941–981. doi: 10.1109/5.30749

El-Hamad, F., Lambert, E., Abbott, D., and Baumert, M. (2015). Relation between QT interval variability and muscle sympathetic nerve activity in normal subjects. *Am. J. Physiol. Hear. Circ. Physiol.* 309, H1218–H1224. doi: 10.1152/ajpheart.00230.2015

Finlay, M. C., Lambiase, P. D., Ben-Simon, R., and Taggart, P. (2016). Effect of mental stress on dynamic electrophysiological properties of the endocardium and epicardium in humans. *Heart Rhythm* 13, 175–182. doi: 10.1016/j.hrthm.2015.08.011

Hanson, B., Child, N., Van Duijvenboden, S., Orini, M., Chen, Z., Coronel, R., et al. (2014). Oscillatory behavior of ventricular action potential duration in heart failure patients at respiratory rate and low frequency. *Front. Physiol.* 5:414. doi: 10.3389/fphys.2014.00414

Hasan, M. A., Abbott, D., and Baumert, M. (2012). Relation between beat-to-beat QT interval variability and t-wave amplitude in healthy subjects. *Ann. Noninvasive Electrocardiol.* 17, 195–203. doi: 10.1111/j.1542-474X.2012.00508.x

Hilz, M. J., Stadler, P., Gryc, T., Nath, J., Habib-Romstoeck, L., Stemper, B., et al. (2014). Music induces different cardiac autonomic arousal effects in young and older persons. *Auton. Neurosci. Basic Clin.* 183, 83–93. doi: 10.1016/j.autneu.2014.02.004

Hlawatsch, F., and Boudreaux-Bartels, G. F. F. (1992). Linear and quadratic time-frequency signal representations. *IEEE Signal. Process. Mag.* 9, 21–67. doi: 10.1109/79.127284

Koelsch, S. (2014). Brain correlates of music-evoked emotions. *Nat. Rev. Neurosci.* 15, 170–180. doi: 10.1038/nrn3666

Koelsch, S., Fritz, T., Cramon, D. Y. V., Müller, K., and Friederici, A. D. (2006). Investigating emotion with music: an fMRI study. *Hum. Brain Mapp.* 27, 239–250. doi: 10.1002/hbm.20180

Koelsch, S., and Jancke, L. (2015). Music and the heart. *Eur. Heart J.* 36, 3043–3048. doi: 10.1093/eurheartj/ehv430

Krabs, R. U., Enk, R., Teich, N., and Koelsch, S. (2015). Autonomic effects of music in health and Crohn's disease: the impact of isochronicity, emotional valence, and tempo. *PLoS One* 10:e0126224. doi: 10.1371/journal.pone.0126224

Kreibig, S. D. (2010). Autonomic nervous system activity in emotion: a review. *Biol. Psychol.* 84, 394–421. doi: 10.1016/j.biopsycho.2010.03.010

Lampert, R. (2016). Mental stress and ventricular arrhythmias. *Curr. Cardiol. Rep.* 18:118. doi: 10.1007/s11886-016-0798-796

Lampert, R., Shusterman, V., Burg, M., McPherson, C., Batsford, W., Goldberg, A., et al. (2009). Anger-induced T-Wave alternans predicts future ventricular arrhythmias in patients with implantable cardioverter-defibrillators. *J. Am. Coll. Cardiol.* 53, 774–778. doi: 10.1016/j.jacc.2008.10.053

Lampert, R., Shusterman, V., Burg, M. M., Lee, F. A., Earley, C., Goldberg, A., et al. (2005). Effects of psychologic stress on repolarization and relationship to autonomic and hemodynamic factors. *J. Cardiovasc. Electrophysiol.* 16, 372–377. doi: 10.1046/j.1540-8167.2005.40580.x

Lane, R. D., Reis, H. T., Hsu, C.-H., Kern, K. B., Couderc, J. P., Moss, A. J., et al. (2018). Abnormal repolarization duration during everyday emotional arousal in long QT syndrome and Coronary Artery disease. *Am. J. Med.* 131:565-572.e2. doi: 10.1016/j.amjmed.2017.12.017

Oosterhoff, P., Tereshchenko, L. G., Van Der Heyden, M. A. G., Ghanem, R. N., Fetics, B. J., Berger, R. D., et al. (2011). Short-term variability of repolarization predicts ventricular tachycardia and sudden cardiac death in patients with structural heart disease: a comparison with QT variability index. *Heart Rhythm* 8, 1584–1590. doi: 10.1016/j.hrthm.2011.04.033

Orini, M., Bailón, R., Enk, R., Koelsch, S., Mainardi, L., and Laguna, P. (2010). A method for continuously assessing the autonomic response to music-induced emotions through HRV analysis. *Med. Biol. Eng. Comput.* 48, 423–433. doi: 10.1007/s11517-010-0592-3

Orini, M., Bailón, R., Laguna, P., Mainardi, L. T., and Barbieri, R. (2012a). A multivariate timefrequency method to characterize the influence of respiration over heart period and arterial pressure. *EURASIP J. Adv. Signal Process.* 2012:214. doi: 10.1186/1687-6180-2012-2214

Orini, M., Bailón, R., Mainardi, L., and Laguna, P. (2012b). Synthesis of HRV signals characterized by predetermined time-frequency structure by means of

time-varying ARMA models. *Biomed. Signal. Process. Control* 7, 141–150. doi: 10.1016/j.bspc.2011.05.003

Orini, M., Bailon, R., Mainardi, L. T., Laguna, P., and Flandrin, P. (2012c). Characterization of dynamic interactions between cardiovascular signals by time-frequency coherence. *IEEE Trans. Biomed. Eng.* 59, 663–673. doi: 10.1109/TBME.2011.2171959

Orini, M., Laguna, P., Mainardi, L. T. T., and Bailón, R. (2012d). Assessment of the dynamic interactions between heart rate and arterial pressure by the cross time–frequency analysis. *Physiol. Meas.* 33, 315–331. doi: 10.1088/0967-3334/33/3/315

Orini, M., Nanda, A., Yates, M., Di Salvo, C., Roberts, N., Lambiase, P. D., et al. (2017a). Mechanoelectrical feedback in the clinical setting: current perspectives. *Prog. Biophys. Mol. Biol.* 130(Pt B), 365–375. doi: 10.1016/j.pbiomolbio.2017.06.001

Orini, M., Tinker, A., Munroe, P. B., and Lambiase, P. D. (2017b). Long-term intra-individual reproducibility of heart rate dynamics during exercise and recovery in the UK Biobank cohort. *PLoS One* 12:e0183732. doi: 10.1371/journal.pone.0183732

Orini, M., Pueyo, E., Laguna, P., and Bailon, R. (2018). A time-varying nonparametric methodology for assessing changes in QT variability unrelated to heart rate variability. *IEEE Trans. Biomed. Eng.* 65, 1443–1451. doi: 10.1109/TBME.2017.2758925

Orini, M., Taggart, P., Srinivasan, N., Hayward, M., and Lambiase, P. D. (2016). Interactions between activation and repolarization restitution properties in the intact human heart: in-vivo whole-heart data and mathematical description. *PLoS One* 11:e0161765. doi: 10.1371/journal.pone.0161765

Orini, M., Yanni, J., Taggart, P., Hanson, B., Hayward, M., Smith, A., et al. (2019). Mechanistic insights from targeted molecular profiling of repolarization alternans in the intact human heart. *Europace* 21, 981–989. doi: 10.1093/europace/euz007

Pollatos, O., Herbert, B. M., Matthias, E., and Schandry, R. (2007). Heart rate response after emotional picture presentation is modulated by interoceptive awareness. *Int. J. Psychophysiol.* 63, 117–124. doi: 10.1016/j.ijpsycho.2006.09.003

Porta, A., Bari, V., De Maria, B., and Baumert, M. (2017). A network physiology approach to the assessment of the link between sinoatrial and ventricular cardiac controls. *Physiol. Meas.* 38, 1472–1489. doi: 10.1088/1361-6579/aa6e95

Porta, A., Tobaldini, E., Gnecchi-Ruscone, T., and Montano, N. (2010). RT variability unrelated to heart period and respiration progressively increases during graded head-up tilt. *Am. J. Physiol. Heart Circ. Physiol.* 298, H1406–H1414. doi: 10.1152/ajpheart.01206.2009

Porter, B., Bishop, M. J., Claridge, S., Child, N., Van Duijvenboden, S., Bostock, J., et al. (2019). Left ventricular activation-recovery interval variability predicts spontaneous ventricular tachyarrhythmia in patients with heart failure. *Heart Rhythm* 16, 702–709. doi: 10.1016/j.hrthm.2018.11.013

Pueyo, E., Orini, M., Rodríguez, J. F. J. F., and Taggart, P. (2016). Interactive effect of betaadrenergic stimulation and mechanical stretch on low-frequency oscillations of ventricular action potential duration in humans. *J. Mol. Cell. Cardiol.* 97, 93–105. doi: 10.1016/j.yjmcc.2016.05.003

Schneider, R. H., Alexander, C. N., Staggers, F., Rainforth, M., Salerno, J. W., Hartz, A., et al. (2005). Long-term effects of stress reduction on mortality in persons =55 years of age with systemic hypertension. *Am. J. Cardiol.* 95, 1060–1064. doi: 10.1016/j.amjcard.2004.12.058

Srinivasan, N. T., Orini, M., Providencia, R., Simon, R., Lowe, M., Segal, O. R., et al. (2019). Differences in the upslope of the precordial body surface ECG T wave reflect right to left dispersion of repolarization in the intact human heart. *Heart Rhythm* 16, 943–951. doi: 10.1016/j.hrthm.2018.12.006

Steptoe, A., and Brydon, L. (2009). Emotional triggering of cardiac events. *Neurosci. Biobehav. Rev.* 33, 63–70. doi: 10.1016/j.neubiorev.2008.04.010

Steptoe, A., and Kivimäki, M. (2012). Stress and cardiovascular disease. *Nat. Rev. Cardiol.* 9, 360–370. doi: 10.1038/nrcardio.2012.45

Taggart, P., Boyett, M. R., Logantha, S. J. R. J., and Lambaise, P. D. (2011a). Anger, emotion, and arrythimias: from brain to heart. *Front Physiol.* 2:67. doi: 10.3389/fphys.2011.00067

Taggart, P., Critchley, H., and Lambiase, P. D. (2011b). Heart-brain interactions in cardiac arrhythmia. *Heart* 97, 698–708. doi: 10.1136/hrt.2010.209304

Taggart, P., Sutton, P., Redfern, C., Batchvarov, V. N., Hnatkova, K., Malik, M., et al. (2005). The effect of mental stress on the non-dipolar components of the T wave: modulation by hypnosis. *Psychosom. Med.* 67, 376–383. doi: 10.1097/01.psy.0000160463.10583.88

Tereshchenko, L. G., Fetics, B. J., Domitrovich, P. P., Lindsay, B. D., and Berger, R. D. (2009). Prediction of ventricular tachyarrhythmias by intracardiac repolarization variability analysis. *Circ. Arrhythmia Electrophysiol.* 2, 276–284. doi: 10.1161/CIRCEP.108.829440

Van Duijvenboden, S., Orini, M., Child, N., Gill, J. S., Taggart, P., and Hanson, B. (2016). Investigation of causal interactions between ventricular action potential duration, blood pressure and respiration. *Comput. Cardiol.* 42, 621–624. doi: 10.1109/CIC.2015.7410987

Ziegelstein, R. C. (2007). Acute emotional stress and cardiac arrhythmias. *J. Am. Med. Assoc.* 298, 324–329. doi: 10.1001/jama.298.3.324

Conflict of Interest: The authors declare that the research was conducted in the absence of any commercial or financial relationships that could be construed as a potential conflict of interest.

frontiers in Physiology

ORIGINAL RESEARCH
published: 17 December 2019
doi: 10.3389/fphys.2019.01510

Long-Term Microgravity Exposure Increases ECG Repolarization Instability Manifested by Low-Frequency Oscillations of T-Wave Vector

Saúl Palacios[1], Enrico G. Caiani[2], Federica Landreani[2], Juan Pablo Martínez[1,3†] and Esther Pueyo[1,3†]*

[1] BSICoS Group, Aragón Institute of Engineering Research, IIS Aragón, Universidad de Zaragoza, Zaragoza, Spain, [2] Dipartimento di Elettronica, Informazione e Bioingegneria, Politecnico di Milano, Milan, Italy, [3] CIBER en Bioingeniería, Biomateriales y Nanomedicina, Madrid, Spain

OPEN ACCESS

Edited by:
George E. Billman,
The Ohio State University,
United States

Reviewed by:
Ruben Coronel,
University of Amsterdam, Netherlands
Emilio Vanoli,
University of Pavia, Italy

***Correspondence:**
Saúl Palacios
spalacios@unizar.es

[†] These authors have contributed equally to this work as last authors

Specialty section:
This article was submitted to Cardiac Electrophysiology, a section of the journal Frontiers in Physiology

Received: 26 August 2019
Accepted: 29 November 2019
Published: 17 December 2019

Citation:
Palacios S, Caiani EG, Landreani F, Martínez JP and Pueyo E (2019) Long-Term Microgravity Exposure Increases ECG Repolarization Instability Manifested by Low-Frequency Oscillations of T-Wave Vector. Front. Physiol. 10:1510. doi: 10.3389/fphys.2019.01510

Ventricular arrhythmias and sudden cardiac death during long-term space missions are a major concern for space agencies. Long-duration spaceflight and its ground-based analog head-down bed rest (HDBR) have been reported to markedly alter autonomic and cardiac functioning, particularly affecting ventricular repolarization of the electrocardiogram (ECG). In this study, novel methods are developed, departing from previously published methodologies, to quantify the index of Periodic Repolarization Dynamics (PRD), an arrhythmic risk marker that characterizes sympathetically-mediated low-frequency oscillations in the T-wave vector. PRD is evaluated in ECGs from 42 volunteers at rest and during an orthostatic tilt table test recorded before and after 60-day –6° HDBR. Our results indicate that tilt test, on top of enhancing sympathetic regulation of heart rate, notably increases PRD, both before and after HDBR, thus supporting previous evidence on PRD being an indicator of sympathetic modulation of ventricular repolarization. Importantly, long-term microgravity exposure is shown to lead to significant increases in PRD, both when evaluated at rest and, even more notably, in response to tilt test. The extent of microgravity-induced changes in PRD has been associated with arrhythmic risk in prior studies. An exercise-based, but not a nutrition-based, countermeasure is able to partially reverse microgravity-induced effects on PRD. In conclusion, long-term exposure to microgravity conditions leads to elevated low-frequency oscillations of ventricular repolarization, which are potentiated following sympathetic stimulation and are related to increased risk for repolarization instabilities and arrhythmias. Tested countermeasures are only partially effective in counteracting microgravity effects.

Keywords: microgravity, periodic repolarization dynamics (PRD), ventricular repolarization, autonomous nervous system, electrocardiogram (ECG) processing, tilt table test

1. INTRODUCTION

After almost 60 years of human spaceflight, there is good evidence on detrimental effects on the human body associated with long-term space missions (Williams et al., 2009; Garrett-Bakelman et al., 2019). Two of the main causes underlying those effects are ionizing radiation and changes in gravity conditions. Specifically, microgravity-induced cardiac arrhythmias are a major concern for national space agencies, as very prolonged periods of time in the International Space Station or in a mission to Mars or the Moon might set the stage for the development of ventricular tachycardia or ventricular fibrillation that could end up in sudden cardiac death (Anzai et al., 2014; Caiani et al., 2016). Although the probability of undergoing serious cardiac arrhythmias in the course of a space mission is low, with the estimated probability of suffering a life-threatening event being of 1% per year in short to mid-duration spaceflights (Russomano et al., 2013), currently available data are limited and more sophisticated techniques should be employed to identify potential in-flight abnormalities in the electrical activity of the heart (Convertino, 2009).

Several factors may enhance predisposition to ventricular arrhythmias during spaceflight. Commonly reported bradycardia (Meck et al., 2001), changes in electrolyte composition of blood plasma (Smith and Zwart, 2008), psychological stress (Kanas et al., 2001) and, very relevantly, adaptation of cardiac autonomic modulation (Fritsch-Yelle et al., 1996) may all concur to adversely affect ventricular electrophysiology. In particular, reported alterations in the sympathetic nervous system might contribute to the documented increase in spatio-temporal inhomogeneity of ventricular repolarization, thus potentially providing an electrophysiological substrate for arrhythmias (Caiani et al., 2016). Nevertheless, further evidence on elevated arrhythmic risk during long-term space missions and its underlying mechanisms is yet to be established.

Studies assessing microgravity effects on ventricular repolarization during or immediately after spaceflight are limited. Major findings indicate that long-duration spaceflight prolongs cardiac repolarization, as measured by the QT corrected interval of the electrocardiogram (ECG) (D'Aunno et al., 2003). Due to the limited opportunities to obtain data from humans in space missions, mainly related to the hazards and high costs of spaceflight investigations, several ground-based models have been used to simulate space conditions, explore potential adverse effects associated with weightlessness and assess the effectiveness of proposed countermeasures. Long-term head-down (−6°) bed rest (HDBR) is a ground-based analog widely utilized to simulate microgravity effects on the human body (Pavy-Le Traon et al., 2007; Hargens and Vico, 2016). Relevant alterations in ventricular repolarization have been reported in HDBR studies. In a 90-day HDBR investigation, several subjects were reported to develop QRS-T angles above 100° (Sakowski et al., 2011), with these elevated values having been associated with 3- to 5-fold increased risk for cardiovascular mortality and sudden death in previous works (Kardys et al., 2003; Yamazaki et al., 2005). In another study of only 9- to 16-day HDBR, simulated microgravity was shown to lead to an increase in microvolt T-wave alternans (Grenon et al., 2005), a well-known marker of ventricular arrhythmias and sudden cardiac death. Of note, HDBR-induced increases in T-wave alternans correlated with changes in sympathetic function. In another short-term HDBR study (Martín-Yebra et al., 2015) TWA was, however, shown not to increase during stress-test and tilt-table test after 5- and 21-day HDBR experiments. Interestingly, subjects suffering a more marked orthostatic intolerance after HDBR were found to be those presenting greater values of TWA, even before exposure to simulated microgravity.

A myriad of indices have been reported in the literature to assess ECG repolarization, including prolongation of the QTc interval (Mitchell and Meck, 2004), QT rate adaptation (Pueyo et al., 2004, 2008), QT interval variability (Piccirillo et al., 2009), T-wave alternans (Rosenbaum et al., 1994; Martinez and Olmos, 2005), or T-wave morphological variability (Adam et al., 1984; Badilini et al., 1997; Acar et al., 1999; Baumert et al., 2011; Ramírez et al., 2017a,b), among others. An index of Periodic Repolarization Dynamics (PRD) has been recently proposed to assess sympathetic modulation of ventricular repolarization by measuring low-frequency (below 0.1 Hz) oscillations in the T-wave vector (Rizas et al., 2014). PRD accounts for variability not limited to a specific time interval, as the QT interval or the T-peak-to-T-end interval, but more generally integrating all the spatio-temporal information in the T-wave vector, which can allow for a more robust characterization of beat-to-beat repolarization variations and can provide a better marker to anticipate electrical instabilities (Rizas et al., 2014, 2016).

In this study, ECG signals from healthy volunteers undergoing 60-day HDBR are analyzed. PRD is hypothesized to be able to characterize the effects of sustained simulated microgravity on ventricular repolarization, particularly in response to an orthostatic Tilt-Table Test (TTT), a common procedure used to assess autonomic nervous system function (Zygmunt and Stanczyk, 2010). To overcome identified issues related to angle quantification as part of the PRD technique, a number of updates on the originally reported methods (Rizas et al., 2014, 2016) are also proposed. Additionally, the effectiveness of two different countermeasures, based on exercise and nutrition, to mitigate or reduce microgravity-induced effects on ventricular repolarization during HDBR are assessed.

2. MATERIALS AND METHODS

2.1. Study Population

Data from two 60-day −6° HDBR campaigns organized by the European Space Agency (ESA) as part of ESA bed rest studies were analyzed in this work. These studies were conducted between 2015 and 2017 in the :envihab facility of the Institute of Aerospace Medicine at the German Aerospace Center-DLR (Cologne, Germany) and at the Institute of Space Medicine and Physiology-MEDES (Toulouse, France).

For the experiment in Cologne, 22 male volunteers (29 ± 6 years, 181 ± 5 cm, 77 ± 7 kg) were enrolled and randomly distributed into either the countermeasure group (JUMP), who performed 48 training sessions of a varying number of countermovement jumps on a sledge jump system during the

FIGURE 1 | Phases of the head-down bed rest (HDBR) campaign, with indication of the days when volunteers underwent tilt table tests: 2 days before the start of the HDBR period (BCD-2) and just after completing it (R+0).

HDBR time period (Kramer et al., 2017), or the control group (CTRL), who did not perform any exercise. For the experiment in Toulouse, 20 male volunteers were enrolled (34 ± 7 years, 176 ± 4 cm, 73 ± 7 kg). They were randomly distributed into either the countermeasure group (NUTR), daily receiving a nutritional countermeasure consisting of a cocktail of anti-oxidants and vitamins (daily, 530 mg of polyphenol, 168 mg of vitamin E, 80 μg of Selenium-Solgar®, and 2.1 g of Omega-3—Omacor®), or the control group (CTRL), who did not receive this nutritional integration.

All subjects underwent prior comprehensive medical examination during the selection process and provided written informed consent to participate in the study, which was approved in advance by the respective Ethical Committees for Human Research at the host institutions.

2.2. Experimental Protocol

Both campaigns were divided into three phases: 15 days of PRE-HDBR baseline (BDC-15 to BDC-1), when the subjects became acclimated physiologically and psychologically to the facilities; 60 days of bed rest (HDT1 to HDT60), when subjects were in strict –6° HDBR (24 h/day); and 15 days of POST-HDBR recovery (R+0 to R+14). **Figure 1** illustrates these three phases. From HDT1 to HDT60, subjects carried out all activities at –6° HDBR: eating, hygienic procedures (teeth brushing, bowel movement, showering) and free time activities (reading, watching, or using computer). Also, all subjects had the same scheduled wake-up (at 6:30 a.m. and 7:00 a.m. in DLR and MEDES campaign, respectively) and light off (at 11:00 p.m.). More information about the study protocol is available in Kramer et al. (2017).

Two TTTs were performed, one of them 2 days before the start of the HDBR period (BCD-2) and the other one just after completing it (R+0). In each TTT the subject was tilted head-up to an angle of 80° for up to 15 min. If the subject did not experience any presyncopal episode during that time, he was exposed to Lower Body Negative Pressures (LBNP) following a protocol of 3-min –10 mmHg steps for a maximum duration of 15 min. Thirty out of the 84 analyzed recordings did not present presyncopal episodes, of which 18 corresponded to PRE-HDBR and 12 to POST-HDBR.

High-resolution (1,000 Hz) 24-h Holter 12-lead ECG signals (Mortara Instrument) recorded at days BCD-2 and R+0 (both including a TTT) were available for this study. For each TTT, a 5-min interval prior to the start of the tilt phase, the first 5 min immediately following its start and the last 5 min of the tilt phase (possibly including LBNP) were analyzed (**Figure 2**). If the tilt phase lasted for less than 5 min, its whole duration was analyzed.

2.3. ECG Pre-processing

Raw ECG signals were pre-processed by a 50 Hz notch filter to remove powerline interference. Taking these pre-processed ECG signals as inputs, QRS detection and ECG wave delineation were performed by using a wavelet-based single-lead automatic system (Martinez et al., 2004). The outputs of the detection and delineation system were combined by using rules to obtain multi-lead ECG delineation marks (Martinez et al., 2004). Since subsequent analysis focused on the T-wave, a 40-Hz low-pass filter was applied to remove noise without altering the T-wave shape. Finally, cubic splines interpolation was applied to estimate and remove baseline wander. An example of an ECG recording as originally acquired and after application of different pre-processing steps is shown in **Figure 3**.

2.4. Calculation of Angles Between Consecutive T Waves

An updated method based on the original method proposed in Rizas et al. (2014) was applied onto the pre-processed ECG signals to compute the angles between consecutive T-waves:

1. Orthogonal leads X, Y, Z were obtained from the 12-lead ECG by using the inverse Dower matrix (Edenbrandt and Pahlm, 1988).
2. The onset and end of each T-wave, denoted by T_{on} and T_{off}, were identified by the delineation system described above. When the delineation failed to identify a T-wave onset (T-wave offset, respectively) for a given beat, its location was set based on T_{on} (T_{off}, respectively) locations for adjacent beats with respect to their corresponding QRS positions. Specifically, T_{on} (or T_{off}) was located at a distance from the corresponding QRS fiducial point equal to the median interval between the QRS and T_{on} (or T_{off}) positions of 30 beats around that beat.

   As T-wave boundaries change on a beat-to-beat basis, and may be influenced by delineation errors, the angle between each two consecutive T-waves was computed by defining a unique temporal window for both waves being analyzed. Specifically, for each angle calculation, the window onset was set at the latest T_{on} of both analyzed beats computed with respect to their QRS fiducial points, while the window end was

set at the earliest T_{off} of both beats computed from their QRS fiducial points.
3. A constant value was subtracted from each T wave in each of the analyzed leads so that the amplitude at T_{off} was set to 0 mV. Subsequently, an average T-wave vector was calculated for each T-wave. The angle dT° between two consecutive T-waves, which is associated with the instantaneous degree of repolarization instability, was calculated by using the dot product of each pair of consecutive average T-wave vectors.
4. The dT° time series was filtered by using a 10th-order median filter to attenuate outliers and avoid very abrupt changes in the time series.

2.5. PRD Computation

Two different methods, based on Continuous Wavelet Transform (CWT) and Phase-Rectified Signal Averaging (PRSA), respectively, were developed based on the initial methodology proposed in Rizas et al. (2014, 2016). These methods were tested for quantification of the low-frequency components of the beat-to-beat dT° series. The steps followed in each of the two methods are depicted in **Figure 4**.

2.5.1. PRD Computation Using Continuous Wavelet Transform

CWT is one of the most widely-used tools for time-frequency analysis (Addison, 2005). Based on the dT° series calculated as described in section 2.4, the next steps were followed to compute PRD (Rizas et al., 2014):

5. The dT° series was linearly interpolated at 2 Hz and a 10-sample moving average filter was used to remove artifacts.
6. CWT was computed at all scales from 1 to 40 by using a 4th-order Gaussian wavelet to quantify low-frequency oscillations of dT°. Wavelet coefficients were obtained for each scale at each time point and an average wavelet coefficient was computed for each scale.
7. Scales (a) were converted to pseudo-frequencies (F_a, expressed in Hz) according to the following equation (Abry, 1997):

$$F_a = \frac{F_c}{a \cdot \Delta} \quad (1)$$

where F_c is the center frequency of the mother wavelet, in Hz, and Δ denotes the sampling period, in seconds.

PRD_{CWT} was defined as the average wavelet coefficient in the frequency range between 0.025 and 0.1 Hz.

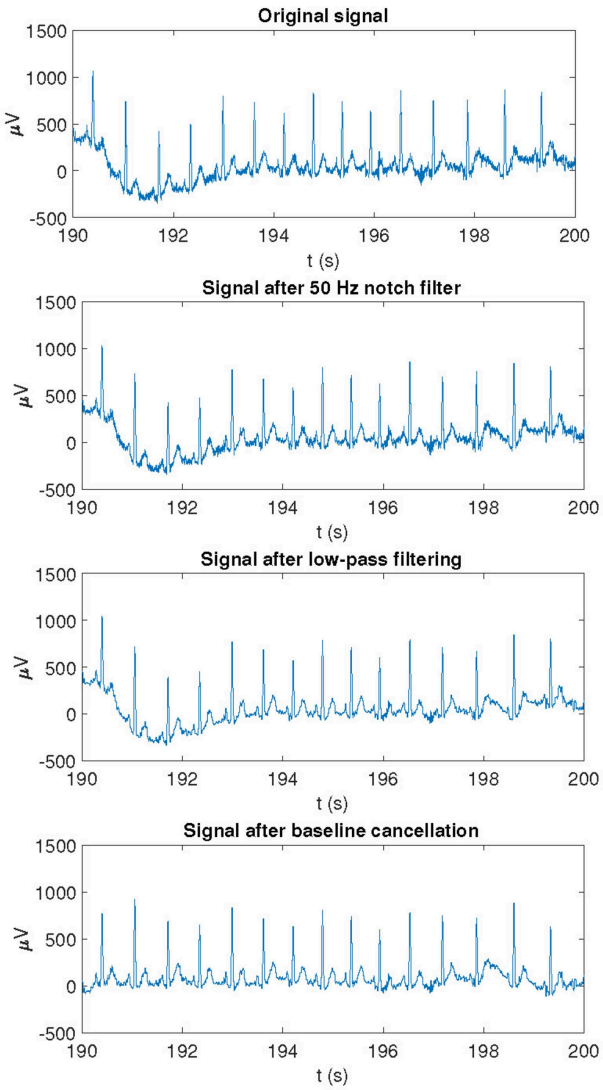

FIGURE 3 | Example of an ECG recording as originally acquired and after application of different pre-processing steps.

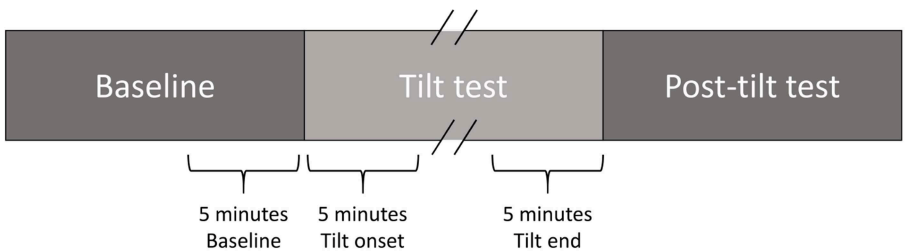

FIGURE 2 | 5-min analysis intervals in each TTT.

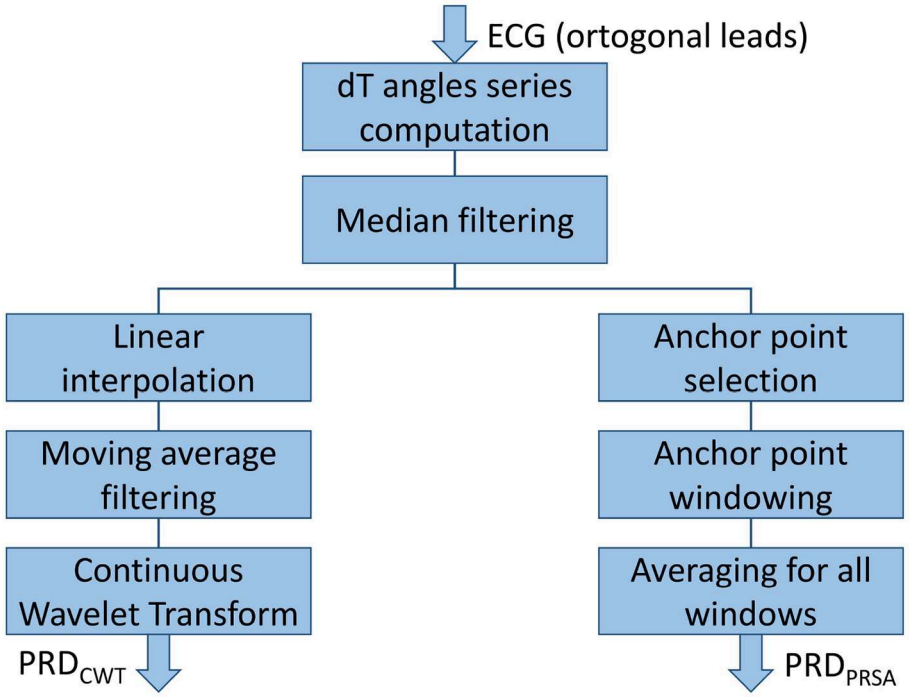

FIGURE 4 | Steps applied to calculate PRD (both CWT- and PRSA-method).

2.5.2. PRD Computation Using Phase-Rectified Signal Averaging

An alternative method to compute oscillatory fluctuations, with less computational requirements, has been proposed based on PRSA (Bauer et al., 2006). The following steps were followed to compute PRD from the dT° series (Rizas et al., 2016):

1. Anchor points were defined by comparing averages of $M = 9$ values of the dT° series previous and posterior to the anchor point candidate (x_i). A beat i is considered an anchor point if:

$$\frac{1}{M}\sum_{j=0}^{M-1} x_{i+j} > \frac{1}{M}\sum_{j=1}^{M} x_{i-j} \quad (2)$$

2. Windows of 2 L values were defined around each anchor point. If an anchor point was so close to the beginning or to the end of the dT° series that there were not enough samples before or after it, it was disregarded. In this study, $L = 20$ was chosen because it was the minimum value to detect frequencies in the range of interest (0.025–0.1) Hz.
3. PRSA series were obtained by averaging the dT° series over all defined windows.

PRD_{PRSA} was defined as the difference between maximum and minimum values of the PRSA series.

2.6. Heart Rate Variability Analysis

RR interval series were computed from the QRS detection marks obtained in section 2.3 for all analyzed 5-min segments at baseline as well as at the beginning and end of TTT. Instantaneous heart rate (HR) variability (HRV) series were calculated following the method described in Bailón et al. (2011). For each segment, the power spectral density (PSD) of HRV was computed by using the periodogram method. A high-frequency band (HF, [0.15, 0.4] Hz) and a low-frequency band (LF, [0.04, 0.15] Hz) were defined for HRV analysis in the frequency domain and the LF and HF powers were calculated by integrating the power spectrum in each of those two bands, respectively. The normalized LF power (LFn), the normalized HF power (HFn) and the ratio between the power in the LF and HF bands (LF/HF) were computed (Malik et al., 1996). Also the median HR (HR_{median}) was computed.

2.7. Statistical Analysis

The Mann-Whitney U-test (or Wilcoxon rank-sum test) was used to compare independent samples, as when comparing each countermeasure (JUMP or NUTR) subgroup vs the corresponding CTRL subgroup. Wilcoxon signed-rank test was used for comparison of paired samples, as when comparing changes induced by HDBR or by TTT in a given group of subjects. Spearman's correlation coefficient ρ and Kendall's τ were used to quantify rank correlation between CWT and PRSA. All statistical analyses were carried out using MATLAB R2017a (9.2).

3. RESULTS

3.1. Comparison of PRD Computed by CWT- and PRSA-Based Methods

Figure 5 shows the two analyzed recordings, at PRE-HDBR and POST-HDBR, from a volunteer presenting small and

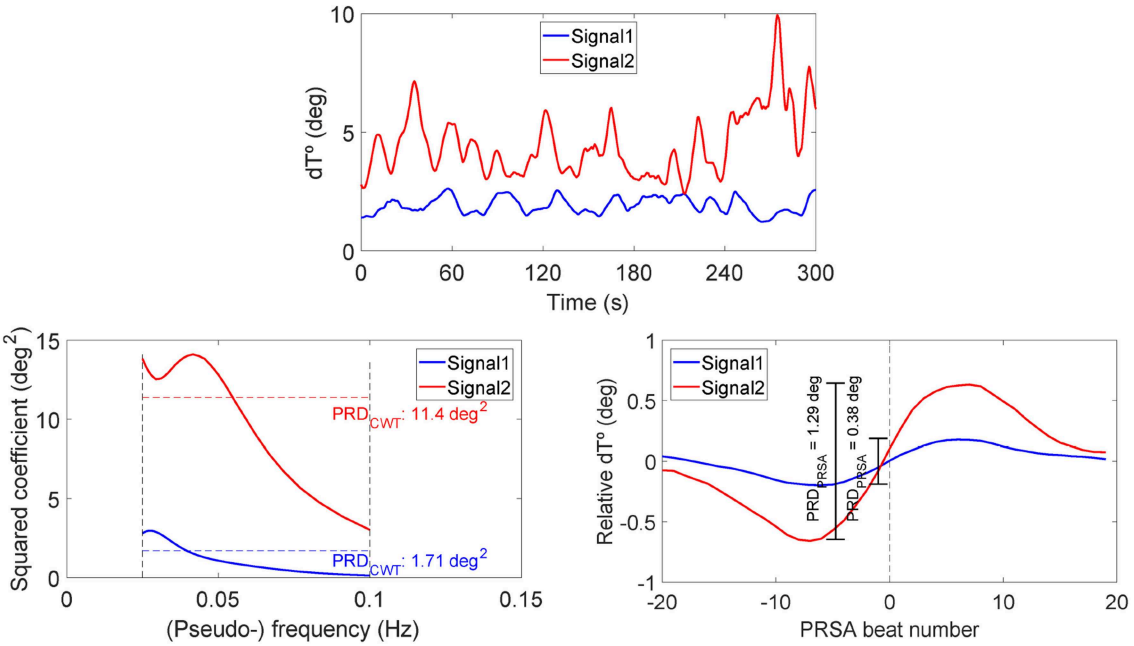

FIGURE 5 | Examples of dT° series (upper), frequency pseudospectra (bottom left), and PRSA series (bottom right) for two ECG segments from a volunteer of the study, at PRE-HDBR and at POST-HDBR, presenting remarkably different magnitudes of low-frequency oscillations in ventricular repolarization. Associated PRD values are indicated in the bottom panels, as computed using CWT- and PRSA-based methods.

large magnitudes of low-frequency oscillations in ventricular repolarization, respectively. The three plots represent the dT° series, the frequency pseudospectra (in terms of squared wavelet coefficients) and the PRSA series. The blue line corresponds to the ECG segment at PRE-HDBR and the red one to the ECG segment at POST-HDBR. Note that the case shown in blue presents low-frequency oscillations in dT° of small magnitude, which translates into low values of PRD_{CWT} and PRD_{PRSA}. The red case, in contrast, presents low-frequency oscillations in dT° of larger magnitude and is associated with considerably higher PRD values, both when measured by using CWT- and PRSA-based methods.

Figure 6 shows the correlation of PRD values computed by using the CWT-based method (X-axis) and the PRSA-based method (Y-axis) for all analyzed segments (baseline, beginning, and end of the tilt phase) in the CTRL group of DLR and MEDES campaigns, for both PRE-HDBR and POST-HDBR. The scatterplot shows a strong correlation between both methods. Rank correlation coefficients were: Spearman's $\rho = 0.93$ ($p < 10^{-50}$), Kendall's $\tau = 0.79$ ($p < 10^{-35}$). In the following, all presented results use the PRSA-based method.

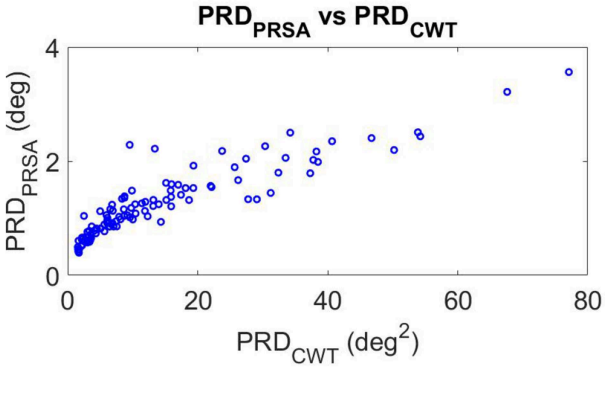

FIGURE 6 | Scatterplot of PRD values measured by CWT- and PRSA-based methods.

3.2. Tilt Test-Induced Effects on PRD

Figure 7, top panel, shows the results of the analysis of three 5-min segments of the dT° series, corresponding to baseline (prior to the tilt) as well as to beginning and end of the tilt phase, for all volunteers in the CTRL group of both campaigns (DLR and MEDES). Results are separately presented for PRE-HDBR (before HDBR) and POST-HDBR (after HDBR). As can be observed from the figure, PRD increased following tilt as compared to baseline, being the results statistically significant when the segment at the beginning of the tilt phase was analyzed. This was true for both PRE-HDBR and POST-HDBR. Results on the effects of tilt on the HRV indices LFn and LF/HF are presented in the bottom panels of **Figure 7**. Both indices showed significantly larger values in response to tilt, indicating increased sympathetic drive during orthostatic stress, both at PRE-HDBR and POST-HDBR. The effect of tilt on other HR and HRV indices is presented in **Figure S1**, which shows a significant increase of HR_{median} and a significant decrease of HFn in response to tilt.

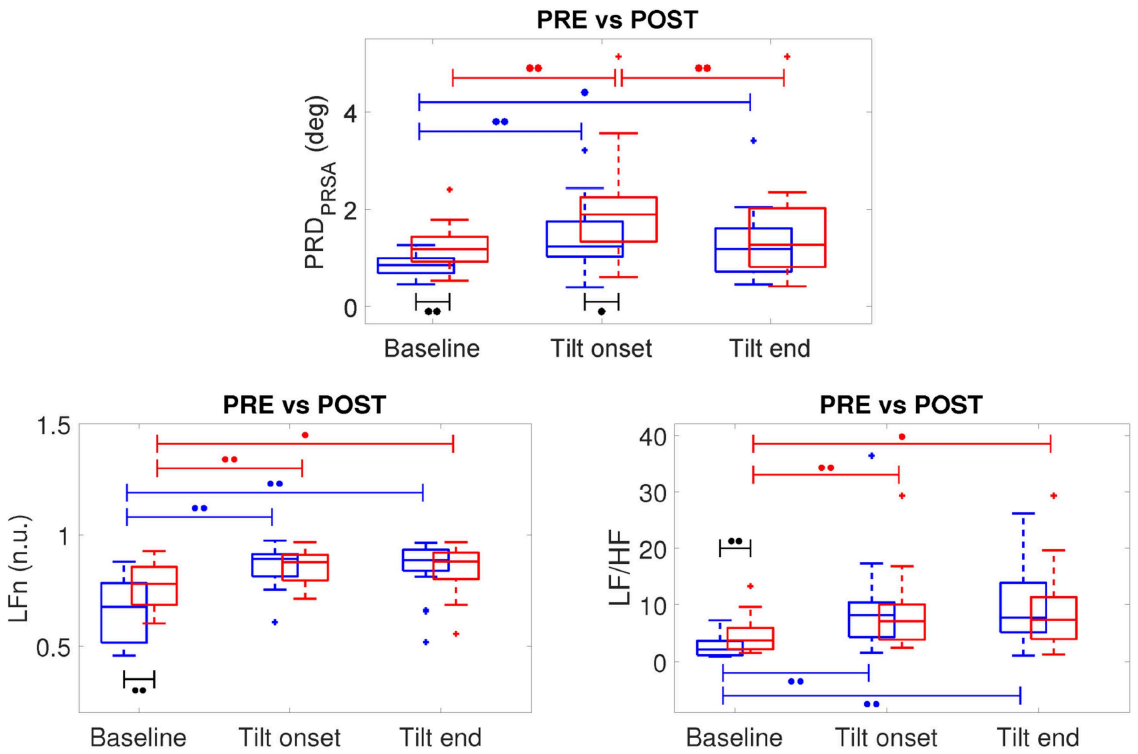

FIGURE 7 | Boxplots of PRD, LFn and LF/HF at PRE-HDBR (in blue) and POST-HDBR (in red) evaluated at baseline and at the beginning and end of the tilt phase. $^{\bullet\bullet}p < 0.01$, $^{\bullet}p < 0.05$ (Wilcoxon signed-rank test).

3.3. Microgravity-Induced Effects on PRD

The effects of microgravity exposure on PRD obtained by comparing PRE-HDBR and POST-HDBR for CTRL group of DLR and MEDES campaigns can be observed from **Figure 7**. At baseline (before TTT), PRD was significantly increased at POST-HDBR with respect to PRE-HDBR, changing from 0.85 [0.31] deg at PRE-HDBR to 1.18 [0.51] deg at POST-HDBR ($p < 0.01$), as presented in the left columns of **Figure 7**.

Considering the analysis at the onset of the tilt phase, PRD was also increased at POST-HDBR with respect to PRE-HDBR, changing from 1.24 [0.72] deg at PRE-HDBR to 1.89 [0.91] deg at POST-HDBR ($p < 0.05$), as shown in the middle columns of **Figure 7**.

No statistically significant differences in PRD at POST-HDBR vs. PRE-HDBR were observed when analyzed at the end of the tilt phase (right columns in **Figure 7**), although there was a trend to increased PRD at POST-HDBR as compared to PRE-HDBR. Specifically, PRD increased from 1.18 [0.88] deg at PRE-HDBR to 1.27 [1.21] deg at POST-HDBR (n.s.).

In the case of the HRV indices LFn and LF/HF, statistically significant microgravity-induced increases were observed when the baseline period was analyzed (see **Figure 7**). Specifically, LFn changed from 0.67 [0.27] n.u. at PRE-HDBR to 0.78 [0.17] n.u. at POST-HDBR ($p < 0.01$). LF/HF changed from 2.12 [2.51] at PRE-HDBR to 3.74 [3.78] at POST-HDBR ($p < 0.01$). The index HFn significantly decreased from PRE-HDBR to POST-HDBR when evaluated at baseline, whereas HR_{median} was significantly augmented due to microgravity either when evaluated at baseline or at the beginning and end of the tilt test (see **Figure S1**).

3.4. PRD and HRV Relation

Figure S2 shows the relationship between tilt-induced changes in PRD and in HR or HRV indexes (LFn, LF/HF and HR_{median}) at PRE-HDBR and POST-HDBR. No significant correlation could be found between PRD and HR or HRV, with Spearman's correlation coefficient ρ being below 0.15 in all evaluated cases (n.s.).

3.5. Effectiveness of Exercise-Based Countermeasure

The ability of a jump-based countermeasure to reverse the effects of microgravity was evaluated by comparing PRD values at PRE-HDBR and POST-HDBR in each of the CTRL and JUMP subgroups of the DLR campaign. The values for PRD measured for each phase of the TTT are presented in **Table 1**. Although there were increases in PRD values from PRE-HDBR to POST-HDBR in both CTRL and JUMP subgroups, the increase was much more attenuated in the JUMP subgroup. Significant differences were found at the beginning of tilt for both CTRL and JUMP subgroups. Illustration of the effects of the JUMP countermeasure are presented in **Figure 8** (left panel), which shows values of ΔPRD, calculated as the PRD value at POST-HDBR minus the PRD value at PRE-HDBR for each subject. From the figure it is clear that whereas values of ΔPRD were

TABLE 1 | PRD values (median [IQR]) at all phases of TTT for PRE-HDBR and POST-HDBR in CTRL and JUMP subgroup.

	PRD	PRE-HDBR (deg)	POST-HDBR (deg)
Baseline	CTRL	0.78 [0.40]	0.93 [0.79]
	JUMP	0.72 [0.34]	0.81 [0.47]
Tilt onset	CTRL	1.32 [1.40]	2.04 [0.99]*
	JUMP	0.77 [0.29]	1.28 [0.77]*
Tilt end	CTRL	0.95 [0.98]	1.48 [1.12]
	JUMP	0.85 [0.51]	1.02 [0.59]

*$p < 0.05$ (with respect to PRE-HDBR).

clearly positive in the CTRL subgroup, particularly during the tilt phase, values were remarkably closer to 0 in the JUMP subgroup.

3.6. Effectiveness of Nutrition-Based Countermeasure

Results on the effectiveness of a nutrition-based countermeasure are presented in **Table 2**. **Figure 8** (right panel) illustrates these results in terms of ΔPRD (differences between POST-HDBR and PRE-HDBR calculated for each subject in the analyzed subgroups). As can be observed from **Table 2**, baseline PRD increased significantly from PRE-HDBR to POST-HDBR in both the CTRL and NUTR subgroups of the MEDES campaign. When evaluation was performed at the beginning of the tilt test, PRD increased at POST-HDBR with respect to PRE-HDBR, although differences were not statistically significant. At the end of the tilt phase, PRD showed a trend of increase in the NUTR group but not in the CTRL group. Results shown in **Figure 8** (right panel) confirm the lack of effectiveness of the evaluated nutrition-based countermeasure.

4. DISCUSSION

This study aimed at investigating alterations in ventricular repolarization associated with long-term exposure to simulated microgravity conditions elicited by 60-day HDBR. Two methods have been developed for quantification of low-frequency oscillations in the T-wave of the ECG, departing from the original methodology proposed in Rizas et al. (2014, 2016). These methods, one using CWT and the other one using PRSA, have been shown to render concordant results in terms of the index of Periodic Repolarization Dynamics, PRD, a marker of low-frequency repolarization oscillations whose increase has been shown to be predictor of ventricular arrhythmias and sudden cardiac death (Rizas et al., 2014, 2016). This study has proved that microgravity remarkably enhances PRD, particularly when evaluated in response to sympathetic stimulation induced by tilt test. An exercise-based countermeasure has been shown to partially reverse microgravity-induced effects on PRD, whereas a nutrition-based countermeasure has been shown not to be effective at all.

The methods developed in this study for PRD quantification departed from the CWT- and PRSA-based methods proposed in Rizas et al. (2014, 2016), respectively. Whereas, the CWT-based method in Rizas et al. (2014) used spherical coordinates, our method used Cartesian coordinates, which rendered improved results for cases where T-wave vectors were close to the axes. Also, our method introduced a refinement on the temporal window used for T-wave definition so as to guarantee that the two consecutive T-waves involved in each angle computation had comparable T-wave window beginnings and ends with respect to their corresponding QRS fiducial points. An additional difference regards the number of samples used for the moving average filter, which was 30 in Rizas et al. (2014) and 10 in our study to minimize distortion of relevant information in the frequency band of interest. For our updated CWT- and PRSA-based methods, correlation analysis has confirmed a strong agreement between them. Although our PRD values are notably different from those obtained in Rizas et al. (2014, 2016), the agreement between CWT- and PRSA-based methods is in concordance with the findings reported in Rizas et al. (2016), where an approach based on PRSA was presented as an alternative to the approach using the CWT technique. The advantage of the PRSA approach is that it highly reduces the computational cost associated with PRD computation.

The analysis conducted in this work has shown that the autonomic changes induced by TTT are manifested as an increase in PRD, both when measured at PRE-HDBR and at POST-HDBR. Such PRD changes could be attributable to an increased sympathetic drive, as indicated by increases in the HRV indices LFn and LF/HF, in line with many other HRV studies, including the ones pioneering spectral HRV analysis during TTT (Pagani et al., 1986, 1988). It is well-known that sympathetic stimulation influences ventricular repolarization and modifies the characteristics of the T-wave in the ECG (Ramirez et al., 2011). Our results showing an increase in PRD in response to TTT are in line with the changes in PRD reported in response to variations in sympathetic activity or β-adrenergic modulation (Rizas et al., 2014, 2016). In our study, those changes are shown not to be explained by HRV changes but to reflect direct autonomic modulation of the ventricular myocardium, in accordance with the findings reported in Rizas et al. (2014, 2016). *In vivo* studies in patients have demonstrated that the same low-frequency oscillatory behavior of ventricular repolarization occurs locally, as measured from activation recovery intervals (ARIs) obtained from unipolar epicardial electrograms during ventricular pacing (Hanson et al., 2014; Porter et al., 2018). In those studies, heightened arousal of the sympathetic nervous system was elicited and maintained by mental stress or by Valsalva maneuver, which allowed characterization of low-frequency oscillations in ARI, a surrogate of action potential duration (APD), showing that those oscillations are coupled to oscillations in systolic and diastolic blood pressure (Hanson et al., 2014; Porter et al., 2018). Computational studies have provided insight into the mechanisms underlying sympathetically-mediated low-frequency oscillations of APD and the observed inter-individual differences (Pueyo et al., 2016; Sampedro-Puente et al., 2019). Specifically, phasic changes in both β-adrenergic stimulation and hemodynamic loading, a known accompaniment of enhanced sympathetic activity, have been demonstrated to contribute to

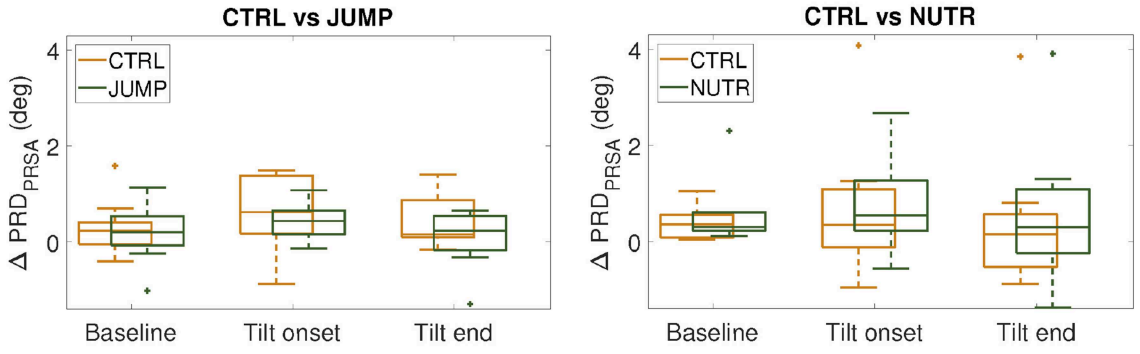

FIGURE 8 | ΔPRD values (median ± IQR) measured respect to PRE-HDBR for the CTRL subgroups (in orange) and the countermeasure (JUMP or NUTR) subgroups (in green) at baseline, beginning and end of the tilt phase. (n.s., Wilcoxon rank-sum test).

low-frequency oscillations in APD, with these two actions being synergistic (Pueyo et al., 2016). Ionic differences in the densities of the L-type calcium (I_{CaL}), rapid delayed rectifier potassium (I_{Kr}), and inwardly rectifier potassium (I_{K1}) currents have been identified as the main drivers of inter-individual differences in the magnitude of low-frequency APD oscillations (Sampedro-Puente et al., 2019).

Importantly, our results have provided evidence on significant effects of long-duration microgravity simulation on cardiac electrical activity. In line with previously published studies, this work has confirmed that microgravity markedly alters ventricular repolarization (D'Aunno et al., 2003; Grenon et al., 2005; Sakowski et al., 2011; Bolea et al., 2012, 2013; Caiani et al., 2013), with those alterations being more manifested when evaluated in response to sympathetic stimulation. This study adds one more T-wave characteristic to the list of ECG repolarization properties proved to be modulated by microgravity. The quantified PRD index represents a form of temporal variability in ventricular repolarization, specifically focused on oscillations of frequencies below 0.1 Hz. Although other measures of ECG temporal variability have been investigated during or immediately after simulated microgravity exposure (Sakowski et al., 2011; Bolea et al., 2013), PRD can provide a more robust characterization of repolarization instability by encompassing global T-wave vector information. Also, the PRD index, by accounting for frequencies below 0.1 Hz, has been proven to be related to sympathetic modulation of ventricular repolarization (Rizas et al., 2016). On the basis that augmented sympathetic activity is associated with adverse outcomes in different patient populations (Verrier and Antzelevitch, 2004), the evaluated PRD index is of great interest for risk prediction. The enhancement of spatial and/or temporal ventricular heterogeneities observed in this and other studies in relation to long-term exposure to microgravity conditions suggest that microgravity could accentuate repolarization instability and thus increase ventricular arrhythmic risk, especially immediately upon gravity restoration. In particular, this study has shown that PRD quantified following 60-day HDBR is highly elevated, up to 50% at rest and up to 100% in response to TTT, with respect to PRE-HDBR values. The extent of change in PRD values measured immediately after 60-day HDBR could be associated with high arrhythmic risk taking as a reference previous studies on risk assessment in post-myocardial infarction patients, where those extents of change were found in patients who died vs. those who survived during follow-up (Rizas et al., 2014, 2017). This is in line with other studies that have reported on subjects presenting long-term microgravity-induced changes in ECG repolarization of an extent similar to those associated with more than 3-fold increased hazard ratio for sudden cardiac death in general populations (Sakowski et al., 2011).

TABLE 2 | PRD values (median [IQR]) at all phases of TTT for PRE-HDBR and POST-HDBR in CTRL and NUTR subgroup.

	PRD	PRE-HDBR (deg)	POST-HDBR (deg)
Baseline	CTRL	0.92 [0.19]	1.32 [0.33]**
	NUTR	1.10 [0.51]	1.22 [1.04]*
Tilt onset	CTRL	1.22 [0.23]	1.59 [0.98]
	NUTR	1.32 [1.02]	1.93 [1.72]
Tilt end	CTRL	1.27 [0.88]	1.13 [0.96]
	NUTR	1.19 [0.74]	1.41 [1.76]

$^{**}p < 0.01$, $^{*}p < 0.05$ (with respect to PRE-HDBR).

Additionally, this study has assessed two countermeasures in their ability to counteract microgravity-induced effects on ventricular repolarization. The first applied countermeasure, based on an exercise training protocol, although markedly attenuated microgravity effects as measured by changes in the PRD index, it was not able to completely reverse them. These results on partial effectiveness of exercise-based countermeasures are in line with the findings reported in Kramer et al. (2017), Maggioni et al. (2018), and Caiani et al. (2018), which investigated the same jump-based countermeasure to reverse musculoskeletal and cardiovascular deconditioning. In other studies, exercise-based countermeasures have shown to be very effective in preserving bone and muscular conditions (McRae et al., 2012; Kramer et al., 2017; Maggioni et al., 2018).

The second tested countermeasure, a nutritional supplementation composed of an anti-oxidant and anti-inflammatory dietary mix, has been shown to be far from

being effective in reducing microgravity-induced effects on ventricular repolarization. This is in agreement with other studies pointing out to lack of effectiveness of this countermeasure in counteracting microgravity exposure effects on bone turnover (Austermann et al., 2019). Importantly, the intake of omega-3 fatty acids, which are components of the dietary mix, and their possible protection of cardiovascular health should additionally be viewed in relation to the potentially increased risk for ventricular arrhythmias. Such a relation is, nevertheless, controversial, with some studies suggesting that they have detrimental arrhythmogenic effects, whereas other postulate minimal effects or highly anti-arrhythmic potential (Albert, 2012; von Schacky, 2012; Coronel, 2017; Tribulova et al., 2017). Although one reason to include this type of acid in a dietary support was its protective effects on bones (Zwart et al., 2010), the findings of the present study point out that the dietary mix could not reduce adverse cardiac effects of microgravity simulation. Further studies including larger number of subjects are needed to confirm or refute these findings. Also, it is relevant to note that, when evaluating the effects of the tested countermeasures, the CTRL subgroups of the JUMP and NUTR studies did not share the same ventricular repolarization characteristics as evaluated by PRD, despite the subjects of both studies having similar physical conditions. Specifically, subjects in the CTRL subgroup of the JUMP study presented higher values of PRD, both at PRE-HDBR and POST-HDBR. Because of that reason, our results on countermeasure effects were assessed in relative terms. Nevertheless, the inclusion of a larger number of subjects would definitely allow more robust analysis of absolute and relative microgravity-induced changes. Additionally, future studies could test other types of nutritional supplements to improve the ability to counteract deleterious effects associated with long-term microgravity exposure (Cena et al., 2003). Based on the results of this study and the concordance with the outcomes of other studies, a modified jump training or a combination of exercise- and nutrition-based countermeasure (Schneider et al., 2009; Konda et al., 2019; Kramer et al., 2019), possibly including other components like pharmacological agents or artificial gravity (Evans et al., 2018), would be suggested to compensate for adverse microgravity-induced effects on ventricular repolarization.

5. CONCLUSIONS

The effects of long-duration microgravity on ventricular repolarization have been assessed by evaluation of the PRD index, a marker of low-frequency repolarization oscillations whose increase is related to high risk for ventricular arrhythmias and sudden cardiac death. Two methods have been developed for robust quantification of PRD, which have shown to present very good agreement. Long-term microgravity exposure has been proven to markedly elevate PRD, particularly when evaluated in response to enhanced sympathetic activity induced by a tilt table test. A countermeasure based on exercise training has been shown to partially counteract microgravity-induced changes in ventricular repolarization as assessed immediately upon gravity restoration.

DATA AVAILABILITY STATEMENT

The datasets analyzed in this article are not publicly available. Requests to access the datasets should be directed to European Space Agency.

ETHICS STATEMENT

The studies involving human participants were reviewed and approved by Institute of Aerospace Medicine—German Aerospace Center-DLR and by Institute of Space Medicine and Physiology-MEDES. The patients/participants provided their written informed consent to participate in this study.

AUTHOR CONTRIBUTIONS

EP and JM devised the project, the main conceptual ideas and proof outline, and were responsible for overseeing the research and providing critical insight and recommendations regarding the focus, structure, and content of the paper. SP performed computational simulations and analyzed the data results. EC was responsible for the definition of the bed rest data acquisition protocols and contributed with technical details and analysis support. FL contributed by managing on-site data acquisition in both campaigns. All authors participated in writing and proofreading throughout the publication process.

FUNDING

This work was supported by projects ERC-2014-StG 638284 (ERC), DPI2016-75458-R (MINECO) and Aragón Government (Reference Group BSICoS T39-17R and project LMP124-18) cofunded by FEDER 2014-2020 *Building Europe from Aragon.* We also acknowledge the support of the Italian Space Agency (contract 2018-7-U.0, PI and recipient EC).

SUPPLEMENTARY MATERIAL

The Supplementary Material for this article can be found online at: https://www.frontiersin.org/articles/10.3389/fphys.2019.01510/full#supplementary-material

REFERENCES

Abry, P. (1997). *Ondelettes et Turbulences: Multirésolutions, Algorithmes de Décomposition, Invariance D'échelle et Signaux de Pression.* Paris: Nouveaux essais. Diderot éd.

Acar, B., Yi, G., Hnatkova, K., and Malik, M. (1999). Spatial, temporal and wavefront direction characteristics of 12-lead t-wave morphology. *Med. Biol. Eng. Comput.* 37, 574–584.

Adam, D. R., Smith, J. M., Akselrod, S., Nyberg, S., Powell, A. O., and Cohen, R. J. (1984). Fluctuations in t-wave morphology

and susceptibility to ventricular fibrillation. *J. Electrocardiol.* 17, 209–218.

Addison, P. S. (2005). Wavelet transforms and the ECG: a review. *Physiol. Measure.* 26, R155–R199. doi: 10.1088/0967-3334/26/5/r01

Albert, C. M. (2012). Omega-3 fatty acids, ventricular arrhythmias, and sudden cardiac death. *Circ. Arrhythm. Electrophysiol.* 5, 456–459. doi: 10.1161/CIRCEP.112.971416

Anzai, T., Frey, M. A., and Nogami, A. (2014). Cardiac arrhythmias during long-duration spaceflights. *J. Arrhythm.* 30, 139–149. doi: 10.1016/j.joa.2013.07.009

Austermann, K., Baecker, N., Zwart, S. R., Smith, S. M., and Heer, M. (2019). Effects of antioxidants on bone turnover markers in 6° head-down tilt bed rest. *Front. Physiol.* 9:48. doi: 10.3389/conf.fphys.2018.26.00048

Badilini, F., Fayn, J., Maison-Blanche, P., Leenhardt, A., Forlini, M. C., Denjoy, I., et al. (1997). Quantitative aspects of ventricular repolarization: relationship between three-dimensional T wave loop morphology and scalar qt dispersion. *Ann. Noninvasive Electrocardiol.* 2, 146–157.

Bailón, R., Laouini, G., Grao, C., Orini, M., Laguna, P., and Meste, O. (2011). The integral pulse frequency modulation model with time-varying threshold: application to heart rate variability analysis during exercise stress testing. *IEEE Trans. Biomed. Eng.* 58, 642–652. doi: 10.1109/TBME.2010.2095011

Bauer, A., Kantelhardt, J. W., Bunde, A., Barthel, P., Schneider, R., Malik, M., et al. (2006). Phase-rectified signal averaging detects quasi-periodicities in non-stationary data. *Phys. A Stat. Mech. Appl.* 364, 423–434. doi: 10.1016/j.physa.2005.08.080

Baumert, M., Lambert, E., Vaddadi, G., Sari, C. I., Esler, M., Lambert, G., et al. (2011). Cardiac repolarization variability in patients with postural tachycardia syndrome during graded head-up tilt. *Clin. Neurophysiol.* 122, 405–409. doi: 10.1016/j.clinph.2010.06.017

Bolea, J., Caiani, E. G., Pueyo, E., Laguna, P., and Almeida, R. (2012). "Microgravity effects on ventricular response to heart rate changes," in *Engineering in Medicine and Biology Society (EMBC), 2012 Annual International Conference of the IEEE* (San Diego, CA: IEEE), 3424–3427.

Bolea, J., Laguna, P., Caiani, E. G., and Almeida, R. (2013). "Heart rate and ventricular repolarization variabilities interactions modification by microgravity simulation during head-down bed rest test," in *Computer-Based Medical Systems (CBMS), 2013 IEEE 26th International Symposium on* (Porto: IEEE), 552–553.

Caiani, E., Landreani, F., Costantini, L., Mulder, E., Gerlach, D., Vaïda, P., et al. (2018). "Effectiveness of high-intensity jump training countermeasure on mitral and aortic flow after 58-days head-down bed-rest assessed by phase-contrast MRI," in *International Astronautical Congress*, Vol. 2018 (Bremen), 135–141.

Caiani, E. G., Martin-Yebra, A., Landreani, F., Bolea, J., Laguna, P., and Vaïda, P. (2016). Weightlessness and cardiac rhythm disorders: current knowledge from space flight and bed-rest studies. *Front. Astron. Space Sci.* 3:27. doi: 10.3389/fspas.2016.00027

Caiani, E. G., Pellegrini, A., Bolea, J., Sotaquira, M., Almeida, R., and Vaïda, P. (2013). Impaired T-wave amplitude adaptation to heart-rate induced by cardiac deconditioning after 5-days of head-down bed-rest. *Acta Astron.* 91, 166–172. doi: 10.1016/j.actaastro.2013.05.016

Cena, H., Sculati, M., and Roggi, C. (2003). Nutritional concerns and possible countermeasures to nutritional issues related to space flight. *Eur. J. Nutr.* 42, 99–110. doi: 10.1007/s00394-003-0392-8

Convertino, V. A. (2009). Status of cardiovascular issues related to space flight: implications for future research directions. *Respir. Physiol. Neurobiol.* 169, S34–S37. doi: 10.1016/j.resp.2009.04.010

Coronel, R. (2017). The pro- or antiarrhythmic actions of polyunsaturated fatty acids and of cholesterol. *Pharmacol. Ther.* 176, 40–47. doi: 10.1016/j.pharmthera.2017.02.004

D'Aunno, D. S., Dougherty, A. H., DeBlock, H. F., and Meck, J. V. (2003). Effect of short-and long-duration spaceflight on QTc intervals in healthy astronauts. *Am. J. Cardiol.* 91, 494–497. doi: 10.1016/s0002-9149(02)03259-9

Edenbrandt, L., and Pahlm, O. (1988). Vectorcardiogram synthesized from a 12-lead ECG: superiority of the inverse Dower matrix. *J. Electrocardiol.* 21, 361–367.

Evans, J. M., Knapp, C. F., and Goswami, N. (2018). Artificial gravity as a countermeasure to the cardiovascular deconditioning of spaceflight: gender perspectives. *Front. Physiol.* 9:716. doi: 10.3389/fphys.2018.00716

Fritsch-Yelle, J. M., Whitson, P. A., Bondar, R. L., and Brown, T. E. (1996). Subnormal norepinephrine release relates to presyncope in astronauts after spaceflight. *J. Appl. Physiol.* 81, 2134–2141.

Garrett-Bakelman, F. E., Darshi, M., Green, S. J., Gur, R. C., Lin, L., Macias, B. R., et al. (2019). The NASA Twins Study: a multidimensional analysis of a year-long human spaceflight. *Science* 364:eaau8650. doi: 10.1126/science.aau8650

Grenon, S. M., Xiao, X., Hurwitz, S., Ramsdell, C. D., Sheynberg, N., Kim, C., et al. (2005). Simulated microgravity induces microvolt T wave alternans. *Ann. Noninvasive Electrocardiol.* 10, 363–370. doi: 10.1111/j.1542-474X.2005.00654.x

Hanson, B., Child, N., Van Duijvenboden, S., Orini, M., Chen, Z., Coronel, R., et al. (2014). Oscillatory behavior of ventricular action potential duration in heart failure patients at respiratory rate and low frequency. *Front. Physiol.* 5:414. doi: 10.3389/fphys.2014.00414

Hargens, A. R., and Vico, L. (2016). Long-duration bed rest as an analog to microgravity. *J. Appl. Physiol.* 120, 891–903. doi: 10.1152/japplphysiol.00935.2015

Kanas, N., Salnitskiy, V., Gushin, V., Weiss, D. S., Grund, E. M., Flynn, C., et al. (2001). Asthenia–does it exist in space? *Psychosom. Med.* 63, 874–880. doi: 10.1097/00006842-200111000-00004

Kardys, I., Kors, J. A., van der Meer, I. M., Hofman, A., van der Kuip, D. A., and Witteman, J. C. (2003). Spatial QRS-T angle predicts cardiac death in a general population. *Eur. Heart J.* 24, 1357–1364. doi: 10.1016/S0195-668X(03)00203-3

Konda, N. N., Karri, R. S., Winnard, A., Nasser, M., Evetts, S., Boudreau, E., et al. (2019). A comparison of exercise interventions from bed rest studies for the prevention of musculoskeletal loss. *npj Microgravity* 5:12. doi: 10.1038/s41526-019-0073-4

Kramer, A., Kümmel, J., Mulder, E., Gollhofer, A., Frings-Meuthen, P., and Gruber, M. (2017). High-intensity jump training is tolerated during 60 days of bed rest and is very effective in preserving leg power and lean body mass: an overview of the Cologne RSL Study. *PLOS ONE* 12:e0169793. doi: 10.1371/journal.pone.0169793

Kramer, A., Poppendieker, T., and Gruber, M. (2019). Suitability of jumps as a form of high-intensity interval training: effect of rest duration on oxygen uptake, heart rate and blood lactate. *Eur. J. Appl. Physiol.* 119, 1149–1156. doi: 10.1007/s00421-019-04105-w

Maggioni, M. A., Castiglioni, P., Merati, G., Brauns, K., Gunga, H.-C., Mendt, S., et al. (2018). High-intensity exercise mitigates cardiovascular deconditioning during long-duration bed rest. *Front. Physiol.* 9:1553. doi: 10.3389/fphys.2018.01553

Malik, M., Bigger, J. T., Camm, A. J., Kleiger, R. E., Malliani, A., Moss, A. J., et al. (1996). Heart rate variability: standards of measurement, physiological interpretation, and clinical use. *Eur. Heart J.* 17, 354–381.

Martinez, J. P., Almeida, R., Olmos, S., Rocha, A. P., and Laguna, P. (2004). A wavelet-based ECG delineator: evaluation on standard databases. *IEEE Trans. Biomed. Eng.* 51, 570–581. doi: 10.1109/TBME.2003.821031

Martinez, J. P., and Olmos, S. (2005). Methodological principles of T wave alternans analysis: a unified framework. *IEEE Trans. Biomed. Eng.* 52, 599–613. doi: 10.1109/TBME.2005.844025

Martín-Yebra, A., Caiani, E. G., Monasterio, V., Pellegrini, A., Laguna, P., and Martínez, J. P. (2015). Evaluation of T-wave alternans activity under stress conditions after 5 d and 21 d of sedentary head-down bed rest. *Physiol. Meas.* 36, 2041–2055. doi: 10.1088/0967-3334/36/10/2041

McRae, G., Payne, A., Zelt, J. G., Scribbans, T. D., Jung, M. E., Little, J. P., et al. (2012). Extremely low volume, whole-body aerobic–resistance training improves aerobic fitness and muscular endurance in females. *Appl. Physiol. Nutr. Metab.* 37, 1124–1131. doi: 10.1139/h2012-093

Meck, J. V., Reyes, C. J., Perez, S. A., Goldberger, A. L., and Ziegler, M. G. (2001). Marked exacerbation of orthostatic intolerance after long- vs. short-duration spaceflight in veteran astronauts. *Psychosom. Med.* 63, 865–873. doi: 10.1097/00006842-200111000-00003

Mitchell, B. M., and Meck, J. V. (2004). Short-duration spaceflight does not prolong QTc intervals in male astronauts. *Am. J. Cardiol.* 93, 1051–1052. doi: 10.1016/j.amjcard.2003.12.060

Pagani, M., Lombardi, F., Guzzetti, S., Rimoldi, O., Furlan, R., Pizzinelli, P., et al. (1986). Power spectral analysis of heart rate and arterial pressure variabilities as a marker of sympatho-vagal interaction in man and conscious dog. *Circ. Res.* 59, 178–193.

Pagani, M., Malfatto, G., Pierini, S., Casati, R., Masu, A. M., Poli, M., et al. (1988). Spectral analysis of heart rate variability in the assessment of autonomic diabetic neuropathy. *J. Auton. Nervous Syst.* 23, 143–153.

Pavy-Le Traon, A., Heer, M., Narici, M. V., Rittweger, J., and Vernikos, J. (2007). From space to Earth: advances in human physiology from 20 years of bed rest studies (1986–2006). *Eur. J. Appl. Physiol.* 101, 143–194. doi: 10.1007/s00421-007-0474-z

Piccirillo, G., Magrì, D., Ogawa, M., Song, J., Chong, V. J., Han, S., et al. (2009). Autonomic nervous system activity measured directly and QT interval variability in normal and pacing-induced tachycardia heart failure dogs. *J. Am. Coll. Cardiol.* 54, 840–850. doi: 10.1016/j.jacc.2009.06.008

Porter, B., van Duijvenboden, S., Bishop, M. J., Orini, M., Claridge, S., Gould, J., et al. (2018). Beat-to-beat variability of ventricular action potential duration oscillates at low frequency during sympathetic provocation in humans. *Front. Physiol.* 9:147. doi: 10.3389/fphys.2018.00147

Pueyo, E., Malik, M., and Laguna, P. (2008). A dynamic model to characterize beat-to-beat adaptation of repolarization to heart rate changes. *Biomed. Signal Process. Control* 3, 29–43. doi: 10.1016/j.bspc.2007.09.005

Pueyo, E., Orini, M., Rodríguez, J. F., and Taggart, P. (2016). Interactive effect of beta-adrenergic stimulation and mechanical stretch on low-frequency oscillations of ventricular action potential duration in humans. *J. Mol. Cell. Cardiol.* 97, 93–105. doi: 10.1016/j.yjmcc.2016.05.003

Pueyo, E., Smetana, P., Caminal, P., de Luna, A. B., Malik, M., and Laguna, P. (2004). Characterization of QT interval adaptation to RR interval changes and its use as a risk-stratifier of arrhythmic mortality in amiodarone-treated survivors of acute myocardial infarction. *IEEE Trans. Biomed. Eng.* 51, 1511–1520. doi: 10.1109/TBME.2004.828050

Ramírez, J., Orini, M., Mincholé, A., Monasterio, V., Cygankiewicz, I., Bayés de Luna, A., et al. (2017a). Sudden cardiac death and pump failure death prediction in chronic heart failure by combining ECG and clinical markers in an integrated risk model. *PLOS ONE* 12:e0186152. doi: 10.1371/journal.pone.0186152

Ramírez, J., Orini, M., Tucker, J. D., Pueyo, E., and Laguna, P. (2017b). Variability of ventricular repolarization dispersion quantified by time-warping the morphology of the T-waves. *IEEE Trans. Biomed. Eng.* 64, 1619–1630. doi: 10.1109/TBME.2016.2614899

Ramirez, R. J., Ajijola, O. A., Zhou, W., Holmström, B., Lüning, H., Laks, M. M., et al. (2011). A new electrocardiographic marker for sympathetic nerve stimulation: modulation of repolarization by stimulation of stellate ganglia. *J. Electrocardiol.* 44, 694–699. doi: 10.1016/j.jelectrocard.2011.07.030

Rizas, K. D., Hamm, W., Kääb, S., Schmidt, G., and Bauer, A. (2016). Periodic repolarisation dynamics: a natural probe of the ventricular response to sympathetic activation. *Arrhythm. Electrophysiol. Rev.* 5, 31–36. doi: 10.15420/aer.2015:30:2

Rizas, K. D., McNitt, S., Hamm, W., Massberg, S., Kääb, S., Zareba, W., et al. (2017). Prediction of sudden and non-sudden cardiac death in post-infarction patients with reduced left ventricular ejection fraction by periodic repolarization dynamics: MADIT-II substudy. *Eur. Heart J.* 38, 2110–2118. doi: 10.1093/eurheartj/ehx161

Rizas, K. D., Nieminen, T., Barthel, P., Zürn, C. S., Kähönen, M., Viik, J., et al. (2014). Sympathetic activity-associated periodic repolarization dynamics predict mortality following myocardial infarction. *J. Clin. Invest.* 124, 1770–1780. doi: 10.1172/JCI70085

Rosenbaum, D. S., Jackson, L. E., Smith, J. M., Garan, H., Ruskin, J. N., and Cohen, R. J. (1994). Electrical alternans and vulnerability to ventricular arrhythmias. *New Engl. J. Med.* 330, 235–241.

Russomano, T., Baers, J. H., Velho, R., Cardoso, R. B., Ashcroft, A., Rehnberg, L., et al. (2013). A comparison between the 2010 and 2005 basic life support guidelines during simulated hypogravity and microgravity. *Extreme Physiol. Med.* 2:11. doi: 10.1186/2046-7648-2-11

Sakowski, C., Starc, V., Smith, S. M., and Schlegel, T. T. (2011). Sedentary long-duration head-down bed rest and ECG repolarization heterogeneity. *Aviat. Space Environ. Med.* 82, 416–423. doi: 10.3357/asem.2945.2011

Sampedro-Puente, D. A., Fernandez-Bes, J., Porter, B., van Duijvenboden, S., Taggart, P., and Pueyo, E. (2019). Mechanisms underlying interactions between low-frequency oscillations and beat-to-beat variability of celullar ventricular repolarization in response to sympathetic stimulation: implications for arrhythmogenesis. *Front. Physiol.* 10:916. doi: 10.3389/fphys.2019.00916

Schneider, S. M., Lee, S. M. C., Macias, B. R., Watenpaugh, D. E., and Hargens, A. R. (2009). WISE-2005: exercise and nutrition countermeasures for upright VO2pk during bed rest. *Med. Sci. Sports Exerc.* 41, 2165–2176. doi: 10.1249/mss.0b013e3181aa04e5

Smith, S. M., and Zwart, S. R. (2008). Nutritional biochemistry of spaceflight. *Adv. Clin. Chem.* 46, 87–130. doi: 10.1016/S0065-2423(08)00403-4

Tribulova, N., Szeiffova Bacova, B., Egan Benova, T., Knezl, V., Barancik, M., and Slezak, J. (2017). Omega-3 index and anti-arrhythmic potential of omega-3 PUFAs. *Nutrients* 9:1191. doi: 10.3390/nu9111191

Verrier, R. L., and Antzelevitch, C. (2004). Autonomic aspects of arrhythmogenesis: the enduring and the new. *Curr. Opin. Cardiol.* 19, 2–11. doi: 10.1097/00001573-200401000-00003

von Schacky, C. (2012). Omega-3 fatty acids: anti-arrhythmic, pro-arrhythmic, or both? *Front. Physiol.* 3:88. doi: 10.3389/fphys.2012.00088

Williams, D., Kuipers, A., Mukai, C., and Thirsk, R. (2009). Acclimation during space flight: effects on human physiology. *CMAJ* 180, 1317–1323. doi: 10.1503/cmaj.090628

Yamazaki, T., Froelicher, V. F., Myers, J., Chun, S., and Wang, P. (2005). Spatial QRS-T angle predicts cardiac death in a clinical population. *Heart Rhythm* 2, 73–78. doi: 10.1016/j.hrthm.2004.10.040

Zwart, S. R., Pierson, D., Mehta, S., Gonda, S., and Smith, S. M. (2010). Capacity of omega-3 fatty acids or eicosapentaenoic acid to counteract weightlessness-induced bone loss by inhibiting nf-κb activation: from cells to bed rest to astronauts. *J. Bone Miner. Res.* 25, 1049–1057. doi: 10.1359/jbmr.091041

Zygmunt, A., and Stanczyk, J. (2010). Methods of evaluation of autonomic nervous system function. *Arch. Med. Sci.* 6, 11–18. doi: 10.5114/aoms.2010.13500

Conflict of Interest: The authors declare that the research was conducted in the absence of any commercial or financial relationships that could be construed as a potential conflict of interest.

frontiers in Physiology

ORIGINAL RESEARCH
published: 14 January 2020
doi: 10.3389/fphys.2019.01547

Time Course of Low-Frequency Oscillatory Behavior in Human Ventricular Repolarization Following Enhanced Sympathetic Activity and Relation to Arrhythmogenesis

David Adolfo Sampedro-Puente[1]*, *Jesus Fernandez-Bes*[1], *Norbert Szentandrássy*[2,3], *Péter Nánási*[2,3], *Peter Taggart*[4] and *Esther Pueyo*[1,5]

[1] BSICOS Group, I3A, IIS Aragón, University of Zaragoza, Zaragoza, Spain, [2] Department of Physiology, Faculty of Medicine, University of Debrecen, Debrecen, Hungary, [3] Department of Dental Physiology and Pharmacology, Faculty of Dentistry, University of Debrecen, Debrecen, Hungary, [4] Department of Cardiovascular Sciences, University College London, London, United Kingdom, [5] Center for Biomedical Research in the Network in Bioengineering, Biomaterials and Nanomedicine (CIBER-BBN), Zaragoza, Spain

OPEN ACCESS

Edited by:
T. Alexander Quinn, Dalhousie University, Canada

Reviewed by:
Crystal M. Ripplinger, University of California, Davis, United States
Matthew W. Kay, George Washington University, United States

***Correspondence:**
David Adolfo Sampedro-Puente
sampedro@unizar.es

Specialty section:
This article was submitted to Cardiac Electrophysiology, a section of the journal Frontiers in Physiology

Received: *12 September 2019*
Accepted: *09 December 2019*
Published: *14 January 2020*

Citation:
Sampedro-Puente DA, Fernandez-Bes J, Szentandrássy N, Nánási P, Taggart P and Pueyo E (2020) Time Course of Low-Frequency Oscillatory Behavior in Human Ventricular Repolarization Following Enhanced Sympathetic Activity and Relation to Arrhythmogenesis. Front. Physiol. 10:1547. doi: 10.3389/fphys.2019.01547

Background and Objectives: Recent studies in humans and dogs have shown that ventricular repolarization exhibits a low-frequency (LF) oscillatory pattern following enhanced sympathetic activity, which has been related to arrhythmic risk. The appearance of LF oscillations in ventricular repolarization is, however, not immediate, but it may take up to some minutes. This study seeks to characterize the time course of the action potential (AP) duration (APD) oscillatory behavior in response to sympathetic provocations, unveil its underlying mechanisms and establish a potential link to arrhythmogenesis under disease conditions.

Materials and Methods: A representative set of human ventricular computational models coupling cellular electrophysiology, calcium dynamics, β-adrenergic signaling, and mechanics was built. Sympathetic provocation was modeled via phasic changes in β-adrenergic stimulation (β-AS) and mechanical stretch at Mayer wave frequencies within the 0.03–0.15 Hz band.

Results: Our results show that there are large inter-individual differences in the time lapse for the development of LF oscillations in APD following sympathetic provocation, with some cells requiring just a few seconds and other cells needing more than 3 min. Whereas, the oscillatory response to phasic mechanical stretch is almost immediate, the response to β-AS is much more prolonged, in line with experimentally reported evidences, thus being this component the one driving the slow development of APD oscillations following enhanced sympathetic activity. If β-adrenoceptors are priorly stimulated, the time for APD oscillations to become apparent is remarkably reduced, with the oscillation time lapse being an exponential function of the pre-stimulation level. The major mechanism underlying the delay in APD oscillations appearance is related to the slow I_{Ks} phosphorylation kinetics, with its relevance being modulated by the I_{Ks} conductance of each individual cell. Cells presenting short oscillation time lapses

are commonly associated with large APD oscillation magnitudes, which facilitate the occurrence of pro-arrhythmic events under disease conditions involving calcium overload and reduced repolarization reserve.

Conclusions: The time course of LF oscillatory behavior of APD in response to increased sympathetic activity presents high inter-individual variability, which is associated with different expression and PKA phosphorylation kinetics of the I_{Ks} current. Short time lapses in the development of APD oscillations are associated with large oscillatory magnitudes and pro-arrhythmic risk under disease conditions.

Keywords: low-frequency oscillations, beta-adrenergic stimulation, cardiac cell models, ventricular repolarization, sympathetic activity, arrhythmogenesis

1. INTRODUCTION

Ventricular repolarization has been shown to exhibit a low-frequency (LF) oscillatory pattern following enhanced sympathetic activity. In humans, this has been demonstrated by quantification of so-called periodic repolarization dynamics in the T-wave vector of the electrocardiogram (ECG) (Rizas et al., 2014, 2016) as well as by *in vivo* evaluation of LF components in activation recovery intervals (ARI) of ventricular electrograms (Hanson et al., 2014; Porter et al., 2018). In post-infarction patients, an increased magnitude of LF oscillations in ECG repolarization has been proved to be a significant predictor of total mortality and sudden cardiac death (Rizas et al., 2017). Most notably, a very recent study has shown that those periodic repolarization dynamics are able to predict the efficacy of implanting a cardioverter defibrillator in patients undergoing primary prophylactic treatment (Bauer et al., 2019). *In silico* studies have provided insight into the cellular mechanisms underlying this oscillatory pattern of ventricular repolarization, which have been explained by the synergistic effect of phasic β-adrenergic stimulation (β-AS) and mechanical stretch, both accompanying enhanced sympathetic nerve activity. In brief, differential phosphorylation kinetics of calcium (I_{Ca}) and potassium (I_K) currents upon phasic β-AS as well as changes in calcium cycling and the action of stretch-activated channels (SACs) in response to phasic mechanical stretch have been shown to generate LF oscillations in cellular action potential (AP) duration (APD) (Pueyo et al., 2016). Subsequent studies have additionally investigated inter-individual differences in LF oscillations of ventricular APD, concluding that calcium and potassium currents, I_{Ca} and I_K (specifically, the rapid delayed rectifier I_{Kr} and inward rectifier I_{K1}), are major ionic modulators of such inter-individudal differences (Sampedro-Puente et al., 2019). Importantly, these identified ionic factors are key for the development of arrhythmic events following enhancement of APD oscillations' magnitude. A very recent investigation has experimentally confirmed in an arrhythmogenic *in vivo* dog model that ventricular remodeling associated with chronic atrioventricular block (CAVB) augments LF oscillations of APD (Sprenkeler et al., 2019). Most importantly, the oscillation magnitude has been reported to be larger in dogs susceptible to dofetilide-induced Torsades de Pointes arrhythmias as compared to non-inducible dogs (Sprenkeler et al., 2019).

For LF oscillations in the ventricular APD to become clearly manifested following increased sympathetic activity, computational research has shown that some tens of seconds or even a few minutes are required (Pueyo et al., 2016). This requisite on a relatively long exposure to enhanced sympathetic activity for repolarization oscillations to develop may explain why experimentally measured APD oscillations appear to come and go and do not remain as sustained oscillations for long recording periods (Hanson et al., 2014). Pueyo et al. (2016) and Sampedro-Puente et al. (2019) have shown that, upon a sympathetic rise, the cellular ventricular APD shows a global trend of shortening, or brief prolongation followed by more prominent shortening, which masks concurrent LF oscillations overlapping with the global APD trend. The individual and combined roles of β-AS and mechanical stretch in determining the time lapse for LF oscillations to become visibly manifested are yet to be explored. Experimental investigations in canine ventricular myocytes have shown that APD presents slow time-dependent changes following application of a constant dose of the β-adrenergic agonist isoproterenol (ISO) (Ruzsnavszky et al., 2014). The slow activation of I_K currents (in particular, slow I_{Ks} and rapid I_{Kr} delayed rectifier currents), as compared to the very fast activation of the I_{Ca} current, has been demonstrated to be behind such APD lag following sudden ISO exposure. The distinctively slow response of I_{Ks} to β-AS and its implications in terms of APD adaptation time have been also described in other species, like the rabbit (Liu et al., 2012). On the other hand, APD dynamicity in response to constant mechanical stretch or to the combination of constant β-AS and mechanical stretch has been less studied experimentally.

The present study investigates the cellular ventricular APD response to phasic, rather than constant, β-AS and mechanical stretch, in closer correspondence with the experimentally reported LF patterns of efferent sympathetic nerve activity (Pagani et al., 1997; Furlan et al., 2000). The global trend of APD response is in this case expected to be concurrent with periodic changes in APD occurring at the frequency of sympathetic activity. For this investigation, a population of computational cellular AP models representative of experimentally reported human ventricular electrophysiological characteristics is

developed and coupled to models of β-AS and mechanics. By using the developed models, the amount of time required for LF fluctuations of APD to arise in response to phasic sympathetic activation is characterized and the ionic mechanisms underlying cell-to-cell differences in APD time lag are dissected. Experimental confirmation of the obtained results is obtained. A relationship between the quantified time lapse and the magnitude of APD oscillations is established, which serves to set links to pro-arrhythmic risk under disease conditions associated with Ca^{2+} overload and reduced repolarization reserve (RRR), both being commonly present in failing hearts.

2. METHODS

2.1. Experimental Data

Ventricular myocytes were isolated from the left ventricular wall of adult beagle dogs as described in Ruzsnavszky et al. (2014). The isolation procedure followed a protocol approved by the local ethical committee according to the principles outlined in the 1964 Declaration of Helsinki and its later amendments. The cells used for this study were obtained from the subepicardial layer.

Transmembrane potentials were measured at 37°C by using 3 M KCl-filled sharp glass microelectrodes with tip resistance 20–40 MΩ (Ruzsnavszky et al., 2014). The electrodes were connected to the input of an Axoclamp-2B amplifier (Molecular Devices, Sunnyvale, CA, USA). Cardiomyocytes were paced at 1 s using 1-ms wide rectangular current pulses with 120% threshold amplitude until steady-state. ISO was applied at a concentration of 10 nM for 5 min. APs were sampled by periods of 30 s following ISO application, with a sampling frequency of 200 kHz using Digidata 1200 A/D card (Axon Instruments Inc., Foster City, CA, USA).

2.2. Electrophysiology Model

A population of human ventricular AP models representative of a wide range of experimentally observed electrophysiological characteristics was built based on the O'Hara-Virág-Varró-Rudy (ORd) epicardial model (O'Hara et al., 2011). The population was obtained by varying the ionic conductances of eight ionic currents in the ORd model, namely: I_{Ks}, slow delayed rectifier potassium current; I_{Kr}, rapid delayed rectifier potassium current; I_{to}, transient outward potassium current; I_{CaL}, L-type calcium current; I_{K1}, inward rectifier potassium current; I_{Na}, sodium current; I_{NaK}, sodium-potassium pump current; and I_{NaCa}, sodium-calcium exchanger current.

Initially, 500 models were generated by using the Latin Hypercube Sampling method to sample the conductances of the above described currents in the range ±100% (McKay et al., 1979; Pueyo et al., 2016). A set of calibration criteria based on experimentally available human ventricular measures of steady-state AP characteristics (Jost et al., 2008; Grandi et al., 2010; Guo et al., 2011; O'Hara et al., 2011; Britton et al., 2017) were imposed, as described in **Table 1**. AP characteristics used for model calibration included: $APD_{90|50}$, which represents steady-state AP duration (APD) at 90|50% repolarization corresponding to 1 Hz pacing (expressed in ms); RMP, representing resting membrane potential (in mV); V_{peak}, representing peak membrane potential measured in the AP upstroke (in mV); and ΔAPD_{90}, representing the percentage of change in APD_{90} with respect to baseline following individual inhibitions of I_{Ks}, I_{Kr}, or I_{K1} currents (measured in ms). Of the initial 500 models, only 218 meeting all the calibration criteria were selected. Additionally, models showing pro-arrhythmic behavior at baseline and/or under sympathetic provocation were discarded, which led to a population of 188 models for the analysis of this study.

TABLE 1 | Calibration criteria applied onto human ventricular cell models.

AP characteristic	Min. acceptable value	Max. acceptable value
Under baseline conditions (Guo et al., 2011; O'Hara et al., 2011; Britton et al., 2017)		
APD_{90} (ms)	178.1	442.7
APD_{50} (ms)	106.6	349.4
RMP (mV)	−94.4	−78.5
V_{peak} (mV)	7.3	–
Under 90% I_{Ks} block (O'Hara et al., 2011)		
ΔAPD_{90} (%)	−54.4	62
Under 70% I_{Kr} block (Grandi et al., 2010)		
ΔAPD_{90} (%)	34.25	91.94
Under 50% I_{K1} block (Jost et al., 2008)		
ΔAPD_{90} (%)	−5.26	14.86

2.3. PKA Phosphorylation Model

A modified version of the Xie et al. (2013) β-adrenergic signaling model was used as a basis to describe phosphorylation levels of cellular protein kinase A (PKA) substrates, as described in Pueyo et al. (2016) and Sampedro-Puente et al. (2019). The Xie et al. (2013) model represents an evolution from the Soltis and Saucerman (2010) signaling model in which I_{Ks} phosphorylation and dephosphorylation rate constants were updated to better match experimental observations reported in Liu et al. (2012). Also, as described in Xie et al. (2013), PKA-mediated phosphorylation of phospholemman (PLM) involved an increase in the Na^+-K^+-ATPase (NKA) affinity for the intracellular Na^+ concentration. In the modified Xie et al. (2013) model of this study, ryanodine receptors (RyR) phosphorylation was defined by using the formulation described in Heijman et al. (2011).

For a specific set of simulations, I_{Ks} phosphorylation and dephosphorylation kinetics were defined as reported in Soltis and Saucerman (2010) to assess the effects of faster phosphorylation kinetics on the time lapse for APD oscillations development.

2.4. Mechanics Model

An updated version of the Niederer et al. (2006) model was employed to describe cell mechanics, with the values of some constants being adjusted to represent human cell characteristics as in Weise and Panfilov (2013) and Pueyo et al. (2016). I_{SAC}, denoting the current through SACs, was accounted for as in Pueyo et al. (2016). Specifically, I_{SAC} was defined as the current through non-specific cationic SACs plus the current through K^+-selective SACs.

2.5. Simulation of Enhanced Sympathetic Activity

Enhanced sympathetic activity was simulated by the combination of phasic β-AS and mechanical stretch effects. Phasic β-AS was simulated by a periodic stepwise profile of the β-adrenergic agonist ISO according to muscle sympathetic nerve activity patterns in humans (Pagani et al., 1997). The periodicity of the ISO profile corresponded to a frequency of 0.05 Hz, this being within the reported Mayer wave frequency range (0.03–0.15 Hz). The 20 s ISO period was composed of a 10 s time interval where the ISO concentration was set to 1 μM and a subsequent 10 s time interval where the ISO concentration was 0. Phasic changes in hemodynamic loading, a known accompaniment of enhanced sympathetic activity, were simulated by phasic mechanical stretch changes at the same 0.05 Hz frequency. Specifically, stretch ratio was varied during the 20 s period by following a sinusoidal waveform with maximal change being 10%, being such level of change in line with those of previous experimental and computational studies (Niederer and Smith, 2007; Iribe et al., 2014). Phasic β-AS and mechanical stretch effects were defined to be in-phase. Five hundred beats at baseline and 500 beats following enhanced sympathetic activity were simulated while pacing at 1 Hz frequency.

2.6. Simulation of Disease Conditions

For specific simulations, disease conditions were simulated by Reduced Repolarization Reserve (RRR) and Ca^{2+} overload. RRR was defined by concomitant inhibition of I_{Kr} and I_{Ks} currents by 30 and 80%, respectively. Ca^{2+} overload was defined by a 4-fold increment in the extracellular Ca^{2+} level.

2.7. Quantification of APD Time Lag in Response to Constant β-AS and/or Mechanical Stretch

APD was evaluated at 90% repolarization in both simulations and experiments. The simulated or experimentally measured APD time series following β-AS and/or mechanical stretch is denoted by $a[k]$, where the discrete index k represents cycle number. Thus, k varies from 0 to K, with K being the number of cycles following β-AS and/or mechanical stretch.

The time lapse, τ_{APD}, for APD to reach a new steady-state following application of β-AS and/or stretch was defined as the time taken by the APD time series to attain convergence, with convergence characterized by the derivative of the APD time series being below a predefined threshold. Specifically, the following steps were used to compute the APD time lapse:

1. **Smoothing**
   To remove short-term variability and make the estimation of the convergence time more robust, moving average smoothing was applied onto the APD time series $a[k]$ to obtain a smooth version of it, $\widehat{a}[k]$:

$$\widehat{a}[k] = \frac{1}{T}\sum_{k'=k}^{k+T} a[k'] \tag{1}$$

   where T was set to the period in cycles of the sympathetic activity, $T = 20$ cycles.
2. **Numerical derivative**
   From $\widehat{a}[k]$, the derivative $d[k]$ was numerically estimated by computing the central difference for the interior data points of $\widehat{a}[k]$ and single-side difference for the edges of $\widehat{a}[k]$:

$$d[k] = \frac{\widehat{a}[k+1] - \widehat{a}[k-1]}{2}, \quad 0 < k < K \tag{2}$$

$$d[0] = \widehat{a}[1] - \widehat{a}[0] \tag{3}$$

$$d[K] = \widehat{a}[K] - \widehat{a}[K-1] \tag{4}$$

3. **Time lapse calculation**
   A threshold on the maximum allowed variation in the derivative of the APD time series for convergence to be attained was defined in this study by setting θ = 0.5 ms. The number of cycles, k_{APD}, for APD convergence following β-AS and/or stretch was defined as:

$$k_{APD} = \min_{0 \le k \le K} \left\{ \left| \sum_{k'=k}^{K} d[k'] \right| < \theta \right\} \tag{5}$$

   The time lapse τ_{APD} was obtained by converting k_{APD} into minutes:

$$\tau_{APD} = k_{APD}\ \frac{CL}{60} \tag{6}$$

   where CL is the cycle length in seconds (constant period between stimuli applied to the cells to elicit APs).

   Values of τ_{APD} equal to 0 represent cases where convergence of the APD time series was immediate.

3. RESULTS

3.1. Time Lapse for Development of LF Oscillations in APD

Figure 1 shows examples of APD time series for two different human ventricular cells of our simulated population presenting LF oscillations following sympathetic provocation. From this figure, it is clear that not only the magnitude of the oscillations is different for the two cells but also the time lapse required for LF oscillations of APD to become evident is remarkably distinct. For the first virtual cell illustrated in **Figure 1**, the time lapse was τ_{APD} = 139 s, whereas for the second virtual cell, τ_{APD} = 0 s. The characteristics of these two cells in terms of ionic current conductances are presented in **Table 2**.

Figure 2, left panel, presents a histogram of the time lapse for APD oscillations developed in response to a rise in sympathetic activity for all the cells in our virtual population. Inter-individual differences in the ionic characteristics of the virtual cells had an impact on τ_{APD}, which ranged from just a few seconds for some virtual cells to more than 3 min for other cells. Similarly, **Figure 2**, right panel, shows a histogram of the power in the LF band (PLF) for APD oscillations under sympathetic provocation, represented

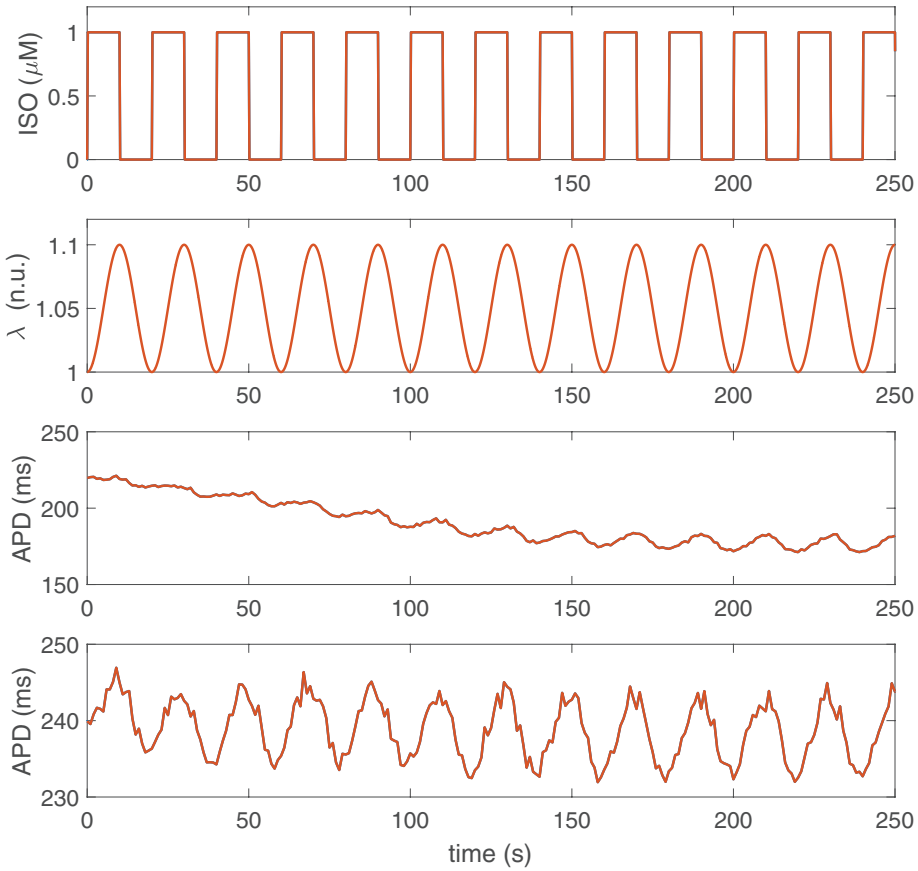

FIGURE 1 | Simulation of sympathetic provocation and APD response of two different cells in the population. First row: Phasic ISO application at a frequency of 0.05 Hz. Second row: Phasic stretch ratio variations at the same frequency. Third and fourth rows: APD time series corresponding to two cells (virtual cell 1 and virtual cell 2) presenting LF oscillations in response to sympathetic provocation.

in terms of log(PLF). Large inter-individual variability also exists in log(PLF), with values covering from 0 to 10 ms^2, although most cells present PLF values below 5 ms^2.

3.2. Contribution of β-AS and Mechanical Stretch to Time Lapse of LF Oscillations in APD

The individual and combined contributions of phasic β-AS and mechanical stretch to the time lapse in the occurrence of LF oscillations of APD is presented in **Figure 3**, left panel. As can be observed from the figure, individual application of phasic β-AS had a major role in the time required for APD oscillations to develop, whereas individual mechanical stretch had a more marginal influence, with the vast majority of simulated cells developing LF oscillations in response to phasic stretch in less than 1 min. When the effects of β-AS and stretch were combined, the APD convergence time was reduced with respect to that corresponding to only β-AS for practically all cells.

Additionally, **Figure 3**, right panel, illustrates the oscillation magnitudes in terms of log(PLF) for individual and combined β-AS and mechanical stretch. Individual mechanical stretch led to the largest oscillations magnitudes, in association with the shortest time delays, whereas individual β-adrenergic stimulation led to the smallest magnitudes, in association with the largest time lapses. Nevertheless, high inter-individual variability could be observed in all cases.

TABLE 2 | Factors multiplying ionic conductances of virtual cells 1 and 2 illustrated in **Figure 1**.

Ionic factors	θ_{Ks}	θ_{Kr}	θ_{to}	θ_{CaL}	θ_{K1}	θ_{Na}	θ_{NaCa}	θ_{NaK}
Virtual cell 1	1.83	0.88	0.78	0.46	1.16	1.70	0.40	1.37
Virtual cell 2	0.49	1.11	1.98	1.37	1.34	0.42	1.82	1.97

3.3. Comparison of APD Time Lapse Following β-AS in Experiments and Simulations

Based on the results presented in sections 3.1 and 3.2 and the fact that LF oscillations of APD are superimposed to the general

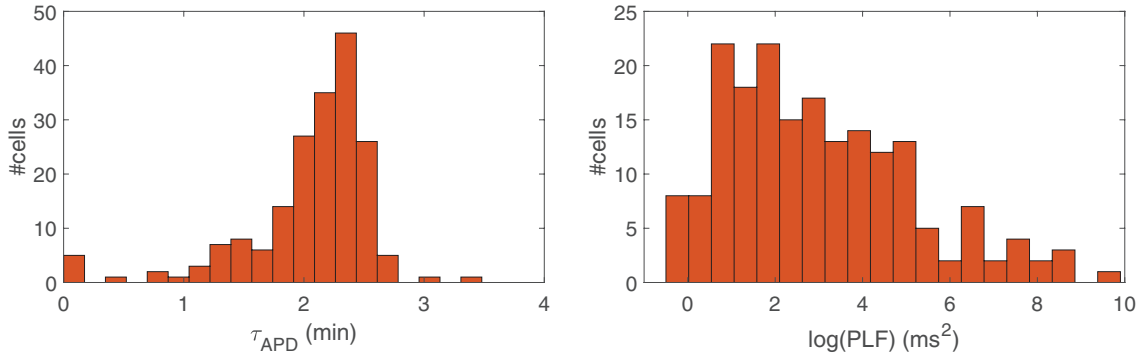

FIGURE 2 | Histogram of the time lapse (**Left**) and LF power (**Right**) of APD in response to increased sympathetic activity for all cells in the simulated population.

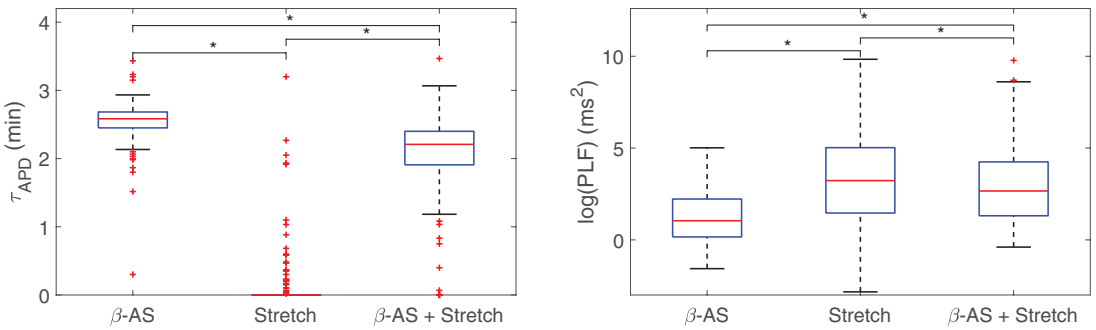

FIGURE 3 | Boxplots representing the time lapse **(left)** and the power in the LF band **(right)** for oscillations of APD to develop in response to phasic β-AS (ISO 1 μM), mechanical stretch (10%) and the combination of both. Statistically significant differences by Wilcoxon signed-rank test (p-value < 0.05) are denoted by *. Since the statistical significance in the comparison of simulated data highly depends on the number of simulated cases, smaller subsets of virtual cells were used to prove that $p < 0.05$ had already been achieved with a much smaller number of virtual cells than those in the whole population.

trend of APD decrease following enhanced sympathetic activity, the time lapse for the development of APD oscillations can equivalently be determined by the time required for APD to converge to steady-state following constant β-AS.

The temporal evolution of APD following constant application of an ISO dose of 10 nM was investigated in simulations based on our generated population of cells and compared with our experimental data recorded by using the same β-AS protocol with the same ISO dose. **Figure 4** presents ΔAPD, calculated by subtracting the mean APD value at baseline (prior to ISO application) to the APD time series measured following β-AS, for both simulated and experimental data from single ventricular myocytes. It can be noted from the figure that large cell-to-cell variability exists in the time lag of measured APD responses, with the transition times required to reach steady-state following ISO application varying by several minutes. This cell-to-cell heterogeneity in the APD response to constant β-AS serves as a basis to explain the cell-to-cell differences in the data presented in **Figure 3** (left column), corresponding to phasic β-AS at a 1 μM ISO dose, which includes APD oscillations overlapped with the decrease in APD. Of note, the simulated time lags in our virtual population of cells are representative of the values measured experimentally in ventricular cardiomyocytes.

3.4. Reduction in Time Lapse for LF Oscillations of APD by Prior Low-Level β-AS

The possibility that prior stimulation of β-adrenoceptors could reduce the time required for APD to develop LF oscillations in response to enhanced sympathetic activity was next explored. **Figure 5** presents results of the time lapse for oscillations development in response to phasic 1 μM ISO application for eight different cases with prior β-AS corresponding to ISO levels varying from 0 to 0.07 μM in 0.01 μM-steps, with each of these pre-stimulation periods applied for 500 beats at 1 Hz pacing frequency. From this figure, it is clear that the time lapse was remarkably reduced as a function of the pre-stimulation level. For a prior stimulation with an ISO dose of 0.05 μM, i.e., 50 nM, most virtual cells developed LF oscillations in APD practically in an instantaneous way after applying the maximal ISO dose of 1 μM. There are still some cells for which the time lapse is above 3 min even if β-adrenoceptors were previously stimulated. Pre-stimulation

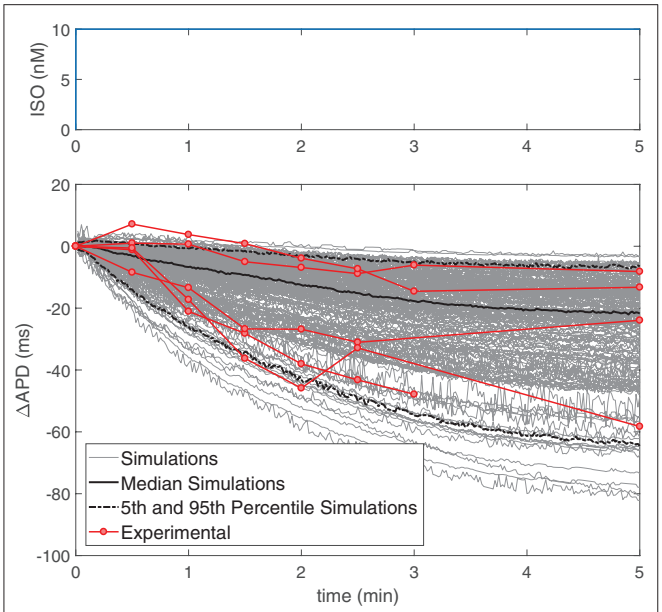

FIGURE 4 | (**Top**) ISO dose in nM, where time zero indicates the time when the solution containing ISO arrived to the cells and analogously for simulations. (**Bottom**) Change in APD with respect to baseline following application of a constant 10 nM ISO dose in experiments (n = 5, red) and simulations (gray) on single ventricular myocytes.

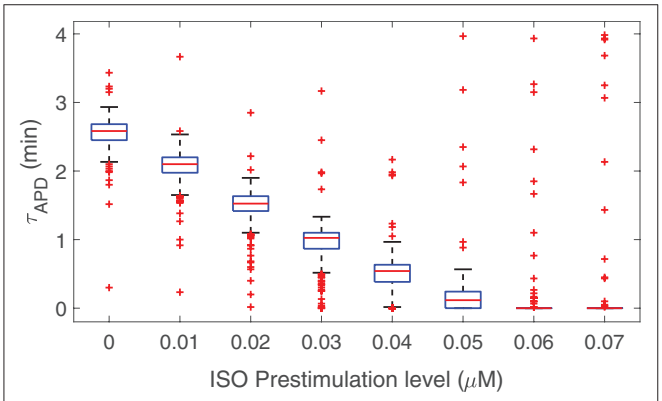

FIGURE 5 | Time lapse for LF oscillations of APD to develop in response to phasic β-AS with 1 μM ISO dose as a function of prior phasic β-AS with lower ISO doses varying from 0 to 0.07 μM.

did not have any remarkable effect on the magnitude of the APD oscillations.

3.5. Ionic Mechanisms Underlying Time Lapse in LF Oscillations of APD

To ascertain the ionic mechanisms underlying the time required for APD to develop LF oscillations following phasic β-AS, the effect of phosphorylation and dephosphorylation kinetics of all cellular PKA substrates was investigated. **Figure 6**, left panel, presents the phosphorylation levels of all these substrates in response to 5 min adrenergic stimulation. As can be observed from the figure, the substrates presenting slower phosphorylation responses are the slow delayed rectifier channels, associated with the I_{Ks} current, and ryanodine receptors, RyR.

To assess the extent to which variations in the phosphorylation and dephosphorylation kinetics of I_{Ks} influenced the time for development of APD oscillations, simulations were run where the I_{Ks} phosphorylation and dephosphorylation rate constants were increased to the values described in Soltis and Saucerman (2010) from which an update was presented in a subsequent study by Xie et al. (2013) to more reliably recapitulate PKA-dependent regulation of I_{Ks}. Specifically, the I_{Ks} phosphorylation rate constant was changed from 8.52 to 84 s^{-1} and the I_{Ks} dephosphorylation rate constant was changed from 0.19 to 1.87 s^{-1}. According to the results presented in **Figure 6**, right panel, it is clear that the time lapse for APD oscillations was very notably reduced after increasing those rate constants, thus indicating the dependence of the APD oscillatory time lapse on I_{Ks} phosphorylation kinetics. On the other hand, variations in the phosphorylation kinetics of RyR had no impact on the time lapse for APD oscillations to develop, even if these were varied by a factor of up to ten times their nominal values.

Based on the above results, and considering that cell-to-cell differences in our population of models correspond to different ionic current conductance contributions, it was hypothesized that inter-individual differences in the time lapse for APD oscillation development was based on their differential I_{Ks} contributions. Simulations were run where I_{Ks} was inhibited at different levels and a monotonic decrease in oscillation time lapse could be quantified for increasingly larger inhibitions, as illustrated in **Figures S1, S2**. For full I_{Ks} blockade, APD oscillations became apparent almost immediately.

3.6. Relationship Between Time Lapse and Magnitude of LF Oscillations of APD

To assess the relationship between the time lapse for development of LF oscillations in APD and the magnitude of such oscillations, a set of models was built in such a way that they all share the same characteristics of the ORd-Xie coupled electrophysiology-β-adrenergic signaling model, except for I_{Ks} phosphorylation and dephosphorylation rate constants, which were varied from model to model so that they covered from the slowest dynamics reported in Xie et al. (2013) to the fastest dynamics reported in Soltis and Saucerman (2010). **Figure 7**, left panel, shows the relation between the magnitude of LF oscillations in APD, quantified by the LF power in the 0.04–0.15 Hz band denoted by PLF, and the time lapse for oscillation development, quantified by τ_{APD}. It can be observed from the figure that the models with the fastest I_{Ks} phosphorylation dynamics are those presenting the shortest time lapse and the highest APD oscillatory magnitude.

To substantiate this result, **Figure 7**, right panel, shows I_{Ks} phosphorylation levels calculated according to the signaling models in Xie et al. (2013) and Soltis and Saucerman (2010), corresponding to the two most extreme points shown in **Figure 7**, left panel. It can be observed from the graphic that, for the model in Soltis and Saucerman (2010), not only are the I_{Ks} phosphorylation dynamics faster but also the associated oscillations are of larger magnitude. These enhanced oscillations

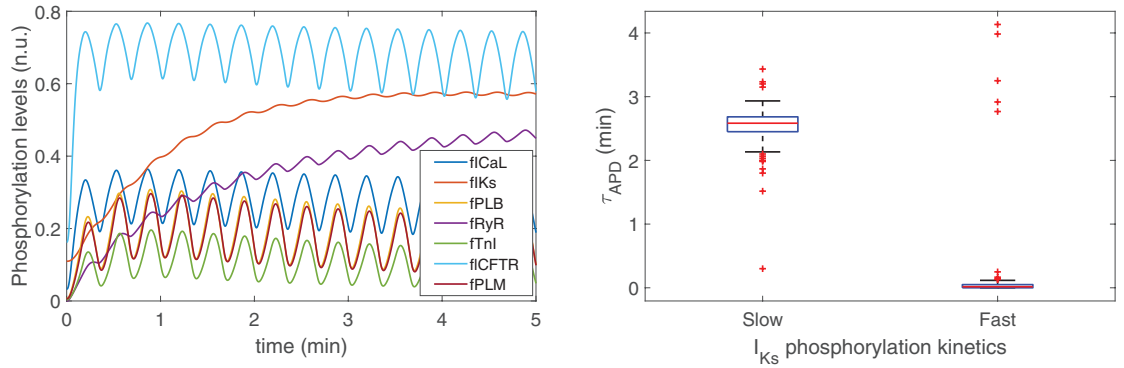

FIGURE 6 | (**Left**) Phosphorylation levels calculated as described in section 2.3. (**Right**) Time lapse for LF oscillations of APD to develop in response to phasic β-AS when using PKA models with slow [**Left**, Xie et al. (2013)] and fast [**Right**, Soltis and Saucerman (2010)] I_{Ks} phosphorylation and dephosphorylation kinetics.

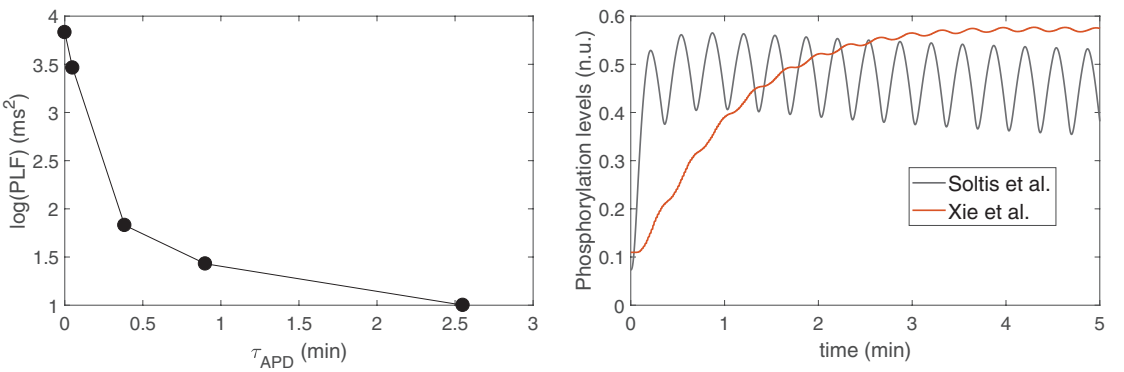

FIGURE 7 | (**Left**) PLF vs. τ_{APD} for varying I_{Ks} phosphorylation and dephosphorylation rate constants ranging from the values in Soltis and Saucerman (2010) to the values in Xie et al. (2013). (**Right**) I_{Ks} phosphorylation levels for the models with I_{Ks} phosphorylation and dephosphorylation rate constants as in Soltis and Saucerman (2010) (gray line) and as in Xie et al. (2013) (red line).

in I_{Ks} phosphorylation have an impact on the AP, which is manifested by a larger oscillatory magnitude of APD.

In the whole population of virtual cells, where all cells present the same phosphorylation kinetics but the conductance of I_{Ks} varies from one cell to another, consequently modulating the influence of I_{Ks} phosphorylation fluctuations on APD oscillatory behavior, the inverse relationship between PLF and τ_{APD} can still be appreciated. This is shown in **Figure 10**, which presents PLF vs τ_{APD} for cells under healthy conditions divided into two groups depending on the presence/absence of pro-arrhythmic effects when disease conditions were simulated, as described in the next section.

3.7. Effect of Disease Conditions in Time Lapse of LF Oscillations of APD and Relation to Arrhythmogenesis

Simulation of disease conditions by Ca^{2+} overload and RRR in our population of models led to a sharp decrease in the APD oscillatory time lapse following increased sympathetic activity. This is illustrated in **Figure 8**, left panel, which shows zero-mean APD time series (after subtraction of the corresponding baseline value to facilitate comparison) for one of the cells in the virtual population under healthy and pathological conditions. The value of τ_{APD} decreased from 130 to 0 ms due to the effects of disease. **Figure 8**, right panel, summarizes the observed changes in τ_{APD} when simulating disease conditions in the subpopulation of cells that did not present pro-arrhythmic events. Whereas Ca^{2+} overload had mild effects on τ_{APD}, the effects of RRR, individually or in the presence of Ca^{2+} overload, contributed to a very remarkable reduction in the oscillatory time lapse.

When disease conditions were simulated as accompanied by an increase in the conductance of non-specific cationic SACs in accordance with experimental evidences (Kamkin et al., 2000; Guinamard et al., 2006), arrhythmogenic events were generated in some of the virtual cells of the population following sympathetic provocation. These were in the form of afterdepolarizations and spontaneous beats and occurred in 46.34% of the virtual cells that did not show any pro-arrhythmic manifestation at baseline. Examples are illustrated in **Figure 9**. To assess whether individual cell oscillatory characteristics evaluated under healthy conditions were related to pro-arrhythmicity, the

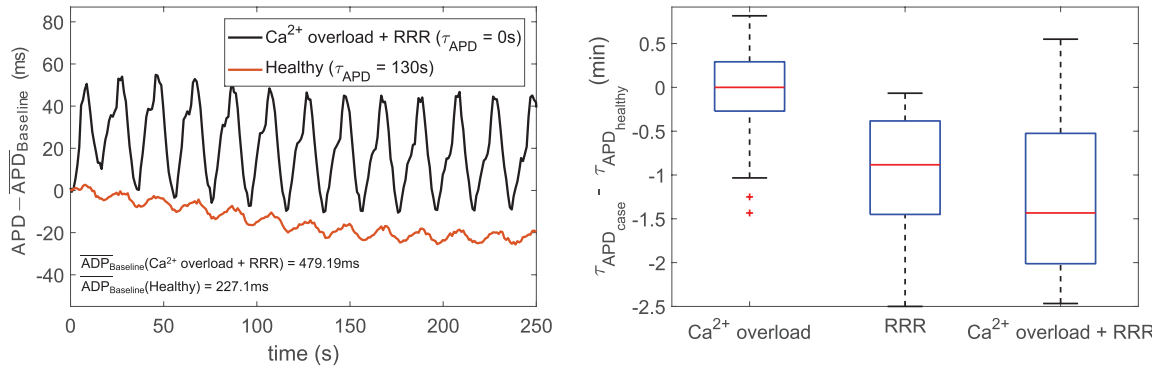

FIGURE 8 | (**Left**) Zero-mean APD series (APD - $\overline{APD}_{Baseline}$) in response to sympathetic provocation, for healthy (red line) and disease (black line) conditions simulated for a virtual cell of the population. (**Right**) Differences in τ_{APD} due to Ca^{2+} overload and/or RRR with respect to healthy conditions.

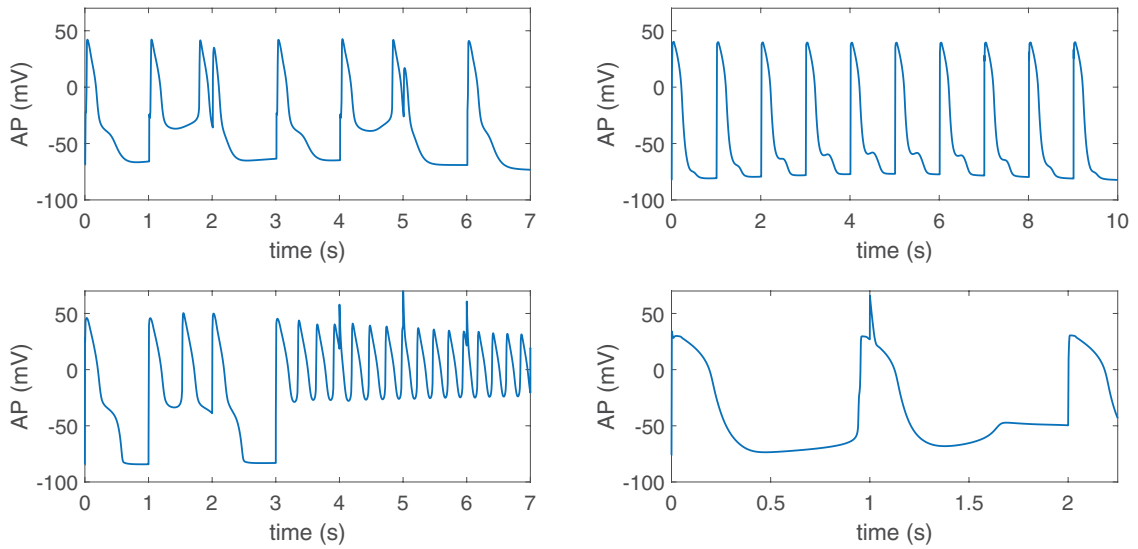

FIGURE 9 | Pro-arrhythmic events in virtual cells in response to increased sympathetic activity under diseased conditions simulated by Ca^{2+} overload, reduced repolarization reserve and increased G_{SAC}. Phase 2 and phase 3 early afterdepolarizations (EADs) **(top panels)**, EAD bursts **(bottom left)** and spontaneous beats **(bottom right)** could be observed.

time lapse, quantified by τ_{APD}, and the magnitude of APD oscillations, quantified by PLF, were compared between the groups of cells presenting and not presenting arrhythmogenic events. Results are presented in **Figure 10**, left and middle panels. As can be observed from the figure, little differences in the mean or median τ_{APD} were found between the two groups. On the other hand, larger differences in PLF were seen between the groups, with the one presenting arrhythmogenic events in response to increased sympathetic activity being associated with remarkably larger mean and median PLF (note that the logarithm of PLF is represented in **Figure 10**). Boxplots of τ_{APD} and log(PLF) for the groups of cells presenting and not presenting arrhythmogenic events are shown in **Figure S3**.

The relationship between PLF and τ_{APD} in the population of cells prior to introducing disease conditions is presented in **Figure 10**, right panel, for the pro-arrhythmic and non-pro-arrhythmic groups. In both groups, larger values of PLF were associated with shorter values of τ_{APD}, although high inter-individual variability could be noticed. The Spearman correlation coefficient was $\rho = -0.82$ in the pro-arrhythmic group and $\rho = -0.57$ in the non-pro-arrhythmic group.

4. DISCUSSION

4.1. Inter-individual Differences in the Time Lapse for Development of LF Oscillations of APD Following Enhanced Sympathetic Activity

The research presented in this study has shown that LF oscillations of human ventricular repolarization, reported in the T-wave of the ECG and locally in ARIs of unipolar epicardial

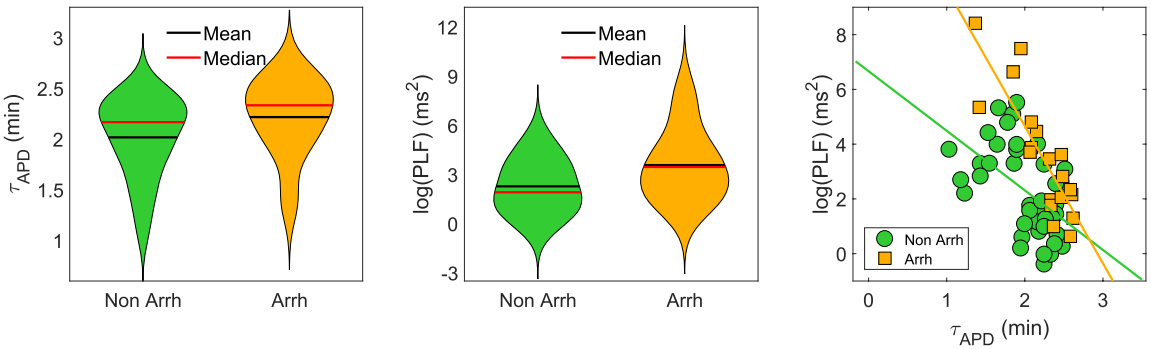

FIGURE 10 | (Left and middle): Violin representations of τ_{APD} and log(PLF), respectively, calculated under healthy conditions for subpopulations of cells presenting and not presenting pro-arrhythmic events when disease conditions were simulated while pacing at CLs of 1,000, 2,000, and 2,500 ms. **(Right)** τ_{APD} vs. log(PLF) for the same two subpopulations. The slopes of the regression lines for the subpopulations presenting (orange) and not presenting (green) pro-arrhythmic events were statistically significantly different by univariate analysis of variance (p-value < 0.05).

electrograms, do not develop immediately upon a sympathetic rise but take some time to become apparent. An algorithm has been proposed to robustly quantify the time lapse required for APD to develop sympathetically-mediated LF oscillations. This time lapse has been shown to be highly variable from one cell to another, ranging from just a few seconds to more than 3 min depending on the ionic characteristics of each individual cell. Following enhanced sympathetic activity, the APD shows a trend of shortening, or brief prolongation followed by more sustained shortening, which masks overlapping oscillations. Only when such APD shortening has been completed, APD oscillations become manifest.

The range of time lags for APD oscillatory behavior following sympathetic provocation is of the order of adaptation lags reported for the QT interval of the ECG in response to increases in sympathetic activity leading to abrupt heart rate increases, either measured from ambulatory Holter recordings (Pueyo et al., 2004) or following tilt test (Pueyo et al., 2008; Nosakhare et al., 2014). Those repolarization dynamics have also been recently investigated in experimental studies using fully innervated Langendorff-perfused mouse and rabbit hearts, where the APD response to bilateral sympathetic nerve stimulation has been described (Wang et al., 2019). In those studies ventricular repolarization was modulated both by direct sympathetic action on the ventricular myocardium as well as indirectly by heart rate-related effects. In the present study, CL was kept constant and the ventricular response was thus only assessed as due to sympathetic effects on the ventricle, as in *in vivo* electrogram recordings from patients where LF oscillations of ARI have been characterized while controlling CL with right ventricular pacing (Hanson et al., 2014; Porter et al., 2018).

The prolonged time lapses for LF oscillatory behavior of APD following enhanced sympathetic activity quantified in this study can help to explain why oscillations seem to appear and disappear, as observed in *in vivo* studies (Hanson et al., 2014), where APD oscillatory behavior could only be measured at certain time intervals of the analyzed recordings. Those time intervals could be speculated to be associated with sustained sympathetic activation so that enough time was allowed for LF oscillations in APD to develop.

In this work sympathetic provocation was simulated by concomitant phasic changes in β-AS and mechanical stretch. The involvement of each of these two components in the protracted LF oscillatory response to a sympathetic rise has been assessed. Our results have determined that mechanical stretch induces LF oscillations of APD in an almost instantaneous manner, whereas β-AS entails much longer APD time courses until LF oscillations can be clearly appreciated. Based on the fact that the time lapse is mainly due to the slow response to β-AS, this study has next validated the calculated time lapses against *in vitro* data from ventricular myocytes following sudden exposure to ISO. Both in the experiments and the simulations of this study, the time required for APD to reach steady-state following sudden β-AS was found to highly vary from cell to cell. Simulated time lapses were comprised within the experimental limits quantified for the ventricular myocytes of this and other studies (Liu et al., 2012; Ruzsnavszky et al., 2014), thus confirming validation of our population of models to reproduce available evidences on the APD time course in response to β-AS.

To further support our conclusions on the key role of β-AS in determining the time lapse for LF oscillations of APD to develop, the effects of pre-stimulating ventricular cells with a lower dose of the β-adrenergic agonist ISO have been tested. Results have confirmed that the oscillatory time lapse is highly dependent on β-adrenoceptors' state. The higher the prior stimulation level of β-adrenoceptors, the shorter the time for development of LF oscillations. This reduction in the oscillatory time lapse by prior ISO exposure agrees with common knowledge on pre-stimulation of β-adrenoceptors altering the impact of β-AS. Under conditions associated with high sympathetic tone, as in failing or aged ventricles, sympathetic surge would thus be expected to induce LF oscillations of repolarization with shorter latency. Consequently, due to the less stringent requirements on the time period of sustained sympathetic activation for LF oscillatory behavior to ensue in failing or aged ventricles, this is anticipated to facilitate the occurrence of such oscillations, with the corresponding potentially adverse consequences (Rizas et al., 2014, 2017; Pueyo et al., 2016; Sampedro-Puente et al., 2019).

4.2. Major Role of I_{Ks} Phospohorylation Kinetics in Determining the Time Lapse for LF Oscillations of APD

The mechanisms underlying the slow appearance of APD oscillations following sympathetic provocation, particularly related to the protracted response to β-AS, have been ascertained in this work by comparing the phosphorylated levels of all cellular substrates accounted for in the modified β-adrenergic signaling model by Xie et al. (2013) used as a basis for this study. Two cellular substrates, namely I_{Ks} and RyR, have been shown to present responses to β-AS being remarkably slower than those of all other substrates. The time required for I_{Ks} and RyR phosphorylation levels to reach steady-state upon β-AS is around 3 min, this being close to the maximum time lapse for APD oscillations to appear in our simulated population of models, while the phosphorylation levels of the remaining cellular substrates reach steady-state in no more than 20–30 s. In other β-adrenergic signaling models, as in the model by Heijman et al. (2011), I_{Ks} and RyR present slow kinetics too, although there are other substrates, like the Na^+-K^+-ATPase current, with even slower kinetics.

The impact of the slow I_{Ks} and RyR phosphorylation kinetics on the APD time course following sympathetic stimulation has been assessed by varying their phosphorylation and dephosphorylation rate constants. Whereas variations in the kinetics of I_{Ks} are proved to have relevant effects on the time lapse for APD oscillations, the influence of variations in the RyR kinetics is negligible. The irrelevant role of RyR phosphorylation on τ_{APD} as compared to that of I_{Ks} phosphorylation can be explained on the basis of their very distinct impact on APD. RyR phosphorylation has been described in this study according to the formulation proposed in Heijman et al. (2011), where it has been shown that disabling RyR phosphorylation leads to little variations in APD with respect to measurements when all substrates are phosphorylated. On the other hand, I_{Ks} phosphorylation has much more prominent effects on APD (Xie et al., 2013). To further support the role of I_{Ks} in determining the APD oscillatory latency, this current has been inhibited to various extents and it has been confirmed that the larger the I_{Ks} current amplitude, the longer the latency. These results lead us to conclude that the high inter-individual variability in the time lapse for APD oscillations characterized in our population of models can be explained by differential I_{Ks} contributions from one cell to another.

The important role of I_{Ks} during β-AS has been pointed out in numerous studies (Volders et al., 2003; Johnson et al., 2010, 2013; Hegyi et al., 2018; Varshneya et al., 2018). Reduced I_{Ks} responsiveness to β-AS has been suggested to increase arrhythmia susceptibility in a heart failure animal model (Hegyi et al., 2018). In ventricular myocytes, loss of I_{Ks} current has been experimentally shown to exaggerate beat-to-beat APD variability in response to β-AS (Johnson et al., 2010, 2013) and computationally proved to facilitate the generation of pro-arrhythmic early afterdepolarizations (Varshneya et al., 2018). Our results provide additional support to the role of I_{Ks} during β-AS, as reduced I_{Ks} shortens the oscillatory latency and thus facilitates the occurrence of LF oscillations of APD. This oscillatory behavior of ventricular repolarization can be seen as a particular form of beat-to-beat variability restricted to frequencies in the Mayer wave frequency range (0.03–15 Hz).

4.3. Increased Arrhythmic Risk as a Function of the Time Lapse and Magnitude of LF Oscillations of APD

RRR, individually or combined with Ca^{2+} overload, has been found to dramatically reduce the time lapse for sympathetically-induced oscillatory behavior. This can be understood on the basis that under RRR the amount of I_{Ks} current is reduced and, provided phosphorylation kinetics are not varied, this leads to a reduction in the oscillation time lag of the APD. Since the above holds for each of the virtual cells in the population built this study, the time lapse values measured under pathological conditions are lower than the ones corresponding to non-pathological conditions.

A comparison for time lapses calculated for cells under healthy conditions has been established while considering two groups of interest, one composed of cells presenting and the other one not presenting arrhythmogenic events after simulation of disease conditions. Results have been shown to be comparable. However, in both the pro-arrhythmic and non-pro-arrhythmic groups, there is an inverse relationship between the magnitude of LF oscillations of APD, measured by PLF, and the time required for such oscillations to develop. These findings indicate that cells in which APD oscillations appear rapidly in response to enhanced sympathetic activity are associated with larger oscillatory magnitudes. Although the inverse relationship between PLF and the oscillatory time lapse holds true for both groups, such a relationship is steeper in the pro-arrhythmic group, with given low time lapse values associated with larger oscillatory magnitudes. Those enhanced magnitudes may facilitate the occurrence of arrhythmic events that can act as triggers for arrhythmias and at the same time they may contribute to a more vulnerable substrate by increasing spatial repolarization inhomogeneities between regions being at different oscillating phases. This increased arrhythmia susceptibility associated with elevated LF oscillations of repolarization has been postulated by *in silico* studies (Pueyo et al., 2016; Sampedro-Puente et al., 2019) and confirmed by *in vivo* research on a CAVB dog model (Sprenkeler et al., 2019) as well as clinical studies in post-infarction patients. (Rizas et al., 2017). These results are in line with studies associating higher levels of temporal repolarization variability, in the form of alternans or in other forms, with increased arrhythmic risk (Rosenbaum, 2001; Porter et al., 2019).

The role of I_{Ks} expression and phosphorylation dynamics in pro-arrhythmia that has been uncovered in the present study is in line with previous studies investigating ventricular repolarization response to β-AS. The slow I_{Ks} phosphorylation kinetics as compared to the fast I_{Ca} kinetics have been reported to be behind the generation of transient arrhythmogenic early afterdepolarizations (Liu et al., 2012; Xie et al., 2013) and APD alternans (Xie et al., 2014b) upon sudden ISO application. In our study, the fact of simulating a whole population of cells allows to additionally reveal the importance of I_{Ks} conductance in determining τ_{APD}, as I_{Ks} conductance modulates the relevance

of I_{Ks} dynamics on APD time course during β-AS. Additionally, differential I_{Ks} and I_{Ca} activation kinetics in response to sudden β-AS have been shown to promote the transition from ventricular tachycardia to ventricular fibrillation by transiently steepening APD restitution in simulated ventricular tissues (Xie et al., 2014a). This same ionic mismatch has been suggested as a plausible mechanism underlying a transitory increase in the risk for arrhythmias by application of sudden adrenergic stress in isolated innervated rabbit hearts treated with a potassium channel blocker and subjected to sustained parasympathetic stimulation (Winter et al., 2018).

4.4. Study Limitations

In this study, simulations have been run to quantify the time lapse for development of sympathetically-mediated LF oscillations of APD in a large population of human ventricular AP models developed based on available experimental data. After confirming the role of β-AS, over the role of mechanical stretch, in determining such oscillatory time lapse, our simulated results were compared with available *in vitro* data from isolated canine ventricular myocytes in response to sudden administration of a β-adrenergic agonist. Despite differences between species, experimental studies have shown that ventricular repolarization characteristics of canine cardiomyocytes closely resemble those of human cardiomyocytes (Szabó et al., 2005; Szentandrássy et al., 2005). If additional *in vitro* and/or *in vivo* data became available to analyze the time required for ARI or APD oscillations to become manifest following sympathetic provocation, further validation of the results obtained in the present study could be performed.

The simulated results presented in this study correspond to single cells. As a continuation of this investigation, tissue models built on the basis of the present population of AP models could be used to assess whether other tissue-specific factors could play a relevant role in the time required for APD oscillations to develop, in the magnitude of such oscillations as well as in the associated consequences in terms of pro-arrhythmic risk.

The population of human ventricular computational models built in this study used the O'Hara et al. (2011) model as a basis to describe human ventricular electrophysiology and calcium dynamics, whereas mechanics were described by a modified version of the Niederer et al. (2006) model. For β-adrenergic signaling, the Xie et al. (2013) model was used as a basis and the Soltis and Saucerman (2010) model was used for additional comparisons. These selections might have an impact on the conclusions reached in this study, particularly regarding quantitative values for the time required for LF oscillations of APD to develop. Nevertheless, in Pueyo et al. (2016), different human and animal cell models were tested for APD oscillatory behavior, confirming model-independence in qualitative terms with only some quantitative differences between different electrophysiological models, particularly for different species. Future studies could address the investigations conducted in this study while using other cellular models as a basis for construction of a population of models representative of human or animal ventricular electrophysiological characteristics reported experimentally and compare with the results of this study.

The developed population of human ventricular AP models was deterministic. Future work could include incorporation of stochasticity into the main ionic currents active during AP repolarization. This would allow accounting for beat-to-beat repolarization variability, which might have an effect in the time course for development of LF oscillations of APD.

An ISO dose of 0 μM was used to represent β-AS under baseline conditions. Although results are anticipated to be very similar to those obtained for a low ISO dose slightly above 0, somewhat different time lapse values for APD oscillations might be quantified.

5. CONCLUSIONS

Human ventricular repolarization presents low-frequency oscillations that develop following enhanced sympathetic activity at time lapses varying from a few seconds to more than 3 min depending on individual cells characteristics. The latency in the oscillatory development is due to the slow ventricular response to β-adrenergic stimulation and, specifically, it is associated with the slow phosphorylation kinetics of the I_{Ks} current. Prior stimulation of β-adrenoceptors reduces the time required for the development of repolarization oscillations. Short time lapses are associated with large APD oscillatory magnitudes, particularly in cells susceptible to develop arrhythmogenic events in response to sympathetic stimulation.

DATA AVAILABILITY STATEMENT

The datasets generated for this study are available on request to the corresponding author.

AUTHOR CONTRIBUTIONS

EP and PT devised the project, the main conceptual ideas and proof outline, and were responsible for overseeing the research and providing critical insight and recommendations regarding the focus, structure and content of the paper. DS-P and JF-B performed computational simulations and analyzed the data results. NS and PN contributed with technical details and analysis support. All authors participated in writing and proofreading throughout the publication process.

FUNDING

This work was supported by the European Research Council through grant ERC-2014-StG 638284, by MINECO (Spain) through project DPI2016-75458-R, by MULTITOOLS2HEART-ISCIII, by Gobierno de Aragón through project LMP124-18 and Reference Group BSICoS T39-17R cofunded by FEDER 2014-2020, by European Social Fund (EU) and Gobierno de Aragón through a personal predoctoral grant to DS-P, by National Research Development and Innovation Office (Hungary) through project NKFIH-K115397, and by European

Regional Development Fund cofunded by National Research Development and Innovation Office (Hungary) through GINOP-2.3.2.-15-2016-00040 and EFOP-3.6.2-16-2017-00006 projects. Computations were performed by ICTS NANBIOSIS (HPC Unit at University of Zaragoza).

SUPPLEMENTARY MATERIAL

The Supplementary Material for this article can be found online at: https://www.frontiersin.org/articles/10.3389/fphys.2019.01547/full#supplementary-material

REFERENCES

Bauer, A., Klemm, M., Rizas, K. D., Hamm, W., von Stülpnagel, L., Dommasch, M., et al. (2019). Prediction of mortality benefit based on periodic repolarisation dynamics in patients undergoing prophylactic implantation of a defibrillator: a prospective, controlled, multicentre cohort study. *Lancet* 394, 1344–1351. doi: 10.1016/S0140-6736(19)31996-8

Britton, O. J., Bueno-Orovio, A., Virág, L., Varró, A., and Rodriguez, B. (2017). The electrogenic Na+/K+ pump is a key determinant of repolarization abnormality susceptibility in human ventricular cardiomyocytes: a population-based simulation study. *Front. Physiol.* 8:278. doi: 10.3389/fphys.2017.00278

Furlan, R., Porta, A., Costa, F., Tank, J., Baker, L., Schiavi, R., et al. (2000). Oscillatory patterns in sympathetic neural discharge and cardiovascular variables during orthostatic stimulus. *Circulation* 101, 886–892. doi: 10.1161/01.cir.101.8.886

Grandi, E., Pasqualini, F. S., and Bers, D. M. (2010). A novel computational model of the human ventricular action potential and Ca transient. *J. Mol. Cell. Cardiol.* 48, 112–121. doi: 10.1016/j.yjmcc.2009.09.019

Guinamard, R., Demion, M., Magaud, C., Potreau, D., and Bois, P. (2006). Functional expression of the TRPM4 cationic current in ventricular cardiomyocytes from spontaneously hypertensive rats. *Hypertension* 48, 587–594. doi: 10.1161/01.HYP.0000237864.65019.a5

Guo, D., Liu, Q., Liu, T., Elliott, G., Gingras, M., Kowey, P. R., et al. (2011). Electrophysiological properties of HBI-3000: a new antiarrhythmic agent with multiple-channel blocking properties in human ventricular myocytes. *J. Cardiovasc. Pharmacol.* 57, 79–85. doi: 10.1097/FJC.0b013e3181ffe8b3

Hanson, B., Child, N., Van Duijvenboden, S., Orini, M., Chen, Z., Coronel, R., et al. (2014). Oscillatory behavior of ventricular action potential duration in heart failure patients at respiratory rate and low frequency. *Front. Physiol.* 5:414. doi: 10.3389/fphys.2014.00414

Hegyi, B., Bányász, T., Izu, L. T., Belardinelli, L., Bers, D. M., and Chen-Izu, Y. (2018). β-adrenergic regulation of late Na^+ current during cardiac action potential is mediated by both PKA and CaMKII. *J. Mol. Cell. Cardiol.* 123, 168–179. doi: 10.1016/j.yjmcc.2018.09.006

Heijman, J., Volders, P. G., Westra, R. L., and Rudy, Y. (2011). Local control of β-adrenergic stimulation: effects on ventricular myocyte electrophysiology and Ca^2+-transient. *J. Mol. Cell. Cardiol.* 50, 863–871. doi: 10.1016/j.yjmcc.2011.02.007

Iribe, G., Kaneko, T., Yamaguchi, Y., and Naruse, K. (2014). Load dependency in force-length relations in isolated single cardiomyocytes. *Prog. Biophys. Mol. Biol.* 115, 103–114. doi: 10.1016/j.pbiomolbio.2014.06.005

Johnson, D. M., Heijman, J., Bode, E. F., Greensmith, D. J., van der Linde, H., Abi-Gerges, N., et al. (2013). Diastolic spontaneous calcium release from the sarcoplasmic reticulum increases beat-to-beat variability of repolarization in canine ventricular myocytes after β-adrenergic stimulation. *Circ. Res.* 112, 246–256. doi: 10.1161/CIRCRESAHA.112.275735

Johnson, D. M., Heijman, J., Pollard, C. E., Valentin, J.-P., Crijns, H. J., Abi-Gerges, N., et al. (2010). I(Ks) restricts excessive beat-to-beat variability of repolarization during beta-adrenergic receptor stimulation. *J. Mol. Cel. Cardiol.* 48, 122–130. doi: 10.1016/j.yjmcc.2009.08.033

Jost, N., Varro, A., Szuts, V., Kovacs, P. P., Seprényi, G., Biliczki, P., et al. (2008). Molecular basis of repolarization reserve differences between dogs and man. *Circulation* 118:S342.

Kamkin, A., Kiseleva, I., and Isenberg, G. (2000). Stretch-activated currents in ventricular myocytes: amplitude and arrhythmogenic effects increase with hypertrophy. *Cardiovasc. Res.* 48, 409–420. doi: 10.1016/s0008-6363(00)00208-x

Liu, G.-X., Choi, B.-R., Ziv, O., Li, W., de Lange, E., Qu, Z., et al. (2012). Differential conditions for early after-depolarizations and triggered activity in cardiomyocytes derived from transgenic LQT1 and LQT2 rabbits. *J. Physiol.* 590, 1171–1180. doi: 10.1113/jphysiol.2011.218164

McKay, M. D., Beckman, R. J., and Conover, W. J. (1979). A comparison of three methods for selecting values of input variables in the analysis of output from a computer code. *Technometrics* 21, 239–245. doi: 10.2307/1268522

Niederer, S., Hunter, P., and Smith, N. (2006). A quantitative analysis of cardiac myocyte relaxation: a simulation study. *Biophys. J.* 90, 1697–1722. doi: 10.1529/biophysj.105.069534

Niederer, S. A., and Smith, N. P. (2007). A mathematical model of the slow force response to stretch in rat ventricular myocytes. *Biophys. J.* 92, 4030–4044. doi: 10.1529/biophysj.106.095463

Nosakhare, E., Verghese, G. C., Tasker, R. C., and Heldt, T. (2014). "Qt interval adaptation to changes in autonomic balance," in *Computing in Cardiology, Vol. 41* (Cambridge, MA: IEEE), 605–608. Available online at: https://ieeexplore.ieee.org/xpl/conhome/7035785/proceeding

O'Hara, T., Virág, L., Varró, A., and Rudy, Y. (2011). Simulation of the undiseased human cardiac ventricular action potential: model formulation and experimental validation. *PLoS Comput. Biol.* 7:e1002061. doi: 10.1371/journal.pcbi.1002061

Pagani, M., Montano, N., Porta, A., Malliani, A., Abboud, F. M., Birkett, C., et al. (1997). Relationship between spectral components of cardiovascular variabilities and direct measures of muscle sympathetic nerve activity in humans. *Circulation* 95, 1441–1448. doi: 10.1161/01.cir.95.6.1441

Porter, B., Bishop, M. J., Claridge, S., Child, N., Van Duijvenboden, S., Bostock, J., et al. (2019). Left ventricular activation-recovery interval variability predicts spontaneous ventricular tachyarrhythmia in patients with heart failure. *Heart Rhythm* 16, 702–709. doi: 10.1016/j.hrthm.2018.11.013

Porter, B., Van Duijvenboden, S., Bishop, M. J., Orini, M., Claridge, S., Gould, J., et al. (2018). Beat-to-beat variability of ventricular action potential duration oscillates at low frequency during sympathetic provocation in humans. *Front. Physiol.* 9:147. doi: 10.3389/fphys.2018.00147

Pueyo, E., Malik, M., and Laguna, P. (2008). A dynamic model to characterize beat-to-beat adaptation of repolarization to heart rate changes. *Biomed. Signal Process. Control* 3, 29–43. doi: 10.1016/j.bspc.2007.09.005

Pueyo, E., Orini, M., Rodríguez, J. F., and Taggart, P. (2016). Interactive effect of beta-adrenergic stimulation and mechanical stretch on low-frequency oscillations of ventricular action potential duration in humans. *J. Mol. Cell. Cardiol.* 97, 93–105. doi: 10.1016/j.yjmcc.2016.05.003

Pueyo, E., Smetana, P., Caminal, P., DeLuna, A., Malik, M., and Laguna, P. (2004). Characterization of QT interval adaptation to RR interval changes and its use as a risk-stratifier of arrhythmic mortality in amiodarone-treated survivors of acute myocardial infarction. *IEEE Trans. Biomed. Eng.* 51, 1511–1520. doi: 10.1109/TBME.2004.828050

Rizas, K. D., Hamm, W., Kääb, S., Schmidt, G., and Bauer, A. (2016). Periodic repolarisation dynamics: a natural probe of the ventricular response to sympathetic activation. *Arrhythm Electrophysiol. Rev.* 5, 31–36. doi: 10.15420/aer.2015:30:2

Rizas, K. D., McNitt, S., Hamm, W., Massberg, S., Kääb, S., Zareba, W., et al. (2017). Prediction of sudden and non-sudden cardiac death in post-infarction patients with reduced left ventricular ejection fraction by periodic repolarization dynamics: MADIT-II substudy. *Eur. Heart J.* 38, 2110–2118. doi: 10.1093/eurheartj/ehx161

Rizas, K. D., Nieminen, T., Barthel, P., Zürn, C. S., Kähönen, M., Viik, J., et al. (2014). Sympathetic activity–associated periodic repolarization dynamics predict mortality following myocardial infarction. *J. Clin. Invest.* 124, 1770–1780. doi: 10.1172/JCI70085

Rosenbaum, D. S. (2001). T wave alternans: a mechanism of arrhythmogenesis comes of age after 100 years. *J. Cardiovasc. Electrophysiol.* 12, 207–209. doi: 10.1046/j.1540-8167.2001.00207.x

Ruzsnavszky, F., Hegyi, B., Kistamás, K., Váczi, K., Horváth, B., Szentandrássy, N., et al. (2014). Asynchronous activation of calcium and potassium currents by isoproterenol in canine ventricular myocytes. *Naunyn-Schmiedeberg's Arch. Pharmacol.* 387, 457–467. doi: 10.1007/s00210-014-0964-6

Sampedro-Puente, D. A., Fernandez-Bes, J., Porter, B., van Duijvenboden, S., Taggart, P., and Pueyo, E. (2019). Mechanisms underlying interactions between low-frequency oscillations and beat-to-beat variability of celullar ventricular repolarization in response to sympathetic stimulation: implications for arrhythmogenesis. *Front. Physiol.* 10:916. doi: 10.3389/fphys.2019.00916

Soltis, A. R., and Saucerman, J. J. (2010). Synergy between CaMKII substrates and β-adrenergic signaling in regulation of cardiac myocyte Ca2+ handling. *Biophys. J.* 99, 2038–2047. doi: 10.1016/j.bpj.2010.08.016

Sprenkeler, D. J., Beekman, J. D. M., Bossu, A., Dunnink, A., and Vos, M. A. (2019). Pro-arrhythmic ventricular remodeling is associated with increased respiratory and low-frequency oscillations of monophasic action potential duration in the chronic atrioventricular block dog model. *Front. Physiol.* 10:1095. doi: 10.3389/fphys.2019.01095

Szabó, G., Szentandrássy, N., Bíró, T., Tóth, B. I., Czifra, G., Magyar, J., et al. (2005). Asymmetrical distribution of ion channels in canine and human left-ventricular wall: epicardium versus midmyocardium. *Pfluegers Arch. Eur. J. Physiol.* 450, 307–316. doi: 10.1007/s00424-005-1445-z

Szentandrássy, N., Bányász, T., Biro, T., Szabó, G., Toth, B., Magyar, J., et al. (2005). Apico-basal inhomogeneity in distribution of ion channels in canine and human ventricular myocardium. *Cardiovasc. Res.* 65, 851–860. doi: 10.1016/j.cardiores.2004.11.022

Varshneya, M., Devenyi, R. A., and Sobie, E. A. (2018). Slow delayed rectifier current protects ventricular myocytes from arrhythmic dynamics across multiple species. *Circ. Arrhythm. Electrophysiol.* 11:e006558. doi: 10.1161/CIRCEP.118.006558

Volders, P. G., Stengl, M., van Opstal, J. M., Gerlach, U., Spätjens, R. L., Beekman, J. D., et al. (2003). Probing the contribution of I_{Ks} to canine ventricular repolarization. *Circulation* 107, 2753–2760. doi: 10.1161/01.CIR.0000068344.54010.B3

Wang, L., Morotti, S., Tapa, S., Francis Stuart, S. D., Jiang, Y., Wang, Z., et al. (2019). Different paths, same destination: divergent action potential responses produce conserved cardiac fight-or-flight response in mouse and rabbit hearts. *J. Physiol.* 597, 3867–3883. doi: 10.1113/JP278016

Weise, L. D., and Panfilov, A. V. (2013). A discrete electromechanical model for human cardiac tissue: effects of stretch-activated currents and stretch conditions on restitution properties and spiral wave dynamics. *PLoS ONE* 8:e59317. doi: 10.1371/journal.pone.0059317

Winter, J., Tipton, M. J., and Shattock, M. J. (2018). Autonomic conflict exacerbates long QT associated ventricular arrhythmias. *J. Mol. Cell. Cardiol.* 116, 145–154. doi: 10.1016/j.yjmcc.2018.02.001

Xie, Y., Grandi, E., Bers, D. M., and Sato, D. (2014a). How does β-adrenergic signalling affect the transitions from ventricular tachycardia to ventricular fibrillation? *Europace* 16, 452–457. doi: 10.1093/europace/eut412

Xie, Y., Grandi, E., Puglisi, J. L., Sato, D., and Bers, D. M. (2013). β-adrenergic stimulation activates early afterdepolarizations transiently via kinetic mismatch of PKA targets. *J. Mol. Cell. Cardiol.* 58, 153–161. doi: 10.1016/j.yjmcc.2013.02.009

Xie, Y., Izu, L. T., Bers, D. M., and Sato, D. (2014b). Arrhythmogenic transient dynamics in cardiac myocytes. *Biophys. J.* 106, 1391–1397. doi: 10.1016/j.bpj.2013.12.050

Conflict of Interest: The authors declare that the research was conducted in the absence of any commercial or financial relationships that could be construed as a potential conflict of interest.

frontiers in Physiology

ORIGINAL RESEARCH
published: 22 January 2020
doi: 10.3389/fphys.2019.01582

Complex Interaction Between Low-Frequency APD Oscillations and Beat-to-Beat APD Variability in Humans Is Governed by the Sympathetic Nervous System

*Stefan Van Duijvenboden[1†], Bradley Porter[2†], Esther Pueyo[3,4], David Adolfo Sampedro-Puente[3], Jesus Fernandez-Bes[3], Baldeep Sidhu[2], Justin Gould[2], Michele Orini[5], Martin J. Bishop[2], Ben Hanson[6], Pier Lambiase[1], Reza Razavi[2], Christopher A. Rinaldi[7], Jaswinder S. Gill[7] and Peter Taggart[1]**

[1] Institute of Cardiovascular Science, University College London, London, United Kingdom, [2] School of Imaging Sciences and Biomedical Engineering, King's College London, London, United Kingdom, [3] BSICOS Group, I3A, IIS Aragón, University of Zaragoza, Zaragoza, Spain, [4] CIBER-BBN, Madrid, Spain, [5] Department of Clinical Pharmacology, Queen Mary University of London, London, United Kingdom, [6] Department of Mechanical Engineering, University College London, London, United Kingdom, [7] Guy's and St Thomas' NHS Foundation Trust, London, United Kingdom

Background: Recent clinical, experimental and modeling studies link oscillations of ventricular repolarization in the low frequency (LF) (approx. 0.1 Hz) to arrhythmogenesis. Sympathetic provocation has been shown to enhance both LF oscillations of action potential duration (APD) and beat-to-beat variability (BVR) in humans. We hypothesized that beta-adrenergic blockade would reduce LF oscillations of APD and BVR of APD in humans and that the two processes might be linked.

Methods and Results: Twelve patients with normal ventricles were studied during routine electrophysiological procedures. Activation-recovery intervals (ARI) as a conventional surrogate for APD were recorded from 10 left and 10 right ventricular endocardial sites before and after acute beta-adrenergic adrenergic blockade. Cycle length was maintained constant with right ventricular pacing. Oscillatory behavior of ARI was quantified by spectral analysis and BVR as the short-term variability. Beta-adrenergic blockade reduced LF ARI oscillations (8.6 ± 4.5 ms^2 vs. 5.5 ± 3.5 ms^2, $p = 0.027$). A significant correlation was present between the initial control values and reduction seen following beta-adrenergic blockade in LF ARI ($r_S = 0.62$, $p = 0.037$) such that when initial values are high the effect is greater. A similar relationship was also seen in the beat-to beat variability of ARI ($r_S = 0.74$, $p = 0.008$). There was a significant correlation between the beta-adrenergic blockade induced reduction in LF power of ARI and the witnessed reduction of beat-to-beat variability of ARI ($r_S = 0.74$, $p = 0.01$). These clinical results accord with recent computational modeling studies which provide mechanistic insight into the interactions of LF oscillations and beat-to-beat variability of APD at the cellular level.

OPEN ACCESS

Edited by:
Tobias Opthof, Academic Medical Center (AMC), Netherlands

Reviewed by:
Jordi Heijman, Maastricht University, Netherlands
Daniel M. Johnson, University of Birmingham, United Kingdom
Marmar Vaseghi, UCLA Cardiac Arrhythmia Center, United States

***Correspondence:**
Peter Taggart
p.taggart@ucl.ac.uk

[†]These authors share first authorship

Specialty section:
This article was submitted to Cardiac Electrophysiology, a section of the journal Frontiers in Physiology

Received: *04 September 2019*
Accepted: *17 December 2019*
Published: *22 January 2020*

Citation:
Van Duijvenboden S, Porter B, Pueyo E, Sampedro-Puente DA, Fernandez-Bes J, Sidhu B, Gould J, Orini M, Bishop MJ, Hanson B, Lambiase P, Razavi R, Rinaldi CA, Gill JS and Taggart P (2020) Complex Interaction Between Low-Frequency APD Oscillations and Beat-to-Beat APD Variability in Humans Is Governed by the Sympathetic Nervous System. Front. Physiol. 10:1582. doi: 10.3389/fphys.2019.01582

Conclusion: Beta-adrenergic blockade reduces LF oscillatory behavior of APD (ARI) in humans *in vivo*. Our results support the importance of LF oscillations in modulating the response of BVR to beta-adrenergic blockers, suggesting that LF oscillations may play role in modulating beta-adrenergic mechanisms underlying BVR.

Keywords: action potential duration, beat-to-beat variability, oscillations, human heart, sympathetic, beta-adrenergic blockade

INTRODUCTION

Factors which influence the stability of ventricular repolarization are important in arrhythmogenesis. Enhanced oscillation of ventricular repolarization in the low frequency range and increased beat-to-beat variability (BVR) of ventricular repolarization are two of the strongest predictors of arrhythmia and sudden cardiac death (Atiga et al., 1998; Haigney et al., 2004; Thomsen et al., 2004; Gallacher et al., 2007; Tereshchenko et al., 2009; Abi-Gerges et al., 2010; Hinterseer et al., 2010; Jacobson et al., 2011; Średniawa et al., 2012; Rizas et al., 2014, 2016, 2017; Baumert et al., 2016; Bauer et al., 2019). Both are enhanced by sympathetic stimulation and recent studies suggest a possible interactive mechanism (Porter et al., 2018). However, the mechanisms underlying the effect of beta-adrenergic stimulation on LF oscillations of repolarization and beat-to-beat variability of repolarization remain unclear.

Oscillations of ventricular repolarization measured from the ECG T-wave vector referred to as periodic repolarisation dynamics (PRD) have been attributed to oscillations in APD at the frequency of the sympathetic nerves (approx. 0.05–0.1 Hz). Ventricular action potential duration (APD) measured as activation-recovery intervals (ARI) has recently been shown to oscillate in this frequency range (Hanson et al., 2014). The LF power of APD has been shown to be increased by sympathetic provocation (Porter et al., 2018). The recent finding of LF oscillations in short term variability of ventricular APD (Porter et al., 2018) raises the possibility of an association between LF oscillations of APD and BVR.

Computational modeling has provided early insight into the mechanisms underlying these oscillations of APD, the effect of beta-adrenergic stimulation and their relationship to the initiation of ventricular arrhythmias (Pueyo et al., 2016a,b). More recent studies on the effect of beta-adrenergic blockade suggest that the cellular mechanisms underlying modulation of LF APD and BVR of APD are strongly influenced by the initial conditions of APD (Sampedro-Puente et al., 2019). One of the objectives of the present study was to examine this hypothesis in humans *in vivo*.

We have studied 12 patients during cardiac catheterization allowing us to measure ARIs as an approximation for APD at 10 right ventricular (RV) and 10 left ventricular (LV) endocardial sites in order to investigate the effect of acute beta-adrenergic blockade on LF oscillations of ventricular APD and on BVR of APD, and the possible interaction between the two. Cycle length was held constant with RV pacing to avoid confounding effects due to the cycle length dependency of APD.

MATERIALS AND METHODS

Ethical Approval

The study was approved by the Ethics Committee of Guy's and Thomas' Hospitals and conformed to the standards set by the Declaration of Helsinki (latest revision: 59th World Medical Association General Assembly). All patients gave written, informed consent.

Subjects

Studies were performed in 12 patients (10 males, 2 females, aged 41–69, median 61) during the course of routine clinical radiofrequency ablation procedures for atrial fibrillation. Four patients had paroxysmal atrial fibrillation, and eight patients had persistent atrial fibrillation. All subjects had normal biventricular systolic function. **Table 1** demonstrates further patient characteristics. Studies were performed in the un-sedated state and cardio-active medications (beta-blockers, non-dihydropyridine calcium channel blockers, digoxin, and flecainide) were discontinued for 5 days before the study.

Protocol

Utilizsing the routine transseptal puncture of an AF ablation, a decapolar catheter was placed in the left ventricle via the left atrium and mitral valve. The pacing catheter and second decapolar catheter were placed in the right ventricle. Routine AF ablation femoral venous access was utilized for placement of all catheters. The transseptal puncture was conducted under radiographic guidance. **Figure 1A** shows the set-up of both recording decapolar catheters and the pacing catheter. Subjects were paced from the right ventricular apex using a Biotronik (Berlin, Germany) stimulator (model UHS 3000) at 2x diastolic

TABLE 1 | Patient characteristics.

Diabetes	2 (17%)
Sleep apnoea	0 (0%)
Hypertension	5 (42%)
Left atrial diameter	4.2±0.4 cm
Presence of left ventricular hypertrophy	2 (17%)
Presence of diastolic dysfunction	2 (17%)
Beta-blocker	7 (60%)
Non-dihydropyridine calcium channel blocker	1 (8%)
Amiodarone	0 (0%)
Digoxin	1 (8%)
Flecainide	1 (8%)

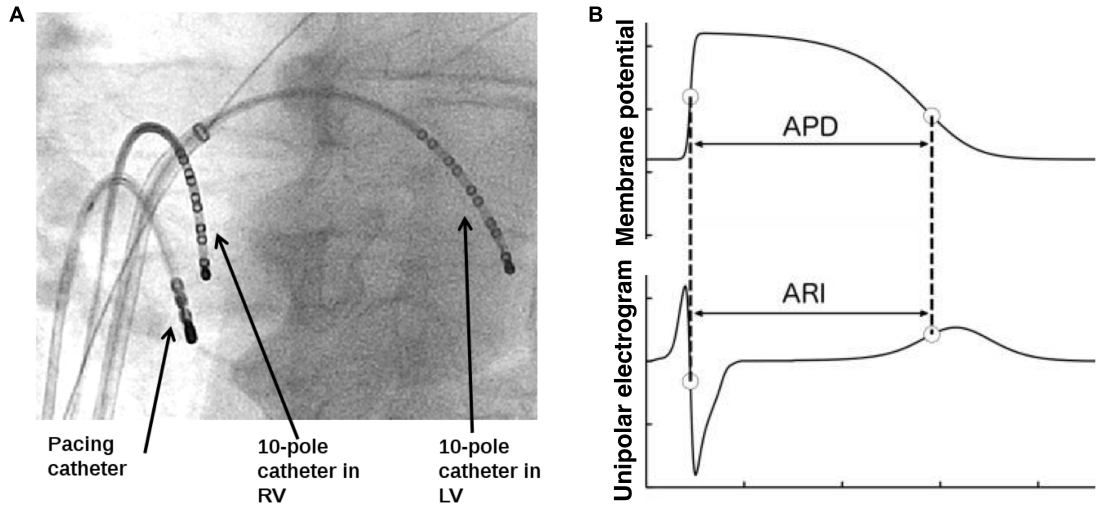

FIGURE 1 | Diagram of **(A)** decapolar catheter electrodes in RV and LV and pacing wire and **(B)** the schematic illustration of relation between the activation recovery interval (ARI) in the unipolar EGM and the ventricular action potential duration (APD).

threshold and 2 ms pulse width, at a cycle length >20 beats/min faster than the intrinsic AF rate (median: 500 ms; range: 360–500 ms) to avoid breakthrough of intrinsic beats. A 2-min period of adaptation to the paced cycle length was applied before starting a controlled breathing protocol. Breathing was controlled throughout the protocol at 0.25 and 0.5 Hz. Recordings took place for 90s during each controlled breathing cycle. First, a control period was established with the breathing protocol performed in absence of any autonomic blocking agents. Pacing was then stopped and the subject received metoprolol at a dose sufficient to reduce the intrinsic heart rate by 10 beats/min (iv; dose range, 2–10 mg), and after a further 10 min for equilibration the pacing (at the same paced cycle length as the control) and breathing protocol was repeated as above. The entire study protocol was completed prior to conducting the AF ablation.

Measurements

Continuous synchronous recordings of femoral arterial blood pressure and unipolar electrograms (UEGs) at 10 endocardial RV and 10 endocardial LV sites (**Figure 1A**) were obtained before routine clinical radiofrequency ablation procedures for atrial fibrillation in the cardiac catheterization lab at St Thomas' Hospital in London, as described previously (Hanson et al., 2012; van Duijvenboden et al., 2015). UEGs and blood pressure recordings were digitized at 1,200 Hz (Ensite 3000; Endocardial Solutions) and analyzed offline.

Data Analysis

UEGs were analyzed for ventricular APDs at each recording site by measuring activation-recovery intervals (ARIs) using the Wyatt method (Wyatt et al., 1981). This method has been validated in theoretical, computational, and experimental studies (Wyatt et al., 1981; Haws and Lux, 1990; Coronel et al., 2006; Potse et al., 2009). According to this method, activation is measured at the moment of minimum dV/dt of the QRS complex of the UEG and repolarization at the moment of maximum dV/dt of the T-wave (**Figure 1B**). ARIs were measured automatically using in house developed algorithms. Heuristic-based screening was used to identify and discount any cases where the T-wave was indistinct or corrupt. Blood pressure recordings were analyzed for systolic blood pressure (SBP) and the maximum rate of systolic pressure increase (dP/dt_{max}) as a measure of myocardial contractility. Measurement of dP/dt_{max} from the femoral artery has been shown to provide good tracking of left ventricular contractility (Monge Garcia et al., 2018).

To establish evenly sampled series, any beats for which ARI, SBP or dP/dt_{max} measurements could not be determined were replaced by linear interpolation between the surrounding beats. Recordings were rejected from the analysis if these surrogate beats constituted more than 10% of any series.

The low frequency (LF) power in each ARI series was estimated by calculating the bandpower in the low-frequency band (0.04–0.15 Hz) using the Thomson's multitaper method with three Slepian tapers, which is known to be robust against noise (Thomson, 1982). The same analysis was applied to the calculate the high frequency (HF) power in in a frequency band of the breathing frequency (either 0.25 or 0.5 Hz) ± 10%. The LF and HF powers were then averaged for RV and LV poles.

Beat-to-beat variability of ARI was assessed by computing the short term variability (STV) of ARIs for each endocardial recording site over the entire recording as per established STV measures (Johnson et al., 2013; Baumert et al., 2016). The STV ARI (STV-ARI) was computed using a moving window of 10 consecutive beats:

$$STV = \frac{\sum |ARI_{i-1} - ARI_i|}{N\sqrt{2}}$$

where ARI_i is the ARI at the ith beat and N is the number of beats. For each pole, we computed the mean STV in time and then averaged these values across poles. The STV of SBP (STV-SBP)

and dP/dt_{max} (STV-dP/dt_{max}) were computed using the same formula and number of beats as for ARI.

Statistical Analysis

Results were averaged across the two separate breathing cycles for both control recordings and following introduction of beta-adrenergic blockade. Results are presented as mean ± standard deviation for normally distributed variables and as median and interquartile range (IQR) for non-normally distributed variables. The effect of beta-adrenergic blockade on LF power for ARI, SBP and dP/dt_{max} was tested for statistical significance using the two-tailed paired Wilcoxon signed–rank test. To evaluate whether there were different responses in ARI STV between individual electrodes ($n = 20$), we used the non-parametric Kruskal–Wallis test. Results were considered significant at $p < 0.05$.

RESULTS

Effect of Beta-Adrenergic Blockade on Combined Group Data

Example ARI, SBP and dP/dt_{max} time series of one patient breathing at 15 breaths/min (0.25 Hz) during control and following beta-adrenergic blockade are shown in **Figure 2**. In this example, clear LF oscillations are visible in all traces during control. which are attenuated following beta-adrenergic blockade. At the same time, there is a clear reduction in the STV.

In the group data, beta-adrenergic blockade resulted in a significant reduction of LF power of ARI (8.6 ± 4.5 ms^2 vs. 5.5 ± 3.5 ms^2, $p = 0.027$) (**Figure 3A**) and the LF power of SBP ($1.4 \times 10^{-3} \pm 1.2 \times 10^{-3}$ mmHg^2 vs. $0.4 \times 10^{-3} \pm 0.5 \times 10^{-3}$ mmHg^2, $p = 0.027$) (**Figure 3B**). A trend to reduction was observed for the LF power of dP/dt_{max} ($0.7 \times 10^{-6} \pm 1 \times 10^{-6}$ vs. $0.1 \times 10^{-6} \pm 0.2 \times 10^{-6}$ mmHg^2/s^2, $p = 0.129$) (**Figure 3C**).

No effect of beta-adrenergic blockade was seen on the HF power of ARI ($6.5 \times 10^{-3} \pm 3 \times 10^{-3}$ ms^2 vs. $6.1 \times 10^{-3} \pm 3.4 \times 10^{-3}$ ms^2, $p = 0.91$), SBP ($1.9 \times 10^{-3} \pm 1 \times 10^{-3}$ mmHg^2 vs. $1.7 \times 10^{-3} \pm 1 \times 10^{-3}$ mmHg^2, $p = 0.424$), nor dP/dt_{max} ($7.6 \times 10^{-7} \pm 7.4 \times 10^{-7}$ mmHg^2/s^2 vs. 3.2 ± 3.9 mmHg^2/s^2, $p = 0.052$).

No immediate effect of beta-adrenergic blockade was seen on mean ARI for group data (186.9 ± 22.8 vs. 186.5 ± 20.5 ms, $p = 0.4$) or the beat-to-beat variability (STV-ARI: 4.26 ± 1.3 vs. 4.03 ± 0.96 ms, $p = 0.97$). We also did not observe an effect on the beat-to-beat variability of SBP (STV-SBP: 5.52 ± 2.25 vs. 4.75 ± 2.68 mmHg, $p = 0.380$), but the STV dP/dt_{max} was significantly reduced (STV-dP/dt_{max} 166 ± 102 vs. 102 ± 80 mmHg/s, $p = 0.005$).

The ARI STV response to beta-adrenergic blockade was not different across breathing frequencies: mean ARI STV reduction −0.1 (±0.7) for 15 breaths/min versus 0.2 (±1.4) ms for 30 breaths/min, $p = 0.8$. Furthermore, as shown in **Figure 4**, there were no significant differences in ARI STV reduction between electrode sites in the RV and LV ($p = 0.87$ and $p = 0.56$ for RV and LV, respectively). We also tested the differences in STV baseline and reduction between RV and LV. Mean values of STV baseline and reduction were slightly higher in the LV, but the differences were not

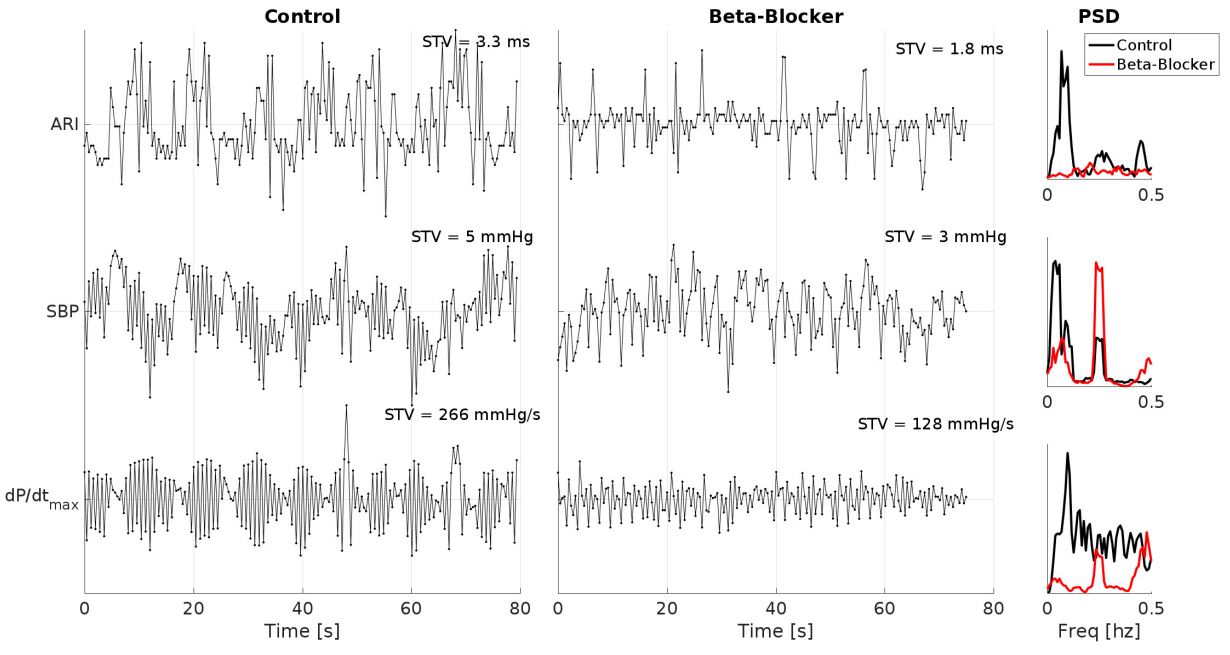

FIGURE 2 | Example ARI, SBP and dP/dt_{max} time series of one patient breathing at 15 breaths/min (0.25 Hz) during control and following beta-adrenergic blockade. Clear low-frequency oscillations are visible in all traces during control, which are attenuated following beta-adrenergic blockade. Also note the reduction in the short time variability (STV) measures. PSD, power spectral density.

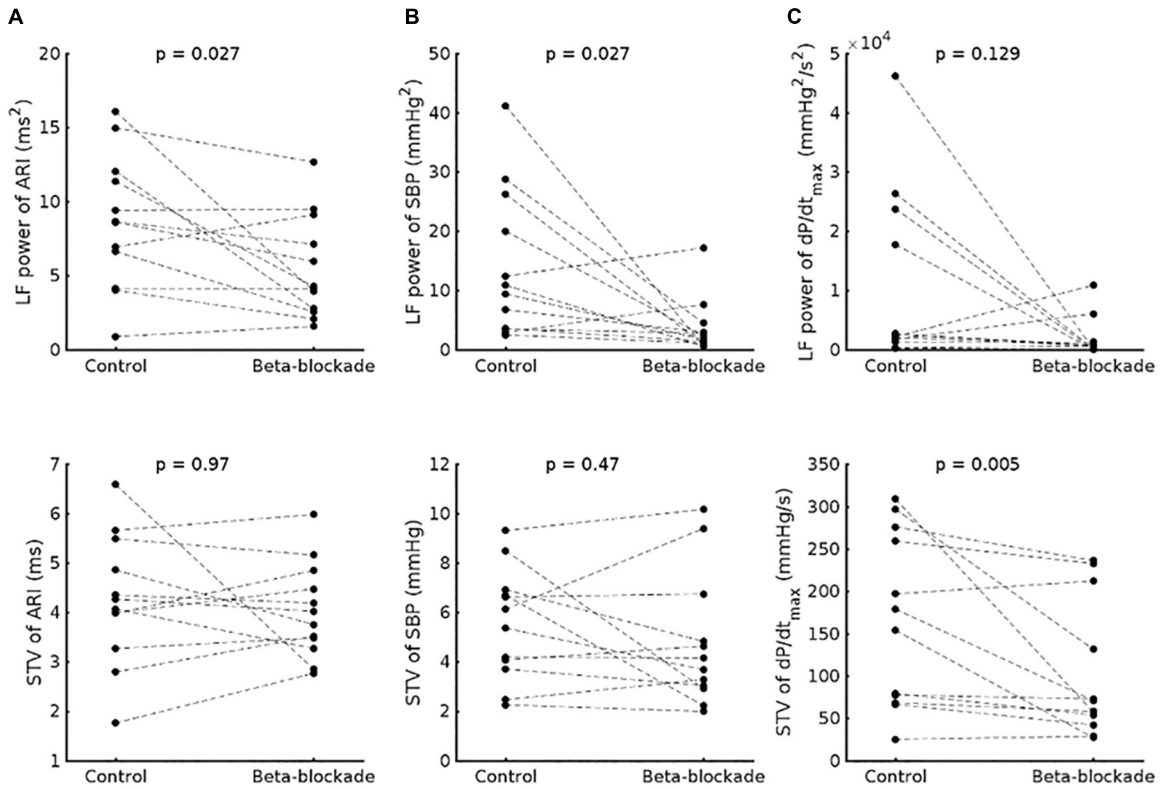

FIGURE 3 | Effect of beta-adrenergic blockade on the low frequency (LF) power (top) and short-term variability (STV) (bottom) of **(A)** activation-recovery intervals (ARIs), **(B)** systolic blood pressure (SBP) and **(C)** the maximum rate of systolic pressure increase (dP/dt$_{max}$).

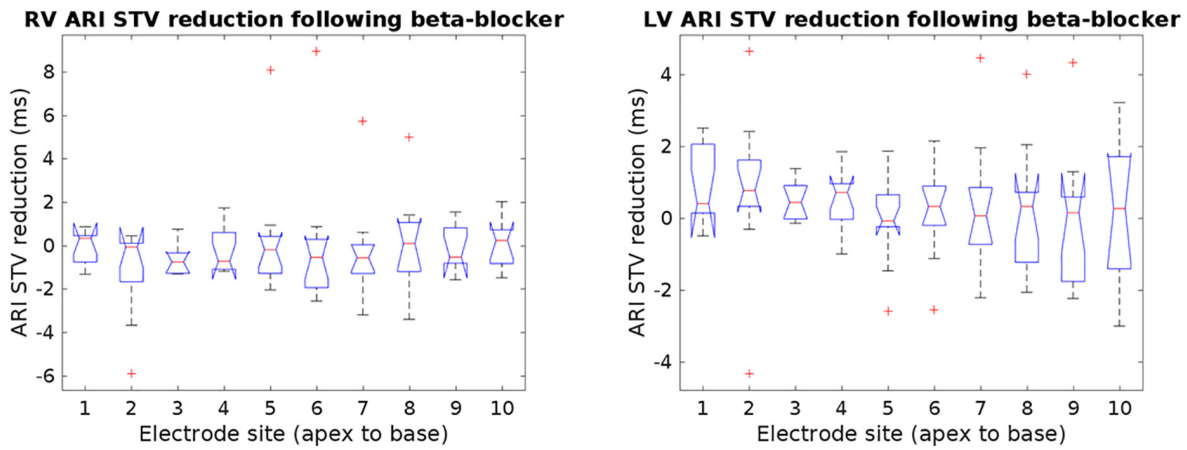

FIGURE 4 | Reduction of ARI short-time variability (STV) following beta-blocker from individual electrodes in the right and left ventricle (RV and LV). No significant changes in STV reduction were found across electrode sites. Outliers are marked by crosses.

statistically significant: mean ARI STV baseline: 8.7 ± 8.1 vs. 9.3 ± 5.0 ms, p = 0.4; mean ARI STV reduction: −0.1 ± 1.8 vs. 0.3 ± 1.0, p = 0.1, for RV and LV, respectively. Finally, we also investigated whether the LF power and STV response to beta-adrenergic blockade was different in patients who had previously been treated with beta-blocker (n = 7, **Table 1**) compared to those who had not (n = 5). Although medication was discontinued for 5 days before the study in all patients, we found that the average response in both ARI LF power and ARI STV was slightly higher in patients treated with beta-blockers, but the numbers were too small to allow robust statistical analysis (mean reduction in LF power: 4.3 ± 5.3 vs. 1.5 ± 1.3 ms^2; mean reduction in ARI STV reduction: 0.7 ± 1.5 vs. −0.4 ± 0.5 ms).

Influence of Initial Values on the Response to Beta-Adrenergic Blockade

The effect of beta-adrenergic blockade on the group data was small. However, a wide range of control values was evident and when our results were expressed in relation to control values a highly significant effect of beta-adrenergic blockade was apparent. Subjects in whom the initial control values of LF of ARI were large showed a greater change in the magnitude of the oscillations following beta-adrenergic blockade compared to subjects in whom the initial values were low. When control oscillations of ARI were large beta-adrenergic blockade reduced their magnitude. When control oscillations were small the response to beta-adrenergic blockade was minimal or variable (r_s = 0.62, p = 0.037) (**Figure 5A**). A similar relationship was observed for ARI-STV (rs = 0.74, p = 0.008) (**Figure 5B**), and the LF power of SBP and dP/dt_{max} (r_s = 0.78, p = 0.004 and r_s = 0.84, p = 0.001, respectively) (**Figures 5C,D**).

Relationship Between Low Frequency Power and Beat-to-Beat Variability of ARI

There was a strong relationship between the reduction in LF power of ARI and the reduction of STV-ARI in response to beta-adrenergic blockade (rs = 0.72, p = 0.01) (**Figure 6**). No significant relationships were found between the reduction of LF power and SBP-STV (rs = 0.42, p = 0.2) or dP/dt_{max}-STV (rs = 0.36, p = 0.3). There was also no significant relationships between the reduction in HF power and STV for ARI, SBP, and dP/dt_{max}: (ARI-STV: rs = 0.48, p = 0.1. SBP-STV: rs = 0.38, p = 0.3; dP/dt_{max} –STV: rs = 0.56, p = 0.06).

DISCUSSION

We studied the effect of acute beta-adrenergic blockade on LF oscillations of ventricular APD (approximated by ARI) and on beat-to-beat APD variability. LF power and STV ARI measurements were made from 10 RV and 10 LV sites and then averaged in patients with normal ventricles. Cycle length was maintained constant with right ventricular pacing to eliminate confounding effects of cycle length dependency and breathing was controlled throughout the protocol at 0.25 and 0.5 Hz. Our main findings were: (1) we observed a wide variation of control values of LF power and beat-to-beat variability of ARI, SBP and dP/dt_{max}; (2) beta-adrenergic blockade was associated with a significant reduction of LF power of ARI and SBP, (3) individually no clear impact of beta-adrenergic blockade on the beat-to-beat variability of ARI, SBP and dP/dt_{max} was demonstrated, however, (4) there was a strong correlation between the reduction seen in the LF power of ARI, SBP, and dP/dt_{max} following beta-adrenergic blockade, and the reduction in beat-to-beat variability.

Whereas oscillations in heart rate variability have long been recognized and the underlying mechanisms the subject of much debate (Parati et al., 2006), oscillations of ventricular APD at the low frequency have only relatively recently been identified (Hanson et al., 2014). These LF APD oscillations identified in

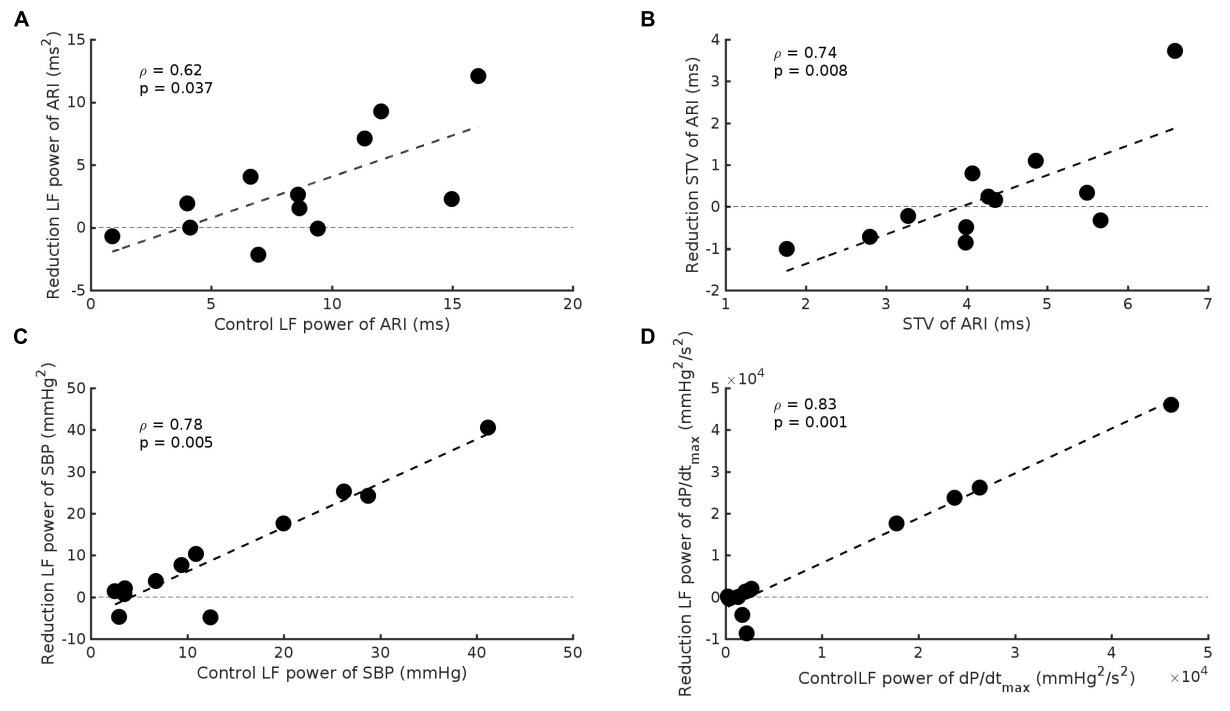

FIGURE 5 | Scatterplots demonstrating the significant relationship between baseline values and the reduction seen following beta-adrenergic blockade in: **(A)** LF power of ARI, **(B)** beat-to-beat variability of ARI (STV ARI), **(C)** LF power of systolic blood pressure (SBP), and **(D)** the LF power of the maximum rate of systolic pressure increase (dP/dt_{max}).

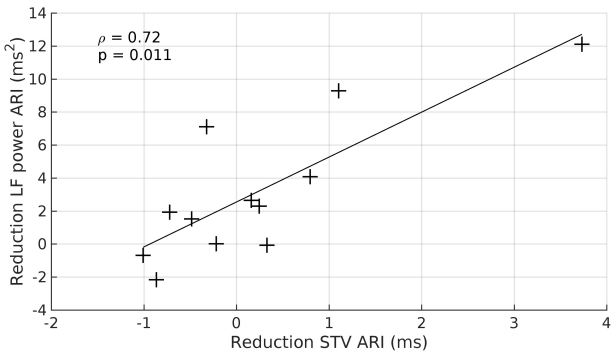

FIGURE 6 | Scatterplot demonstrating the significant relationship between the beta-adrenergic blockade induced reduction in the LF power ARI and the witnessed reduction in beat-to-beat variability of ARI (STV ARI). +, data point.

humans using ARI recordings from the ventricular myocardium, are independent of variation in R-R interval and independent of respiration (Hanson et al., 2014). They frequently occur in association with LF oscillations in blood pressure (Mayer waves) (Julien, 2006). Oscillation of ventricular repolarization at the low frequency has recently been identified from the body surface ECG T-wave vector and these are also independent of R-R interval variability and respiration and are attributed to LF oscillation of ventricular APD (Rizas et al., 2014). When enhanced these oscillations are strongly predictive of arrhythmia and sudden cardiac death (Rizas et al., 2014, 2016, 2017, 2019; Hamm et al., 2017). The magnitude of both ARI and T-wave vector oscillations is increased during sympathetic stimulation (Rizas et al., 2014; Porter et al., 2017, 2018) and it has been suggested they may be related to the intrinsic low frequency oscillation of sympathetic nerve activity.

Enhanced beat-to-beat variability of repolarization, measured clinically as QT variability or experimentally as APD variability, is well known to predispose to malignant ventricular arrhythmias (Atiga et al., 1998; Haigney et al., 2004; Thomsen et al., 2004; Gallacher et al., 2007; Tereshchenko et al., 2009; Abi-Gerges et al., 2010; Hinterseer et al., 2010; Jacobson et al., 2011; Średniawa et al., 2012; Baumert et al., 2016). BVR has been shown to be enhanced by beta-adrenergic stimulation (Johnson et al., 2010, 2013; Porter et al., 2017). Paradoxically studies using beta-adrenergic blockade have shown a mixed response of BVR in QT interval measurements with either no change or an increase or decrease (Baumert et al., 2016). In this work we demonstrate firstly a strong dependence of the effect of beta blockade on initial conditions, and secondly a possible interaction between LF power and beat-to-beat variability of ARI. Importantly, we observed that changes in beat-to-beat variability were more enhanced following beta-adrenergic blockade when LF power was reduced. In contrary, small or no changes were observed in beat-to-beat variability in individuals for which the LF power was not modulated. Although these findings may have important mechanistic implications in this context, it should be noted that beat-to-beat variability and low frequency power are both measures of variability, hence the observed relationship between LF power and beat-to-beat variability could also be a mathematical consequence. Nevertheless, the results could provide an explanation on the conflicting results reported on the effect of beta-adrenergic blockade on beat-to-beat variability. Recently it has also been observed that the intrinsic beat-to-beat variation in APD also exhibits phasic variation at the low frequency, which is enhanced during increased sympathetic stimulation (Porter et al., 2018), which may further support a possible interaction between LF ARI and intrinsic beat-to-beat variation in ARI. Interestingly, preliminary data from this study shows that the response of LF ARI power and beat-to-beat variability following beta-adrenergic blockade were more pronounced in individuals that had previously been treated with beta-blockers. While the number were too small to draw any final conclusions, it might highlight a role of the dynamic nature of beta-adrenergic receptors, but it is also possible that these patients had a higher sympathetic tone during control. Future work will further investigate this finding.

The present work was conducted in patients with normal hearts and we cannot exclude the possibility that the relationships we observed may have been different in patients with arrhythmias. However, in this context the following observations in patients with arrhythmias are worth mention. In a recent study in heart failure patients ARI recordings as a measure of local action potential duration were obtained from the left ventricular epicardial lead of an implanted cardiac defibrillator device. 11 of 43 patients received appropriate shock treatment for sustained ventricular tachycardia or fibrillation, and ARI variability was significantly higher in these patients compared to patients who did not develop arrhythmia (Porter et al., 2019). In the present paper we observed a relationship between the initial BVR and the corresponding reduction following beta blockade. Consequently beta-adrenergic blockade may have a greater effect on BVR in individuals at increased arrhythmic risk compared to those at low risk.

Clinical conditions associated with high arrhythmia risk are commonly accompanied by adverse ventricular remodeling with downregulation of ionic currents and dysregulation of Ca2+handling and reduced repolarization reserve (Armoundas et al., 2001). Beta-adrenergic stimulation in the presence of reduced repolarization reserve (Iks block) has been shown to dramatically increase BVR and be proarrhythmic (Johnson et al., 2010). The importance of downregulation of IKs in promoting excess BVR during beta-adrenergic stimulation was further demonstrated in a study identifying a role of calcium mediated mechanisms in the generation of arrhythmias (Johnson et al., 2013). In a recent study in the chronic AV block dog model using monophasic action potential recordings, remodeling resulted in an increase of low frequency oscillations of ventricular MAP duration. Furthermore, low frequency BVR measured as beat to beat differences of MAP duration, also increased. Increased low frequency power was positively related to Torsades de Pointes inducibility (Sprenkeler et al., 2019). These results suggest an interaction between the remodeling process,

low frequency oscillation and beat to beat variability of ventricular repolarization as playing an important role in arrhythmogenesis. The findings are in keeping with recent computational modeling studies involving phasic low frequency beta-adrenergic and mechanical stimulation. When remodeling was simulated by reducing repolarization reserve (reduced Ikr) and incorporating calcium overload early after depolarizations and triggered activity were readily induced (Pueyo et al., 2016b; Sampedro-Puente et al., 2019).

While a number of studies have investigated the cellular mechanisms underlying modulation of BVR by beta-adrenergic stimulation and the consequent effect on arrhythmia initiation (Johnson et al., 2010, 2013; Szentandrássy et al., 2015), only a few have so far examined mechanisms underlying low frequency oscillation of ventricular APD (Pueyo et al., 2016b; Sampedro-Puente et al., 2019). Regarding BVR ion channel stochasticity and calcium cyclical variation have both been identified as major contributors. Regarding low frequency oscillations of ventricular APD a direct action of beta-adrenergic stimulation and mechano-electric feedback has been suggested.

Recent computational research has shown that the major ionic contributors to inter-individual differences in LF oscillations of APD and beat-to-beat APD variability are I_{Kr}, I_{CaL}, and I_{K1} (Sampedro-Puente et al., 2019). In this study, a set of stochastic human ventricular action potential models was developed by individually varying the ionic conductances of I_{Kr}, I_{CaL}, and I_{K1} from their nominal values in the O'Hara-Virág-Varró-Rudy (ORd) action potential model (O'Hara et al., 2011). Beta-adrenergic and mechanical stretch effects were included in the models to simulate sympathetic modulation of ventricular electrophysiology at the cell level (Pueyo et al., 2016b; Sampedro-Puente et al., 2019). For each of the simulated models, normalized measures of LF oscillation magnitude of APD (nmLF) and beat-to-beat APD variability (STV-APD) were computed before and after beta-adrenergic blockade. In accordance with the clinical observations of this study, beta-adrenergic blockade in these simulated cells led to a remarkable reduction in nmLF and also in STV-APD. Importantly, these simulations showed a wide range of nmLF and STV-APD initial values as well as of their changes in response to beta-adrenergic blockade. In line with the presented clinical data, higher nmLF and STV-APD initial values were associated with larger beta-adrenergic blockade-induced decreases in the magnitudes of both markers. A strong correlation was observed between the effects of beta-adrenergic blockade on nmLF and STV-APD.

The reduction in nmLF in response to beta-adrenergic blockade, which could be observed to a greater or lesser extent in all the virtual cells, can be explained on the basis of beta-adrenergic stimulation enhancing LF oscillations of APD via differential phosphorylation and dephosphorylation kinetics of cellular PKA targets (mainly I_{CaL} and I_{Ks}) (Pueyo et al., 2016b; Sampedro-Puente et al., 2019). For STV-APD, the reduction induced by beta-adrenergic blockade is justified by the fact that beta-adrenergic stimulation modulates, on the one hand, the LF oscillations of APD and, on the other hand, the stochastic gating of ionic currents active during the repolarization phase (Sampedro-Puente et al., 2019).

Mechanoelectric feedback (MEF) has been suggested to contribute to the development of LF oscillations and BVR of APD in humans *in vivo* (Hanson et al., 2014) and by computational simulation, these adrenergic and mechanical actions have been shown to synergistically potentiate the oscillatory behavior and temporal variability of cellular ventricular repolarization (Pueyo et al., 2016b; Sampedro-Puente et al., 2019), in accord with the well-known potentiation of MEF effects by beta-adrenergic stimulation (Horner et al., 1996; Puglisi et al., 2013). The role of MEF, possibly through stretch-activated channels, in contributing to BVR is supported by experimental evidence in the chronic atrioventricular-block dog model, where beat-to-beat preload changes have been shown to increase short-term variability of monophasic APD (Stams et al., 2016). The timing of electro-mechanical coupling may also be important. In a canine model IKs block prolonged APD altering the timing of ventricular repolarization in relation to the ventricular pressure curve. Under these conditions the addition of left stellate stimulation induced Torsades de Points (ter Bekke et al., 2019).

The importance of risk stratification for arrhythmia and sudden death to guide patient selection for ICD implantation has already been stressed. A number of non-invasive markers of risk have been proposed including amongst others heart rate variability, baroreflex sensitivity, microvolt T-wave alternans, heart rate turbulence, Tpeak-Tend as an index of dispersion of repolarization and QT interval variability, all of which are modulated by autonomic activity (Baumert et al., 2016; Priori et al., 2016; Tse et al., 2017). However, despite showing promise none of these has so far influenced clinical practice. Numerous studies have examined the predictive power of BVR estimated in humans as QT variability or intracardiac QT interval as have been comprehensively summarized by Baumert et al. (2016). While many studies showed encouraging results a significant number were less so. It was concluded by these authors that analysis of joint RR and QT dynamics seems to allow detecting repolarization stability preceding malignant ventricular arrhythmias in patients post MI, and prospective studies are needed on the predictive value of QTV as part of a multivariate risk stratification procedure in different well-defined populations. The variable that has shown the most consistent association with sudden cardiac death is reduced left ventricular ejection fraction and remains the gold standard for risk stratification of patients with ischemic heart disease and primary prevention (Priori et al., 2016). A conceptually attractive aspect of the application of BVR is that experimental work in a canine complete AV block model indicates that the strong association with inducible TdP/VF reflects ventricular remodeling which is a characteristic feature of at-risk patients (Smoczynska et al., 2019). A recent multicenter prospective clinical trial involving 44 centers in 15 EU countries now provides convincing evidence for enhanced low frequency oscillations of ventricular repolarization, measured from the ECG T-wave vector referred to as Periodic Repolarization Dynamics (PRD), to be one of the strongest predictors of ventricular arrhythmia and sudden death in post MI

patients (Bauer et al., 2019). Comparison of the potential clinical value of each of these various biomarkers is hindered by the fact that most studies have focused on just one or a small number of these parameters and the lack of any standardization of methodology and study population. Future research should focus on evaluating the prognostic value of possible combinations of these biomarkers in prospective multivariate analysis in specific patient populations.

Limitations

The study population were patients with ostensibly normal ventricles undergoing routine ablation procedures for supraventricular arrhythmias. Eight of the 12 patients had persistent atrial fibrillation and therefore the possibility of some ventricular remodeling cannot be excluded. However, the routine procedure for atrial fibrillation ablation involves transseptal puncture to allow access to the left atrium from the right atrium. This enables placement of an LV decapolar catheter for the research procedure (right atrium to left atrium to left ventricle via the mitral valve) without the need for arterial puncture for retrograde access to the left ventricle. In many years experience of acquiring basic electrophysiological data from the *in vivo* human heart in order to complement laboratory studies, we have always considered it a priority to integrate the research protocol with the clinical protocol avoiding additional invasive procedures. We recognize that it would be ideal to have longer recordings when studying LF related parameters, but to comply with clinical studies we designed the study with view to limiting the duration of the study as much as possible.

Recordings were made from 20 localized right and left ventricular endocardial sites and then averaged. It is possible that other regions may have yielded different results. Furthermore, averaging may confound local beat-to-beat variabilities, although we did not find evidence for this when comparing the STV reduction across electrode sites and between left and right ventricle. In addition, breathing frequency may also play a role. In this work we report averaged data from two different breathing frequencies (15 and 30 breaths/min), but the reduction in ARI STV between the two breathing frequencies was not found to be significantly different.

Clinical Implications

Understanding the mechanisms underlying the interaction between beta-adrenergic stimulation, the LF oscillatory behavior of APD and beat-to-beat APD variability is important for the development of therapeutic strategies for the prevention of arrhythmia and sudden cardiac death. Enhanced oscillations of ventricular repolarization in the LF range measured from the ECG T-wave vector and referred to as periodic repolarization dynamics (PRD) have emerged as one of the strongest predictors of arrhythmia and sudden cardiac death in cardiac patients and are the subject of ongoing clinical trials (Rizas et al., 2014, 2016, 2017, 2019; Hamm et al., 2017; Bauer et al., 2019). The present work identifies several specific features of the interaction between beta-adrenergic stimulation, the LF oscillatory behavior of APD and beat-to-beat APD variability that are reproducible by computational modeling which enables mechanistic insight to be gained at the cellular level.

CONCLUSION

In patients with normal ventricles acute beta-adrenergic blockade modulated LF oscillatory behavior of ventricular APD (measured as ARIs) and beat-to-beat variability of APD in a manner that was dependent on baseline APD variability. A strong correlation was present between the effect of beta-adrenergic blockade on LF oscillation of APD and beat-to-beat variability of APD. These findings are discussed in relation to computational modeling which reproduced the clinical findings and investigated cellular mechanisms. These observations provide valuable insight into the strong association of LF oscillations of ventricular repolarization and arrhythmic and sudden cardiac death. Further work is warranted to improve our understanding in order to develop therapeutic strategies.

DATA AVAILABILITY STATEMENT

The datasets generated for this study are available on request to the corresponding author.

ETHICS STATEMENT

The studies involving human participants were reviewed and approved by the Ethics Committee of Guy's and Thomas' Hospitals. The patients/participants provided their written informed consent to participate in this study.

AUTHOR CONTRIBUTIONS

BP, SV, JG, and PT conceived and designed the experiments. All authors took responsibility in analyzing and interpreting the data, contributed to drafting or revising the manuscript, and approved the final version of the manuscript.

FUNDING

BP was funded by an Abbott educational grant. MB acknowledges the support of the Medical Research Council United Kingdom through a New Investigator Research Grant Number MR/N011007/1. The research was supported by the National Institute for Health Research (NIHR) Clinical Research Facility at Guy's and St Thomas' NHS Foundation Trust, NIHR Biomedical Research Centre based at Guy's and St Thomas' NHS Foundation Trust, and King's College London. The views expressed are those of the authors and not necessarily those of the NHS, the NIHR, or the Department of Health.

REFERENCES

Abi-Gerges, N., Valentin, J. P., and Pollard, C. E. (2010). Dog left ventricular midmyocardial myocytes for assessment of drug-induced delayed repolarization: short-term variability and proarrhythmic potential. *Br. J. Pharmacol.* 159, 77–92. doi: 10.1111/j.1476-5381.2009.00338.x

Armoundas, A. A., Wu, R., Juang, G., Marbán, E., and Tomaselli, G. F. (2001). Electrical and structural remodeling of the failing ventricle. *Pharmacol. Ther.* 92, 213–230. doi: 10.1016/S0163-7258(01)00171-171

Atiga, W. L., Calkins, H., Lawrence, J. H., Tomaselli, G. F., Smith, J. M., and Berger, R. D. (1998). Beat-to-beat repolarization lability identifies patients at risk for sudden cardiac death. *J. Cardiovasc. Electrophysiol.* 9, 899–908. doi: 10.1111/j.1540-8167.1998.tb00130.x

Bauer, A., Klemm, M., Rizas, K. D., Hamm, W., von Stülpnagel, L., Dommasch, M., et al. (2019). Prediction of mortality benefit based on periodic repolarisation dynamics in patients undergoing prophylactic implantation of a defibrillator: a prospective, controlled, multicentre cohort study. *Lancet* 394, 1344–1351. doi: 10.1016/S0140-6736(19)31996-8

Baumert, M., Porta, A., Vos, M. A., Malik, M., Couderc, J. P., Laguna, P., et al. (2016). QT interval variability in body surface ECG: measurement, physiological basis, and clinical value: position statement and consensus guidance endorsed by the European heart rhythm association jointly with the ESC working group on cardiac cellular electroph. *Europace* 18, 925–944. doi: 10.1093/europace/euv405

Coronel, R., de Bakker, J. M. T., Wilms-Schopman, F. J. G., Opthof, T., Linnenbank, A. C., Belterman, C. N., et al. (2006). Monophasic action potentials and activation recovery intervals as measures of ventricular action potential duration: experimental evidence to resolve some controversies. *Hear. Rhythm* 3, 1043–1050. doi: 10.1016/j.hrthm.2006.05.027

Gallacher, D. J., Van de Water, A., van der Linde, H., Hermans, A. N., Lu, H. R., Towart, R., et al. (2007). In vivo mechanisms precipitating torsades de pointes in a canine model of drug-induced long-QT1 syndrome. *Cardiovasc. Res.* 76, 247–256. doi: 10.1016/j.cardiores.2007.06.019

Haigney, M. C., Zareba, W., Gentlesk, P. J., Goldstein, R. E., Illovsky, M., McNitt, S., et al. (2004). QT interval variability and spontaneous ventricular tachycardia or fibrillation in the Multicenter Automatic Defibrillator Implantation Trial (MADUT) II patients. *J. Am. Coll. Cardiol.* 44, 1481–1487. doi: 10.1016/j.jacc.2004.06.063

Hamm, W., Rizas, K. D., Stülpnagel, L. V., Vdovin, N., Massberg, S., Kääb, S., et al. (2017). Implantable cardiac monitors in high-risk post-infarction patients with cardiac autonomic dysfunction and moderately reduced left ventricular ejection fraction: design and rationale of the SMART-MI trial. *Am. Heart J.* 190, 34–39. doi: 10.1016/j.ahj.2017.05.006

Hanson, B., Child, N., Van Duijvenboden, S., Orini, M., Chen, Z., Coronel, R., et al. (2014). Oscillatory behavior of ventricular action potential duration in heart failure patients at respiratory rate and low frequency. *Front. Physiol.* 5:414. doi: 10.3389/fphys.2014.00414

Hanson, B., Gill, J., Western, D., Gilbey, M. P., Bostock, J., Boyett, M. R., et al. (2012). Cyclical modulation of human ventricular repolarization by respiration. *Front. Physiol.* 3:379. doi: 10.3389/fphys.2012.00379

Haws, C. W., and Lux, R. L. (1990). Correlation between in vivo transmembrane action potential durations and activation-recovery intervals from electrograms. Effects of interventions that alter repolarization time. *Circulation* 81, 281–288. doi: 10.1161/01.CIR.81.1.281

Hinterseer, M., Beckmann, B. M., Thomsen, M. B., Pfeufer, A., Ulbrich, M., Sinner, M. F., et al. (2010). Usefulness of short-term variability of QT intervals as a predictor for electrical remodeling and proarrhythmia in patients with nonischemic heart failure. *Am. J. Cardiol.* 106, 216–220. doi: 10.1016/j.amjcard.2010.02.033

Horner, S. M., Murphy, C. F., Coen, B., Dick, D. J., and Lab, M. J. (1996). Sympathomimetic modulation of load-dependent changes in the action potential duration in the in situ porcine heart. *Cardiovasc. Res.* 32, 148–157. doi: 10.1016/0008-6363(96)00087-9

Jacobson, I., Carlsson, L., and Duker, G. (2011). Beat-by-beat QT interval variability, but not QT prolongation per se, predicts drug-induced torsades de pointes in the anaesthetised methoxamine-sensitized rabbit. *J. Pharmacol. Toxicol. Methods* 63, 40–46. doi: 10.1016/j.vascn.2010.04.010

Johnson, D. M., Heijman, J., Bode, E. F., Greensmith, D. J., Van Der Linde, H., Abi-Gerges, N., et al. (2013). Diastolic spontaneous calcium release from the sarcoplasmic reticulum increases beat-to-beat variability of repolarization in canine ventricular myocytes after β-adrenergic stimulation. *Circ. Res.* 112, 246–256. doi: 10.1161/CIRCRESAHA.112.275735

Johnson, D. M., Heijman, J., Pollard, C. E., Valentin, J. P., Crijns, H. J. G. M., Abi-Gerges, N., et al. (2010). IKs restricts excessive beat-to-beat variability of repolarization during beta-adrenergic receptor stimulation. *J. Mol. Cell. Cardiol.* 48, 122–130. doi: 10.1016/j.yjmcc.2009.08.033

Julien, C. (2006). The enigma of mayer waves: facts and models. *Cardiovasc. Res.* 70, 12–21. doi: 10.1016/j.cardiores.2005.11.008

Monge Garcia, M. I., Jian, Z., Settels, J. J., Hunley, C., Cecconi, M., Hatib, F., et al. (2018). Performance comparison of ventricular and arterial dP/dtmax for assessing left ventricular systolic function during different experimental loading and contractile conditions. *Crit. Care* 22:325. doi: 10.1186/s13054-018-2260-1

O'Hara, T., Virág, L., Varró, A., and Rudy, Y. (2011). Simulation of the undiseased human cardiac ventricular action potential: model formulation and experimental validation. *PLoS Comput. Biol.* 7:e1002061. doi: 10.1371/journal.pcbi.1002061

Parati, G., Mancia, G., Di Rienzo, M., Castiglioni, P., Taylor, J., and Studinger, P. (2006). Point: counterpoint point: counterpoint: cardiovascular variability is / is not an index of autonomic control of circulation. *J. Appl. Physiol.* 101, 676–688. doi: 10.1152/japplphysiol.00446.2006.Point

Porter, B., Bishop, M. J., Claridge, S., Behar, J., Sieniewicz, B. J., Webb, J., et al. (2017). Autonomic modulation in patients with heart failure increases beat-to-beat variability of ventricular action potential duration. *Front. Physiol.* 8:328. doi: 10.3389/fphys.2017.00328

Porter, B., Bishop, M. J., Claridge, S., Child, N., Van Duijvenboden, S., Bostock, J., et al. (2019). Left ventricular activation-recovery interval variability predicts spontaneous ventricular tachyarrhythmia in patients with heart failure. *Hear. Rhythm* 16, 702–709. doi: 10.1016/j.hrthm.2018.11.013

Porter, B., Van Duijvenboden, S., Bishop, M. J., Orini, M., Claridge, S., Gould, J., et al. (2018). Beat-to-Beat variability of ventricular action potential duration oscillates at low frequency during sympathetic provocation in humans. *Front. Physiol.* 9:147. doi: 10.3389/fphys.2018.00147

Potse, M., Vinet, A., Opthof, T., and Coronel, R. (2009). Validation of a simple model for the morphology of the T wave in unipolar electrograms. *Am. J. Physiol. Heart Circ. Physiol.* 297, H792–H801. doi: 10.1152/ajpheart.00064.2009

Priori, S. G., Blomström-Lundqvist, C., Mazzanti, A., Blom, N., Borggrefe, M., Camm, J., et al. (2016). 2015 ESC guidelines for the management of patients with ventricular arrhythmias and the prevention of sudden cardiac death. *Russ. J. Cardiol.* 7, 5–86.

Pueyo, E., Dangerfield, C. E., Britton, O. J., Virág, L., Kistamás, K., Szentandrássy, N., et al. (2016a). Experimentally-based computational investigation into beat-to-beat variability in ventricular repolarization and its response to ionic current inhibition. *PLoS One* 11:e0151461. doi: 10.1371/journal.pone.0151461

Pueyo, E., Orini, M., Rodríguez, J. F., and Taggart, P. (2016b). Interactive effect of beta-adrenergic stimulation and mechanical stretch on low-frequency oscillations of ventricular action potential duration in humans. *J. Mol. Cell. Cardiol.* 97, 93–105. doi: 10.1016/j.yjmcc.2016.05.003

Puglisi, J. L., Negroni, J. A., Chen-Izu, Y., and Bers, D. M. (2013). The force-frequency relationship: insights from mathematical modeling. *Adv. Physiol. Educ.* 37, 28–34. doi: 10.1152/advan.00072.2011

Rizas, K. D., Doller, A. J., Hamm, W., Vdovin, N., von Stuelpnagel, L., Zuern, C. S., et al. (2019). Periodic repolarization dynamics as risk predictor after myocardial infarction: prospective validation study. *Hear. Rhythm* 16, 1223–1231. doi: 10.1016/j.hrthm.2019.02.024

Rizas, K. D., Hamm, W., Kääb, S., Schmidt, G., and Bauer, A. (2016). Periodic repolarisation dynamics: a natural probe of the ventricular response to sympathetic activation. *Arrhythmia Electrophysiol. Rev.* 5, 31–36. doi: 10.15420/aer.2015

Rizas, K. D., McNitt, S., Hamm, W., Massberg, S., Kääb, S., Zareba, W., et al. (2017). Prediction of sudden and non-sudden cardiac death in post-infarction patients with reduced left ventricular ejection fraction by periodic repolarization dynamics: MADIT-II substudy. *Eur. Heart J.* 38, 2110–2118. doi: 10.1093/eurheartj/ehx161

Rizas, K. D., Nieminen, T., Barthel, P., Zürn, C. S., Kähönen, M., Viik, J., et al. (2014). Clinical medicine Sympathetic activity – associated periodic repolarization dynamics predict mortality following myocardial infarction. *J. Clin. Invest.* 124, 1770–1780. doi: 10.1172/JCI70085DS1

Sampedro-Puente, D. A., Fernandez-Bes, J., Porter, B., van Duijvenboden, S., Taggart, P., and Pueyo, E. (2019). Mechanisms underlying interactions between low-frequency oscillations and beat-to-beat variability of celullar ventricular repolarization in response to sympathetic stimulation: implications for arrhythmogenesis. *Front. Physiol.* 10:916. doi: 10.3389/fphys.2019.00916

Smoczynska, A., Beekman, H. D., and Vos, M. A. (2019). The increment of short-term variability of repolarisation determines the severity of the imminent arrhythmic outcome. *Arrhythmia Electrophysiol. Rev.* 8, 166–172. doi: 10.15420/aer.2019.16.2

Sprenkeler, D. J., Beekman, J. D. M., Bossu, A., Dunnink, A., and Vos, M. A. (2019). Pro-Arrhythmic ventricular remodeling is associated with increased respiratory and low-frequency oscillations of monophasic action potential duration in the chronic atrioventricular block dog model. *Front. Physiol.* 10:1095. doi: 10.3389/fphys.2019.01095

Średniawa, B., Kowalczyk, J., Lenarczyk, R., Kowalski, O., Sędkowska, A., Cebula, S., et al. (2012). Microvolt T-wave alternans and other noninvasive predictors of serious arrhythmic events in patients with an implanted cardioverter-defibrillator. *Kardiol. Pol.* 70, 447–455.

Stams, T. R. G., Oosterhoff, P., Heijdel, A., Dunnink, A., Beekman, J. D. M., van der Nagel, R., et al. (2016). Beat-to-beat variability in preload unmasks latent risk of Torsade de Pointes in anesthetized chronic atrioventricular block dogs. *Circ. J.* 80, 1336–1345. doi: 10.1253/circj.CJ-15-1335

Szentandrássy, N., Kistamás, K., Hegyi, B., Horváth, B., Ruzsnavszky, F., Váczi, K., et al. (2015). Contribution of ion currents to beat-to-beat variability of action potential duration in canine ventricular myocytes. *Pflugers Arch. Eur. J. Physiol.* 467, 1431–1443. doi: 10.1007/s00424-014-1581-4

ter Bekke, R. M. A., Moers, A. M. E., de Jong, M. M. J., Johnson, D. M., Schwartz, P. J., Vanoli, E., et al. (2019). Proarrhythmic proclivity of left-stellate ganglion stimulation in a canine model of drug-induced long-QT syndrome type 1. *Int. J. Cardiol.* 286, 66–72. doi: 10.1016/j.ijcard.2019.01.098

Tereshchenko, L. G., Fetics, B. J., and Berger, R. D. (2009). Intracardiac QT variability in patients with structural heart disease on class III antiarrhythmic drugs. *J. Electrocardiol.* 42, 505–510. doi: 10.1016/j.jelectrocard.2009.07.011

Thomsen, M. B., Verduyn, S. C., Stengl, M., Beekman, J. D. M., De Pater, G., Van Opstal, J., et al. (2004). Increased short-term variability of repolarization predicts d-sotalol-induced torsades de pointes in dogs. *Circulation* 110, 2453–2459. doi: 10.1161/01.CIR.0000145162.64183.C8

Thomson, D. J. (1982). Spectrum estimation and harmonic analysis. *Proc. IEEE* 70, 1055–1096. doi: 10.1109/PROC.1982.12433

Tse, G., Gong, M., Wong, W. T., Georgopoulos, S., Letsas, K. P., Vassiliou, V. S., et al. (2017). The tpeak - tend interval as an electrocardiographic risk marker of arrhythmic and mortality outcomes: a systematic review and meta-analysis. *Hear. Rhythm* 14, 1131–1137. doi: 10.1016/j.hrthm.2017.05.031

van Duijvenboden, S., Hanson, B., Child, N., Orini, M., Rinaldi, C. A., Gill, J. S., et al. (2015). Effect of autonomic blocking agents on the respiratory-related oscillations of ventricular action potential duration in humans. *Am. J. Physiol. Heart Circ. Physiol.* 309, H2108–H2117. doi: 10.1152/ajpheart.00560.2015

Wyatt, R. F., Burgess, M. J., Evans, A. K., Lux, R. L., Abildskov, J. A., and Tsutsumi, T. (1981). Estimation of ventricular transmembrane action potential durations and repolarization times from unipolar electrograms. *Am. J. Cardiol.* 47:488. doi: 10.1016/0002-9149(81)91028-6

Conflict of Interest: The authors declare that the research was conducted in the absence of any commercial or financial relationships that could be construed as a potential conflict of interest.

frontiers in Physiology

ORIGINAL RESEARCH
published: 22 January 2020
doi: 10.3389/fphys.2019.01548

Beat-to-Beat Patterning of Sinus Rhythm Reveals Non-linear Rhythm in the Dog Compared to the Human

N. Sydney Moïse[1], Wyatt H. Flanders[2] and Romain Pariaut[1]*

[1] College of Veterinary Medicine, Department of Clinical Sciences, Cornell University, Ithaca, NY, United States, [2] Department of Physics, University of Washington, Seattle, WA, United States

The human and dog have sinus arrhythmia; however, the beat-to-beat interval changes were hypothesized to be different. Geometric analyses (R–R interval tachograms, dynamic Poincaré plots) to examine rate changes on a beat-to-beat basis were analyzed along with time and frequency domain heart rate variability from 40 human and 130 canine 24-h electrocardiographic recordings. Humans had bell-shaped beat-interval distributions, narrow interval bands across time with continuous interval change and linear changes in rate. In contrast, dogs had skewed non-singular beat distributions, wide interval bands {despite faster average heart rate of dogs [mean (range); 81 (64–119)] bpm compared to humans [74.5 (59–103) p = 0.005]} with regions displaying a paucity of intervals (*zone of avoidance)* and linear plus non-linear rate changes. In the dog, dynamic Poincaré plots showed linear rate changes as intervals prolonged until a point of divergence from the line of identity at a mean interval of 598.5 (95% CI: 583.5–613.5) ms (*bifurcation interval*). The dog had bimodal beat distribution during sleep with slower rates and greater variability than during active hours that showed singular interval distributions, higher rates and less variability. During sleep, Poincaré plots of the dog had clustered or branched patterns of intervals. A slower rate supported greater parasympathetic modulation with a branched compared to the clustered distribution. Treatment with atropine eliminated the non-linear patterns, while hydromorphone shifted the bifurcated branching and beat clustering to longer intervals. These results demonstrate the unique non-linear nature of beat-to-beat variability in the dog compared to humans with increases in interval duration (decrease heart rate). These results provoke the possibility that changes are linear with a dominant sympathetic modulation and non-linear with a dominant parasympathetic modulation. The abrupt bifurcation, zone of avoidance and beat-to-beat patterning are concordant with other studies demonstrating the development of exit block from the sinus node with parasympathetic modulation influencing not only the oscillation of the pacing cells, but conduction to the atria. Studies are required to associate the *in vivo* sinus node beat patterns identified in this study to the mapping of sinus impulse origin and exit from the sinus node.

Keywords: sinus arrhythmia, heart rate variability, Poincaré plots, Holter monitoring, parasympathetic, sinus node, non-linear, autonomic nervous system

OPEN ACCESS

Edited by:
Peter Taggart,
University College London,
United Kingdom

Reviewed by:
Vadim V. Fedorov,
The Ohio State University,
United States
Ruben Coronel,
University of Amsterdam, Netherlands

****Correspondence:***
N. Sydney Moïse
nsm2@cornell.edu

Specialty section:
This article was submitted to Cardiac Electrophysiology, a section of the journal Frontiers in Physiology

Received: *14 June 2019*
Accepted: *09 December 2019*
Published: *22 January 2020*

Citation:
Moïse NS, Flanders WH and Pariaut R (2020) Beat-to-Beat Patterning of Sinus Rhythm Reveals Non-linear Rhythm in the Dog Compared to the Human. Front. Physiol. 10:1548. doi: 10.3389/fphys.2019.01548

INTRODUCTION

Arising from the normal sinus node the relationship of each beat to that of the next is dependent on the intrinsic characteristics of the pacing cells (Gao et al., 2010; Nicolini et al., 2012; Monfredi et al., 2013; Yaniv et al., 2014a,b; Valente et al., 2018) and the external forces of the autonomic nervous system (Billman, 2011). Recent studies reveal that the stochastic (unpredictable) (Yaniv et al., 2014b) and chaotic (deterministic) (Nicolini et al., 2012; Yaniv et al., 2014b; Zhang et al., 2015) mechanisms that regulate the beating heart are caused by the complexity of structure (Fedorov et al., 2009; Ambrosi et al., 2012) and function of the sinus node in both the dog and human (Fedorov et al., 2009, 2010, 2012; Glukhov et al., 2013; Csepe et al., 2016; Kalyanasundaram et al., 2019). The sinus node is not simply a cluster of the most rapidly depolarizing cells of the heart. Instead, it is a central core surrounded by a transitional region of specialized cells, fibrous tissue, and atrial myocytes. After spontaneous depolarization a sinus impulse traverses specialized conduction pathways to depolarize the atria (Kalyanasundaram et al., 2019). The rhythm so recognized in the dog of sinus arrhythmia results from dynamic inputs of sympathetic and parasympathetic systems triggered by a combination of central medullary influences, cardiovascular reflexes, and mechanics of respiration (Boineau et al., 1980; Goldberger et al., 1994; Roossien et al., 1997; Brodde et al., 1998; Yasuma and Hayano, 2004; Billman, 2011, 2013; Krohova et al., 2018).

Long-term electrocardiographic (Holter) recordings have permitted the appraisal of rhythm during variation of autonomic input throughout the day. Time, (Malik et al., 1996; Shaffer and Ginsberg, 2017) frequency, (Csepe et al., 2016) and geometric (tachograms, histograms, Poincaré plots) (Esperer et al., 2008; Khandoker et al., 2013; Borracci et al., 2018) domain indices are often used in the assessment of heart rate (sinus) variability (Malik et al., 1996; Billman, 2011; Billman et al., 2015b; Shaffer and Ginsberg, 2017). Furthermore, to understand better the complexity of biophysical oscillators like the sinus node, advanced methods have been developed to analyze heart rate variability such as measures of fractal-like behavior (long-term analysis), detrended fluctuation (Stein et al., 2005) (short-term analysis), disorder (approximate and sample entropy), non-linear dynamical systems (multiscale Poincaré plots) (Henriques et al., 2015; Shaffer and Ginsberg, 2017) and chaotic behavior (Nicolini et al., 2012; Sassi et al., 2015; Zhang et al., 2015; Behar et al., 2018b; Valente et al., 2018).

The dog and human exhibit sinus arrhythmia; however, the variation between beat intervals is greater in the dog (Behar et al., 2018a,b; Kalyanasundaram et al., 2019). The complexity and mechanism for the dramatic variation in the beat intervals so unique to the dog is explained inadequately. The explanation of high parasympathetic tone does not elucidate the underlying mechanism for the variation, nor does it explain the different patterns of sinus arrhythmia commonly identified on the canine electrocardiogram. The integration of G-protein coupled receptors that with activation reduce the heart rate and regulators of G-protein signaling that attenuate the parasympathetic signaling acting through M2 muscarinic and adenosine receptors that control ion channels responsible for the autorhythmic depolarization of the sinus node cells (Mighiu and Heximer, 2012) is key in the dog with normal or abnormal sinus node function.

We, and others, have observed the unique beat patterning of changes in heart rate in the dog using geometric heart rate variability (Moïse et al., 2010; Gladuli et al., 2011; Blake et al., 2018). However, as the heart rhythm is non-stationary and two-dimensional methods do not permit thorough examination, expanded techniques are required to understand the dynamics of heart rate variability. In the observational portion of the study herein, we used new methodologies (three-dimensional tachograms, dynamic Poincaré plots, three-dimensional histographic Poincaré plots) to glean new insights into our understanding of sinus arrhythmia in the dog as it compares to the human. Our observations led to the following hypotheses. We hypothesized that our new methods to examine beat-to-beat dynamics during sinus arrhythmia would reveal a unique non-linear beat patterning in the dog that differed from humans. We hypothesized that particular beat patterning of sinus arrhythmia is associated with different levels of parasympathetic input as indirectly reflected by indices of heart rate variability and through studies in the dog whereby parasympatholytic and parasympathomimetic drugs altered the beat-to-beat patterns. We further hypothesized that the rate at which the beat-to-beat interval in the dog deviates from a linear slowing (bifurcation interval) approximates the intrinsic rate of oscillation of the canine sinus node. Finally, from our data on 130 dogs and 40 humans with clinically normal sinus node function, we propose hypotheses for future studies concerning the mechanistic difference in the patterning of sinus arrhythmia between these two species.

Abbreviations: RMSSD, square root of the mean squared successive interval differences; R–R intervals or beat-to-beat intervals, duration between two QRS complexes (R–R intervals or beat-to-beat intervals) and verified surrogate for P–P intervals for this study; SACP, sinoatrial conduction pathways; SDANN, standard deviation of all 5-min beat interval means; SDNN, Standard deviation of all beat intervals; SDNNIn, mean of all 5-min beat interval standard deviations (index).

MATERIALS AND METHODS

Human Holter Recording Database

The 24-h ambulatory ECG recordings (Holter recordings) from 200 healthy adult humans were accessed from the Telemetric and Holter ECG Warehouse (THEW) maintained by the University of Rochester Medical Center, Rochester, NY, United States. Permission to use these data was approved by the review board after submission of proposal for use via http://www.thew-project.org/. Reasons for performing the Holter recordings were not given for this database. The enrollment criteria for selection from this data set included the following: no overt cardiovascular disease, no history of cardiovascular disease, no systemic hypertension or chronic illnesses, adults > 18-years of age, normal physical examination, no medications that would interfere with sinus rate, normal echocardiographic examination, no pregnancy, no diagnosis of sinus node dysfunction, no sinus

pauses > 2500 ms, < 3.0% or < 4000 ventricular ectopic complexes, < 0.25% atrial ectopic complexes and no abnormal symptoms during Holter recording. It is noted that the only difference in the criteria between the human and dog concerns the duration of sinus pauses. None of the humans had pause durations > 2500 ms. However, this is a common finding in the dog. The goal of these criteria was not to select recordings devoid of any abnormalities, but to select those for which sinus node function was deemed normal and the presence of arrhythmias not of clinical importance.

Canine Holter Recording Database

Holter recordings of dogs were retrieved from the database of the Section of Cardiology Holter Laboratory at the College of Veterinary Medicine, Cornell University, Ithaca, NY, United States (analyzing canine recordings since 1988). A database of > 5000 Holter recordings between 2009 and 2014 was examined to identify only those performed using Forest Medical Holter recorders (Trillium 5000/5900) (Syracuse, NY, United States). Each recording was required to have a minimum of 22 h with 99% artifact free data. All recordings were from clinical patients. Recordings in these dogs were performed to screen for arrhythmias, to determine if suspected arrhythmias identified by either auscultation or during electrocardiographic monitoring were of clinical importance, or to investigate cause of syncope or seizure. Recordings were selected only if sinus node function was determined to be normal. The enrollment criteria for this data set included the following: no overt cardiovascular disease (including myocardial failure or congestive heart failure), no systemic diseases, adult dog > 1-year of age, no physical abnormalities that would affect sinus rate, no medications that would influence sinus rate, no pregnancy, no diagnosis of sinus node dysfunction, no sinus pauses > 5500 ms, no more than 3 pauses > 4000 ms, < 3.0% or < 4000 ventricular ectopic complexes, < 0.25% atrial ectopic complexes and no abnormal clinical signs during Holter recording. Additionally, any Holters that had evidence of vasovagal reflex or Bezold-Jarisch reflex in association with a history of syncope were excluded. Therefore, the goal of these criteria was not to select recordings devoid of any abnormalities (so that aged dogs could be included), but to select those for which sinus node function was deemed normal and the presence of arrhythmias not of clinical importance. Clinical sinus node dysfunction in the dog is characterized by an average heart rate < 60 bpm, minimum heart rate < 30 bpm, time with heart rate < 50 bpm > 350 min, number of pauses > 2 s > 1500, longest sinus pause > 5500 ms and > 3 pauses > 4 s. All 24-h electrocardiographic recordings were performed with the dogs in the home environment.

Owners were given a detailed diary form to complete so that sleep-wake cycles could be documented. The Forest Medical Holter recorders (Trillium® 5000/5900) provide 256 Hz sampling frequency signals (4 ms time resolution) with 8-bit amplitude resolution (5 μV amplitude resolution). Leads were positioned for a 3-lead modified orthogonal X, Y, Z configuration. After downloading the raw data, a technician trained in cardiac rhythm and Holter analysis edited the recordings. All recordings were then over-read by a veterinary cardiologist (NSM) to ensure > 99% accuracy for the identification and classification of P and QRS waves given the importance for heart rate variability analysis (Peltola, 2012). It is emphasized that a veterinary cardiologist with extensive experience in the analysis of canine electrocardiographic recordings reviewed all electrocardiograms to ensure that identified complexes were sinus in origin and not atrial premature complexes. Others unfamiliar with the rhythms of the dog mistakenly identify normal sinus beats as atrial premature complexes because of the prominent sinus arrhythmia. To implement these analyses, software from Forest Medical (Trillium®), was used for the QRS detection, beat annotations, time domain and frequency domain heart rate variability. Additionally, Forest Medical permitted access to the raw data (R–R intervals and annotations) for the development of additional software (WHF).

Sinus Rate Determination

For both the human and canine recordings, the files were examined to ensure that the R–R intervals represented the P–P intervals. Throughout this manuscript the term R–R interval will be used as a surrogate for P–P interval. When referring to the relationship between an R–R interval and the next, the term beat-to-beat interval will be used. Any recordings with atrioventricular conduction block, QRS complexes not preceded by a P wave (e.g., junctional origin) or any other arrhythmias that would be annotated as a normal complex, were not included in the analyses for the assessment of sinus node rate and rhythm. Descriptive data for sinus rate were determined including the average, minimum and maximum rate, time with rate < 50 bpm, time with rate > 120 bpm, number of pauses > 2 s and the longest pause. The density of specific R–R intervals was shown as histograms for each hour and summed for the full 24-h. Additionally, heart rate over time was graphically displayed across time with heart rate tachograms and two- and three-dimensional R–R interval tachograms. On the heart rate tachogram the rolling eight-beat average rate was shown between the minimum and maximum rate for each segment. The two-dimensional tachogram plotted the R–R interval for each hour and over 24-h. Importantly, because each recording contained approximately 100,000 data points, an overlay of points did not permit an appreciation of interval density (number of intervals with same or similar values inadequately identified) and this prompted the development of customized software (WHF).

Heart Rate Variability Analyses

Based on the guidelines for heart rate variability analysis time, (Malik et al., 1996; Shaffer and Ginsberg, 2017) frequency, and geometric domain analyses were performed (Trillium®). Time domain methods included (1) estimate of overall heart rate variability using standard deviation of all beats (SDNN), (2) estimate of long-term components of heart rate variability using standard deviation of all 5-min beat interval means (SDANN) and (3) cycles shorter than 5 min were assessed by the mean of all 5-min beat interval standard deviations (SDNNIn), (4) estimate of short-term components of heart rate variability using the square root of the mean squared successive interval differences

TABLE 1 | Heart rate and heart rate variability comparisons.

(A) Comparisons of populations and 24-h heart rate characteristics boxer versus non-boxer (31 other dog breeds represented). Data shown as median (range) and *p*-value from Wilcoxon Test with Bonferroni correction.

Parameter	Boxer (*n* = 69)	Non-boxer (*n* = 61)	*p*-value
Age	5 (1–12)	9 (1.5–16)	<0.0001
Weight (kg)	27 (16–38)	15 (4–61)	<0.0001
Heart rate (bpm)	81 (66–112)	82 (64–119)	1.0
Minimum heart rate (bpm)	40 (29–59)	41 (32–69)	1.0
Maximum heart rate (bpm)	240 (182–333)	236 (163–301)	1.0
Heart rate < 50 (min)	27 (0–312)	3 (0–432)	1.0
Heart rate > 120 (min)	102 (16–444)	90 (0–726)	1.0
Longest pause (s)	3.2 (2–5.5)	2.6 (0–5.5)	<0.001
Number of pauses > 2 s	157 (2–2737)	40 (0–2082)	<0.001

(B) Comparisons of 24-h heart rate dog versus human heart rate. Data shown as median (range) and *p*-value from Wilcoxon Test with Bonferroni correction.

	Dog (*n* = 130)	Human (*n* = 40)	*p*-value
Heart rate (bpm)	81 (64–119)	74.5 (59–103)	0.005
Minimum heart rate (bpm)	41 (29–69)	51 (34–67)	<0.001
Maximum heart rate (bpm)	236 (163–333)	132 (98–187)	<0.001

(C) Comparisons of 24-h time domain heart rate variability between boxers, non-boxers, and humans. Heart rate variability parameters corrected for heart rate (see text). Data shown are mean and standard deviation. Groups with letter (a–c) in common are not different from each other at $p > 0.05$.

	Boxer (*n* = 69)	Non-boxer (*n* = 61)	Human (*n* = 40)
SDNN (ms)	0.457 (0.056)[a]	0.396 (0.008)[b]	0.176 (0.010)[c]
SDANNIn (ms)	0.376 (0.054)[a]	0.314 (0.079)[b]	0.077 (0.022)[c]
SDANN (ms)	0.249 (0.046)[a]	0.215 (0.068)[b]	0.157 (0.048)[c]
RMSSD (ms)	0.475 (0.075)[a]	0.412 (0.132)[b]	0.045 (0.021)[c]

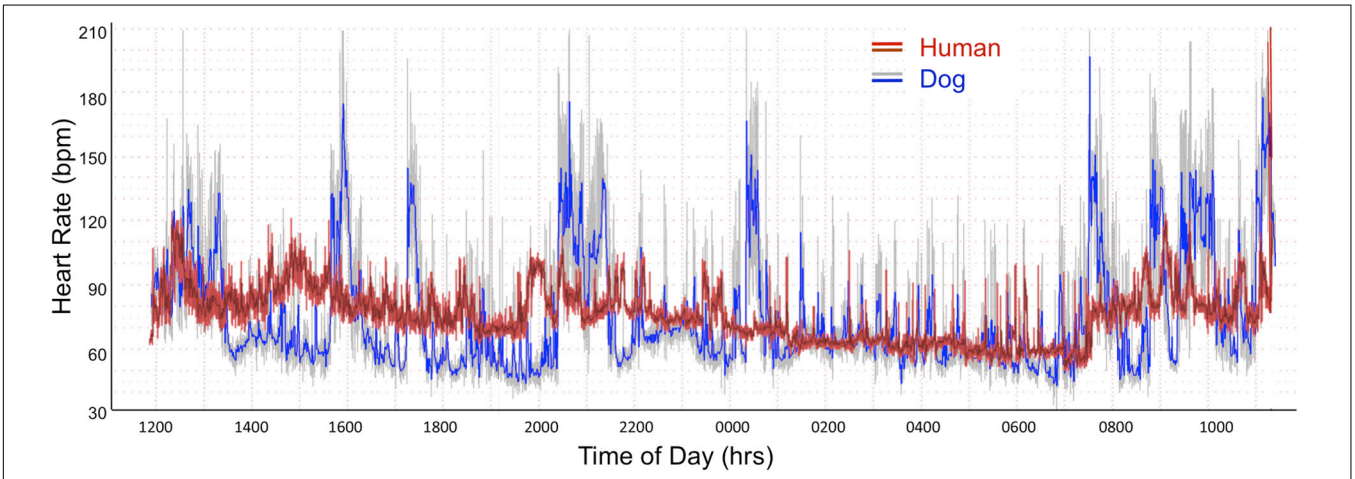

FIGURE 1 | Heart rate tachogram from a human (red/magenta) and dog (gray/blue). The representative patterns exhibited in these two subjects were similar to all. The tachogram shows the heart rate over the course of a 24-h day. The inner magenta (human) and blue (dog) colors indicate the average heart rate as determined by a rolling average of 8 beats. The red (human) and gray (dog) colors indicate the maximum and minimum heart rate during that time. Between the hours of 0100 and 0730 a nocturnal dip (slowing of heart rate) is seen in both the human and dog. In the dog other periods have a similar heart rate slowing associated with sleep as indicated by the diary kept by the owners. The dog has a wider range of heart rates. From the two-dimensional heart rate tachogram the beat-to-beat distribution cannot be determined.

(RMSSD). The frequency domain parameters analyzed were total power and high frequency. For the frequency domain analyses a window of 512 beats with a Hamming filter applied was used. Total power density was determined with frequencies < 0.4 Hz and high frequency was in the range of 0.15–0.4 Hz. During the hour-windows of the frequency analysis, the 512 beat window

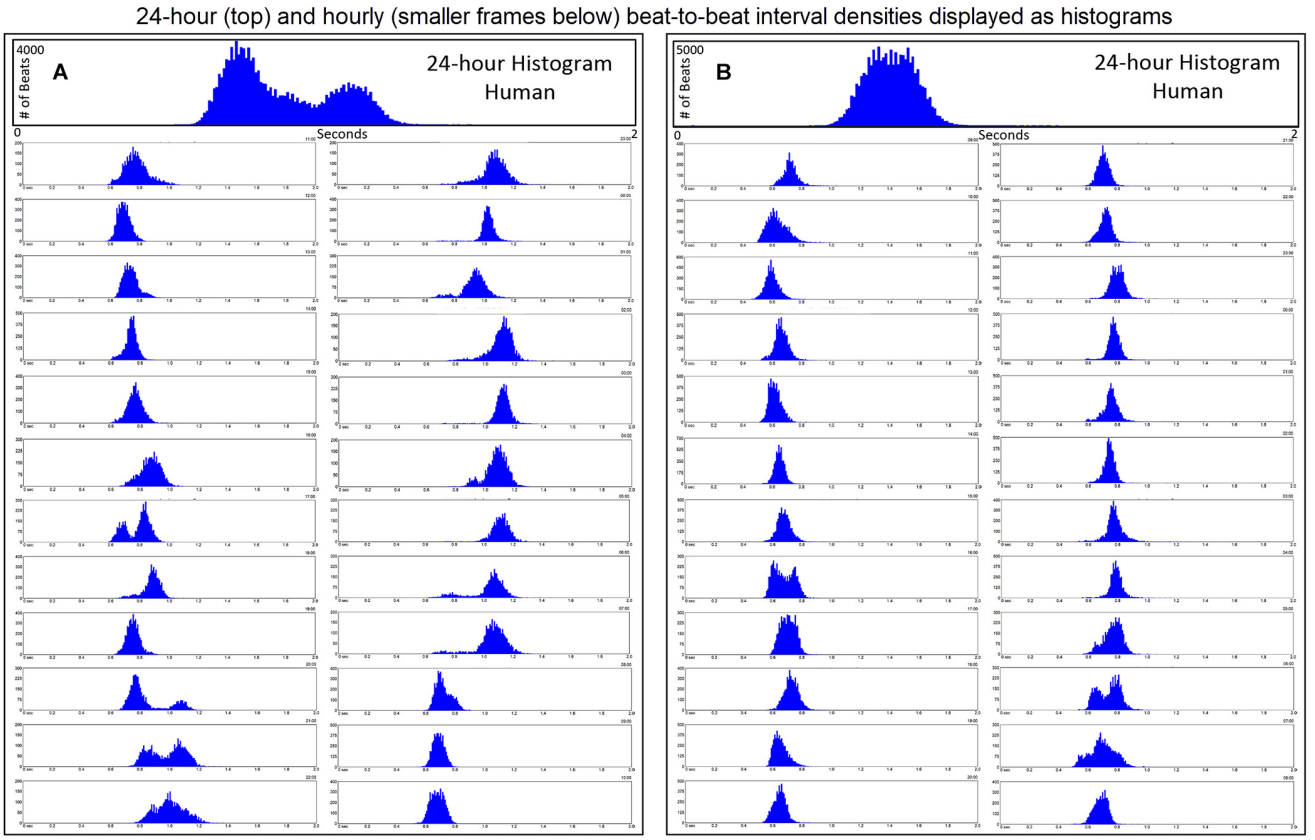

FIGURE 2 | R–R interval histograms from 24-h ECG recordings from two different humans. All of the human R–R interval histograms were either similar to these two individuals or a mixture of these two types of distributions. The top expanded frame is the summation of all R–R intervals over the 24 h. Note the different density distribution of R–R intervals (thus, heart rates) in these two individuals. The individual in frame **(A)** has more time at longer R–R intervals compared to the individual in frame **(B)**. Below the 24-h summary frames the corresponding 1-h histograms for each individual are shown. The summation of these 24 single 1-h histograms form the composite shown at the top for each individual. In general, depending on physiologic needs, the heart rate over a 1-h period primarily has a Gaussian-shaped distribution. Some hours have more than one Gaussian-shaped distribution. This type of distribution exists likely because the heart rate decreases and increases linearly.

was initially selected at the midpoint in the hour so long as the average heart rate approximated that of the average for that hour ± 5 bpm. The window was moved from the midpoint before or after until this heart rate was found. During sleep hours with stable rate and rhythm, time and frequency domain parameters were corrected for heart rate. To correct for the mathematical influence of rate on variability, time domain indices were divided by the average interval of the examined period and frequency domain indices were divided by the square of the average interval in seconds (Sacha and Pluta, 2008; Billman, 2013; Sacha et al., 2013; Billman et al., 2015b).

Beat-to-Beat and Three-Dimensional Analyses

All Holter recordings were examined using geometric domain heart rate variability to identify beat-to-beat patterns. Two-dimensional Poincaré plots were constructed for each hour and 24-h by plotting an R–R interval on the x-axis and the next interval (R–R + 1 interval) on the y-axis. In order to examine the beat-to-beat patterning it was necessary to create the ability to select periods for analysis such as hours of activity or stable sleep hour, while also having the ability to visualize the formation of the Poincaré plots in two and three-dimensions. Therefore, advanced geometric domain analyses including dynamic Poincaré plots, three-dimensional histographic Poincaré and three-dimensional R–R interval tachograms were developed by one of us (WHF) using JavaScript HTML and GLSL[1,2], after integration with the time series R–R intervals. Three-dimensional histographic Poincaré plots were generated by sorting the interval data and logarithmically adding onto a GPU based on different regions. A user interface was developed for a web-based amalgamation to permit interval and time selection. The dynamic Poincaré plots were used to specifically follow the patterns during acceleration and slowing of the heart rate. Examination of these plots, in addition to the R–R interval tachograms, prompted the development

[1]http://wyattflanders.com/poincare/

[2]http://wyattflanders.com/poincareplot/

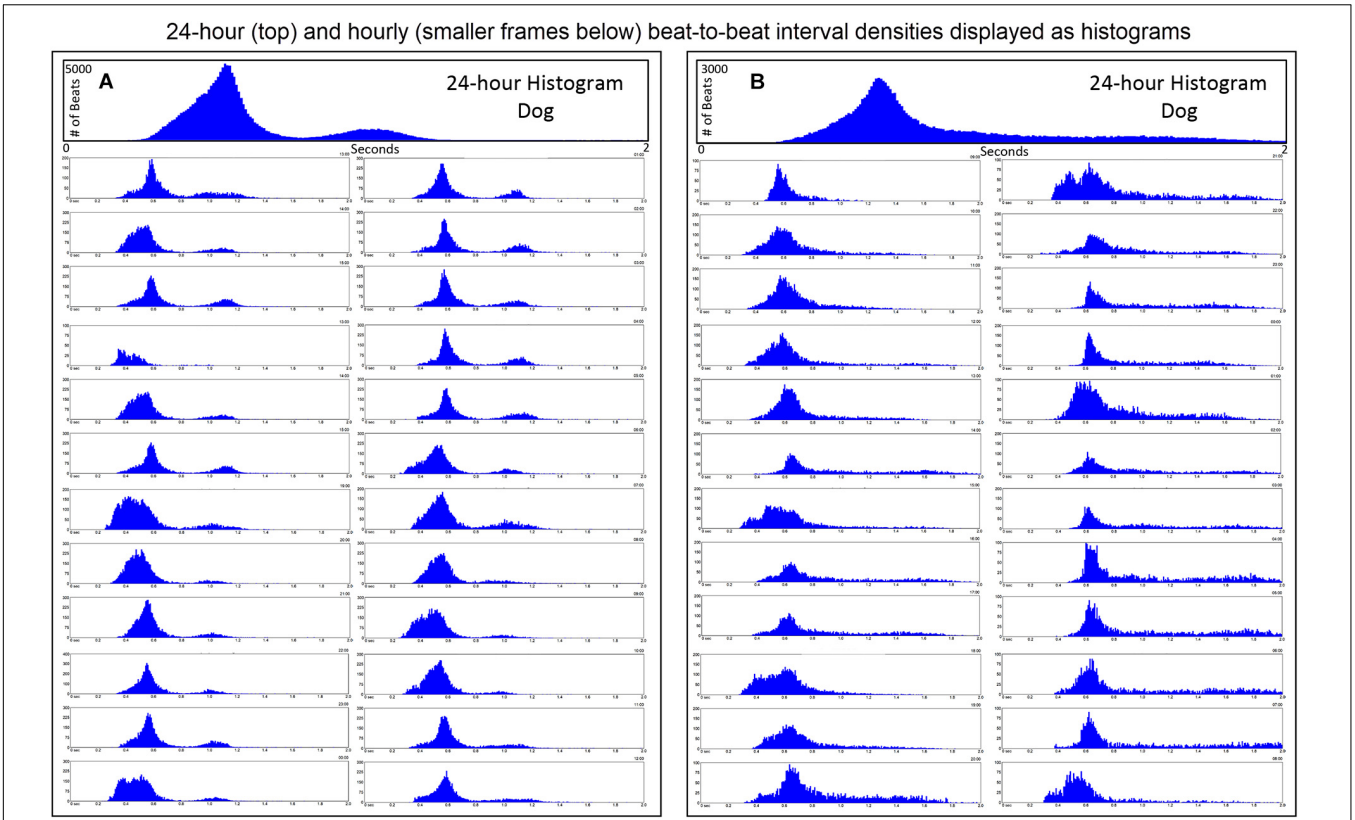

FIGURE 3 | R–R interval histograms from 24-h electrocardiographic recordings from two different dogs. These two dogs represented the basic patterns seen in all dogs. The top expanded frame is the summation of all R–R intervals over the 24-h. Note the different density distribution of R–R intervals (thus, heart rates) in these two examples. Below the 24-h summary frames, the corresponding single 1-h histograms for each dog are shown. The summation of these 24 single 1-h histograms form the composite shown at the top for each dog. Note the more complicated beat distribution of the dog when compared to the human. Dog **(A)** tends to have different distributions within a given hour. Shorter R–R intervals (more leftward distribution) tend to merge with the dominant distribution centered at approximately 550 ms (109 bpm) with a paucity of beats centered at approximately 800 ms (75 bpm). A small number of beats (but not time spent at these intervals) with the distribution centered at approximately 1050 ms (57 bpm) is seen. Dog **(B)** has a dominant distribution of R–R intervals centered at 600 ms (100 bpm) with a tail of more diffusely distributed long R–R intervals. Dog **(A)** was a boxer and dog **(B)** a Doberman pincher.

of pattern classification that then led to further analyses and comparisons.

(1) Regions with a paucity (also coined as a 'zone of avoidance') (Moïse et al., 2010) of R–R intervals seen on the tachograms and beat-to-beat intervals seen on the Poincaré plots.
(2) Regions with clustered beat-to-beat intervals (defined as discontinuous and isolated intervals on the Poincaré plots coupled with dense banding separated by a paucity of R–R intervals on the tachogram and bimodal distribution on histograms) (13 boxers/12 non-boxers).
(3) Regions with branched beat-to-beat intervals (defined as continuous intervals on the Poincaré plots coupled with broad spreading of R–R intervals on the tachogram and rightward-skewed distribution on histograms) (13 boxers/12 non-boxers).
(4) R–R interval bifurcation (this interval determined as the average of the three shortest intervals during a stable sleep hour in 25 boxers and 25 non-boxers).

Parasympatholytic and Parasympathomimetic Drug Effects

The findings of beat patterning during spontaneous sinus rhythm in the dog strongly suggested the influence of the parasympathetic nervous system. After approval from the Institutional Animal Care and Use Committee, 8 beagles had 24-h electrocardiographic recordings to assess the geometric beat-to-beat patterning as influenced by parasympatholytic and parasympathomimetic agents. Atropine (0.04 mg/kg intravenously) and hydromorphone (0.2 mg/kg intravenously) were administered on separate days after a baseline recording was obtained. Regions of the recordings associated with these treatments were analyzed for beat-to-beat patterns. The corresponding time of the baseline recording served as the control period.

Statistical Analysis

The following comparisons were made (1) 24-h data for boxer dog breed, non-boxer breeds and human (2) hour for all dogs with bimodal versus singular interval density, and (3) stable

TABLE 2 | Comparisons of bimodal versus singular histogram distributions within dog and clustered versus branched beat-to-beat interval patterns between dogs.

(A) Within dog (n = 128) (paired data) comparison of an hour with a large paucity of beats resulting in a bimodal distribution and an hour with a small paucity of beats characterized as a single distribution. Heart rate variability parameters corrected for heart rate (see text). Data shown as median (range) and p-value from Wilcoxon Signed Rank Test with Bonferroni correction.

Parameter	Bimodal	Singular	p-value
Average heart rate (bpm)	68 (50–130)	110 (75–163)	<0.001
Beat-to-beat interval (ms)	882 (462–1200)	546 (368–800)	<0.001
Minimum heart rate (bpm)	48 (32–139)	69 (34–108)	<0.001
Maximum heart rate (bpm)	147 (80–236)	199 (123–313)	<0.001
SDNN (ms)	0.38 (0.22–0.58)	0.27 (0.07–1.35)	<0.001
SDANNIn (ms)	0.34 (0.15–0.49)	0.20 (0.05–0.55)	<0.001
SDANN (ms)	0.11 (0.03–0.50)	0.16 (0.03–0.59)	0.032
RMSSD (ms)	0.47 (0.18–0.69)	0.24 (0.04–0.57)	<0.001
Frequency domain total power (ms^2)	24486 (1379–66913)	4493 (335–31063)	<0.001
Frequency domain HRV-HF (ms^2)	19311 (33–59924)	312 (14–10770)	<0.001

(B) Comparison of beat patterning (clustered versus branched) during a single sleep hour in 50 dogs (13/12 boxers/non-boxers each group). Heart rate variability parameters corrected for rate/interval (see text). Data shown as median (range) and p-value from Wilcoxon Test with Bonferroni correction.

	Clustered (n = 25)	Branched (n = 25)	p-value
Average heart rate (bpm)	71 (57–93)	54 (46–92)	<0.001
Beat-to-beat interval (ms)	845 (645–1053)	1111 (652–1304)	<0.001
Minimum heart rate (bpm)	55 (42–68)	41 (34–71)	<0.001
Maximum heart rate (bpm)	144 (103–196)	137 (112–174)	0.99
Number of pauses	1 (0–16)	24 (0–374)	0.006
SDNN (ms)	0.349 (0.156–0.468)	0.409 (0.273–0.467)	0.008
SDANNIn (ms)	0.312 (0.128–0.424)	0.369 (0.245–0.426)	0.02
SDANN (ms)	0.099 (0.049–0.205)	0.118 (0.038–0.226)	0.36
RMSSD (ms)	0.477 (0.167–0.619)	0.481 (0.373–0.686)	0.99
Frequency domain total power (ms^2)	19036 (6352–59061)	33541 (11492–86423)	<0.001
Frequency domain HRV-HF (ms^2)	15856 (4107–55894)	19741 (5205–44501)	0.2

sleep hour with clustered versus branched interval distribution in the dogs. Additionally, the bifurcation interval in the dog was examined relative to age, average heart rate and time domain indices of heart rate variability SDNN (the latter after correction for heart rate). Distribution of all continuous variables was assessed for normality. Difference between groups for variables with normal distribution were analyzed using a t-test and data is presented as mean and standard deviation. Differences between those variables showing a non-normal distribution were analyzed with non-parametric methods (Wilcoxon Rank Sum test, also called Mann–Whitney-Test) and data is presented as median and range. Adjustments for p-values controlling for multiple comparisons was done using Bonferroni correction. The relationship between variables of heart rate and heart rate variability with age for each group (boxers, non-boxers, and humans) was examined by a regression analysis with slopes and standard error reported. Differences in the time domain parameters between these groups was tested with a one-way ANOVA followed with a *post hoc* multiple comparisons with Tukey correction. Differences between groups for categorical variables were tested using Fisher's exact test. Differences for paired data (singular/bimodal distribution) within a category (boxer, non-boxer) were achieved with paired data non-parametric Wilcoxon Signed Rank test. Correlation between continuous variables was explored by using Pearson correlation for parametric data and Spearman for non-parametric. To determine relationship bivariate analysis was performed for specific variables. All analyses were performed in JMP (v.12.0.1 and v. 14.0.0, SAS Institute, Cary, NC, United States).

RESULTS

Human and Canine Holter Recordings

After review of recordings in THEW, Holter recordings from 40 humans were studied that met the criteria. It is noted that none of the reviewed recordings in the bank had pauses > 2.5 s. Equal numbers of males and females were included with a median age of 41.7 years (range 18–80 years). Holter recordings from 130 dogs were studied. Canine recordings included 69 boxers (41 females/28 males) and 61 (32 females/29 males) non-boxers (no difference in sex distribution; p-value = 0.32). Of the 61 non-boxers, 31 different breeds were represented. Those with more than one dog per breed included eight mixed breed, six Shi Tzu, four Labrador retrievers, four miniature schnauzers, three great Danes, three Doberman pinschers, and two dachshunds. Boxers were overrepresented

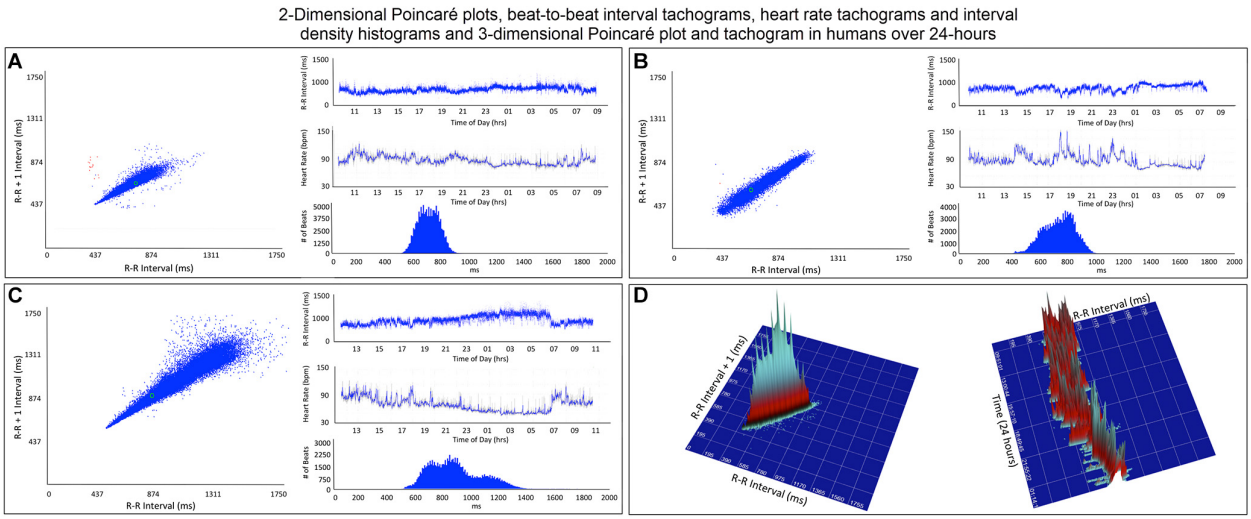

FIGURE 4 | This figure illustrates in four humans the beat-to-beat relationship shown by two-dimensional Poincaré plots and the beat distribution identified by R–R interval tachograms, heart rate tachograms and R–R interval histograms. The recording in frame **(A)** shows an individual with the fastest average heart rate (85 bpm) (red dots indicate low numbers of ventricular premature complexes) and the recording in frame **(C)** shows an individual with the slowest average heart rate (67 bpm). These three recordings **(A–C)** illustrate that although the density of R–R intervals (heart beat distribution) varies from fast to slow depending on physiologic needs, the heart rate in humans tends to change linearly along the line of identity. In some, the spread of intervals increases at longer intervals. Two-dimensional Poincaré plots and R–R interval tachograms do not provide an appreciation of the number of beats at a given interval. In frame **(D)**, three-dimensional plots of the R–R intervals from a 24-h recording from a normal human are shown as a histographic Poincaré plot (left) and tachogram (right). These type of plots provide an appreciation of the beat density for a given R–R interval on a beat-to-beat basis (histographic Poincaré plot) or over the course of time (three-dimensional interval tachogram). The amount of time examined can be selected(http://wyattflanders.com/poincare/ and http://wyattflanders.com/poincareplot/).

because of the high number of screenings performed for breeding animals; therefore, boxers and non-boxers were compared. The age and weight data are shown in **Table 1A**. The boxers were significantly younger and larger than the non-boxers.

Hour Sinus Rate

Heart Rate Human Versus Dog

As shown in **Table 1A** the only significant differences between boxers and non-boxers concerning heart rate were the number of sinus pauses > 2 s and the duration of the longest pause with boxers having more sinus pauses and the longest pause of greater duration. The average, minimum and maximum heart rates of the dogs were compared to humans (**Table 1B**). All variables characterizing sinus heart rate were significantly different between dogs and humans. Although the average heart rate in the humans was slower, the spread of heart rate was greater in the dog with lower minimum and higher maximum heart rate. **Figure 1** illustrates these characteristics of the sinus heart rate in the human and dog.

Hour Heart Rate Variability

Heart Rate Variability Boxer, Non-boxer, and Human

Table 1C shows the difference between groups of 24-h time domain heart rate corrected indices. All groups were different from each other; however, the values in humans were markedly lower than in all dogs.

Heart Rate Variability and Age

Supplementary Table 1 shows the relationship of age to heart rate and each of the 24-h time domain (heart rate corrected) indices of heart rate variability. Higher heart rate was associated with advancing age in the non-boxers. However, this group of dogs had a wider age range with numerous geriatric animals when compared to the boxers. In this population of humans relationship to age was not identified. However, time domain parameters were significantly related to age in humans. No relationship of age to time domain parameters were found in the dogs.

Histogram Beat-Interval Distribution

R–R Interval Histograms Human Versus Dog

Further examination of heart rate/R–R interval distribution using histogram plots of R–R intervals showed differences between humans and dogs. **Figure 2** shows representative distributions in two humans that were similar to all recordings. The 24-h summation is a composite of R–R intervals shown for each hour. A shifting left or right of the interval densities approximates a Gaussian distribution. In contrast, **Figure 3** shows examples of two dogs with typical histogram distributions of R–R intervals. The 24-h summed distributions are not from shifts of singular shifting Gaussian patterns, but instead are from bimodal or trimodal distributions and skewed R–R intervals to the right/longer intervals. These patterns were seen across all breeds of dogs. Singular Gaussian patterns were seen in dogs during hours with documented activity or the hour during application or removal of the Holter recorder.

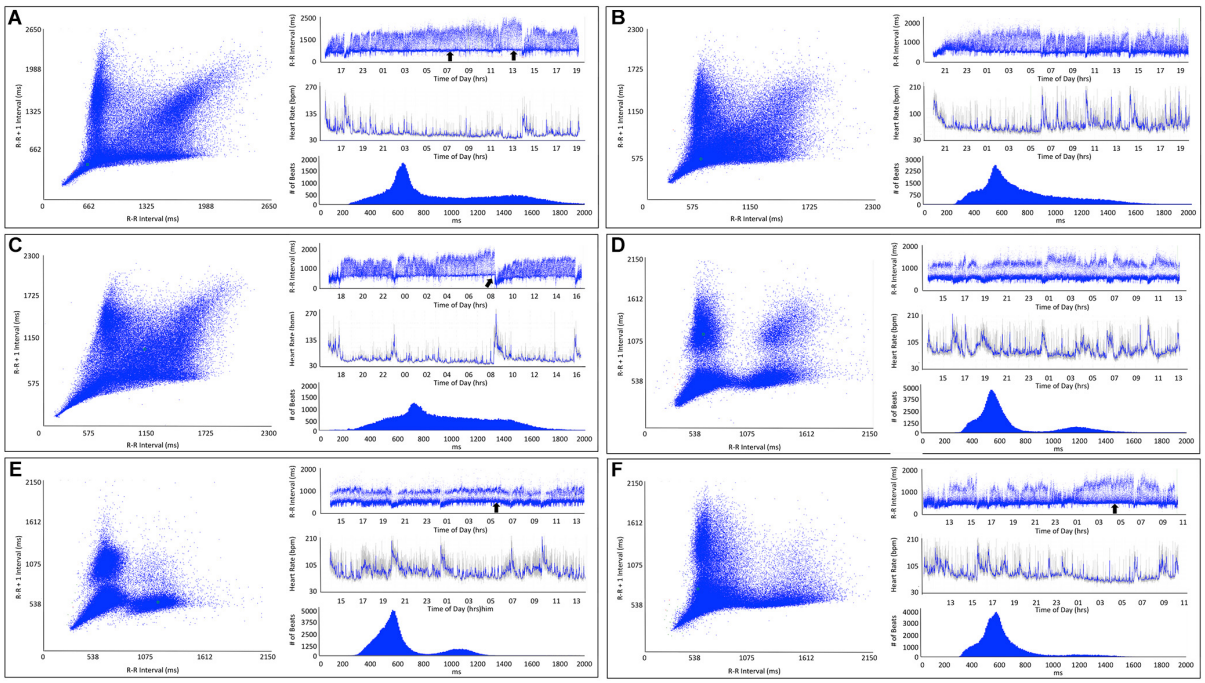

FIGURE 5 | This figure illustrates in six dogs the beat-to-beat relationship shown by two-dimensional Poincaré plots and beat distribution identified by R–R interval tachograms, heart rate tachograms and R–R interval histograms. All dogs had these types of the distributions. It is important to realize that on a two-dimensional plot each of the R–R intervals, when they are the same, they overlay each other such that the beat density (actual number of beats at a particular interval) are only partially appreciated. The geometric images of heart rate variability illustrate the difference in the distribution of heart beats not only between dogs and humans (compare to **Figure 4**), but also amongst dogs. When the dog is compared to the human, the beat distribution characteristics include: (1) Slowing of the heart rate that is non-linear after a bifurcation, such that heart rate changes are not restricted to the line of identity (diagonal line from lower left corner to upper right corner). (2) Wider distribution of R–R intervals with a varying degree of a paucity of beats ('zone of avoidance') identified in the Poincaré plots, R–R interval tachograms and R–R interval histograms. The 'zone of avoidance' cannot be appreciated from the heart rate tachogram. The similarities among the dogs in the Poincaré plots include a 'stalk' showing faster beat-to-beat intervals likely because of higher sympathetic modulation and lower parasympathetic modulation. The beat-to-beat distribution spreads/bifurcates when the R–R interval extends beyond approximately 600 ms. As illustrated in frames (**A–F)**, dogs differed in the Poincaré plots by the degree of beat-to-beat 'branching' versus the amount of beat-to-beat 'clustering,' the paucity of beat-to-beat intervals and the appearance of long–long intervals resulting in a 'cloud.' When the branches are parallel to the axes this indicates that as the long interval increases the short interval stays more constant (frame **A**). When the arm deviates up on the x-axis or right on the Y axis this indicates that the short intervals are increasing as the long intervals increase (frame **C**). Frames (**A–C)** show faster beat-to-beat relationships that with slowing results in branching that spreads as wide bands with the long–short/short–long relationship of sinus arrhythmia. Additionally, a region of long–long R–R intervals shown as a 'cloud' extends with an upper border along the line of identity. Of these three dogs (**A–C**) the one in frame **(A)** has the most obvious region with a paucity of R–R intervals. Frames (**D–F)** show a more distinct zone of avoidance. Additionally, **(D,E)** have beat clustering evident not only in the Poincaré plots but also throughout the R–R interval tachograms. Also evident on the R–R interval tachogram is the appearance of a thick line (broad black arrows in frames **A,E,F**). The R–R intervals appear to protrude downward with sharp spikes from this relatively constant 'line' that at approximately 600 ms. The R–R interval of this line approximated the bifurcation interval (see **Table 3**) seen on the Poincaré plots. Note in frame **(C)** that the dog suddenly has an increase in heart rate (decrease in R–R interval) indicated with the broad angled black arrow. This was due to sudden excitement noted on the diary. For the rest of the Holter the paucity of beats (zone of avoidance) is less apparent during a period of changing heart rate. See text and additional figures for explanation.

The more common bimodal distributions corresponded to time-periods with the most distinct zone of avoidance and during the sleep hours.

Singular Versus Bimodal Histographic Distribution in the Dog

Time domain and frequency domain heart rate variability were used to determine if the bimodal versus the singular interval distribution was associated with greater parasympathetic modulation as qualitatively judged by heart rate variability for each of 128 dogs. To accomplish this, hours were selected with the greatest (bimodal) and least (singular) paucity of R–R intervals. Singular distributions were during the Holter application. Hours with the bimodal distribution had greater heart rate variability as judged by time domain parameters and greater power density overall. The latter was the result of markedly higher high frequency power (**Table 2A**). During a given hour or 24-h, an additional beat distribution at short R–R intervals associated with activity could be identified making a trimodal distribution. Histographic representation of these shorter R–R intervals often overlapped with the largest density that was characterized by a distribution that centered around 600 ms (**Figure 3**). The longer R–R interval distribution was either a Gaussian-shape distribution or flat with greater range of intervals. These two types of distributions were further evaluated (see below).

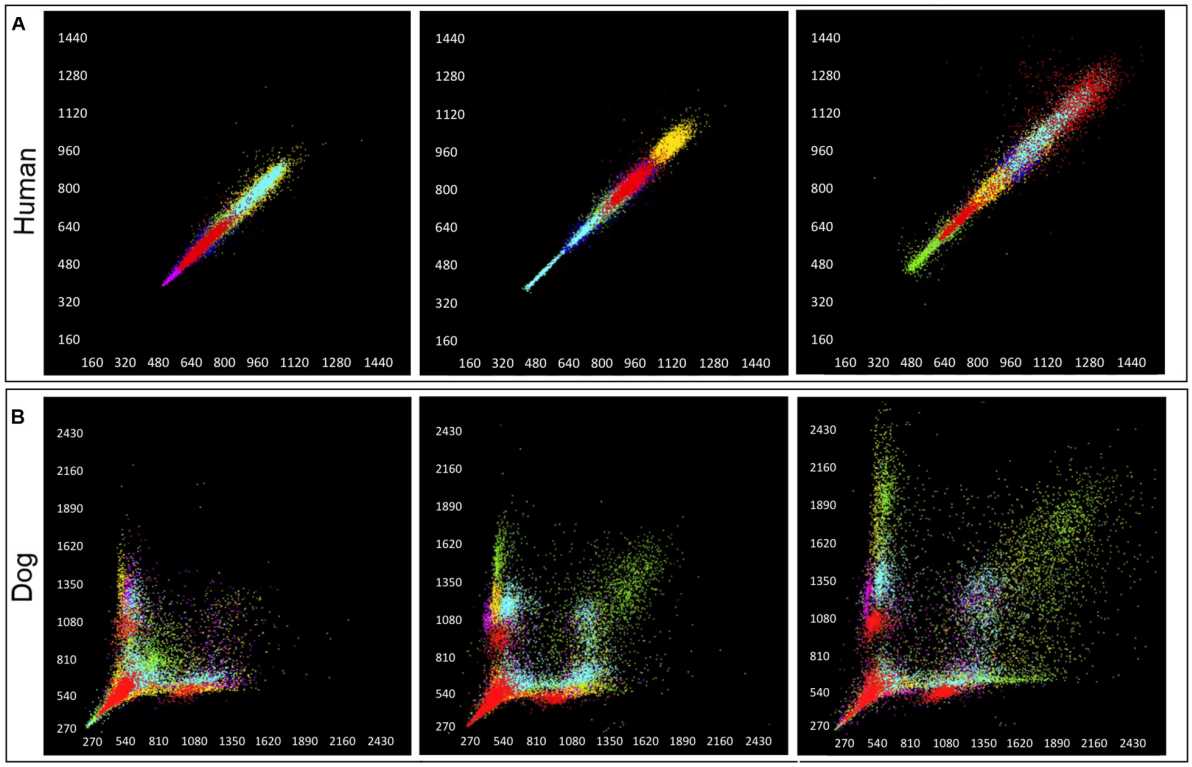

FIGURE 6 | (**Supplementary Videos 1, 2**) Examination that is limited to still frames of two-dimensional geometric heart rate variability restricts understanding of the beat-to-beat dynamics. Here, frames captured from dynamic/animated two-dimensional Poincaré plots of five humans **(A)** and five dogs **(B)** provide the ability to examine heart rate dynamics in the human and dog.http://wyattflanders.com/poincare/ Each individual dog or human is represented by a different color. The R–R interval (X axis) and R–R + 1 interval (Y-axis) (intervals are in 'ms') are plotted with the ability to change the number of intervals represented (for clarity, labeling for these axes is omitted). The associated videos (**Supplementary Videos 1, 2**) for these frames illustrate the difference between the dog and human concerning the beat-to-beat increasing and decreasing of heart rate and associated beat-to-beat changes. In the human, these changes occur primarily along the line of identity (diagonal line from lower left corner to upper right corner). In the dog as the beat-to-beat intervals increase they do so along the line of identity until approximately 600 ms when a bifurcation develops resulting in two 'branches' or 'clusters' along the X and Y axes. In the dog, a paucity of beats is noted for certain beat-to-beat intervals (zone of avoidance). The latter will not be evident if an excessive number of beats are shown. Additionally, some dogs develop a 'cloud' of long–long R–R intervals with an upper border along the line of identity. These videos can also have lines added and the speed adjusted so that the exact beat-to-beat interval relationships are seen (see **Figure 8** and **Supplementary Videos 3–6**). **Supplementary Videos 1, 2** correspond with this figure.

R–R Interval Tachograms Human Versus Dog

R–R interval tachograms showed consistent differences between humans and dogs (**Figures 4**, **5**). The patterns shown in these figures represent those that were seen for all subjects. Each dot represents an R–R interval. Tachograms in humans had the appearance of a narrow band that would move up and down as the intervals lengthened and shortened (**Figure 4**). In contrast, the patterns in dogs were more complex. Three general features characterized the tachograms of the dogs (**Figure 5**):

(1) Broader spread of longer intervals. This region of longer intervals varied in its spread between dogs or within dog depending on the wake-sleep cycle. The greatest spread occurred during documented sleep.
(2) Regions of lower beat density (infrequent R–R intervals) that looked like a 'white-band' separating shorter and longer R–R intervals. Often this low beat density band was consistent over the day (this region identified as the zone of avoidance). Two general characteristics were noted: (1) low beat density separated by two distinct wide bands of R–R intervals and (2) region of lower beat density with more diffuse band at longer R–R intervals. During times of heart rate change, these banding characteristics were less distinct.
(3) A denser region of shorter R–R intervals that appeared as a 'dark-band' that also was consistent over the day. This band tended to have the appearance of a 'line' demarcating the shortest intervals. Shorter intervals did interrupt this 'line' and correlated with abrupt increases in heart rate (shorter intervals), and often associated with artifact indicating body movement (exercise/excitement).

Beat-to-Beat Analyses: Poincaré Plots

Two-Dimensional Poincaré Plots

To gain a better understanding of the unique patterns identified in the dog when compared to the human, beat-to-beat analyses were performed. As shown in **Figures 4**, **5**, the two-dimensional

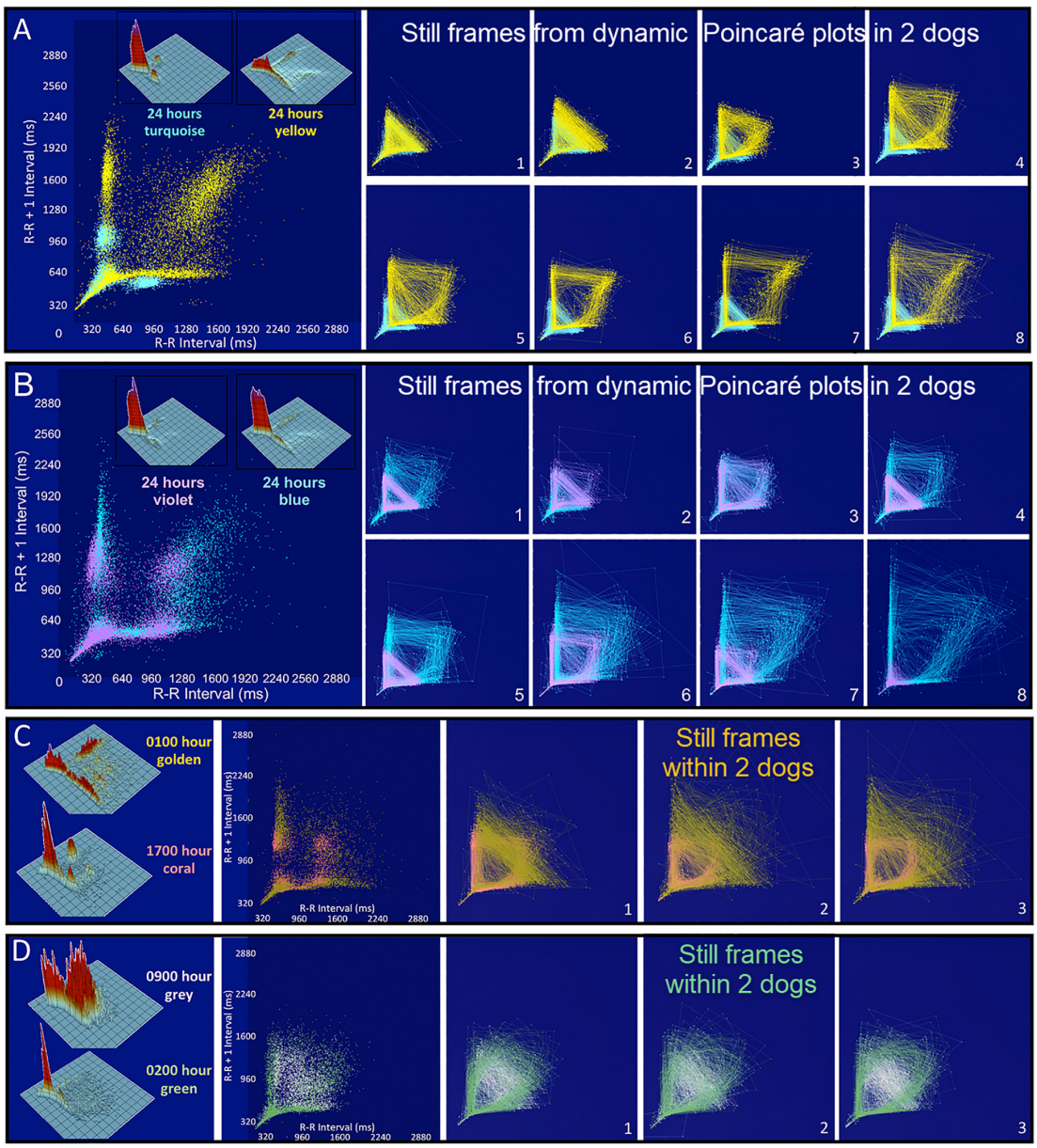

FIGURE 7 | (**Supplementary Videos 3–6**) Still frames from dynamic Poincaré plots (http://wyattflanders.com/poincareplot/) of six different dogs demonstrate the varied R–R interval patterns between dogs (frames **A,B**) and within dogs (frames **C,D**). In frames **(A,B)** large Poincaré plots without connecting lines contain 10,000 beat intervals and above this plot, the corresponding three-dimensional histographic Poincaré plots of the entire 24-h are shown. Below the three-dimensional histographic plots, a color code is stated for that dog that corresponds with the animated Poincaré plot in this figure and in the accompanying **Supplementary Videos**. To the right of this panel, from the dynamic two-dimensional Poincaré plots still frames of 1000 intervals with lines, the beat-to-beat relationships are presented. The still frames were captured at different time points during 24-h electrocardiographic recordings (Frames **1–8**). In frame **(A)**, the dog in aqua (boxer) has a clustered pattern with no long–long intervals while the dog in yellow (small mixed-breed) has a long-branched pattern with a long–long R–R interval cloud. Compare the beat density of the dog in yellow (Frame **A**) to the dog in blue (Frame **B**). In frame **(B)** a boxer with a clustered pattern (color violet) also has the central cloud of long–long intervals. The Doberman pinscher in blue shows a large variation in long–long intervals. Frames **(C,D)** illustrate the varied patterns within dog. The hour of the day and color representing that hour for the dynamic Poincaré plots are indicated to the right of the three-dimensional histographic Poincaré plot for each dog. The pattern of sinus arrhythmia can change over time with varying autonomic input. This also shows that if the entire 24 h is considered at one time the true dynamics of the interval relationships can be masked. The dog in frame **(C)** (boxer) during the sleep hour 0100 (golden) has a 'branched' pattern with slower rates; however, a more clustered pattern with faster rate is identified during an hour of wakefulness (coral). The dog in frame **(C)** (Wheaton Terrier) during the 0900 h (gray) was noted to have wide swings in heart rate associated with different activities as documented in the diary. This resulted in many transitions of rate with a more dense pattern; however, during the sleep hour (green) a different pattern was identified with the zone of avoidance evident. **Supplementary Videos 3–6** provided with this figure.

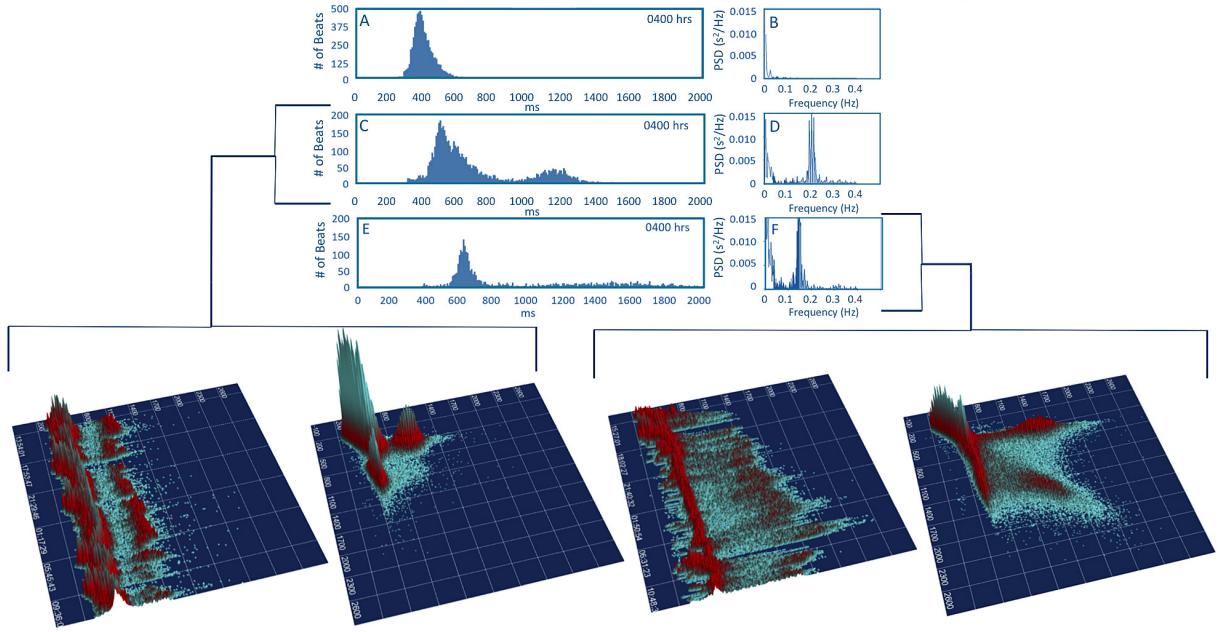

FIGURE 8 | To assist in understanding some of the geometric patterns identified in the dog analyses were performed after visual inspection to categorize major beat-to-beat patterns. Initially, the hourly R–R interval histograms were inspected to identify those with a single Gaussian-shaped distributions and those with two or more distributions apparent that also had a region with a paucity of beats (Frames **A,C,E**). Statistics regarding time domain and frequency domain characteristics are provided in **Table 2**. In this figure, examples of the two-dimensional histogram and corresponding power spectrum/frequency domain profile of heart rate variability (Frames **B,D,F**) are shown. The three-dimensional R–R interval tachograms and histographic Poincaré plots for the two different dogs shown in frames **(C,D)** and frames **(E,F)** are bracketed below. Each of these dogs was a boxer.

Poincaré plots of the human and dog are distinctly different. In the human, as the heart rate changes with shorter to longer intervals the beat-to-beat changes occur along the line of identity of the Poincaré plot. In **Figure 4D** a three-dimensional histographic Poincaré plot more clearly illustrates the beat-to-beat distribution along the line of identity and the three-dimensional tachogram shows the change in beat intervals throughout the day. Importantly, is the notation that these graphs show number intervals; however, this does not give a representation of the amount of time and at shorter versus longer intervals. That is, the lower density of the longer intervals should not be interpreted as minimal or infrequent because the 'time spent' may be greater. In contrast, two-dimensional Poincaré plots in the dog (**Figure 5**) illustrate that beat intervals occur along the line of identity until a point at which a bifurcation occurs resulting in a wide spread corresponding to long–short and short–long intervals. In the dog, two-dimensional Poincaré plots could be described as branched or clustered (see section "Materials and Methods") with a paucity of interval beats of varying degree. Because these plots were a summation of the entire 24-h, it was necessary to examine shorter times to understand the formation of these patterns.

Dynamic Poincaré Plots

Dynamic (animated) Poincaré plots were developed to examine both human and canine data sets (**Figure 6** and **Supplementary Videos 1, 2**). This new methodology illustrated the difference in the increasing and decreasing of heart rate on a beat-to-beat basis between the human and dog. Humans consistently changed rate in a linear fashion, but dogs had a visual bifurcation at a relatively stable point on the graph. However, the spread of beat intervals after the bifurcation point differed amongst the dogs (**Figures 7**, **8**). Examination of individual hours with lines connecting each successive beat interval provided the ability to see the sequence of heartbeat intervals (**Figure 9**). From these data it was apparent that dogs had different patterns after the bifurcation from the consistent shorter intervals (**Figures 7A,B** and **Supplementary Videos 3, 4**). Moreover, an individual dog could have different patterns throughout the day (**Figure 7C** and **Supplementary Videos 5, 6**). The dynamic Poincaré plots with lines illustrating sequence clearly showed the paucity of beats/zone of avoidance for both clustered and branched R–R interval distributions.

Three-Dimensional Tachograms and Histographic Poincaré Plots

Three-dimensional plots revealed a truer representation of beat distributions (**Figures 4**, **8**) permitting selection of 25 clustered and 25 branched R–R interval patterns (**Figure 8**). Time domain and frequency domain analyses of heart rate variability revealed slower heart rates and mixed evidence of greater parasympathetic modulation with beat distribution characterized as branched

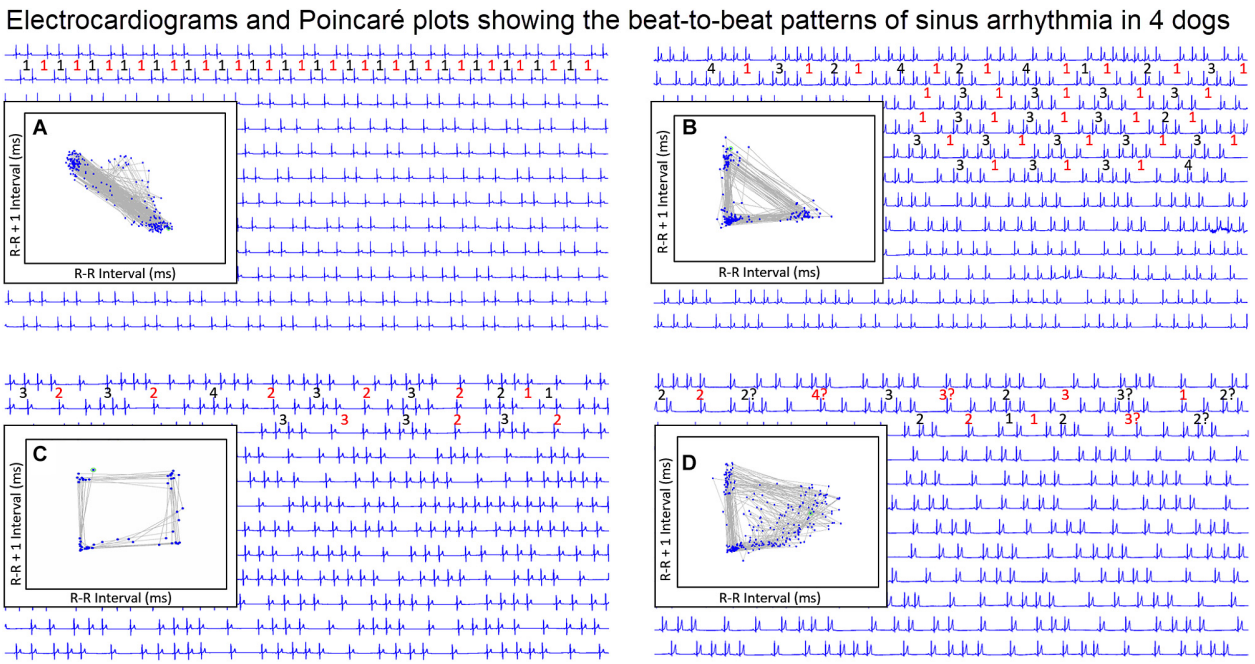

FIGURE 9 | During stable sleep hours, focused intervals were identified on the electrocardiogram and compared to the Poincaré plots. This figure illustrates four common patterns. Each line is 30 s. The inset is the Poincaré plot of the ECG frame shown (for clarity the specific R–R interval in milliseconds is omitted). Frame **(A)** shows the Poincaré plot when the sinus arrhythmia has primarily a ratio of one-short R–R interval to one-long R–R interval. Because there are no consecutive short-short R–R intervals, no clusters of intervals are seen in the lower left region of the Poincaré plot. Frame **(B)** shows the Poincaré plot when the primary ratio is one-long R–R interval to two to four-short R–R intervals. The short-short intervals are in the lower left region and the single long interval between the clusters of short intervals results in a triangular shape (long–short interval followed by short intervals followed by short–long interval). Frame **(C)** shows the pattern when the sinus arrhythmia has primarily two-long R–R intervals with clusters of short intervals. The long–long intervals result in a cloud in the upper right region beginning at the line of identity. The resulting shape is that of a polygon. Frame **(D)** illustrates the shape of the Poincaré plot with more variability in the R–R intervals creating a long–long cloud of intervals. From frame **(D)** the R–R intervals before the speeding of the rate are more variable than the long R–R interval that follows the short sequence. That is, with sinus arrhythmia the long interval after the faster rate is more consistent then the long interval before the faster rate. It is important to note that these examples were taken during a time when each of the dogs was displaying a sinus arrhythmia with presumed high parasympathetic tone and not interrupted by marked increases in sympathetic tone. Without a sympathetic surge note that none of the short-short intervals goes below a specific point. Although for clarity the scale is omitted, this was approximately 600 ms. This corresponds to the limit of the R–R interval seen on the R–R interval tachogram (see **Figure 7** and **Table 3**). For each frame, the numbers in red are long R–R intervals and numbers in black are short R–R intervals. If a '?' follows the number, this indicates that some uncertainty exists concerning the exact number of intervals defined as long or short (e.g., R–R interval duration is medium).

versus clustered (**Figure 8** and **Table 2B**). Beats clustered more with a sequence of short–long intervals. That is, the last beat sequence of short–long intervals was more consistent than that of a long–short interval. When examining these plots it is important to keep in mind that the interval density mathematically will show a greater density for the short intervals rather than the longer intervals, but this does not reflect the 'time' the heart spent at shorter or longer rates.

Electrocardiographic Relationship to Beat-to-Beat Patterns

Beat-to-Beat Pattern With Slowing Heart Rate

To understand the beat patterns identified in the dog the dynamic Poincaré plots were examined in conjunction with visualization of the electrocardiogram. **Figure 9** illustrates this examination of four dogs during a stable sleep hour revealing the differing patterns of sinus arrhythmia and corresponding Poincaré plots. Note that during these stable sleep times with likely low sympathetic input, no short-short R–R intervals along the line of identity are present (compare with **Figures 7**, **8**). However, the bifurcation point is consistent and is identified in the dog when the heart rate slows after a sympathetic stimulation associated with excitement (**Figure 10** and **Supplementary Video 7**). The human heart rate slows linearly throughout the full range of beat intervals; however, although the dog heart slows initially along the line of identity when the heart rate slows to a particular interval, a bifurcation develops. This interval was coined the 'bifurcation interval.' An additional finding from the comparison of the Poincaré plots with the electrocardiogram is the 'cloud' of longer intervals. The cloud associated with long–long (**Figure 5D**) intervals in many dogs formed a mass effect of intervals widely spread around the line of identity.

Bifurcation Interval/Zone

It was noted that amongst dogs the bifurcation interval was visually within a narrow range of beat-to-beat intervals. Moreover, this bifurcation interval or zone corresponded

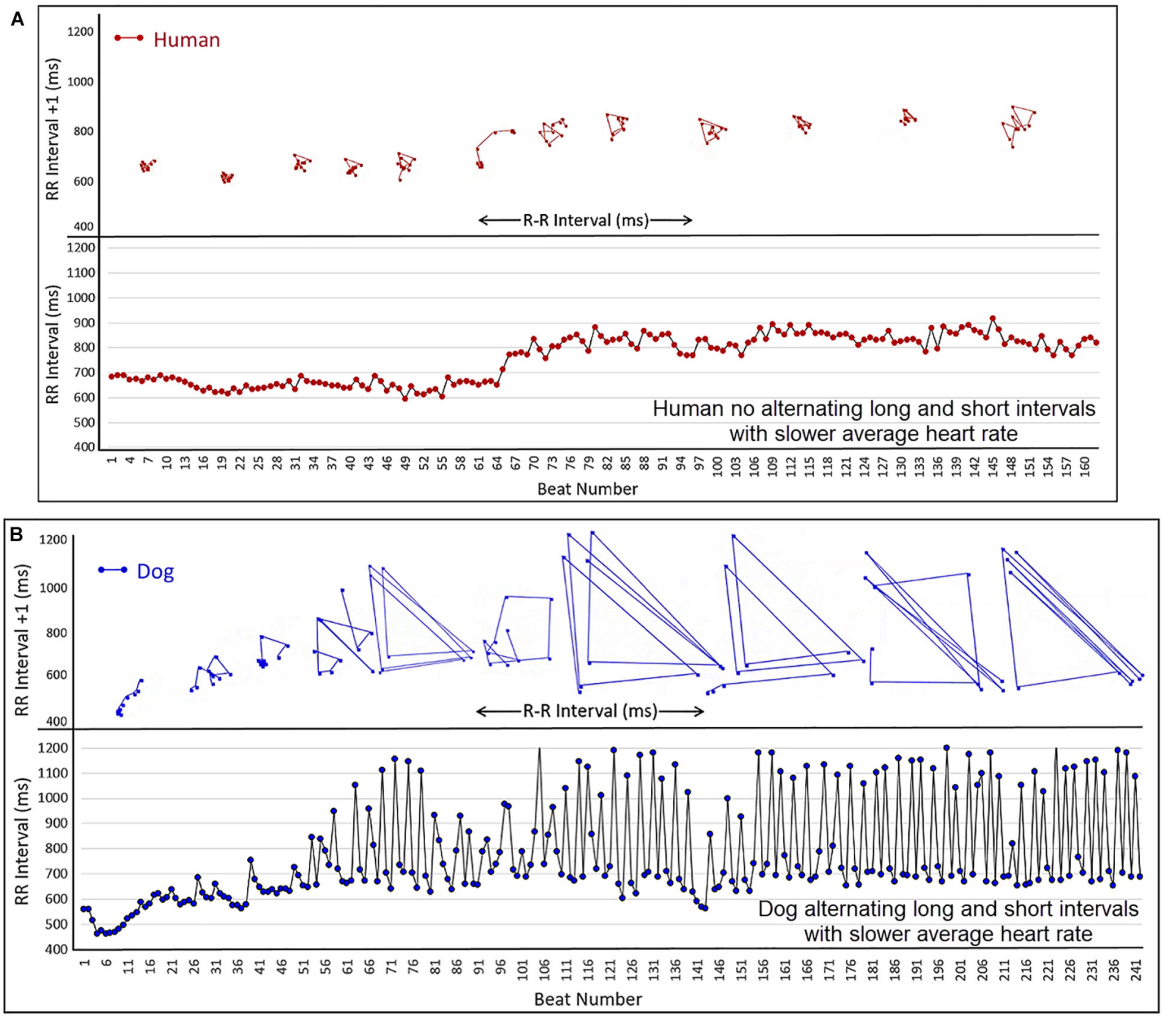

FIGURE 10 | (**Supplementary Video 7**) This figure illustrates the slowing of the sinus rhythm in the human and dog. As the human sinus node slows the beat-to-beat variation is confined along the line of identity (Frame **A**). As the dog sinus node slows (Frame **B**), the rate slows along the line of identity, just as in the human, until approximately 600 ms when a bifurcation occurs with long–short R–R intervals. This is shown in the Poincaré plots as well as the tachogram in this focused illustration. For clarity, the scale for Poincaré plots on the x-axis is not shown. **Supplementary Video 7** complements this figure.

to the same visual point identified on the tachogram as a 'line' of 'usually' shortest-intervals during stable sleep (see **Figure 5**). Therefore, measurement from the canine data set during a stable sleep hour in 25 boxers and 25 non-boxers was performed to determine the range for the bifurcation interval, its relationship to overall heart rate and its relationship to a measure of parasympathetic modulation using the overall time domain variable, SDNN corrected for heart rate. Data were normally distributed with results in **Table 3**. The average heart rate during the sleep hour was correlated modestly with the bifurcation interval and rate corrected SDNN; that is, the longer the bifurcation interval, the slower the heart rate and the higher the SDNN. The bifurcation interval had a 95% confidence interval (**Table 3**) that was equivalent to a heart rate range of 97.8–102.8 bpm. The bifurcation interval was not correlated with SDNN.

Parasympatholytic and Parasympathomimetic Drug Effects

The beat-to-beat patterns after both atropine and hydromorphone were compared to baseline during and following the peak of drug effects (**Figures 11–14** and **Supplementary Videos 8, 9**). After treatment with the parasympatholytic drug atropine, the heart rate increased (decrease in beat-to-beat interval) as expected. Additionally, the beat-to-beat interval did change below the identified bifurcation interval in a linear fashion. Over time, dynamic Poincaré plots and tachograms revealed that as the parasympatholytic effects waned

TABLE 3 | Pairwise correlation of bifurcation interval measured during stable sleep hour in 50 dogs* with heart rate, R–R-interval, rate corrected SDNN, and age.

Parameter	Mean	*SD*	95% CI
Bifurcation interval (ms)	598.5	54.3	583.5–613.5
Age (years)	6.5	3.32	5.6–7.4
Average heart rate (bpm)	63.6	11.1	60.4–66.7
Average R–R-interval (ms)	971	164	924–1018
SDNN (ms)	0.364	0.07	0.343–0.386

Variable	By variable	Correlation *r*	95% CI of *r*	*p*-value
Bifurcation interval (ms)	Age (years)	−0.102	−0.367 to 0.182	0.48
Bifurcation interval (ms)	Average heart rate (bpm)	−0.572	−0.733 to −0.349	<0.001
Bifurcation interval	SDNN (ms)	−0.235	−0.482 to 0.05	0.10
Average heart rate (bpm)	SDNN (ms)	−0.342	−0.566 to −0.070	0.02

*CI, confidence interval. *Boxers and non-boxers were combined because data for each of these variables were not different for these data.*

a bifurcation and non-linear slowing of the heart rate (increase in beat-to-beat interval) developed (**Figures 11**, **12**, **14** and **Supplementary Video 8**). Treatment with hydromorphone with its parasympathomimetic effects (Deo et al., 2008) not only showed a slowing of rate with an increase in the beat-to-beat interval, but also a loss of linear heart rate changes. The zone of avoidance or paucity of beats as seen on the Poincaré plots was expanded (**Figures 11**, **13**, **14** and **Supplementary Video 9**). Each of the features described above was noted in all eight dogs.

DISCUSSION

The present study investigated the unique beat-to-beat patterning of sinus rhythms in the dog compared to the human. To accomplish the study objectives, additional tools of geometric beat-to-beat analyses were developed. The major findings in this study include: (1) During sinus arrhythmia the dog has a unique non-Gaussian and non-linear patterning when compared to humans as revealed by interval distributions (histograms and tachograms) and beat-to-beat maps (two- and three-dimensional and dynamic Poincaré plots). (2) Dogs have distinctive beat-to-beat distributions with regions of low beat density (zone of avoidance) and patterns (clustered and branched) associated with potentially different parasympathetic and sympathetic influence as reflected by qualitative assessment of time and frequency domain indices of heart rate variability. Furthermore, administration of parasympatholytic and parasympathomimetic drugs supported the role of the parasympathetic system in dictating the patterns identified. (3) The patterns of beat-to-beat variability in the dog evidenced by the dynamic Poincaré plots revealed a consistent region or zone (bifurcation interval) at which the long- and short- intervals of sinus arrhythmia became non-linear. Moreover, the results of this study in a clinical population of dogs under the influence of spontaneous changes in autonomic input, is congruent with the hypotheses of experimental canine studies (Fedorov et al., 2009, 2010; Glukhov et al., 2013; Lou et al., 2013, 2014; Kalyanasundaram et al., 2019) of the sinus node that demonstrate the likelihood of parasympathetic influence on the sinoatrial conduction pathways (SACPs). Finally, these studies serve as a background to the potential understanding of not only normal sinus node function in the dog, but of potential mechanisms of sinus node dysfunction.

Different Ways to Speed and Slow

Each of the geometric heart rate indices used in the assessment of beat-to-beat changes in rate showed clear differences between the human and dog. The unique pattern identified in the dog may be related to key structural components of the sinus node complex and the electrophysiologic consequences of parasympathetic modulation and how these target the key receptors of spontaneous depolarization of pacing cells and the exit to the surrounding atrial tissue. Numerous investigations of structure and function of the sinus node conclude a similarity between the human and dog (Fedorov et al., 2009, 2010, 2012; Nikolaidou et al., 2012; Csepe et al., 2015, 2016; Kalyanasundaram et al., 2019) however, the influence of vagal modulation may be more profound in the dog. In contrast to smaller species (e.g., mouse, rabbit) with a thinner atrium and a sinus node that functions more similarly to a two-dimensional structure, the canine and human have a three-dimensional structure (Fedorov et al., 2009, 2010, 2012; Nikolaidou et al., 2012; Li et al., 2017). In the larger hearts, specific SACP connect the sinus node to the atrium (Fedorov et al., 2009, 2010, 2012; Nikolaidou et al., 2012; Glukhov et al., 2013; Lou et al., 2014; Csepe et al., 2015; Li et al., 2017; Kalyanasundaram et al., 2019). These discrete exit pathways (2–5 in the dog) have been identified by thorough investigations of structure and function using high-resolution optical mapping, action potential morphologies, immunostaining and histologic confirmation (Opthof, 2000). Because these narrow SACP slow the impulse velocity from the pacing cells, charge accumulates to overcome the source-sink mismatch between the sinus node and atria. These studies and others have demonstrated that the stimulation of the heart beat is the result of not only the pacing cells within the complex compartmentalized sinus node, but also dependent on the conduction of these impulses reaching the atrial myocardium through the SACP. Just as the spontaneous depolarization rate shifts in the location of the

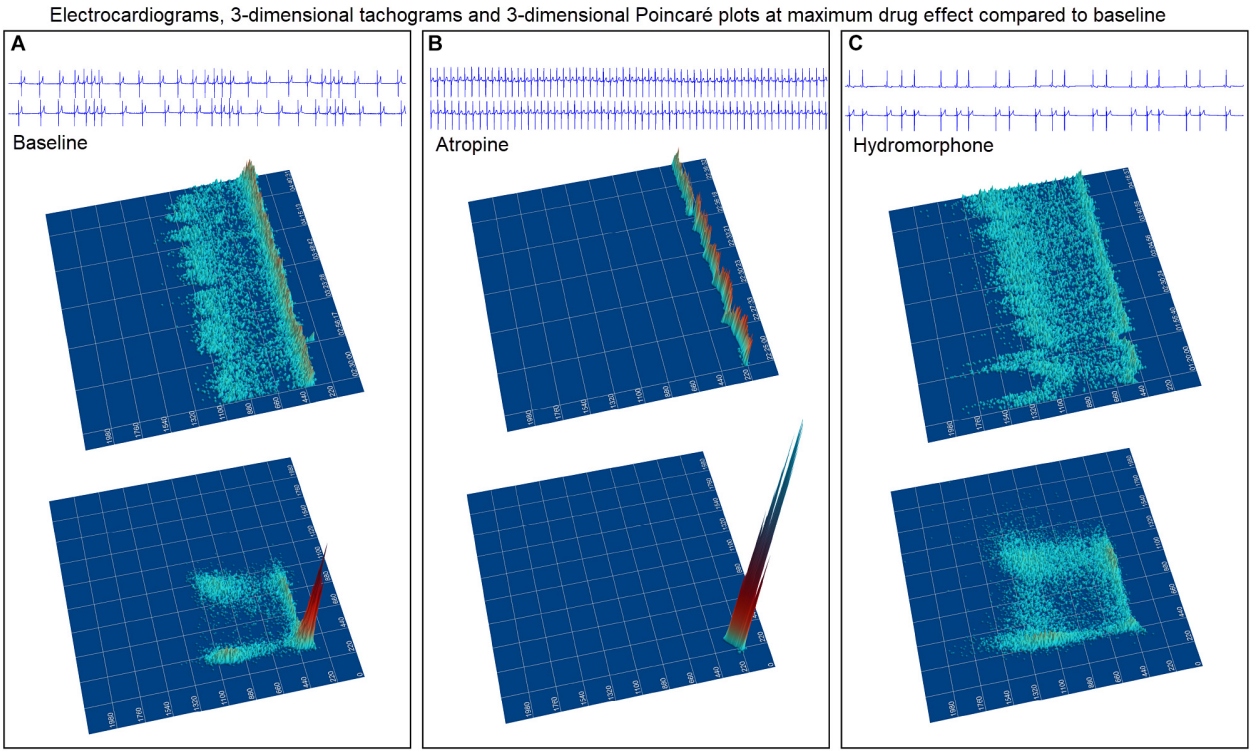

FIGURE 11 | The peak effects of atropine (0.04 mg/kg given intravenously) (Frame **A**) and hydromorphone (0.2 mg/kg given intravenously) (Frame **B**) compared to baseline (Frame **C**) are shown in the electrocardiograms, three-dimensional tachograms and Poincaré plots of beagle 5. During the baseline recording the sinus arrhythmia has a pattern with a paucity of beat intervals that can be identified on both the tachogram and Poincaré plots. At the longest intervals a cloud appears near the line of identity. After the administration of atropine (Frame **B**) that results in a decrease in parasympathetic modulation, the heart rate not only increases with a loss of sinus arrhythmia but the pattern of beat-to-beat intervals becomes linear. After the administration of hydromorphone (Frame **C**) that results in an increase in parasympathetic modulation, the heart rate slows and the bifurcation interval increases with a paucity of beat intervals (zone of avoidance). Scaling of all images is the same to show proportionality.

leading sinus pacing cells, SACP are substantially influenced by mediators of autonomic tone. For example, depending on the dose of adenosine or acetylcholine, not only are the membrane (I_f current) and voltage (Ca^{2+}) clocks suppressed to slow depolarization (Gao et al., 2010; Lou et al., 2013; Li et al., 2017), but conduction through the SACP is slowed (Opthof, 2000; Fedorov et al., 2009, 2010, 2012; Nikolaidou et al., 2012; Glukhov et al., 2013; Lou et al., 2013, 2014; Kalyanasundaram et al., 2019). Exit block through the SACP can develop in the dog with high levels of acetylcholine corresponding to high vagal tone potentially obtained during sleep (Glukhov et al., 2013; Kalyanasundaram et al., 2019). Although the intrinsic sinus rate of the dog (Evans et al., 1990; Du et al., 2017) and human (Opthof, 2000; Li et al., 2017) are similar, the higher parasympathetic tone in the dog is associated with a more pronounced sinus arrhythmia that we hypothesize based on the identified patterning of intervals in this study is, in part, the consequence of a more profound effect on the SACP resulting in exit block. Moreover, although variations in the non-linear patterns of sinus rhythm were seen in the dog, those with greater clustering of beats with 'shorter' short–long intervals had less variability than those with greater branching suggesting a possible difference in the balance between the rhythmicity of the parasympathetic and sympathetic tone. Of course, further studies are require to confirm these hypotheses.

SACP and Bifurcation Interval

Detailed and expansive studies of the canine sinus node support the existence of SACP that are subject to exit block during certain perturbations that mimic parasympathetic modulation. Moreover, the potential for decremental conduction would support modulation of exit block and this would then explain the inexact multiples and clustering of intervals. Experimental studies show that acetylcholine or adenosine can influence pacing cell depolarization and conduction through the SACP (Fedorov et al., 2009, 2010, 2012; Glukhov et al., 2013; Lou et al., 2013, 2014). Therefore, it is reasonable to hypothesize that our results, which demonstrate clustered and branched patterns related to the ratio of short- and long- intervals in the dog, could follow the same modulation of rate and rhythm via exit block through the SACP and slowed phase four-depolarization of pacing cells. In dogs with the longer beat-to-beat intervals a 'cloud' widely surrounding the line of identity may indicate a more profound effect of impulse initiation rather than conduction out the SACP. This type of pattern

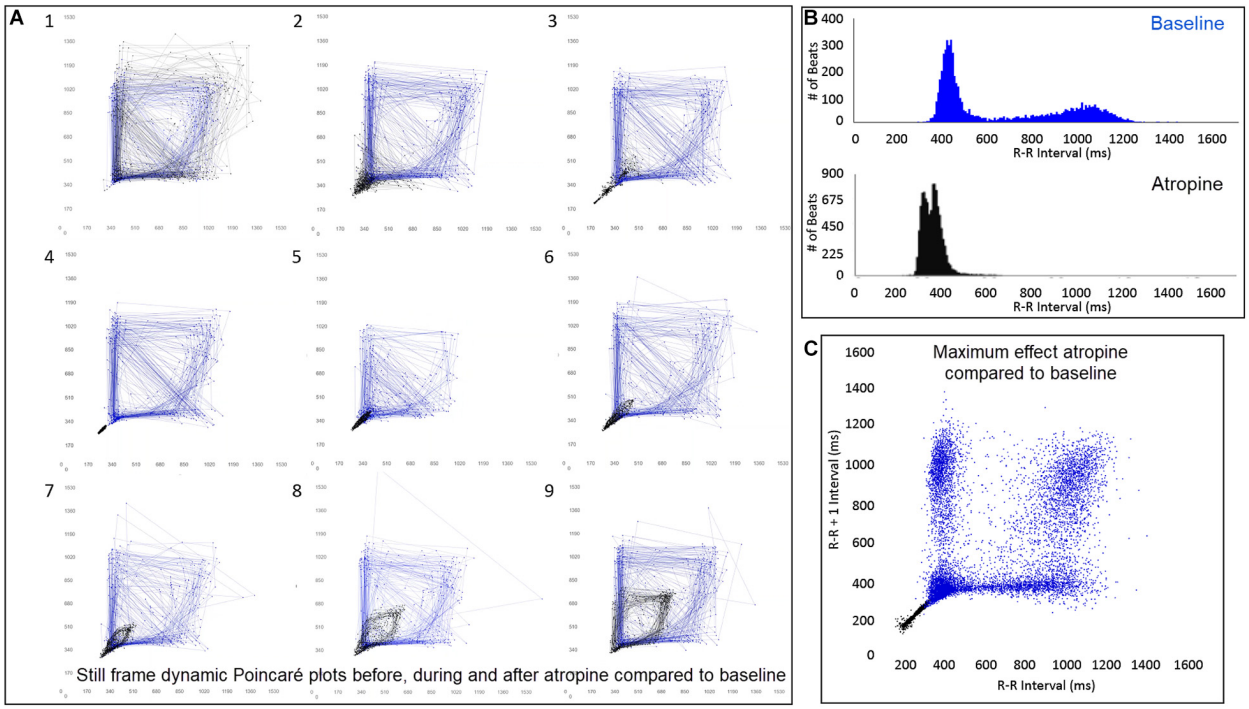

FIGURE 12 | (**Supplementary Video 8**) Still frames from dynamic Poincaré plots (Frame **A1–9**) from the electrocardiographic recordings from two different days during a stable rest period (blue) and just before, during and after administration of atropine (black) (0.04 mg/kg given intravenously) in beagle 8. Dots represent the beat-to-beat interval (R–R interval surrogate for P–P interval with all these verified to be sinus in origin) with lines connecting the next beat-to-beat interval. Each frame shows 500 beat-to-beat intervals. After atropine, the parasympatholytic effects result in the beat-to-beat intervals becoming shorter (Frames **1–4**) and as parasympathetic modulation returns, the beat-to-beat intervals become longer (Frames **5–9**). Note that after treatment with atropine the beat-to-beat patterning characterized by a bifurcation collapses to short intervals that hug the line of identity. When the heart rate slows (longer beat-to-beat intervals) with the decreasing drug effect, the bifurcation is identified again. In frame **(B)**, the number of beats at a particular beat interval are shown for the stable rest time (blue) and during treatment with atropine (black). The double peak during the atropine treatment represents the faster rate during the intravenous injection followed by the true drug effect and its short beat-to-beat intervals. In frame **(C)**, the Poincaré plot illustrates a comparison without the connecting lines of the entire baseline period and the time of maximum effect of atropine. **Supplementary Video 8** complements this figure.

was identified in all dogs administered hydromorphone which is known to have a parasympathomimetic effect on the sinus node. This observation maybe concordant with saturation of the parasympathetic effect on the sinus node decreasing the respiratory modulation of heart rate variability. The latter is identified in trained athletes (Goldberger et al., 1994). We corrected for the mathematical biased inherent in time and frequency analyses by dividing by the standard deviation or standard deviation squared, respectively (Sacha and Pluta, 2008; Billman, 2011, 2013; Billman et al., 2015b; Sacha et al., 2013). Finally, it is intriguing that the bifurcation interval at which point slowing of the heart rate in the dog becomes non-linear, a very narrow 95% confidence range of 97.8–102.8 beats per minute (583.5–613.5 ms) approximates the intrinsic sinus node rate of the adult and older dog. The intrinsic rate of the sinus node is that which is inherent to spontaneous depolarization of the sinus node cells without autonomic input (Billman et al., 2015a). How autonomic input is subtracted (e.g., pharmacological blockade, surgical denervation, explanted heart) influences this value (Evans et al., 1990). Also, age is an important determinant of the intrinsic rate with young dogs (168 ± 11 bpm) having faster rates compared to adults (120 ± 9 beats per minute) and elderly (88 ± 9 bpm) dogs (Du et al., 2017).

Heart Rate Variability

Heart rate variability is influenced by multiple inputs of central and peripheral parasympathetic and sympathetic modulation (Evans et al., 1990; Goldberger et al., 1994; Cerutti et al., 1995; Roossien et al., 1997; Stein et al., 2005; Billman, 2011, 2013; Billman et al., 2015b; Shaffer and Ginsberg, 2017; Behar et al., 2018a,b). The variability results from complex interactions and cannot be simplified to say that high variability universally indicates high parasympathetic modulation (Goldberger et al., 1994; Costa et al., 2017; Shaffer and Ginsberg, 2017; Hayano and Yuda, 2019). Both groups of dogs in this study had greater variability using traditional time domain indices than in humans. Traditional methods to evaluate the variability of the sinus node driven rate in humans have meaningful limitations particularly when evaluating disease states and this has prompted advanced methods (Hayano and Yuda, 2019). Some indices used in the evaluation of the rhythm in humans are not applicable to the dog. For example, the percentage of successive R–R intervals that differ by more than 50 ms

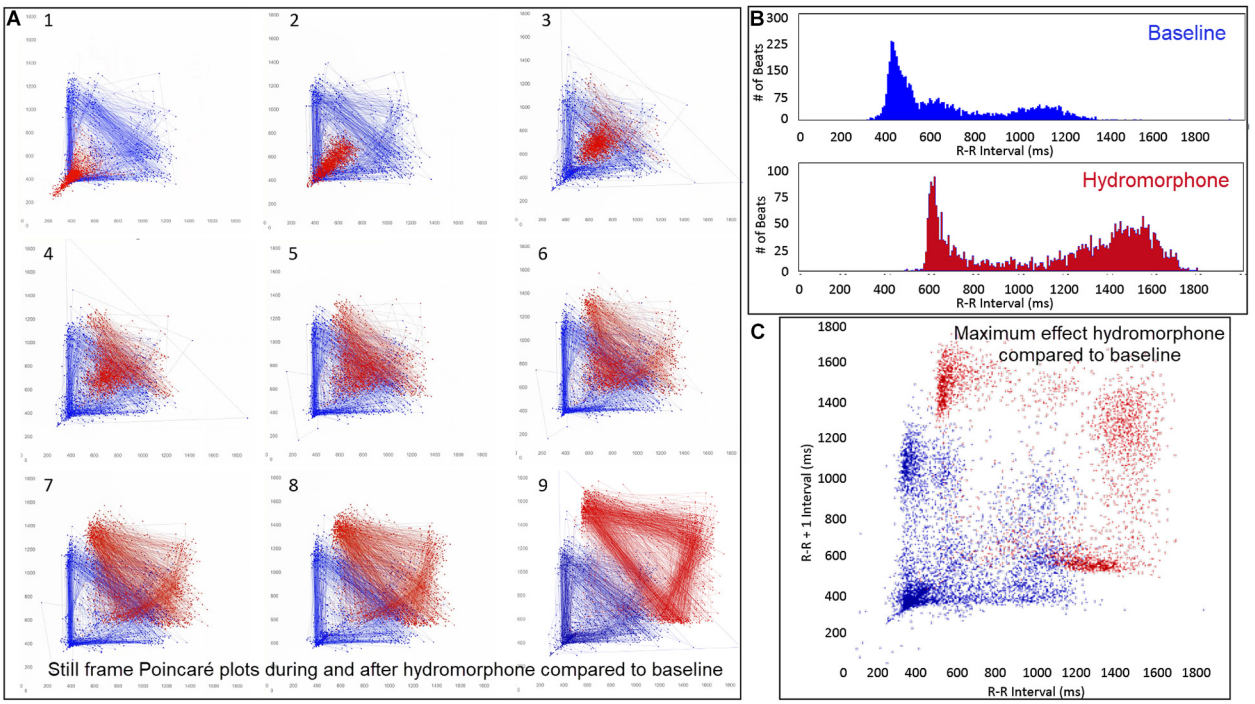

FIGURE 13 | (**Supplementary Video 9**) Still frames from dynamic Poincaré plots (Frame **A1–9**) derived from intervals of 24-h electrocardiographic recordings from two different days during a stable rest period (blue) and just before and after administration of hydromorphone (red) (0.2 mg/kg given intravenously) given to beagle 1. Dots represent the beat-to-beat interval (R–R interval surrogate for P–P interval with all these verified to be sinus in origin) with lines connecting the next beat-to-beat interval. Each frame shows 1500 beat-to-beat intervals. After hydromorphone the beat-to-beat intervals become longer. In frames (**1–5)** the heart rate is faster because the dog is excited during the intravenous administration and then calms as the drug takes effect. The heart rate and beat-to-beat interval pattern changes with increasing drug effect. The characteristic pattern with a paucity of beat intervals (zone of avoidance) and beat intervals that do not hover around the line of identity are seen in the dog with high parasympathetic modulation induced by the hydromorphone. In frame **(B)** the number of beats at a particular beat interval are shown for the stable rest period (blue) and during treatment with hydromorphone (red). In frame **(C)**, the Poincaré plot illustrates a comparison without the connecting lines of the entire baseline period and the time of maximum effect of hydromorphone. **Supplementary Video 9** complements this figure.

(pNN50) because this difference is too small for the dog. The triangular index is not applicable because the dog does not have a singular Gaussian distribution (Shaffer and Ginsberg, 2017). Furthermore, some of the linear measurements used in the evaluation of Poincaré plots in humans are also not valid in the dog because they are derived from the studies of linear changes along the line of identity (Shaffer and Ginsberg, 2017). These include the area of the ellipse (width/length), which represents total heart rate variability, the standard deviation perpendicular to the line of identity and the standard deviation along the line of identity. Newly developed methods to better understand the variability in the sinus rhythm have been developed and deserve further evaluation in different species (Costa et al., 2017).

Beyond Visual Geometric Analyses

Although this study used dynamic Poincaré plots and three-dimensional imaging to demonstrate a difference in beat-to-beat intervals between the dog and human these visual indices are inadequate (Esperer et al., 2008). Moreover, linear quantification are inappropriate, thus non-linear analyses demand exploration. These may include approximate or sample entropy, detrended fluctuation analyses and fractal measures, as well as the development of new methodologies through computer modeling of the beat-to-beat variation (Esperer et al., 2008; Nicolini et al., 2012; Khandoker et al., 2013; Burykin et al., 2014; Yaniv et al., 2014b; Henriques et al., 2015; Shaffer and Ginsberg, 2017; Borracci et al., 2018; Valente et al., 2018). In humans, slowing of the heart rate is a continuum with some having slower rates (e.g., athletes), but in the normal dog slowing of the heart is not a continuous process. We hypothesize that the dog has greater potential for alterations of conduction in the SACP that is linked to the parasympathetic modulation. This hypothesis is supported by the (1) abrupt change of beat-to-beat intervals, (2) paucity and grouping of beats rather than a continuum of beat intervals, and (3) relatively consistent bifurcation interval during basal conditions.

Clinical Relevance

Both humans and dogs can be afflicted with sinus node dysfunction. Such dysfunction may be intrinsic, extrinsic or both. Alterations in the parasympathetic nervous system or molecular targets likely play an important role, thus understanding the relationship of the sinus node complex with the inclusion of the SACP is likely vital to differentiating disease that results in exit block versus those with disease from impulse formation.

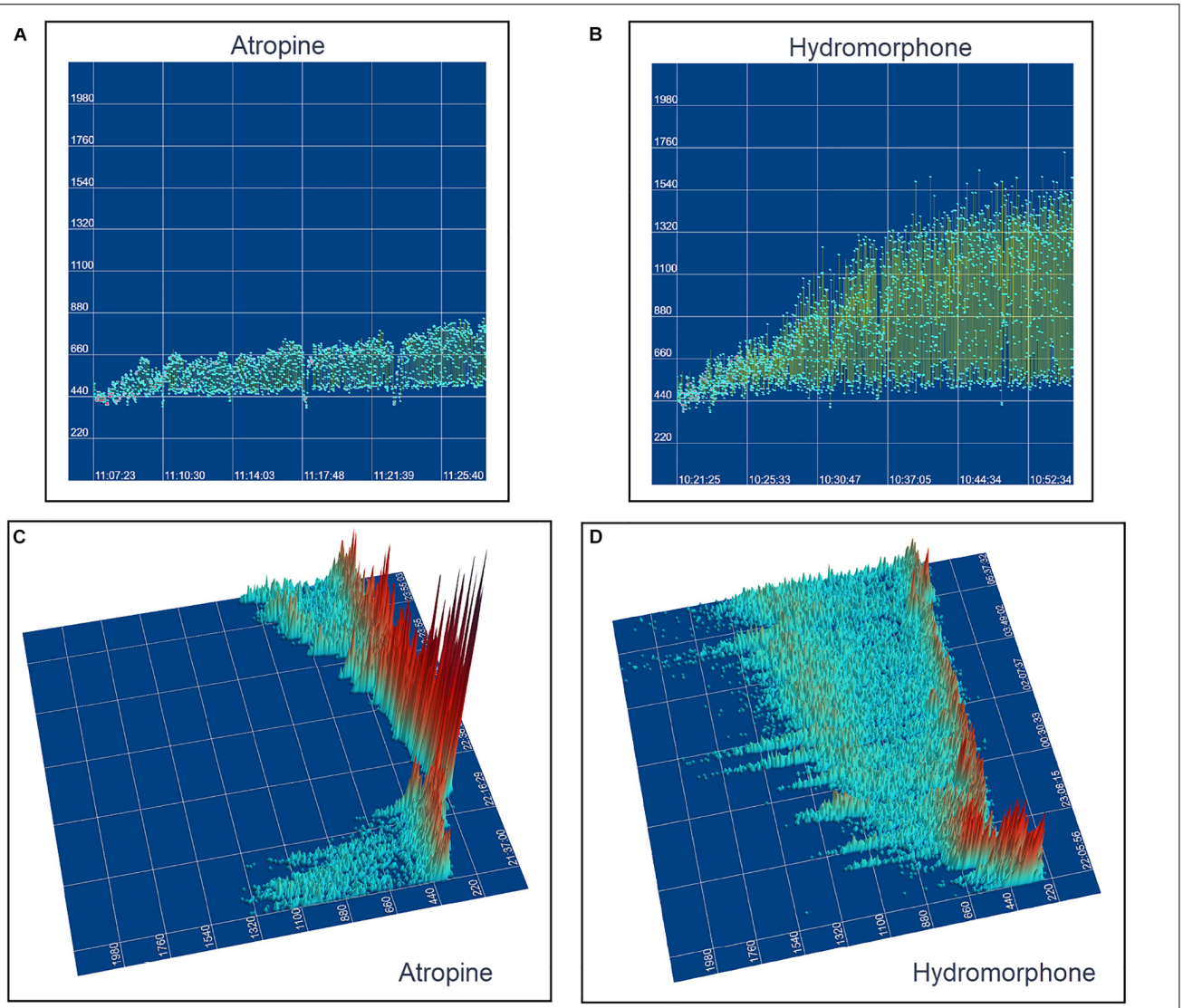

FIGURE 14 | This figure uses two-dimensional **(A,B)** and three-dimensional **(C,D)** tachograms to show the pattern and density of sinus intervals before, during, and after treatment to decrease and increase parasympathetic modulation. Recordings were from two different days for each treatment. Frame **(A)** (beagle 1) illustrates the interval changes (turquoise dots represent interval duration and yellow lines connect sequential intervals) as the drug effects of atropine (0.04 mg/kg given intravenously) dissipate. The decreasing and increasing interval duration associated with the increasing and decreasing drug effects of atropine are seen in frame **(C)** (beagle 1). As the effects of atropine subside the bifurcation interval increases with an increased paucity of beats as sinus arrhythmia returns. Frame **(B,D)** (beagle 8) show increasing interval duration associated with the increasing drug effects of hydromorphone (0.2 mg/kg given intravenously). The effects of hydromorphone result in an increased paucity of beats, an increase in the bifurcation interval and a greater spread of long intervals. Scaling for frames **(C,D)** are equal to show proportionality of the interval density.

The use of the techniques illustrated herein may be valuable in this differentiation.

Limitations

Our study is limited to the surface electrocardiogram without direct assessment of the multiplicity of inputs that control the sinus rhythm. However, the patterning observed supports experimental studies of the sinus node in the dog. The study population of dogs and humans included a wide range of ages; however, the range in age between boxers and non-boxers was different and likely responsible for the difference in the relationship of age to time domain indices of heart rate variability. Equating dog age to human age is known to be difficult, non-linear and highly variable depending on the breed of dog (Cotman and Head, 2008). Consequently, attempts to compare the influence of age between the dog and human from our study is not possible. It is known that sinus node function varies with age, and, thus, this must be taken into consideration. Additionally, because 32 different breeds were studied of varied sizes with 108 dogs neutered, comparison to humans by weight or sex was not undertaken. Although the only entry criteria that differed between the dogs and humans was the duration that

defined a sinus pause, this did not impact the difference in beat-to-beat patterning because the non-linear change occurred at intervals that were more than 1000 ms shorter than the defined pause. It is stressed that autonomic activity was not directly measured, and heart rate variability provides only an indirect qualitative assessment of cardiac parasympathetic activity. More advanced analyses need to be undertaken to further investigate the potential mechanisms for the unique patterning of sinus arrhythmia in the dog.

CONCLUSION

Our study demonstrated distinctive differences in beat-to-beat sinus rhythms in the dog compared to humans. Specific patterns within and between dog were associated with differences in heart rate, time and frequency domain variability. Treatment with atropine as a parasympatholytic agent resulted in small variation in beat intervals that were along the line of identity while treatment with hydromorphone as a parasympathomimetic agent resulted in an expansion and exaggeration of the patterns identified without linear variation in the beat-to-beat intervals. The non-linear rhythms of sinus arrhythmia in the dog require assessment using analyses appropriate to the dynamics. The multiplicity of input that results in the beat-to-beat dynamics identified in the normal canine are concordant with the possibility of not only alterations in the initiation of sinus impulses, but also variable exit block within the SACP. Furthermore, these results may offer insight to the possible mechanisms for sinus node dysfunction seen in the dog that has a disease footprint similar to humans.

DATA AVAILABILITY STATEMENT

The datasets generated for this study are available on request to the corresponding author.

ETHICS STATEMENT

The animal study was reviewed and approved by the Cornell University IACUC for drug studies. Written informed consent was obtained from the owners for the participation of their animals in this study.

AUTHOR CONTRIBUTIONS

NM designed the study, analyzed the data, created all the images, interpreted the data, and wrote the manuscript. WF created the software for the analysis and contributed to the interpretation of the data. RP contributed to the interpretation of the data and reviewed the manuscript.

ACKNOWLEDGMENTS

We wish to sincerely thank Drs. Sabine Mann and Françoise Vermeylen for assistance with statistical analyses; Shari Hemsley for assistance with editing of 24-h Holter recordings; and Kelsey Kearns, Andrea Gladuli, Ellen Gunzel, Emily Herrold, and Caitlin Hokanson for assistance with data management. We are also grateful to Don Greenfield and Forest Medical, Syracuse, NY, United States for permitting us access to the raw Holter data for our investigation. We are appreciative of the investigators who established and maintain the Telemetric and Holter ECG Warehouse (THEW) at the University of Rochester Medical Center, Rochester, NY, United States. Special appreciation is given to Dr. George Billman for critical input.

SUPPLEMENTARY MATERIAL

The Supplementary Material for this article can be found online at: https://www.frontiersin.org/articles/10.3389/fphys.2019.01548/full#supplementary-material

REFERENCES

Ambrosi, C. M., Fedorov, V. V., Schuessler, R. B., Rollins, A. M., and Efimov, I. R. (2012). Quantification of fiber orientation in the canine atrial pacemaker complex using optical coherence tomography. *J. Biomed. Opt.* 17:071309. doi: 10.1117/1.JBO.17.7.071309

Behar, J. A., Rosenberg, A. A., Shemla, O., Murphy, K. R., Koren, G., Billman, G. E., et al. (2018a). A universal scaling relation for defining power spectral bands in mammalian heart rate variability analysis. *Front. Physiol.* 9:1001. doi: 10.3389/fphys.2018.01001

Behar, J. A., Rosenberg, A. A., Weiser-Bitoun, I., Shemla, O., Alexandrovich, A., Konyukhov, E., et al. (2018b). PhysioZoo: a novel open access platform for heart rate variability analysis of mammalian electrocardiographic data. *Front. Physiol.* 9:1390. doi: 10.3389/fphys.2018.01390

Billman, G. E. (2011). Heart rate variability? A historical perspective. *Front. Physiol.* 2:86. doi: 10.3389/fphys.2011.00086

Billman, G. E. (2013). The effect of heart rate on the heart rate variability response to autonomic interventions. *Front. Physiol.* 4:222. doi: 10.3389/fphys.2013.00222

Billman, G. E., Cagnoli, K. L., Csepe, T., Li, N., Wright, P., Mohler, P. J., et al. (2015a). Exercise training-induced bradycardia: evidence for enhanced parasympathetic regulation without changes in intrinsic sinoatrial node function. *J. Appl. Physiol.* 118, 1344–1355. doi: 10.1152/japplphysiol.01111.2014

Billman, G. E., Huikuri, H. V., Sacha, J., and Trimmel, K. (2015b). An introduction to heart rate variability: methodological considerations and clinical applications. *Front. Physiol.* 6:55. doi: 10.3389/fphys.2015.00055

Blake, R. R., Shaw, D. J., Culshaw, G. J., and Martinez-Pereira, Y. (2018). Poincaré plots as a measure of heart rate variability in healthy dogs. *J. Vet. Cardiol.* 20, 20–32. doi: 10.1016/j.jvc.2017.10.006

Boineau, J. P., Schuessler, R. B., Hackel, D. B., Miller, C. B., Brockus, C. W., and Wylds, A. C. (1980). Widespread distribution and rate differentiation of the atrial pacemaker complex. *Am. J. Physiol. Circ. Physiol.* 239, H406–H415. doi: 10.1152/ajpheart.1980.239.3.H406

Borracci, R. A., Montoya Pulvet, J. D., Ingino, C. A., Fitz Maurice, M., Hirschon Prado, A., and Dominé, E. (2018). Geometric patterns of time-delay plots from different cardiac rhythms and arrhythmias using short-term EKG signals. *Clin. Physiol. Funct. Imaging* 38, 856–863. doi: 10.1111/cpf.12494

Brodde, O. E., Konschak, U., Becker, K., Rüter, F., Poller, U., Jakubetz, J., et al. (1998). Cardiac muscarinic receptors decrease with age. In vitro and in vivo studies. *J. Clin. Invest.* 101, 471–478. doi: 10.1172/JCI1113

Burykin, A., Costa, M. D., Citi, L., and Goldberger, A. L. (2014). Dynamical density delay maps: simple, new method for visualising the behaviour of complex systems. *BMC Med. Inform. Decis. Mak.* 14:6. doi: 10.1186/1472-6947-14-6

Cerutti, S., Bianchi, A. M., and Mainardi, L. T. (1995). "Spectral analysis of the heart rate variability signal," in *Heart Rate Variability*, eds M. Malik, and A. J. Camm, (Wiley, NJ: Wiley).

Costa, M. D., Davis, R., and Goldberger, A. L. (2017). Heart rate fragmentation: a new approach to the analysis of cardiac interbeat interval dynamics. *Front. Physiol.* 8:255. doi: 10.3389/fphys.2017.00255

Cotman, C. W., and Head, E. (2008). The canine (dog) model of human aging and disease: dietary, environmental and immunotherapy approaches. *J. Alzheimers Dis.* 15, 685–707. doi: 10.3233/JAD-2008-15413

Csepe, T. A., Kalyanasundaram, A., Hansen, B. J., Zhao, J., and Fedorov, V. V. (2015). Fibrosis: a structural modulator of sinoatrial node physiology and dysfunction. *Front. Physiol.* 6:37. doi: 10.3389/fphys.2015.00037

Csepe, T. A., Zhao, J., Hansen, B. J., Li, N., Sul, L. V., Lim, P., et al. (2016). Human sinoatrial node structure: 3D microanatomy of sinoatrial conduction pathways. *Prog. Biophys. Mol. Biol.* 120, 164–178. doi: 10.1016/j.pbiomolbio.2015.12.011

Deo, S., Barlow, M., Gonzalez, L., Yoshishige, D., and Caffrey, J. (2008). Cholinergic location of δ-opioid receptors in canine atria and SA node. *Am. J. Physiol. Hear. Circ. Physiol.* 294, H829–H838.

Du, J., Deng, S., Pu, D., Liu, Y., Xiao, J., and She, Q. (2017). Age-dependent down-regulation of hyperpolarization-activated cyclic nucleotide-gated channel 4 causes deterioration of canine sinoatrial node function. *Acta Biochim. Biophys. Sin.* 49, 400–408. doi: 10.1093/abbs/gmx026

Esperer, H. D., Esperer, C., and Cohen, R. J. (2008). Cardiac arrhythmias imprint specific signatures on Lorenz plots. *Ann. Noninvasive Electrocardiol.* 13, 44–60. doi: 10.1111/j.1542-474X.2007.00200.x

Evans, J. M., Randall, D. C., Funk, J. N., and Knapp, C. F. (1990). Influence of cardiac innervation on intrinsic heart rate in dogs. *Am. J. Physiol. Circ. Physiol.* 258, H1132–H1137. doi: 10.1152/ajpheart.1990.258.4.H1132

Fedorov, V. V., Chang, R., Glukhov, A. V., Kostecki, G., Janks, D., Schuessler, R. B., et al. (2010). Complex interactions between the sinoatrial node and atrium during reentrant arrhythmias in the canine heart. *Circulation* 122, 782–789. doi: 10.1161/CIRCULATIONAHA.109.935288

Fedorov, V. V., Glukhov, A. V., and Chang, R. (2012). Conduction barriers and pathways of the sinoatrial pacemaker complex: their role in normal rhythm and atrial arrhythmias. *Am. J. Physiol. Circ. Physiol.* 302, H1773–H1783. doi: 10.1152/ajpheart.00892.2011

Fedorov, V. V., Schuessler, R. B., Hemphill, M., Ambrosi, C. M., Chang, R., Voloshina, A. S., et al. (2009). Structural and functional evidence for discrete exit pathways that connect the canine sinoatrial node and atria. *Circ. Res.* 104, 915–923. doi: 10.1161/CIRCRESAHA.108.193193

Gao, Z., Chen, B., Joiner, M. A., Wu, Y., Guan, X., Koval, O. M., et al. (2010). I(f) and SR Ca(2+) release both contribute to pacemaker activity in canine sinoatrial node cells. *J. Mol. Cell. Cardiol.* 49, 33–40. doi: 10.1016/j.yjmcc.2010.03.019

Gladuli, A., Moïse, N. S., Hemsley, S. A., and Otani, N. F. (2011). Poincaré plots and tachograms reveal beat patterning in sick sinus syndrome with supraventricular tachycardia and varying AV nodal block. *J. Vet. Cardiol.* 13, 63–70. doi: 10.1016/j.jvc.2010.12.001

Glukhov, A. V., Hage, L. T., Hansen, B. J., Pedraza-Toscano, A., Vargas-Pinto, P., Hamlin, R. L., et al. (2013). Sinoatrial node reentry in a canine chronic left ventricular infarct model. *Circ. Arrhythmia Electrophysiol.* 6, 984–994. doi: 10.1161/CIRCEP.113.000404

Goldberger, J. J., Ahmed, M. W., Parker, M. A., and Kadish, A. H. (1994). Dissociation of heart rate variability from parasympathetic tone. *Am. J. Physiol. Circ. Physiol.* 266, H2152–H2157. doi: 10.1152/ajpheart.1994.266.5.H2152

Hayano, J., and Yuda, E. (2019). Pitfalls of assessment of autonomic function by heart rate variability. *J. Physiol. Anthropol.* 38:3. doi: 10.1186/s40101-019-0193-2

Henriques, T. S., Mariani, S., Burykin, A., Rodrigues, F., Silva, T. F., and Goldberger, A. L. (2015). Multiscale Poincaré plots for visualizing the structure of heartbeat time series. *BMC Med. Inform. Decis. Mak.* 16:17. doi: 10.1186/s12911-016-0252-0

Kalyanasundaram, A., Li, N., Hansen, B. J., Zhao, J., and Fedorov, V. V. (2019). Canine and human sinoatrial node: differences and similarities in the structure, function, molecular profiles, and arrhythmia. *J. Vet. Cardiol.* 22, 2–19. doi: 10.1016/j.jvc.2018.10.004

Khandoker, A. H., Karmakar, C., Brennan, M., Voss, A., and Palaniswami, M. (2013). *Poincaré Plot Methods for Heart Rate Variability Analysis*. New York, NY: Springer Science+Business Media.

Krohova, J., Czippelova, B., Turianikova, Z., Lazarova, Z., Wiszt, R., Javorka, M., et al. (2018). Information domain analysis of respiratory sinus arrhythmia mechanisms. *Physiol. Res.* 67, S611–S618.

Li, N., Hansen, B. J., Csepe, T. A., Zhao, J., Ignozzi, A. J., Sul, L. V., et al. (2017). Redundant and diverse intranodal pacemakers and conduction pathways protect the human sinoatrial node from failure. *Sci. Transl. Med.* 9:eaam5607. doi: 10.1126/scitranslmed.aam5607

Lou, Q., Glukhov, A. V., Hansen, B., Hage, L., Vargas-Pinto, P., Billman, G. E., et al. (2013). Tachy-brady arrhythmias: the critical role of adenosine-induced sinoatrial conduction block in post-tachycardia pauses. *Hear. Rhythm* 10, 110–118. doi: 10.1016/j.hrthm.2012.09.012

Lou, Q., Hansen, B. J., Fedorenko, O., Csepe, T. A., Kalyanasundaram, A., Li, N., et al. (2014). Upregulation of adenosine A1 receptors facilitates sinoatrial node dysfunction in chronic canine heart failure by exacerbating nodal conduction abnormalities revealed by novel dual-sided intramural optical mapping. *Circulation* 130, 315–324. doi: 10.1161/CIRCULATIONAHA.113.007086

Malik, M., Bigger, J. T., Camm, A. J., Kleiger, R. E., Malliani, A., Moss, A. J., et al. (1996). Heart rate variability: standards of measurement, physiological interpretation, and clinical use. *Eur. Heart J.* 17, 354–381.

Mighiu, A., and Heximer, S. (2012). Controlling parasympathetic regulation of heart rate: a gatekeeper role for RGS proteins in the sinoatrial node. *Front. Physiol.* 3:204. doi: 10.3389/fphys.2012.00204

Moïse, N. S., Gladuli, A., Hemsley, S. A., and Otani, N. F. (2010). "Zone of avoidance": RR interval distribution in tachograms, histograms, and Poincaré plots of a Boxer dog. *J. Vet. Cardiol.* 12, 191–196. doi: 10.1016/j.jvc.2010.07.001

Monfredi, O., Maltseva, L. A., Spurgeon, H. A., Boyett, M. R., Lakatta, E. G., and Maltsev, V. A. (2013). Beat-to-beat variation in periodicity of local calcium releases contributes to intrinsic variations of spontaneous cycle length in isolated single sinoatrial node cells. *PLoS One* 8:e67247. doi: 10.1371/journal.pone.0067247

Nicolini, P., Ciulla, M. M., de Asmundis, C., Magrini, F., and Brugada, P. (2012). The prognostic value of heart rate variability in the elderly, changing the perspective: from sympathovagal balance to chaos theory. *Pacing Clin. Electrophysiol.* 35, 621–637. doi: 10.1111/j.1540-8159.2012.03335.x

Nikolaidou, T., Aslanidi, O. V., Zhang, H., and Efimov, I. R. (2012). Structure-function relationship in the sinus and atrioventricular nodes. *Pediatr. Cardiol.* 33, 890–899. doi: 10.1007/s00246-012-0249-0

Opthof, T. (2000). The normal range and determinants of the intrinsic heart rate in man. *Cardiovasc. Res.* 45, 177–184.

Peltola, M. A. (2012). Role of editing of R–R intervals in the analysis of heart rate variability. *Front. Physiol.* 3:148. doi: 10.3389/fphys.2012.00148

Roossien, A., Brunsting, J. R., Nijmeijer, A., Zaagsma, J., and Zijlstra, W. G. (1997). Effects of vasoactive intestinal polypeptide on heart rate in relation to vagal cardioacceleration in conscious dogs. *Cardiovasc. Res.* 33, 392–399.

Sacha, J., Barabach, S., Statkiewicz-Barabach, G., Sacha, K., Müller, A., Piskorski, J., et al. (2013). How to strengthen or weaken the HRV dependence on heart rate–Description of the method and its perspectives. *Int. J. Cardiol.* 168, 1660–1663. doi: 10.1016/j.ijcard.2013.03.038

Sacha, J., and Pluta, W. (2008). Alterations of an average heart rate change heart rate variability due to mathematical reasons. *Int. J. Cardiol.* 128, 444–447. doi: 10.1016/j.ijcard.2007.06.047

Sassi, R., Cerutti, S., Lombardi, F., Malik, M., Huikuri, H. V., Peng, C.-K., et al. (2015). Advances in heart rate variability signal analysis: joint position statement by the e-Cardiology ESC working group and the european heart rhythm association co-endorsed by the Asia Pacific Heart Rhythm Society. *Europace* 17, 1341–1353. doi: 10.1093/europace/euv015

Shaffer, F., and Ginsberg, J. P. (2017). An overview of heart rate variability metrics and norms. *Front. Public Heal.* 5:258. doi: 10.3389/fpubh.2017.00258

Stein, P. K., Domitrovich, P. P., Hui, N., Rautaharju, P., and Gottdiener, J. (2005). Sometimes higher heart rate variability is not better heart rate variability: results of graphical and nonlinear analyses. *J. Cardiovasc. Electrophysiol.* 16, 954–959. doi: 10.1111/j.1540-8167.2005.40788.x

Valente, M., Javorka, M., Porta, A., Bari, V., Krohova, J., Czippelova, B., et al. (2018). Univariate and multivariate conditional entropy measures for the characterization of short-term cardiovascular complexity under physiological stress. *Physiol. Meas.* 39:014002. doi: 10.1088/1361-6579/aa9a91

Yaniv, Y., Ahmet, I., Liu, J., Lyashkov, A. E., Guiriba, T.-R., Okamoto, Y., et al. (2014a). Synchronization of sinoatrial node pacemaker cell clocks and its autonomic modulation impart complexity to heart beating intervals. *Hear. Rhythm* 11, 1210–1219. doi: 10.1016/j.hrthm.2014.03.049

Yaniv, Y., Lyashkov, A. E., Sirenko, S., Okamoto, Y., Guiriba, T.-R., Ziman, B. D., et al. (2014b). Stochasticity intrinsic to coupled-clock mechanisms underlies beat-to-beat variability of spontaneous action potential firing in sinoatrial node pacemaker cells. *J. Mol. Cell. Cardiol.* 77, 1–10. doi: 10.1016/j.yjmcc.2014.09.008

Yasuma, F., and Hayano, J.-I. (2004). Respiratory sinus arrhythmia: why does the heartbeat synchronize with respiratory rhythm? *Chest* 125, 683–690. doi: 10.1378/chest.125.2.683

Zhang, L., Guo, T., Xi, B., Fan, Y., Wang, K., Bi, J., et al. (2015). Automatic recognition of cardiac arrhythmias based on the geometric patterns of Poincaré plots. *Physiol. Meas.* 36, 283–301. doi: 10.1088/0967-3334/36/2/283

Conflict of Interest: The authors declare that the research was conducted in the absence of any commercial or financial relationships that could be construed as a potential conflict of interest.

frontiers in Physiology

REVIEW
published: 18 March 2020
doi: 10.3389/fphys.2020.00236

Low-Frequency Oscillations in Cardiac Sympathetic Neuronal Activity

Richard Ang[1] and Nephtali Marina[1,2]**

[1] Centre for Cardiovascular and Metabolic Neuroscience, Neuroscience, Physiology and Pharmacology, University College London, London, United Kingdom, [2] Division of Medicine, University College London, London, United Kingdom

Sudden cardiac death caused by ventricular arrhythmias is among the leading causes of mortality, with approximately half of all deaths attributed to heart disease worldwide. Periodic repolarization dynamics (PRD) is a novel marker of repolarization instability and strong predictor of death in patients post-myocardial infarction that is believed to occur in association with low-frequency oscillations in sympathetic nerve activity. However, this hypothesis is based on associations of PRD with indices of sympathetic activity that are not directly linked to cardiac function, such as muscle vasoconstrictor activity and the variability of cardiovascular autospectra. In this review article, we critically evaluate existing scientific evidence obtained primarily in experimental animal models, with the aim of identifying the neuronal networks responsible for the generation of low-frequency sympathetic rhythms along the neurocardiac axis. We discuss the functional significance of rhythmic sympathetic activity on neurotransmission efficacy and explore its role in the pathogenesis of ventricular repolarization instability. Most importantly, we discuss important gaps in our knowledge that require further investigation in order to confirm the hypothesis that low frequency cardiac sympathetic oscillations play a causative role in the generation of PRD.

Keywords: sympathetic, arrhythmia, oscillations, cardiac repolarization, cardiac innervation

OPEN ACCESS

Edited by:
George E. Billman, The Ohio State University, United States

Reviewed by:
Ruben Coronel, University of Amsterdam, Netherlands
Crystal M. Ripplinger, University of California, Davis, United States

***Correspondence:**
Richard Ang
r.ang@nhs.net
Nephtali Marina
n.marina@ucl.ac.uk

Specialty section:
This article was submitted to Cardiac Electrophysiology, a section of the journal Frontiers in Physiology

Received: *19 December 2019*
Accepted: *02 March 2020*
Published: *18 March 2020*

Citation:
Ang R and Marina N (2020) Low-Frequency Oscillations in Cardiac Sympathetic Neuronal Activity. Front. Physiol. 11:236. doi: 10.3389/fphys.2020.00236

INTRODUCTION

Sudden cardiac death caused by ventricular arrhythmias is a leading cause of mortality globally, resulting in approximately 50% of all cardiovascular-related deaths each year (Wong et al., 2019). Excessive sympathetic activity is a crucial factor known to promote myocardial repolarization abnormalities that increase the vulnerability of developing ventricular fibrillation and fatal cardiac arrhythmias (Maling and Moran, 1957; Cao et al., 2000). Recent studies have shown that ventricular repolarization instability after an acute myocardial infarction (MI) exhibits a pronounced rhythmic pattern that is believed to mimic the characteristic low-frequency (LF) oscillations in sympathetic efferent activity (Rizas et al., 2014, 2017; Pueyo et al., 2016). This electrophysiological phenomenon has been termed periodic repolarization dynamics (PRD) and it can be measured non-invasively from the vector angle of the electrocardiogram (ECG) T wave (Rizas et al., 2014).

This article aims to review the available evidence in support of the hypothesis that rhythmic sympathetic nerve traffic to the myocardium underlies the origin of PRD. We first focus on how excessive adrenergic signaling affects myocardial repolarization. We then present a comprehensive

review of published data obtained in rodent brain tissue *in vitro* and in whole animal preparations *in vivo* that prove that sympathetic neuronal networks most likely involved in the control of cardiac function can exhibit LF oscillatory activity under some experimental conditions. We then discuss the mechanisms involved in the generation of rhythmic sympathetic discharges and explore the physiological role of patterned activity in the sympathetic system and its impact on neurotransmission efficacy. In doing so, we identify important gaps in our knowledge that need to be addressed in future studies.

Cardiac Ventricular Repolarization and the Surface ECG T Wave

Cardiomyocyte repolarization represents a complex sequence of electrical events that occur during phases 1 to 3 of the action potential in which the net outward current exceeds the net inward current, causing the return of the membrane potential to its baseline resting state prior to the next depolarization. Cardiac ventricular repolarization is a significant determinant of the QT interval, represented on the surface ECG by the interval between the start of the QRS complex and the end of the T wave (Yan et al., 2003).

There is general agreement that the T wave is the result of voltage gradients that exist within the ventricular myocardium during cardiac repolarization although the precise mechanism appears to differ depending on the species studied and the experimental preparation used. Using arterially perfused canine right ventricular wedge preparations, Antzelevitch found three layers of electrically and functionally distinct cell types of the ventricular myocardium: the epicardial cells, the M cells and the endocardial cells (Antzelevitch, 2006). These studies demonstrated that the T wave arises due to transmural voltage gradients across the ventricular myocardium which develop as a result of the difference in the time course of repolarization of the three layers, with the M cells having the longest action potential duration (APD) followed by the endocardial layer and the epicardial layer. However, mapping studies using arterially perfused left ventricular wedge preparations and intact hearts suggest that transmural repolarization differences do not fully explain T wave genesis (Opthof et al., 2007; Boukens et al., 2015). By comparing electrical and optical mapping of both intact and left ventricular wedge preparation of canine hearts, Boukens et al. (2017) demonstrated that electrical gradients from wedge preparations differed from those of intact hearts, implying that findings from wedge preparations may not extrapolate to the whole heart.

In addition to the transmural electrical gradient, there is also evidence of electrical heterogeneity between the apex to base (Autenrieth et al., 1975; Watanabe et al., 1985; Franz et al., 1987) and left to right ventricles of the heart (Durrer et al., 1970; Srinivasan et al., 2016). Indeed, whole heart studies have shown that the T wave is an index of dispersion of repolarization across the whole heart and not due to transmural electrical gradients (Meijborg et al., 2014; Opthof et al., 2017; Srinivasan et al., 2019).

Effects of Sympathoexcitation on Cardiac Repolarization and Ventricular Arrhythmia

Sympathoexcitation leads to norepinephrine release which activates β-adrenoceptors (β-AR) to modulate myocardial repolarization and contractility. β-AR stimulation increases L-type Ca^{2+} current which leads to an increase in APD but this is counterbalanced by the concomitant increase in outwards K^+ currents via the rapidly (I_{Kr}) and slowly (I_{Ks}) activating delayed rectifier potassium channels (Hartzell, 1988). Sympathoexcitation can lead to both APD shortening or prolongation depending on the net effect of the inwards and outwards currents (Priori and Corr, 1990). This effect is species-dependent and in humans it has been shown to lead to APD prolongation (Jakob et al., 1988; Veldkamp et al., 2001).

The arrhythmogenic effects of excessive noradrenergic tone are exerted at different levels. At the cellular level, β-AR activation leads to cyclic AMP (cAMP) dependent phosphorylation of proteins involved in excitation–contraction coupling which includes L-type Ca^{2+} channels, ryanodine receptors (RyR) and phospholamban, with concomitant increase in sarcoplasmic reticulum (SR) Ca^{2+}-ATPase (SERCA) activity (Hartzell, 1988). This results in an increase in cytosolic and SR Ca^{2+} levels which can result in a triggered action potential via Na^+/Ca^{2+} exchanger (NCX) and membrane depolarizations during phase 4 of the action potential. This process is also known as delayed after depolarizations (DADs) (Pogwizd and Bers, 2004) and pathological processes such as MI and subsequent heart failure are believed to increase the likelihood of DADs by inducing an increase in the expression of NCX (Pogwizd et al., 1999) and by promoting SR Ca^{2+} leak via RyR (Shannon et al., 2003) and a decreased I_{Kr} current (Pogwizd et al., 2001). At the tissue level, a further requirement for arrhythmogenesis is electrical coupling between the focus of origin and the surrounding tissue (Kumar et al., 1996). Electrical coupling through gap junctions silences "unstable" tissue by the surrounding "stable" cells (also described as "source-sink" effect) (Xie et al., 2010). DADs occurring simultaneously in several thousand cells is hence required to generate enough depolarizing current to produce a propagating action potential, which is manifested clinically as premature ventricular complexes (PVCs) (Myles et al., 2012). Adverse remodeling secondary to disease processes can lead to decreased gap junction coupling which results in a lower number of cells with DADs required to generate an abnormal impulse (Poelzing and Rosenbaum, 2004). On a macro level, overt tissue fibrosis can also result in areas of electrically unexcitable tissue which creates the condition for re-entrant arrhythmias to occur (Vaquero et al., 2008). Finally, at the whole heart level, the heterogeneous distribution of sympathetic nerves across the heart may also play an important role in the generation of ventricular arrhythmias. The density of sympathetic nerve terminals appears to be more abundant at the ventricular base compared to the apex and these regional differences may have a profound effect on the APD gradient from endocardial to epicardial layers (Nabauer et al., 1996; Brunet et al., 2004; Ieda et al., 2007; Lorentz et al., 2010). As a result, even under non-pathological

conditions, sympathetic activation would lead to non-uniform changes in APD across the ventricles, increasing the dispersion of repolarization and the potential for re-entrant arrhythmias. In pathological conditions (i.e., diabetes, obesity, MI, and heart failure), where maladaptive cardiac sympathetic innervation remodeling occurs, heterogeneity of APD and repolarization may become even more pronounced (Gardner et al., 2016).

In summary, sympathoexcitation leads to both an increase in triggered activity, and dispersion of repolarization. This leads to abnormalities in activation and propagation of electrical activity in the ventricular myocardium that have been shown in experimental and clinical studies to be pro-arrhythmic (Maling and Moran, 1957; Cao et al., 2000).

Low Frequency Oscillation T Wave Dynamics as a Marker of Sympathoexcitation and Susceptibility to Ventricular Arrhythmia

An area of intense clinical research has been the search for a reliable biomarker of increased susceptibility to potentially fatal ventricular arrhythmia which would help direct clinical intervention such as prophylactic implantation of an implantable cardioverter defibrillator device (ICD). Various non-invasive methods have been studied, including assessments of increased/altered sympathetic tone [heart rate variability (Schmidt et al., 1999) and baroreflex sensitivity (Billman et al., 1982)] and measurements of abnormalities in cardiac repolarization [QT interval (Zhang et al., 2011), QT dispersion (Day et al., 1990), Tpeak to Tend (Panikkath et al., 2011) and microvolt T wave alternans (Verrier et al., 2011)]. However, these methods are not accurate as they only provide an indirect probe of the sympathetic effect on cardiac repolarization. For example, the effect of autonomic tone on sinus node activity is not excluded when studying QT interval as the heart rate is not kept constant and changes in heart rate in itself may affect the QT interval. Furthermore, there may also be concomitant influences of the sympathovagal tone on the vasculatures and on the renin-angiotensin-aldosterone system which may confound the interpretation of the results.

Periodic repolarization dynamics has been proposed as a promising risk marker for susceptibility to ventricular arrhythmia. PRD is assessed using a high resolution ECG recorded in 'Frank lead configuration' with three orthogonal axes *X*-, *Y*-, and *Z*-. Low frequency ($\leq$0.1 Hz) periodic changes of the T wave vector provide an index to measure both sympathetic activity and its effects on ventricular repolarization. In a cohort of 908 patients, increased PRD predicted total and cardiovascular mortality in survivors of MI and was independent of underlying heart rate and respiratory activity. Furthermore, in multivariate analysis PRD provided incremental prognostic value in addition to established risk markers such as LV ejection fraction and measure of T wave alternans (Rizas et al., 2014). A recent 5-year prospective multicenter study (EUropean Comparative Effectiveness Research to Assess the Use of Primary ProphylacTic Implantable Cardioverter Defibrillators, EU-CERT-ICD) showed a strong correlation between the magnitude of the oscillations of ventricular repolarization with both arrhythmia and sudden death in patients with ischemic and non-ischemic cardiomyopathy. Thus, PRD has great potential as a clinical tool for risk stratification of patients who would benefit from implantation of implantable cardioverter defibrillators (Bauer et al., 2019).

The link between PRD and the level of sympathetic activity was demonstrated in clinical studies showing that manipulations that trigger sympathoexcitatory responses (i.e., exercise or the tilt test) enhance the magnitude of PRD whilst pharmacological blockade of β-adrenergic antagonists have the opposite effect (Rizas et al., 2014). The periodicity of the oscillations in ventricular repolarization appears to be in the same frequency range of the LF oscillatory patterns detected in muscle sympathetic nerve activity recordings (MSNA) (Furlan et al., 2000) and in the spontaneous beat-to-beat oscillations in the R–R interval (RRi) (Pagani et al., 1986; Malliani et al., 1991). Other studies have also demonstrated similar rhythmic patterns of APD in patients with heart failure which are coherent with the 0.1 Hz oscillatory frequency of arterial blood pressure Mayer waves (Hanson et al., 2014). Similarly, a recent study has shown that LF oscillations in APD were reduced following β-ADR blockade and were correlated with changes in RRi (Duijvenboden et al., 2019). Together, this evidence has led to the suggestion that LF oscillatory patterns in APD and PRD represent the effect of sympathetic nerve activity on the myocardium (Rizas et al., 2014, 2016). However, this hypothesis is based on associations of PRD with indirect measurements of sympathetic activity which are not anatomically or functionally involved in the regulation of ventricular excitability and repolarization: first, RRi is believed to represent sympathetic influences on the sino-atrial node (Malliani et al., 1991) which explains why PRD is not affected when heart rate variability is eliminated in subjects with fixed atrial pacing (Rizas et al., 2014). Second, arterial blood pressure Mayer waves are believed to result from rhythmic oscillations of muscle vasoconstrictor activity (Julien, 2006). Third, MSNA is a direct measurement of sympathetic vasomotor tone that is usually recorded at the peroneal nerve (Macefield, 2013). Thus, in the following sections we have sought to identify experimental evidence of the existence of oscillatory activity in neuronal networks and peripheral nerves along the neurocardiac axis which might have a more direct role in the regulation of ventricular myocardial excitability.

Rhythmic Sympathetic Activity

One of the most remarkable characteristics of sympathetic neuronal discharges is their rhythmic nature. Autonomic neuroscientists have applied power spectral analysis methods based on fast Fourier transform (FFT) algorithms to detect rhythmic patterns in sympathetic neurons and peripheral nerves both in experimental laboratory animals and in human subjects (Montano et al., 2009).

Rhythmic sympathetic oscillations occur over a wide spectrum of distinct frequencies, ranging from 0.1 to 10 Hz, depending on the sympathetic outflow being measured (Malpas, 1998). In humans, a LF rhythm ($\leq$0.1 Hz) is often found in direct recordings of MSNA (Furlan et al., 2000) and in the variability of

heart rate (HR) and systolic arterial blood pressure (SAP) (Pagani et al., 1986; Malliani et al., 1991). However, these sympathetic outflows are unlikely to have a direct role in the control of cardiac excitability since they are not anatomically linked with the innervation of ventricular cardiomyocytes and their control mechanisms may differ from the systems that control cardiac sympathetic outflow. Since direct measurements of cardiac sympathetic outflows cannot be investigated in human subjects, we will primarily discuss evidence obtained in experimental laboratory animals using invasive techniques for the direct assessment of cardiac sympathetic neuronal activity (CSNA).

Low-frequency oscillations in sympathetic outflows appear to be less ubiquitous than cardiac-related (2–6 Hz) and respiratory-related (1–3 Hz) rhythms. Nevertheless, numerous studies have found that LF rhythms are a robust feature of sympathetic neuronal networks involved in the control of cardiac function. Although none of the studies discussed in the following sections have investigated rhythmic sympathetic oscillations in the context of ventricular repolarization instability, the mechanisms described herein are likely to contribute, at least in part, to the origin, regulation and synchronization of PRD.

LF Oscillations in Brainstem Neuronal Circuits

Sympathetic activity originates in a lower brainstem region known as the rostral ventrolateral medulla (RVLM). The RVLM contains a group of C1 catecholaminergic neurons and a group of non-catecholaminergic neurons believed to produce glutamate (Brown and Guyenet, 1985; Schreihofer and Guyenet, 1997; Guyenet, 2006). RVLM neurons send monosynaptic excitatory inputs to sympathetic preganglionic neurons (spns) within the thoraco-lumbar spinal cord (Amendt et al., 1979; Ross et al., 1981) that are crucial for the maintenance of resting vascular tone and heart rate (Marina et al., 2011).

Low-frequency oscillatory patterns have been identified in single RVLM neurons in experiments conducted in unanesthetized, decerebrated, vagotomised and artificially ventilated cats with denervated baroreceptors (Montano et al., 1995, 1996) and in rats anesthetized with urethane with either intact or denervated baroreceptors (Tseng et al., 2009). RVLM neuronal LF oscillations were shown to be correlated with the LF component of the systolic arterial pressure variability (Montano et al., 1995) and were found to be involved in the generation of coherent LF oscillations in renal sympathetic nerve outflows (Tseng et al., 2009). Although the identity of the target organ innervated by these neurons was not identified in these studies, these data strongly suggest that LF sympathetic oscillations have a central origin as they were detected in the absence of cardio-respiratory and baroreceptor inputs. Experiments conducted in adult decerebrated cats have also identified the presence of 0.1 Hz oscillatory activity in pontine neurons involved in respiratory pattern generation and in medullary raphé neurons that modulate both, sympathetic nerve activity and the activity of brainstem respiratory networks (Morris et al., 2010). LF oscillations in pontine and raphé neurons were coordinated with arterial blood pressure Mayer waves and became synchronized with the central respiratory rhythm after elimination of pulmonary stretch receptor inputs (Morris et al., 2010). Together, these results suggest that LF oscillatory activity originates in a dispersed supraspinal neuronal network that participates in the integration of vasomotor, cardiac-related and respiratory rhythms.

Little is known about the cellular mechanisms that contribute to the origin of LF oscillations in supraspinal neuronal networks. At the single cell level, *in vitro* studies have demonstrated that RVLM neurons have the capability of displaying intrinsic pacemaker activity in conditions of reduced synaptic activity, which suggests that synaptic inputs are only involved in the modulation of rhythmic patterns (Sun et al., 1988a,b). Intracellular recordings conducted in retrogradely identified cells in isolated neonatal spinal cord preparations confirmed that a population of non-adrenergic reticulospinal neurons in the RVLM possess pacemaker-like properties such as an after-hyperpolarization at the end of the spike followed by a slow depolarization with no evidence of excitatory postsynaptic potentials (EPSPs) between action potentials (Sun et al., 1988b). However, single cell recordings in intact preparations (anesthetized rats) failed to support this "pacemaker hypothesis," arguing that pacemaker-like activity recorded in RVLM neurons results from the anatomical or functional elimination of synaptic inputs (Lipski et al., 1996). Thus, a "network" hypothesis has been suggested which proposes that 2- to 6-Hz and 10-Hz oscillatory activities in medullary neurons originate from the influence of synaptic influences from neighboring brainstem oscillators located in the lateral tegmental field (LTF) which can be entrained by baroreceptor inputs (Barman and Gebber, 1987, 1993). Although these results illustrate some general mechanisms underlying the generation of rhythmic activity in bulbospinal neurons, they highlight the lack of evidence that might explain how cardiac presympathetic neurons generate LF oscillatory patterns, in particular in conditions of enhanced sympathetic drive.

LF Oscillations in Sympathetic Preganglionic Neurons of the Spinal Cord

Neurons located across four distinct regions of the thoracolumbar spinal cord integrate descending excitatory inputs from the RVLM and other sympathoexcitatory areas in the hypothalamus. These centers include the intermediolateral cell column (IML), nucleus intermediolateralis thoracolumbalis pars funicularis, intercalated nucleus (IN), and central autonomic area (CA). The axon from the spns exit the spinal cord through the ventral root to make synaptic contact with cardiac sympathetic ganglia via white rami communicans. Anatomical tracing studies in guinea pigs (Dalsgaard and Elfvin, 1981) and cats (Chung et al., 1975, 1979) have shown that spns that control cardiac function are mainly distributed along lower cervical and upper thoracic spinal segments (C8-T11).

Most of the evidence showing LF oscillatory activity in preganglionic neuronal networks comes primarily from *in vivo* studies conducted in whole animal preparations. Neuronal

recordings from thoracic preganglionic axons in anesthetized cats with high spinal transection at the C1 level showed neuronal discharge variability in the range of 0.1 Hz that were temporally synchronized with the oscillations in systemic arterial pressure (Fernandez de Molina and Perl, 1965). Similar recordings conducted in decerebrated, unanesthetized cats confirmed the presence of rhythmic neuronal discharges in the LF range at the level of the third thoracic (T3) white ramus communicans that correlated with the LF component of the R–R interval (Lombardi et al., 1990; Montano et al., 1992). The power of LF oscillations was increased in response to a fall in systemic blood pressure and conversely, was decreased in response to elevations in arterial blood pressure (Montano et al., 1992). In a subsequent study Montano et al. (2000) found that LF preganglionic neuronal oscillations were preserved following acute spinal transection at the C1 level and the rhythmic discharges remained synchronized with the variability of the R–R interval and systolic blood pressure (Montano et al., 2000). In these conditions, the power of LF sympathetic discharges in preganglionic fibers innervating the stellate ganglion was found to increase in response to increases in arterial blood pressure and this effect was abolished when cardiovascular afferent inputs to the spinal cord were physically interrupted by a dorsal rhizotomy (Montano et al., 2000). Together, these data suggest that LF oscillations are generated locally within preganglionic sympathetic neuronal circuits and that positive-feedback spinal reflexes play an important role in the potentiation of LF oscillatory activity in cardiac-related spns.

The rhythmic properties of spns neuronal discharge have been studied primarily *in vitro* using acute spinal cord slices and isolated spinal cord preparations from neonatal rats. These studies have shown that the mechanisms underlying the generation of this rhythmic pattern result from a complex interaction between intrinsic membrane properties in individual neurons, synaptic inputs and network interactions within the spinal cord. At the single cell level, patch-clamp recordings in neonatal rat spinal cord slices revealed the presence of spontaneous membrane potential oscillations in spns independent of excitatory or inhibitory synaptic inputs, which suggests that oscillatory activity arises from intrinsic membrane properties in spns (Spanswick and Logan, 1990; Shen et al., 1994). At the network level, synchronized sympathetic activity is believed to emerge as a consequence of transmission of spontaneous membrane potential oscillations between gap-junction-coupled spns (Logan et al., 1996; Nolan et al., 1999). In support of this network hypothesis, our immunohistochemical studies have revealed that thoracic spns express connexin-36 proteins along somato-dendritic sites of close apposition (Marina et al., 2008) and pharmacological studies in spinal cord slices have shown that blockade of gap junctions attenuates and in some cases abolishes rhythmic activity in spns (Pierce et al., 2010).

Synaptic mechanisms have also been implicated in the generation of rhythmic activity in spns. Several studies have shown that rhythmic oscillations can be induced pharmacologically by activation of 5-HT receptors in spinal cord preparations *in vitro* (Pickering et al., 1994; Lewis and Coote, 1996; Pierce et al., 2010) and in *in situ* "isolated spinal cord preparations" in anesthetized rats (Marina et al., 2006). This suggests that oscillatory activity in preganglionic neuronal networks is generated in response to direct descending serotonergic excitatory inputs from the medulla oblongata (Smith et al., 1998).

Although rhythmic sympathetic activity in the spinal cord has received significant research attention, very little information is available about the putative mechanisms that give rise to the generation of LF oscillations in spns (Su, 2001; Sourioux et al., 2018). Electrophysiological recordings of preganglionic fibers innervating the celiac ganglion revealed the presence of spontaneous bursting activity in the range of <0.1 Hz that was abolished in the presence of a high Mg^{+} solution and was attenuated by application of non-NMDA receptor blockers (Su, 2001). A recent study showed that activation of muscarinic cholinergic receptors (mAchRs) trigger LF oscillatory activity in spns in coordination with somatomotor neuronal activity (Sourioux et al., 2018). These studies have thus identified cholinergic and glutamatergic neurotransmission mechanisms that play an important role in the generation of LF oscillations in spns that innervate visceral organs. Future studies should determine whether similar mechanisms operate in upper thoracic spinal segments which may facilitate the generation of LF oscillatory activity in sympathetic preganglionic networks that control the electrical activity of the heart.

LF Oscillations in Cardiac Sympathetic Postganglionic Fibers

Extra-cardiac sympathetic neurons are located across numerous thoracic ganglia in particular in the stellate, middle cervical, superior cervical and mediastinal ganglia (Janes et al., 1986; Ardell and Armour, 2016). The electrophysiological properties of neurons located within the stellate ganglion and postganglionic axons traveling along the cardiac sympathetic nerve (CSN) have been studied extensively in several animal models *in vivo*, including ambulatory cats (Tsuchimochi et al., 2002), dogs (Han et al., 2012; Chan et al., 2015) sheep (Jardine et al., 2002, 2005, 2007; Charles et al., 2018) and anesthetized cats (Nishikawa et al., 1994). Experiments conducted in conscious and anesthetized cats with either intact or denervated baroreceptors have been the model of choice to study periodic oscillations in CSNA. However, the frequency of rhythmic neuronal oscillations reported so far appears to be dominated by cardiac-related rhythms in the 2-to 6-Hz range (Ninomiya et al., 1989, 1990, 1993; Kocsis et al., 1990; Hedman et al., 1994; Kocsis, 1994; Hedman and Ninomiya, 1995; Kocsis and Gyimesi-Pelczer, 1998; Larsen et al., 2000) or by respiratory-related rhythms in synchrony with the discharge frequency of the phrenic nerve (Kollai and Koizumi, 1980). The presence of LF oscillations in cardiac postganglionic fibers has not been documented yet, which appears to be counterintuitive, since the final synaptic relay in the neurocardiac axis would be expected to follow the same oscillatory pattern generated by either bulbar presympathetic or spinal preganglionic neuronal networks. However, this apparent lack of scientific evidence does not preclude the existence of LF oscillations in cardiac postganglionic fibers, as this might be the consequence of the experimental conditions used to

obtain the data. As mentioned previously, LF oscillations in preganglionic axons have only been detected in decerebrated cats in the absence of general anesthesia (Montano et al., 1992, 2000). Previous studies have shown that anesthetic drugs produce a profound suppression of cardiac sympathetic nerve activity in cats (Matsukawa et al., 1993). This suggests that LF oscillations might have been suppressed and therefore were probably not detected in the studies where animals were anesthetized with chloralose (Kollai and Koizumi, 1980; Kocsis et al., 1990; Kocsis, 1994), sodium pentobarbital (Hedman et al., 1994) or urethane (Kocsis, 1994; Larsen et al., 2000). Another factor that might have interfered with the detection of LF oscillations in cardiac postganglionic fibers is the signal processing methods used for the discrimination of rhythmic components. In the decerebrated cat, cardiac preganglionic fiber power spectra are primarily dominated by a 3.3 Hz component which relates to the rhythm synchronous with the cardiac cycle. In contrast, the power spectral density of LF components in the 0–0.5 Hz range in these preparations is only minor (Lombardi et al., 1990). In order to better identify synchronized preganglionic activity in the LF range, cardiac synchronous rhythmicity needs to be eliminated by filtering the signal with low pass filters with a cut-off frequency of 1 Hz. This allows sampling of the neural signal once per-heart beat and application of autoregressive modeling analysis of sympathetic nerve discharges and R–R interval duration (Lombardi et al., 1990; Montano et al., 1992, 2000). In contrast, the studies assessing cardiac postganglionic nerve discharges cited above did not take measurements to eliminate cardiac-related synchronous activity which may have prevented the detection of LF oscillations (Kocsis et al., 1990; Kocsis, 1994; Kocsis and Gyimesi-Pelczer, 1998; Larsen et al., 2000).

LF Oscillations in Intrinsic Ganglionated Cardiac Plexus

The intrinsic innervation of the heart includes a heterogeneous collection of sympathetic (Moravec and Moravec, 1989; Moravec et al., 1990) and parasympathetic (Yuan et al., 1993) cardiac ganglia collectively termed ganglionated plexus (GP). According to the classification proposed by Beaumont et al. (2013), intracardiac local circuit neurons (LCNs) fall into three main categories: (a) secondary afferent LCNs that detect mechanical and chemical stress signals from different regions of the heart, (b) secondary efferent LCNs that respond to sympathetic and/or parasympathetic neuronal inputs from higher brain centers, medullary networks, spinal preganglionic neurons and thoracic extracardiac ganglia, and (c) convergent LCNs that integrate afferent sensory information with efferent autonomic inputs. LCNs are believed to generate coordinated responses that control chronotropic, dromotropic, inotropic, and lusotropic properties of the heart (Armour, 1997, 2004; Armour et al., 1998).

In vivo studies conducted in anesthetized dogs showed that GP neurons residing in the ventral ventricular GP display spontaneous activity in synchrony to the cardiac cycle and the respiratory rhythm and are exquisitely sensitive to stimulation of β-adrenergic receptors and mechanical stimulation (Ardell et al., 1991). A subsequent study also found that epicardial application of voltage-gated sodium channel agonist veratridine induced robust bursting discharges in the range of 0.1 Hz in both, intrinsic ventricular GP neurons and extrinsic cardiac neurons. However, neuronal discharges were frequently found to be out of synchrony (Armour et al., 1998). In some experiments, transection of sympathetic and vagal neuronal connections also resulted in the generation of bursting activity in intrinsic and middle cervical ganglia neurons (Armour et al., 1998). However, manipulations to produce mechanical activation of carotid sinus baroreceptors failed to produce a significant activation of intrinsic cardiac neurons. These data suggest that LF bursting patterns are primarily displayed by ventricular secondary afferent intracardiac LCNs in response to the detection of chemical clues that are normally released in situations of myocardial damage. Future studies should aim to determine whether LF rhythmic activity generated by intracardiac LCNs is mechanistically linked to the facilitation of LF repolarization instability as observed in PRD.

Cardiac Sympathetic Oscillations Post-MI

Clinical studies have shown that LF oscillations in the variability of muscle sympathetic nerve activity (MSNA) are significantly increased in patients after MI (Martinez et al., 2011). However, sympathetic vasoconstrictor fibers innervate arterioles that determine peripheral resistance which have no anatomical connection with regional cardiac targets. MSNA might be different to CSNA in terms of the regulation of central mechanisms underlying the generation of oscillatory patterns. Thus, increased MSNA is unlikely to be directly linked to the periodic fluctuations in cardiac repolarization observed in patients post-MI (Rizas et al., 2014).

To our best knowledge, there are no studies in experimental animals models of MI that have investigated changes in the power of the LF component in the variability of neuronal discharges of bulbospinal RVLM neurons, spns in the IML and postganglionic sympathetic neurons of the CSN. Electrophysiological studies conducted to investigate the neuronal response properties to MI in anesthetized cats have shown that interruption of the left coronary artery blood flow produced a substantial increase in the discharge of afferent sympathetic fibers that supply the ventricular myocardium and this effect was mimicked by intracoronary administration of bradykinin (Lombardi et al., 1981). Functional changes in sympathetic innervation are thus likely to contribute to post-MI hypersensitivity and may eventually lead to the loss of sympathetic fibers within the infarcted myocardium.

Mi triggers a cardio-cardiac reflex which results in increased activity of preganglionic fibers of the third thoracic white ramus communicans and these responses were found to be preserved in animals with spinal cord transection (Malliani et al., 1969). Experiments in conscious cats (Ninomiya et al., 1986) sheep (Jardine et al., 2005) and dogs (Han et al., 2012) have shown that neuronal discharges of the cardiac postganglionic neurons in the stellate ganglion and CSN increase significantly

immediately after MI. Chronic stellate ganglion nerve activity (SGNA) recordings in ambulatory dogs revealed that increased neuronal excitability was observed in viable recordings for as long as 2 months and these changes were associated with increased nerve density at the stellate ganglion (Han et al., 2012).

A recent study using a porcine model of MI revealed that the spontaneous LF rhythmic firing rate of intracardiac GP neurons in the left ventricle are preserved at the same level following a MI, however, with a significant reduction in the detection of afferent inputs. These functional changes were associated with a significant increase in intracardiac neuron cell size and an upregulation in the expression of the sympathetic neuronal marker Tyrosine Hydroxylase (Rajendran et al., 2016). Future preclinical studies should investigate further whether periodic oscillations in ventricular repolarization in subjects post- MI are related to the function of intracardiac PG neurons.

Functional Significance of Cardiac Sympathetic Oscillatory Activity

The physiological meaning of sympathetic oscillatory activity remains unclear. Many studies support the notion that rhythmic activity promotes the coordination of neuronal firing of individual sympathetic neurons which may lead to a highly coordinated and more efficient release of neurotransmitter at the nerve terminal (Nilsson et al., 1985; Ando et al., 1993; Janssen et al., 1997; Lisman, 1997; Dibona and Sawin, 1999). Also, rhythmicity is believed to allow the coordination of nerve discharges between different sympathetic outflows which may help to generate integrated responses that help maintain homeostasis (Barman and Kenney, 2007).

At present, the physiological mechanisms underlying the genesis of PRD are unknown. In this review article we worked under the unverified assumption that recurrent periods of ventricular repolarization instability follow the LF rhythm of cardiac sympathetic postganglionic activity. In support of this hypothesis, *in vitro* studies conducted in fully innervated isolated rabbit hearts have shown that electrical stimulation of CSN (with a stimulation frequency of 15 Hz for 50 s) changed the spatial dispersion of repolarization (DOR) from apex toward the base to base toward the apex within 15 s following the start of the stimulation (Mantravadi et al., 2007). When sympathetic nerve stimulation was interrupted, DOR returned slowly to baseline levels and to its original direction (i.e., apex to base) after approximately 2 min. Although the dynamics of the responses obtained under these experimental conditions (50 s stimulation) make it difficult to extrapolate these results with the periodicity of PRD reported to occur every 10 s (Rizas et al., 2014, 2016), these data provide important clues about the transfer function between neurotransmitter release from the cardiac sympathetic terminals and the concomitant changes in cardiomyocyte repolarization (Mantravadi et al., 2007). Further work needs to be done using similar experimental models but providing rhythmic bursts of sympathetic stimulation to conclusively determine whether LF oscillatory cardiac sympathetic activity translates into periodic oscillations of ventricular repolarization instability.

CONCLUSION

Since Adrian et al. (1932) published their seminal study on rhythmic spontaneous bursting activity in sympathetic nerves of anesthetized animals, a considerable amount of literature has been generated describing the features, mechanisms and possible physiological implications of sympathetic rhythmic activity. However, the translational potential of this mechanism has remained obscure for almost a century.

The discovery of PRD as a novel marker of CSN traffic and strong predictor of death has recently reignited the interest in the phenomenon of sympathetic rhythmicity. The experimental evidence reviewed here identified sympathetic circuitries contained in the brainstem and in the spinal cord which may have direct connections with the ventricular myocardium and that are capable of generating LF oscillatory activity. However, the hypothesis that PRD is directly driven by sympathetic neuronal oscillations (Rizas et al., 2014, 2016) is still missing crucial pieces of evidence, specifically: (i) can postganglionic sympathetic fibers to the heart exhibit LF oscillations, in particular in conditions associated with increased cardiac sympathetic tone?, (ii) are LF sympathetic oscillations themselves pro-arrhythmogenic?, and (iii) is it the amplitude of PRD oscillations what determines its arrhythmogenic potential? The latter is particular relevant since PRD oscillations can be detected in healthy individuals and their amplitude can be increased in response to pharmacological and physiological sympathoexcitatory interventions (Rizas et al., 2014). However, physiological increases in cardiac sympathetic tone and therefore increases in the amplitude of PRD oscillations in healthy subjects do not appear to have arrhythmogenic effects. In contrast, in a cohort of post-MI patients who did not survive the 5-year follow up period, the amplitude of PRD oscillations appears to be much greater than in surviving patients (Rizas et al., 2014). This suggests that the myocardium in non-survivors is more vulnerable to the arrhythmogenic effects of sympathetic oscillatory activity. Alternatively, we speculate that in post-MI subjects with high mortality risk, increased amplitude of PRD oscillations might reflect a higher degree of synchronization among cardiac presympathetic and preganglionic neurons which would allow the recruitment of previously silent postganglionic fibers that innervate specific targets within the heart, such as the myocardium. This would result in the release of copious amounts of norepinephrine from the sympathetic terminals and perhaps the release of arrhythmogenic co-transmitters such as Neuropeptide Y (Kalla et al., 2019) which may ultimately precipitate profound periodic changes in ventricular repolarization.

AUTHOR CONTRIBUTIONS

NM designed the review and drafted the manuscript. RA contributed to the writing of the final version of the manuscript. Percentage contributions are NM 70% and RA 30%. All authors read and approved the final manuscript.

REFERENCES

Adrian, E. D., Bronk, D. W., and Phillips, G. (1932). Discharges in mammalian sympathetic nerves. *J. Physiol.* 74, 115–133. doi: 10.1113/jphysiol.1932.sp002832

Amendt, K., Czachurski, J., Dembowsky, K., and Seller, H. (1979). Bulbospinal projections to the intermediolateral cell column: a neuroanatomical study. *J. Auton. Nerv. Syst.* 1, 103–107.

Ando, S., Imaizumi, T., and Takeshita, A. (1993). Effects of patterns of sympathetic nerve stimulation on vasoconstricting responses in the hindquarter of rabbits. *J. Auton. Nerv. Syst.* 45, 225–233. doi: 10.1016/0165-1838(93)90054-x

Antzelevitch, C. (2006). Cellular basis for the repolarization waves of the ECG. *Ann. N. Y. Acad. Sci.* 1080, 268–281. doi: 10.1196/annals.1380.021

Ardell, J. L., and Armour, J. A. (2016). Neurocardiology: structure-based function. *Compr. Physiol.* 6, 1635–1653. doi: 10.1002/cphy.c150046

Ardell, J. L., Butler, C. K., Smith, F. M., Hopkins, D. A., and Armour, J. A. (1991). Activity of in vivo atrial and ventricular neurons in chronically decentralized canine hearts. *Am. J. Physiol.* 260(3 Pt 2), H713–H721. doi: 10.1152/ajpheart.1991.260.3.H713

Armour, J. A. (1997). Intrinsic cardiac neurons involved in cardiac regulation possess alpha 1-, alpha 2-, beta 1- and beta 2-adrenoceptors. *Can. J. Cardiol.* 13, 277–284.

Armour, J. A. (2004). Cardiac neuronal hierarchy in health and disease. *Am. J. Physiol. Regul. Integr. Comp. Physiol.* 287, R262–R271. doi: 10.1152/ajpregu.00183.2004

Armour, J. A., Collier, K., Kember, G., and Ardell, J. L. (1998). Differential selectivity of cardiac neurons in separate intrathoracic autonomic ganglia. *Am. J. Physiol.* 274, R939–R949. doi: 10.1152/ajpregu.1998.274.4.R939

Autenrieth, G., Surawicz, B., and Kuo, C. S. (1975). Sequence of repolarization on the ventricular surface in the dog. *Am. Heart J.* 89, 463–469. doi: 10.1016/0002-8703(75)90152-0

Barman, S. M., and Gebber, G. L. (1987). Lateral tegmental field neurons of cat medulla: a source of basal activity of ventrolateral medullospinal sympathoexcitatory neurons. *J. Neurophysiol.* 57, 1410–1424. doi: 10.1152/jn.1987.57.5.1410

Barman, S. M., and Gebber, G. L. (1993). Lateral tegmental field neurons play a permissive role in governing the 10-Hz rhythm in sympathetic nerve discharge. *Am. J. Physiol.* 265(5 Pt 2), R1006–R1013. doi: 10.1152/ajpregu.1993.265.5.R1006

Barman, S. M., and Kenney, M. J. (2007). Methods of analysis and physiological relevance of rhythms in sympathetic nerve discharge. *Clin. Exp. Pharmacol. Physiol.* 34, 350–355. doi: 10.1111/j.1440-1681.2007.04586.x

Bauer, A., Klemm, M., Rizas, K. D., Hamm, W., von Stulpnagel, L., Dommasch, M., et al. (2019). Prediction of mortality benefit based on periodic repolarisation dynamics in patients undergoing prophylactic implantation of a defibrillator: a prospective, controlled, multicentre cohort study. *Lancet* 394, 1344–1351. doi: 10.1016/S0140-6736(19)31996-8

Beaumont, E., Salavatian, S., Southerland, E. M., Vinet, A., Jacquemet, V., Armour, J. A., et al. (2013). Network interactions within the canine intrinsic cardiac nervous system: implications for reflex control of regional cardiac function. *J. Physiol.* 591, 4515–4533. doi: 10.1113/jphysiol.2013.259382

Billman, G. E., Schwartz, P. J., and Stone, H. L. (1982). Baroreceptor reflex control of heart rate: a predictor of sudden cardiac death. *Circulation* 66, 874–880. doi: 10.1161/01.cir.66.4.874

Boukens, B. J., Meijborg, V. M. F., Belterman, C. N., Opthof, T., Janse, M. J., Schuessler, R. B., et al. (2017). Local transmural action potential gradients are absent in the isolated, intact dog heart but present in the corresponding coronary-perfused wedge. *Physiol. Rep.* 5:e13251. doi: 10.14814/phy2.13251

Boukens, B. J., Sulkin, M. S., Gloschat, C. R., Ng, F. S., Vigmond, E. J., and Efimov, I. R. (2015). Transmural APD gradient synchronizes repolarization in the human left ventricular wall. *Cardiovasc. Res.* 108, 188–196. doi: 10.1093/cvr/cvv202

Brown, D. L., and Guyenet, P. G. (1985). Electrophysiological study of cardiovascular neurons in the rostral ventrolateral medulla in rats. *Circ. Res.* 56, 359–369. doi: 10.1161/01.res.56.3.359

Brunet, S., Aimond, F., Li, H., Guo, W., Eldstrom, J., Fedida, D., et al. (2004). Heterogeneous expression of repolarizing, voltage-gated K+ currents in adult mouse ventricles. *J. Physiol.* 559(Pt 1), 103–120. doi: 10.1113/jphysiol.2004.063347

Cao, J. M., Fishbein, M. C., Han, J. B., Lai, W. W., Lai, A. C., Wu, T. J., et al. (2000). Relationship between regional cardiac hyperinnervation and ventricular arrhythmia. *Circulation* 101, 1960–1969. doi: 10.1161/01.cir.101.16.1960

Chan, Y. H., Tsai, W. C., Shen, C., Han, S., Chen, L. S., Lin, S. F., et al. (2015). Subcutaneous nerve activity is more accurate than heart rate variability in estimating cardiac sympathetic tone in ambulatory dogs with myocardial infarction. *Heart Rhythm* 12, 1619–1627. doi: 10.1016/j.hrthm.2015.03.025

Charles, C. J., Jardine, D. L., Rademaker, M. T., and Richards, A. M. (2018). Systemic angiotensin II does not increase cardiac sympathetic nerve activity in normal conscious sheep. *Biosci. Rep.* 38:BSR20180513. doi: 10.1042/BSR20180513

Chung, J. M., Chung, K., and Wurster, R. D. (1975). Sympathetic preganglionic neurons of the cat spinal cord: horseradish peroxidase study. *Brain Res.* 91, 126–131. doi: 10.1016/0006-8993(75)90471-0

Chung, K., Chung, J. M., LaVelle, F. W., and Wurster, R. D. (1979). Sympathetic neurons in the cat spinal cord projecting to the stellate ganglion. *J. Comp. Neurol.* 185, 23–29. doi: 10.1002/cne.901850103

Dalsgaard, C. J., and Elfvin, L. G. (1981). The distribution of the sympathetic preganglionic neurons projecting onto the stellate ganglion of the guinea pig. A horseradish peroxidase study. *J. Auton. Nerv. Syst.* 4, 327–337. doi: 10.1016/0165-1838(81)90036-9

Day, C. P., McComb, J. M., and Campbell, R. W. (1990). QT dispersion: an indication of arrhythmia risk in patients with long QT intervals. *Br. Heart J.* 63, 342–344. doi: 10.1136/hrt.63.6.342

Dibona, G. F., and Sawin, L. L. (1999). Functional significance of the pattern of renal sympathetic nerve activation. *Am. J. Physiol.* 277, R346–R353. doi: 10.1152/ajpregu.1999.277.2.R346

Duijvenboden, S. V., Porter, B., Pueyo, E., Sampedro-Puente, D. A., Fernandez-Bes, J., Sidhu, B., et al. (2019). Complex interaction between low-frequency APD oscillations and beat-to-beat APD variability in humans is governed by the sympathetic nervous system. *Front. Physiol.* 10:1582. doi: 10.3389/fphys.2019.01582

Durrer, D., van Dam, R. T., Freud, G. E., Janse, M. J., Meijler, F. L., and Arzbaecher, R. C. (1970). Total excitation of the isolated human heart. *Circulation* 41, 899–912. doi: 10.1161/01.cir.41.6.899

Fernandez de Molina, A., and Perl, E. R. (1965). Sympathetic activity and the systemic circulation in the spinal cat. *J. Physiol.* 181, 82–102. doi: 10.1113/jphysiol.1965.sp007747

Franz, M. R., Bargheer, K., Rafflenbeul, W., Haverich, A., and Lichtlen, P. R. (1987). Monophasic action potential mapping in human subjects with normal electrocardiograms: direct evidence for the genesis of the T wave. *Circulation* 75, 379–386. doi: 10.1161/01.cir.75.2.379

Furlan, R., Porta, A., Costa, F., Tank, J., Baker, L., Schiavi, R., et al. (2000). Oscillatory patterns in sympathetic neural discharge and cardiovascular variables during orthostatic stimulus. *Circulation* 101, 886–892. doi: 10.1161/01.cir.101.8.886

Gardner, R. T., Ripplinger, C. M., Myles, R. C., and Habecker, B. A. (2016). Molecular mechanisms of sympathetic remodeling and arrhythmias. *Circ. Arrhythm. Electrophysiol.* 9:e001359. doi: 10.1161/CIRCEP.115.001359

Guyenet, P. G. (2006). The sympathetic control of blood pressure. *Nat. Rev. Neurosci.* 7, 335–346. doi: 10.1038/nrn1902

Han, S., Kobayashi, K., Joung, B., Piccirillo, G., Maruyama, M., Vinters, H. V., et al. (2012). Electroanatomic remodeling of the left stellate ganglion after myocardial infarction. *J. Am. Coll. Cardiol.* 59, 954–961. doi: 10.1016/j.jacc.2011.11.030

Hanson, B., Child, N., Van Duijvenboden, S., Orini, M., Chen, Z., Coronel, R., et al. (2014). Oscillatory behavior of ventricular action potential duration in heart failure patients at respiratory rate and low frequency. *Front. Physiol.* 5:414. doi: 10.3389/fphys.2014.00414

Hartzell, H. C. (1988). Regulation of cardiac ion channels by catecholamines, acetylcholine and second messenger systems. *Prog. Biophys. Mol. Biol.* 52, 165–247. doi: 10.1016/0079-6107(88)90014-4

Hedman, A. E., Matsukawa, K., and Ninomiya, I. (1994). Origin of cardiac-related synchronized cardiac sympathetic nerve activity in anaesthetized cats. *J. Auton. Nerv. Syst.* 47, 131–140. doi: 10.1016/0165-1838(94)90074-4

Hedman, A. E., and Ninomiya, I. (1995). Periodicity, amplitude and width of synchronized cardiac sympathetic nerve activity in anaesthetized cats. *J. Auton. Nerv. Syst.* 55, 81–91. doi: 10.1016/0165-1838(95)00031-r

Ieda, M., Kanazawa, H., Kimura, K., Hattori, F., Ieda, Y., Taniguchi, M., et al. (2007). Sema3a maintains normal heart rhythm through sympathetic innervation patterning. *Nat. Med.* 13, 604–612. doi: 10.1038/nm1570

Jakob, H., Nawrath, H., and Rupp, J. (1988). Adrenoceptor-mediated changes of action potential and force of contraction in human isolated ventricular heart muscle. *Br. J. Pharmacol.* 94, 584–590. doi: 10.1111/j.1476-5381.1988.tb11564.x

Janes, R. D., Brandys, J. C., Hopkins, D. A., Johnstone, D. E., Murphy, D. A., and Armour, J. A. (1986). Anatomy of human extrinsic cardiac nerves and ganglia. *Am. J. Cardiol.* 57, 299–309. doi: 10.1016/0002-9149(86)90908-2

Janssen, B. J., Malpas, S. C., Burke, S. L., and Head, G. A. (1997). Frequency-dependent modulation of renal blood flow by renal nerve activity in conscious rabbits. *Am. J. Physiol.* 273(2 Pt 2), R597–R608. doi: 10.1152/ajpregu.1997.273.2.R597

Jardine, D. L., Charles, C. J., Ashton, R. K., Bennett, S. I., Whitehead, M., Frampton, C. M., et al. (2005). Increased cardiac sympathetic nerve activity following acute myocardial infarction in a sheep model. *J. Physiol.* 565(Pt 1), 325–333. doi: 10.1113/jphysiol.2004.082198

Jardine, D. L., Charles, C. J., Frampton, C. M., and Richards, A. M. (2007). Cardiac sympathetic nerve activity and ventricular fibrillation during acute myocardial infarction in a conscious sheep model. *Am. J. Physiol. Heart Circ. Physiol.* 293, H433–H439. doi: 10.1152/ajpheart.01262.2006

Jardine, D. L., Charles, C. J., Melton, I. C., May, C. N., Forrester, M. D., Frampton, C. M., et al. (2002). Continual recordings of cardiac sympathetic nerve activity in conscious sheep. *Am. J. Physiol. Heart Circ. Physiol.* 282, H93–H99. doi: 10.1152/ajpheart.2002.282.1.H93

Julien, C. (2006). The enigma of Mayer waves: facts and models. *Cardiovasc. Res.* 70, 12–21. doi: 10.1016/j.cardiores.2005.11.008

Kalla, M., Hao, G., Tapoulal, N., Tomek, J., Liu, K., Woodward, L., et al. (2019). The cardiac sympathetic co-transmitter neuropeptide Y is pro-arrhythmic following ST-elevation myocardial infarction despite beta-blockade. *Eur Heart J.* doi: 10.1093/eurheartj/ehz852 [Epub ahead of print].

Kocsis, B. (1994). Basis for differential coupling between rhythmic discharges of sympathetic efferent nerves. *Am. J. Physiol.* 267(4 Pt 2), R1008–R1019. doi: 10.1152/ajpregu.1994.267.4.R1008

Kocsis, B., Gebber, G. L., Barman, S. M., and Kenney, M. J. (1990). Relationships between activity of sympathetic nerve pairs: phase and coherence. *Am. J. Physiol.* 259(3 Pt 2), R549–R560. doi: 10.1152/ajpregu.1990.259.3.R549

Kocsis, B., and Gyimesi-Pelczer, K. (1998). Spinal segments communicating resting sympathetic activity to postganglionic nerves of the stellate ganglion. *Am. J. Physiol.* 275, R400–R409. doi: 10.1152/ajpregu.1998.275.2.R400

Kollai, M., and Koizumi, K. (1980). Patterns of single unit activity in sympathetic postganglionic nerves. *J. Auton. Nerv. Syst.* 1, 305–312. doi: 10.1016/0165-1838(80)90025-9

Kumar, R., Wilders, R., Joyner, R. W., Jongsma, H. J., Verheijck, E. E., Golod, D. A., et al. (1996). Experimental model for an ectopic focus coupled to ventricular cells. *Circulation* 94, 833–841. doi: 10.1161/01.cir.94.4.833

Larsen, P. D., Lewis, C. D., Gebber, G. L., and Zhong, S. (2000). Partial spectral analysis of cardiac-related sympathetic nerve discharge. *J. Neurophysiol.* 84, 1168–1179. doi: 10.1152/jn.2000.84.3.1168

Lewis, D. I., and Coote, J. H. (1996). Evidence that the firing pattern of sympathetic preganglionic neurones is determined by an interaction between amines and an excitatory amino acid. *Boll. Soc. Ital. Biol. Sper.* 72, 279–294.

Lipski, J., Kanjhan, R., Kruszewska, B., and Rong, W. (1996). Properties of presympathetic neurones in the rostral ventrolateral medulla in the rat: an intracellular study "in vivo'. *J. Physiol.* 490(Pt 3), 729–744. doi: 10.1113/jphysiol.1996.sp021181

Lisman, J. E. (1997). Bursts as a unit of neural information: making unreliable synapses reliable. *Trends Neurosci.* 20, 38–43. doi: 10.1016/s0166-2236(96)10070-9

Logan, S. D., Pickering, A. E., Gibson, I. C., Nolan, M. F., and Spanswick, D. (1996). Electrotonic coupling between rat sympathetic preganglionic neurones in vitro. *J. Physiol.* 495(Pt 2), 491–502. doi: 10.1113/jphysiol.1996.sp021609

Lombardi, F., Della Bella, P., Casati, R., and Malliani, A. (1981). Effects of intracoronary administration of bradykinin on the impulse activity of afferent sympathetic unmyelinated fibers with left ventricular endings in the cat. *Circ. Res.* 48, 69–75. doi: 10.1161/01.res.48.1.69

Lombardi, F., Montano, N., Finocchiaro, M. L., Ruscone, T. G., Baselli, G., Cerutti, S., et al. (1990). Spectral analysis of sympathetic discharge in decerebrate cats. *J. Auton. Nerv. Syst.* 30(Suppl.), S97–S99. doi: 10.1016/0165-1838(90)90109-v

Lorentz, C. U., Alston, E. N., Belcik, T., Lindner, J. R., Giraud, G. D., and Habecker, B. A. (2010). Heterogeneous ventricular sympathetic innervation, altered beta-adrenergic receptor expression, and rhythm instability in mice lacking the p75 neurotrophin receptor. *Am. J. Physiol. Heart Circ. Physiol.* 298, H1652–H1660. doi: 10.1152/ajpheart.01128.2009

Macefield, V. G. (2013). Sympathetic microneurography. *Handb. Clin. Neurol.* 117, 353–364. doi: 10.1016/B978-0-444-53491-0.00028-6

Maling, H. M., and Moran, N. C. (1957). Ventricular arrhythmias induced by sympathomimetic amines in unanesthetized dogs following coronary artery occlusion. *Circ. Res.* 5, 409–413. doi: 10.1161/01.res.5.4.409

Malliani, A., Pagani, M., Lombardi, F., and Cerutti, S. (1991). Cardiovascular neural regulation explored in the frequency domain. *Circulation* 84, 482–492. doi: 10.1161/01.cir.84.2.482

Malliani, A., Schwartz, P. J., and Zanchetti, A. (1969). A sympathetic reflex elicited by experimental coronary occlusion. *Am. J. Physiol.* 217, 703–709. doi: 10.1152/ajplegacy.1969.217.3.703

Malpas, S. C. (1998). The rhythmicity of sympathetic nerve activity. *Prog. Neurobiol.* 56, 65–96. doi: 10.1016/s0301-0082(98)00030-6

Mantravadi, R., Gabris, B., Liu, T., Choi, B. R., de Groat, W. C., Ng, G. A., et al. (2007). Autonomic nerve stimulation reverses ventricular repolarization sequence in rabbit hearts. *Circ. Res.* 100, e72–e80. doi: 10.1161/01.RES.0000264101.06417.33

Marina, N., Abdala, A. P., Korsak, A., Simms, A. E., Allen, A. M., Paton, J. F., et al. (2011). Control of sympathetic vasomotor tone by catecholaminergic C1 neurones of the rostral ventrolateral medulla oblongata. *Cardiovasc. Res* 91, 703–710. doi: 10.1093/cvr/cvr128

Marina, N., Becker, D. L., and Gilbey, M. P. (2008). Immunohistochemical detection of connexin36 in sympathetic preganglionic and somatic motoneurons in the adult rat. *Auton. Neurosci* 139, 15–23. doi: 10.1016/j.autneu.2007.12.004

Marina, N., Taheri, M., and Gilbey, M. P. (2006). Generation of a physiological sympathetic motor rhythm in the rat following spinal application of 5-HT. *J. Physiol* 571(Pt 2), 441–450. doi: 10.1113/jphysiol.2005.100677

Martinez, D. G., Nicolau, J. C., Lage, R. L., Toschi-Dias, E., de Matos, L. D., Alves, M. J., et al. (2011). Effects of long-term exercise training on autonomic control in myocardial infarction patients. *Hypertension* 58, 1049–1056. doi: 10.1161/HYPERTENSIONAHA.111.176644

Matsukawa, K., Ninomiya, I., and Nishiura, N. (1993). Effects of anesthesia on cardiac and renal sympathetic nerve activities and plasma catecholamines. *Am. J. Physiol.* 265(4 Pt 2), R792–R797. doi: 10.1152/ajpregu.1993.265.4.R792

Meijborg, V. M., Conrath, C. E., Opthof, T., Belterman, C. N., de Bakker, J. M., and Coronel, R. (2014). Electrocardiographic T wave and its relation with ventricular repolarization along major anatomical axes. *Circ. Arrhythm. Electrophysiol.* 7, 524–531. doi: 10.1161/CIRCEP.113.001622

Montano, N., Barman, S. M., Gnecchi-Ruscone, T., Porta, A., Lombardi, F., and Malliani, A. (1995). [Role of low-frequency neuronal activity in the medulla in the regulation of the cardiovascular system]. *Cardiologia* 40, 41–46.

Montano, N., Cogliati, C., da Silva, V. J., Gnecchi-Ruscone, T., Massimini, M., Porta, A., et al. (2000). Effects of spinal section and of positive-feedback excitatory reflex on sympathetic and heart rate variability. *Hypertension* 36, 1029–1034. doi: 10.1161/01.hyp.36.6.1029

Montano, N., Furlan, R., Guzzetti, S., McAllen, R. M., and Julien, C. (2009). Analysis of sympathetic neural discharge in rats and humans. *Philos. Trans. A Math. Phys. Eng. Sci.* 367, 1265–1282. doi: 10.1098/rsta.2008.0285

Montano, N., Gnecchi-Ruscone, T., Porta, A., Lombardi, F., Malliani, A., and Barman, S. M. (1996). Presence of vasomotor and respiratory rhythms in the discharge of single medullary neurons involved in the regulation of cardiovascular system. *J. Auton. Nerv. Syst.* 57, 116–122. doi: 10.1016/0165-1838(95)00113-1

Montano, N., Lombardi, F., Gnecchi Ruscone, T., Contini, M., Finocchiaro, M. L., Baselli, G., et al. (1992). Spectral analysis of sympathetic discharge, R-R interval and systolic arterial pressure in decerebrate cats. *J. Auton. Nerv. Syst.* 40, 21–31. doi: 10.1016/0165-1838(92)90222-3

Moravec, M., and Moravec, J. (1989). Adrenergic neurons and short proprioceptive feedback loops involved in the integration of cardiac function in the rat. *Cell Tissue Res.* 258, 381–385. doi: 10.1007/bf00239458

Moravec, M., Moravec, J., and Forsgren, S. (1990). Catecholaminergic and peptidergic nerve components of intramural ganglia in the rat heart. An immunohistochemical study. *Cell Tissue Res.* 262, 315–327. doi: 10.1007/bf00309887

Morris, K. F., Nuding, S. C., Segers, L. S., Baekey, D. M., Shannon, R., Lindsey, B. G., et al. (2010). Respiratory and Mayer wave-related discharge patterns of raphe and pontine neurons change with vagotomy. *J. Appl. Physiol. (*1985) 109, 189–202. doi: 10.1152/japplphysiol.01324.2009

Myles, R. C., Wang, L., Kang, C., Bers, D. M., and Ripplinger, C. M. (2012). Local beta-adrenergic stimulation overcomes source-sink mismatch to generate focal arrhythmia. *Circ. Res.* 110, 1454–1464. doi: 10.1161/CIRCRESAHA.111.262345

Nabauer, M., Beuckelmann, D. J., Uberfuhr, P., and Steinbeck, G. (1996). Regional differences in current density and rate-dependent properties of the transient outward current in subepicardial and subendocardial myocytes of human left ventricle. *Circulation* 93, 168–177. doi: 10.1161/01.cir.93.1.168

Nilsson, H., Ljung, B., Sjoblom, N., and Wallin, B. G. (1985). The influence of the sympathetic impulse pattern on contractile responses of rat mesenteric arteries and veins. *Acta Physiol. Scand.* 123, 303–309. doi: 10.1111/j.1748-1716.1985.tb07592.x

Ninomiya, I., Akiyama, T., and Nishiura, N. (1990). Mechanism of cardiac-related synchronized cardiac sympathetic nerve activity in awake cats. *Am. J. Physiol.* 259(3 Pt 2), R499–R506. doi: 10.1152/ajpregu.1990.259.3.R499

Ninomiya, I., Malpas, S. C., Matsukawa, K., Shindo, T., and Akiyama, T. (1993). The amplitude of synchronized cardiac sympathetic nerve activity reflects the number of activated pre- and postganglionic fibers in anesthetized cats. *J. Auton. Nerv. Syst.* 45, 139–147. doi: 10.1016/0165-1838(93)90125-e

Ninomiya, I., Matsukawa, K., Honda, T., Nishiura, N., and Shirai, M. (1986). Cardiac sympathetic nerve activity and heart rate during coronary occlusion in awake cats. *Am. J. Physiol.* 251(3 Pt 2), H528–H537. doi: 10.1152/ajpheart.1986.251.3.H528

Ninomiya, I., Nishiura, N., Matsukawa, K., and Akiyama, T. (1989). Fundamental rhythm of cardiac sympathetic nerve activity in awake cats at rest and during body movement. *Jpn. J. Physiol.* 39, 743–753. doi: 10.2170/jjphysiol.39.743

Nishikawa, K., Terai, T., Morimoto, O., Yukioka, H., and Fujimori, M. (1994). Effects of intravenous lidocaine on cardiac sympathetic nerve activity and A-V conduction in halothane-anesthetized cats. *Acta Anaesthesiol. Scand.* 38, 115–120. doi: 10.1111/j.1399-6576.1994.tb03851.x

Nolan, M. F., Logan, S. D., and Spanswick, D. (1999). Electrophysiological properties of electrical synapses between rat sympathetic preganglionic neurones in vitro. *J. Physiol.* 519(Pt 3), 753–764. doi: 10.1111/j.1469-7793.1999.0753n.x

Opthof, T., Coronel, R., Wilms-Schopman, F. J., Plotnikov, A. N., Shlapakova, I. N., Danilo, P., et al. (2007). Dispersion of repolarization in canine ventricle and the electrocardiographic T wave: Tp-e interval does not reflect transmural dispersion. *Heart Rhythm* 4, 341–348. doi: 10.1016/j.hrthm.2006.11.022

Opthof, T., Remme, C. A., Jorge, E., Noriega, F., Wiegerinck, R. F., Tasiam, A., et al. (2017). Cardiac activation-repolarization patterns and ion channel expression mapping in intact isolated normal human hearts. *Heart Rhythm* 14, 265–272. doi: 10.1016/j.hrthm.2016.10.010

Pagani, M., Lombardi, F., Guzzetti, S., Rimoldi, O., Furlan, R., Pizzinelli, P., et al. (1986). Power spectral analysis of heart rate and arterial pressure variabilities as a marker of sympatho-vagal interaction in man and conscious dog. *Circ. Res.* 59, 178–193. doi: 10.1161/01.res.59.2.178

Panikkath, R., Reinier, K., Uy-Evanado, A., Teodorescu, C., Hattenhauer, J., Mariani, R., et al. (2011). Prolonged Tpeak-to-tend interval on the resting ECG is associated with increased risk of sudden cardiac death. *Circ. Arrhythm. Electrophysiol.* 4, 441–447. doi: 10.1161/CIRCEP.110.960658

Pickering, A. E., Spanswick, D., and Logan, S. D. (1994). 5-Hydoxytryptamine evokes depolarizations and membrane potential oscillations in rat sympathetic preganglionic neurones. *J. Physiol.* 480(Pt 1), 109–121. doi: 10.1113/jphysiol.1994.sp020345

Pierce, M. L., Deuchars, J., and Deuchars, S. A. (2010). Spontaneous rhythmogenic capabilities of sympathetic neuronal assemblies in the rat spinal cord slice. *Neuroscience* 170, 827–838. doi: 10.1016/j.neuroscience.2010.07.007

Poelzing, S., and Rosenbaum, D. S. (2004). Altered connexin43 expression produces arrhythmia substrate in heart failure. *Am. J. Physiol. Heart Circ. Physiol.* 287, H1762–H1770. doi: 10.1152/ajpheart.00346.2004

Pogwizd, S. M., and Bers, D. M. (2004). Cellular basis of triggered arrhythmias in heart failure. *Trends Cardiovasc. Med.* 14, 61–66. doi: 10.1016/j.tcm.2003.12.002

Pogwizd, S. M., Qi, M., Yuan, W., Samarel, A. M., and Bers, D. M. (1999). Upregulation of Na(+)/Ca(2+) exchanger expression and function in an arrhythmogenic rabbit model of heart failure. *Circ. Res.* 85, 1009–1019. doi: 10.1161/01.res.85.11.1009

Pogwizd, S. M., Schlotthauer, K., Li, L., Yuan, W., and Bers, D. M. (2001). Arrhythmogenesis and contractile dysfunction in heart failure: roles of sodium-calcium exchange, inward rectifier potassium current, and residual beta-adrenergic responsiveness. *Circ. Res.* 88, 1159–1167. doi: 10.1161/hh1101.091193

Priori, S. G., and Corr, P. B. (1990). Mechanisms underlying early and delayed afterdepolarizations induced by catecholamines. *Am. J. Physiol.* 258(6 Pt 2), H1796–H1805. doi: 10.1152/ajpheart.1990.258.6.H1796

Pueyo, E., Orini, M., Rodriguez, J. F., and Taggart, P. (2016). Interactive effect of beta-adrenergic stimulation and mechanical stretch on low-frequency oscillations of ventricular action potential duration in humans. *J. Mol. Cell. Cardiol.* 97, 93–105. doi: 10.1016/j.yjmcc.2016.05.003

Rajendran, P. S., Nakamura, K., Ajijola, O. A., Vaseghi, M., Armour, J. A., Ardell, J. L., et al. (2016). Myocardial infarction induces structural and functional remodelling of the intrinsic cardiac nervous system. *J. Physiol.* 594, 321–341. doi: 10.1113/JP271165

Rizas, K. D., Hamm, W., Kaab, S., Schmidt, G., and Bauer, A. (2016). Periodic repolarisation dynamics: a natural probe of the ventricular response to sympathetic activation. *Arrhythm. Electrophysiol. Rev.* 5, 31–36. doi: 10.15420/aer.2015:30:2

Rizas, K. D., McNitt, S., Hamm, W., Massberg, S., Kaab, S., Zareba, W., et al. (2017). Prediction of sudden and non-sudden cardiac death in post-infarction patients with reduced left ventricular ejection fraction by periodic repolarization dynamics: MADIT-II substudy. *Eur. Heart J.* 38, 2110–2118. doi: 10.1093/eurheartj/ehx161

Rizas, K. D., Nieminen, T., Barthel, P., Zurn, C. S., Kahonen, M., Viik, J., et al. (2014). Sympathetic activity-associated periodic repolarization dynamics predict mortality following myocardial infarction. *J. Clin. Invest.* 124, 1770–1780. doi: 10.1172/JCI70085

Ross, C. A., Armstrong, D. M., Ruggiero, D. A., Pickel, V. M., Joh, T. H., and Reis, D. J. (1981). Adrenaline neurons in the rostral ventrolateral medulla innervate thoracic spinal cord: a combined immunocytochemical and retrograde transport demonstration. *Neurosci. Lett.* 25, 257–262. doi: 10.1016/0304-3940(81)90401-8

Schmidt, G., Malik, M., Barthel, P., Schneider, R., Ulm, K., Rolnitzky, L., et al. (1999). Heart-rate turbulence after ventricular premature beats as a predictor of mortality after acute myocardial infarction. *Lancet* 353, 1390–1396. doi: 10.1016/s0140-6736(98)08428-1

Schreihofer, A. M., and Guyenet, P. G. (1997). Identification of C1 presympathetic neurons in rat rostral ventrolateral medulla by juxtacellular labeling in vivo. *J. Comp. Neurol.* 387, 524–536. doi: 10.1002/(sici)1096-9861(19971103)387:4<524::aid-cne4>3.0.co;2-4

Shannon, T. R., Pogwizd, S. M., and Bers, D. M. (2003). Elevated sarcoplasmic reticulum Ca2+ leak in intact ventricular myocytes from rabbits in heart failure. *Circ. Res.* 93, 592–594. doi: 10.1161/01.RES.0000093399.11734.B3

Shen, E., Wu, S. Y., and Dun, N. J. (1994). Spontaneous and transmitter-induced rhythmic activity in neonatal rat sympathetic preganglionic neurons in vitro. *J. Neurophysiol.* 71, 1197–1205. doi: 10.1152/jn.1994.71.3.1197

Smith, J. E., Jansen, A. S., Gilbey, M. P., and Loewy, A. D. (1998). CNS cell groups projecting to sympathetic outflow of tail artery: neural circuits involved in heat loss in the rat. *Brain Res.* 786, 153–164. doi: 10.1016/s0006-8993(97)01437-6

Sourioux, M., Bertrand, S. S., and Cazalets, J. R. (2018). Cholinergic-mediated coordination of rhythmic sympathetic and motor activities in the newborn rat spinal cord. *PLoS Biol.* 16:e2005460. doi: 10.1371/journal.pbio.2005460

Spanswick, D., and Logan, S. D. (1990). Spontaneous rhythmic activity in the intermediolateral cell nucleus of the neonate rat thoracolumbar spinal cord in vitro. *Neuroscience* 39, 395–403. doi: 10.1016/0306-4522(90)90276-a

Srinivasan, N. T., Orini, M., Providencia, R., Simon, R., Lowe, M., Segal, O. R., et al. (2019). Differences in the upslope of the precordial body surface ECG T wave reflect right to left dispersion of repolarization in the intact human heart. *Heart Rhythm* 16, 943–951. doi: 10.1016/j.hrthm.2018.12.006

Srinivasan, N. T., Orini, M., Simon, R. B., Providencia, R., Khan, F. Z., Segal, O. R., et al. (2016). Ventricular stimulus site influences dynamic dispersion of repolarization in the intact human heart. *Am. J. Physiol. Heart Circ. Physiol.* 311, H545–H554. doi: 10.1152/ajpheart.00159.2016

Su, C. K. (2001). Intraspinal amino acid neurotransmitter activities are involved in the generation of rhythmic sympathetic nerve discharge in newborn rat spinal cord. *Brain Res.* 904, 112–125. doi: 10.1016/s0006-8993(01)02495-7

Sun, M. K., Hackett, J. T., and Guyenet, P. G. (1988a). Sympathoexcitatory neurons of rostral ventrolateral medulla exhibit pacemaker properties in the presence of a glutamate-receptor antagonist. *Brain Res.* 438, 23–40. doi: 10.1016/0006-8993(88)91320-0

Sun, M. K., Young, B. S., Hackett, J. T., and Guyenet, P. G. (1988b). Reticulospinal pacemaker neurons of the rat rostral ventrolateral medulla with putative sympathoexcitatory function: an intracellular study in vitro. *Brain Res.* 442, 229–239. doi: 10.1016/0006-8993(88)91508-9

Tseng, W. T., Chen, R. F., Tsai, M. L., and Yen, C. T. (2009). Correlation of discharges of rostral ventrolateral medullary neurons with the low-frequency sympathetic rhythm in rats. *Neurosci. Lett.* 454, 22–27. doi: 10.1016/j.neulet.2009.02.057

Tsuchimochi, H., Matsukawa, K., Komine, H., and Murata, J. (2002). Direct measurement of cardiac sympathetic efferent nerve activity during dynamic exercise. *Am. J. Physiol. Heart Circ. Physiol.* 283, H1896–H1906. doi: 10.1152/ajpheart.00112.2002

Vaquero, M., Calvo, D., and Jalife, J. (2008). Cardiac fibrillation: from ion channels to rotors in the human heart. *Heart Rhythm* 5, 872–879. doi: 10.1016/j.hrthm.2008.02.034

Veldkamp, M. W., Verkerk, A. O., van Ginneken, A. C., Baartscheer, A., Schumacher, C., de Jonge, N., et al. (2001). Norepinephrine induces action potential prolongation and early afterdepolarizations in ventricular myocytes isolated from human end-stage failing hearts. *Eur. Heart J.* 22, 955–963. doi: 10.1053/euhj.2000.2499

Verrier, R. L., Klingenheben, T., Malik, M., El-Sherif, N., Exner, D. V., Hohnloser, S. H., et al. (2011). Microvolt T-wave alternans physiological basis, methods of measurement, and clinical utility–consensus guideline by International Society for Holter and Noninvasive Electrocardiology. *J. Am. Coll. Cardiol.* 58, 1309–1324. doi: 10.1016/j.jacc.2011.06.029

Watanabe, T., Rautaharju, P. M., and McDonald, T. F. (1985). Ventricular action potentials, ventricular extracellular potentials, and the ECG of guinea pig. *Circ. Res.* 57, 362–373. doi: 10.1161/01.res.57.3.362

Wong, C. X., Brown, A., Lau, D. H., Chugh, S. S., Albert, C. M., Kalman, J. M., et al. (2019). Epidemiology of sudden cardiac death: global and regional perspectives. *Heart Lung Circ.* 28, 6–14. doi: 10.1016/j.hlc.2018.08.026

Xie, Y., Sato, D., Garfinkel, A., Qu, Z., and Weiss, J. N. (2010). So little source, so much sink: requirements for afterdepolarizations to propagate in tissue. *Biophys. J.* 99, 1408–1415. doi: 10.1016/j.bpj.2010.06.042

Yan, G. X., Lankipalli, R. S., Burke, J. F., Musco, S., and Kowey, P. R. (2003). Ventricular repolarization components on the electrocardiogram: cellular basis and clinical significance. *J. Am. Coll. Cardiol.* 42, 401–409.

Yuan, B. X., Ardell, J. L., Hopkins, D. A., and Armour, J. A. (1993). Differential cardiac responses induced by nicotine sensitive canine atrial and ventricular neurones. *Cardiovasc. Res.* 27, 760–769. doi: 10.1093/cvr/27.5.760

Zhang, Y., Post, W. S., Blasco-Colmenares, E., Dalal, D., Tomaselli, G. F., and Guallar, E. (2011). Electrocardiographic QT interval and mortality: a meta-analysis. *Epidemiology* 22, 660–670. doi: 10.1097/EDE.0b013e318225768b

Conflict of Interest: The authors declare that the research was conducted in the absence of any commercial or financial relationships that could be construed as a potential conflict of interest.

frontiers in Physiology

PERSPECTIVE
published: 12 June 2020
doi: 10.3389/fphys.2020.00582

Autonomic Control of the Heart and Its Clinical Impact. A Personal Perspective

*Maria Teresa La Rovere[1], Alberto Porta[2,3] and Peter J. Schwartz[4]**

[1]Department of Cardiology, IRCCS Istituti Clinici Scientifici Maugeri, Montescano (Pavia), Italy, [2]Department of Biomedical Sciences for Health, University of Milan, Milan, Italy, [3]Department of Cardiothoracic, Vascular Anesthesia and Intensive Care, IRCCS Policlinico San Donato, Milan, Italy, [4]Center for Cardiac Arrhythmias of Genetic Origin and Laboratory of Cardiovascular Genetics, Istituto Auxologico Italiano, IRCCS, Milan, Italy

This essay covers several aspects of the autonomic control of the heart, all relevant to cardiovascular pathophysiology with a direct impact on clinical outcomes. Ischemic heart disease, heart failure, channelopathies, and life-threatening arrhythmias are in the picture. Beginning with an overview on some of the events that marked the oscillations in the medical interest for the autonomic nervous system, our text explores specific areas, including experimental and clinical work focused on understanding the different roles of tonic and reflex sympathetic and vagal activity. The role of the baroreceptors, not just for the direct control of circulation but also because of the clinical value of interpreting alterations (spontaneous or induced) in their function, is discussed. The importance of the autonomic nervous system for gaining insights on risk stratification and for providing specific antiarrhythmic protection is also considered. Examples are the interventions to decrease sympathetic activity and/or to increase vagal activity. The non-invasive analysis of the RR and QT intervals provides additional information. The three of us have collaborated in several studies and each of us contributes with very specific and independent areas of expertise. Here, we have focused on those areas to which we have directly contributed and hence speak with personal experience. This is not an attempt to provide a neutral and general overview on the autonomic nervous system; rather, it represents our effort to share and provide the readers with our own personal views matured after many years of research in this field.

Keywords: heart rate variability, QT interval, baroreflex sensitivity, autonomic nervous system, sympathetic nervous system, vagal activity, long QT syndrome, sudden death

OPEN ACCESS

Edited by:
Peter Taggart, University College London, United Kingdom

Reviewed by:
Ruben Coronel, University of Amsterdam, Netherlands
Mathias Baumert, The University of Adelaide, Australia
Tobias Opthof, Amsterdam University Medical Center (UMC), Netherlands

****Correspondence:***
Peter J. Schwartz
p.schwartz@auxologico.it

Specialty section:
This article was submitted to Cardiac Electrophysiology, a section of the journal Frontiers in Physiology

Received: *23 December 2019*
Accepted: *11 May 2020*
Published: *12 June 2020*

Citation:
La Rovere MT, Porta A and Schwartz PJ (2020) Autonomic Control of the Heart and Its Clinical Impact. A Personal Perspective. Front. Physiol. 11:582. doi: 10.3389/fphys.2020.00582

INTRODUCTION

One of the characteristics of the autonomic nervous system is the waxing and waning of its activity, both afferent and efferent. Similarly, the last 50 years have witnessed the waxing and waning of its interest for clinical cardiologists dealing with cardiac arrhythmias, sudden death, and heart failure.

Especially in the 1970s, but also later, much effort was devoted to the study of neural activity through the recording of single fibers in the sympathetic and vagal nerves (Malliani et al., 1969, 1973; Kunze, 1972; Cerati and Schwartz, 1991), which allowed the description

of important autonomic reflexes (Schwartz et al., 1973). In the 1970s, 1980s, and 1990s, interest for the autonomic nervous system peaked. Some investigators focused on the stimulation of nerves directed to the heart trying to derive information for potential clinical translation (Schwartz, 1985), others focused on various aspects of the analysis of heart rate, either at rest (Kleiger et al., 1987) or in response to stimuli (Billman, 2009); these analyses of tonic or reflex autonomic activity had post-myocardial infarction (post-MI) and heart failure risk stratification as one significant objective (Schwartz et al., 1992a; Mortara et al., 1997; La Rovere et al., 1998, 2003). During the last 20 years, there was a surge of interest for the possibility of modulating autonomic activity, especially the vagal one, also in chronic conditions such as heart failure (Schwartz et al., 2008a, 2015; De Ferrari et al., 2011); however, the combination of unsatisfactory results and superficial analyses (Hauptman et al., 2012; Gold et al., 2016) has somewhat cooled down these hopes. One area where clinical success has fueled interest is the one related to the prevention of life-threatening events by cardiac sympathetic denervation (Schwartz, 2014).

Here, the three of us, who have collaborated in a number of studies, present our unabashed views on some of these topics.

INITIAL OVERVIEW

The neural control of the heart is accomplished throughout a multilevel neural network within the central nervous system and peripheral extracardiac and cardiac ganglia that exert their influence *via* the sympathetic and parasympathetic nervous systems (Levy and Schwartz, 1994; Shivkumar et al., 2016). Cardiac diseases may profoundly affect central and peripheral mechanisms of neural control of cardiac function, thus resulting in maladaptive responses that may be critically involved in the progression of the disease or in the development of arrhythmias. Neural sensory information from the heart (Paintal, 1963; Schwartz et al., 1973), blood vessels, and other organs is processed at different levels within the neuraxis with a first level of integration represented by the intrinsic cardiac nervous system located in the cardiac ganglia within the heart. The intrinsic cardiac nervous system processes sensory information and provides efferent input to the myocardium under the tonic modulation of the extrinsic sympathetic and parasympathetic input. Arterial baroreceptors play a paramount role in the neural control of the cardiovascular system (Eckberg and Sleight, 1992). Arterial baroreceptors are stretch receptors embedded in the adventitia of the carotid sinus and aortic wall. Increases in arterial blood pressure will result in an increased rate of impulse firing to the nucleus tractus solitarius, which modulates sympathetic and parasympathetic output to the cardiovascular system. The baroreflex control of circulatory homeostasis occurs on a negative feedback basis. Thus, the attending reflex decrease in sympathetic activity and increase in vagal activity will reduce heart rate, cardiac contractility, and peripheral resistance. Opposite changes are associated with an arterial pressure decrease.

By complex interactions between the main neurotransmitters [namely, noradrenaline, acetylcholine, and neuropeptide Y; (Dusi et al., 2020)] and their effects on specific receptors of cardiac cells in the sinoatrial node, atrioventricular node, and left ventricle, the autonomic nervous system affects several aspects of cardiac electrophysiology. At the sinus node level, efferent vagal activity decreases while sympathetic activity increases the spontaneous depolarization rate of sinus node cells.

Furthermore, it has been known for many years that sympathetic nervous system stimulation may be pro-arrhythmic, particularly in conditions of acute myocardial ischemia (Harris et al., 1971; Schwartz and Vanoli, 1981; Janse et al., 1985; Schwartz et al., 1985), while vagal nerve stimulation may reduce the potential for lethal arrhythmias (Kent et al., 1973; Vanoli et al., 1991). Thus, by controlling the autonomic traffic to the heart, the baroreceptors are involved in the susceptibility to ventricular and supraventricular arrhythmias. Moreover, by controlling the hemodynamic adjustments to blood pressure changes, they also play a role in the clinical response to sustained rhythm disorders (De Ferrari et al., 1995; Landolina et al., 1997).

Damage to cardiac sensory nerve endings caused by acute myocardial infarction and left ventricular remodeling directly affects the baroreceptor system. The attending reflex autonomic dysfunction, characterized by reduced parasympathetic and increased sympathetic activity coupled with neural remodeling and nerve sprouting (Cao et al., 2000), promotes arrhythmogenesis.

The prominent neurohumoral mechanism at play in heart failure is the sympathetic nervous system whose increased activity coupled with vagal withdrawal is initiated by the arterial baroreflex (Hartupee and Mann, 2017). Although other mediators, including sympatho-excitatory reflexes, humoral factors, and central mechanisms (Floras and Ponikowski, 2015) contribute to the development of sympathetic-parasympathetic imbalance in heart failure, an impairment of baroreflex control of heart rate is a prominent characteristic of the heart failure syndrome and a reliable marker of the severity of the disease (Mortara et al., 1997).

Relevant insights into the pathophysiological implications of heart disease-related baroreflex impairment date back to the early 1970s when it was recognized that baroreceptor reflexes can be modulated by cardiac afferent sympathetic activity activated by mechanical and chemical stimuli (Malliani et al., 1973; Schwartz et al., 1973). An animal model provided the first evidence that reduction in cardiac parasympathetic control is associated with an increased risk for sudden death. In this canine model (Billman et al., 1982; Schwartz et al., 1984), baroreflex sensitivity (BRS) was impaired by myocardial infarction, with the greatest impairment noted in animals particularly susceptible to sudden death (Schwartz et al., 1988). Similarly in humans, a tight relationship between reduced baroreceptor activity and heart disease state was first reported by Eckberg et al. (1971) and was subsequently found to be associated with an increased risk of cardiac mortality and sudden cardiac death in post-MI and heart failure patients (Mortara et al., 1997; La Rovere et al., 1998, 2001).

The initial results with BRS led some investigators to consider the possibility that powerful baroreceptive reflex would imply that the attendant increase in vagal activity to the sinus node would extend to the ventricles as well. The high specificity of

the cardiac innervation (Pagani et al., 1974; Randall, 1984), the central organization of cardiovascular reflexes (Wurster, 1984), and the important report by Inoue and Zipes (1987) indicate clearly that such an extrapolation would be both naïve and unwarranted. Indeed, a heart-rate response indicative of increased vagal activity does not exclude the possibility of a dominant sympathetic activity at ventricular level (e.g., the diving reflex, hypoxia, and inferior myocardial ischemia). Nonetheless, the most frequent reflex response is synergistic, i.e., one limb of the autonomic nervous system is excited with simultaneous inhibition of the other (Wurster, 1984), and the reduction in heart rate produced by the baroreflex is accompanied by a reflex withdrawal of sympathetic activity that is generalized and extends to the ventricles. In the sudden death animal model that played such an important role in the development of the clinical interest for BRS (Schwartz et al., 1984), the dogs with higher BRS were also those with larger heart rate reductions during acute myocardial ischemia despite continuation of exercise (Schwartz et al., 1984). One logical implication is that the animals responding with strong vagal reflexes to blood pressure increases are likely to respond similarly to acute myocardial ischemia. The animals with the greatest sinus node response to the baroreflex test are less prone to sudden death during myocardial ischemia, and conversely, those with the most reduced BRS are more vulnerable to ventricular fibrillation. This does not mean that the baroreflex test predicts the autonomic changes at the ventricular level during myocardial ischemia but indicates that it can often predict the outcome during an ischemic episode, which is what really matters. Although, as correctly stated (Inoue and Zipes, 1987), the use of spontaneous or reflex changes in heart rate as an indicator of what might happen at the ventricular level would certainly be naive, their use to identify individuals at varying risk of life-threatening events is a rational exploitation of the current understanding of cardiovascular pathophysiology.

ASSESSMENT OF CARDIAC AUTONOMIC FUNCTION

As the baroreflex affects the balance between parasympathetic inhibition and sympathetic excitation of the sinoatrial node of the heart, sinus node activity (either spontaneous or in response to a provocation) can provide information on the underlying regulatory system.

Assessment of Arterial Baroreflex Control

Several methods have been developed so far to evaluate arterial baroreflex control in humans (La Rovere et al., 2008; Pinna et al., 2017). The reference method in clinical and research applications entails the assessment of the heart rate response to a physiological provocation (Smyth et al., 1969; La Rovere et al., 2008). In the original method, intravenous injections of small boluses of phenylephrine are used to raise blood pressure transiently, and the resultant reflex bradycardia (expressed as the following heart periods) is used as an index of BRS. A wealth of non-invasive indicators of the arterial-cardiac baroreceptor reflex sensitivity can be obtained by the joint analysis of beat-to-beat spontaneous fluctuations of systolic blood pressure and RR interval series (La Rovere et al., 2008). These methods include: model-free techniques (Robbe et al., 1987; Pinna et al., 2002), interactions among heart period and systolic arterial pressure (Porta et al., 2000; Nollo et al., 2005; Milan-Mattos et al., 2018), models searching for specific patterns of baroreflex origin (Bertinieri et al., 1985) or heart rate responses to systolic pressure changes (Bauer et al., 2010), and others merely requiring a certain degree of association between spontaneous heart period and systolic arterial pressure variations (Westerhof et al., 2004). Some methods lead to an indirect estimate of BRS *via* analysis of the bi-phasic response of the sinus node to a premature ventricular contraction (named heart rate turbulence) that is largely dependent on the baroreflex (Schmidt et al., 1999; La Rovere et al., 2011). Despite indices of baroreflex control derived from spontaneous variability cannot be considered fully equivalent to the interventional ones (Diaz and Taylor, 2006), their value in clinical setting has been proved (La Rovere et al., 2008; Pinna et al., 2017). The reliability of these non-invasive indices has been recently reviewed (Pinna et al., 2015) with special attention to their predictive value (Pinna et al., 2017).

Assessment of Heart Rate Variability

Since the seminal study by Akselrod et al. (1981), autonomic function has been non-invasively inferred from the variability of sinus RR interval obtained from surface electrocardiogram (ECG). The disappearance of RR variability after vagal blockade by high dose atropine not only proved the predominance of vagal over sympathetic cardiac modulation in humans at rest (Pomeranz et al., 1985; Montano et al., 1998) but also confirmed that RR interval variability was related to autonomic control. Indeed, in humans at rest, the primacy of the vagal versus the sympathetic drive leads to a heart rate lower than the intrinsic heart rate of the isolated heart (Jose and Collison, 1970).

The RR mean provides an indication of the tonic balance between sympathetic and vagal mean neural activities (Malik et al., 2019b), while the magnitude of the RR variations about its mean is linked to the balance of the spontaneous variations of vagal and sympathetic neural activities about their correspondent means, usually referred to as vagal and sympathetic modulations (Task Force of the European Society of Cardiology and the North American Society of Pacing and Electrophysiology, 1996; Pagani et al., 1997; Bauer et al., 2017; Malik et al., 2019a). A number of techniques have been developed to quantify the RR interval variability in order to evaluate cardiac autonomic regulation. The measurement of RR interval variability was initially based on simple statistics, such as the standard deviation of RR interval variation and its derivative, and on power spectral analysis that separates and quantifies the various oscillations that exist in the RR interval signal. At variance with the conventional measures of RR interval variability, complexity markers and fractal measures of HRV account for the inherent irregularity, long range correlation, and scale invariance of the spontaneous fluctuations of RR interval (Goldberger, 1996; Porta et al., 2009).

It has been recently stressed that RR variability markers might be biased proxies of autonomic modulation as a result

of the nonlinear relation between mean RR and magnitude of RR changes (Opthof et al., 1984; Boyett et al., 2019; Malik et al., 2019a). The rate-dependency of RR variability markers is the consequence of the direct effect of acetylcholine concentration on the diastolic depolarization rate of the sinus node pacemaker cells producing larger variations of the cycle length if the cycle length is longer (Zaza and Lombardi, 2001). This relation might limit the value of RR variability markers expressed in absolute units because an augmented modulation of the autonomic activity increases RR variability indices but a greater fluctuations of RR might be simply a consequence of bradycardia, regardless of whether it is of autonomic origin or due to modifications of the properties of sinus node pacemaker cells [e.g., I_f modifications; Zaza and Lombardi, (2001); Da Silva et al. (2015); Boyett et al. (2019)]. Since this effect is the mere consequence of the sinus node transduction process, it could affect any marker based on RR changes including BRS. Therefore, the possibility of interpreting RR variability markers as proxies of autonomic modulation is fully preserved as long as the compared populations and/or experimental conditions exhibit the same RR mean. Alternatively, it was suggested to use RR variability indices that feature an intrinsic normalization (Zaza and Lombardi, 2001; Da Silva et al., 2015). Among those indices, normalized high frequency (HF) powers and the low frequency (LF)/HF ratio can be exploited (Pagani et al., 1997). Especially whether the RR mean varies among groups and experimental conditions and, thus, the genuine role of an altered neural modulation is not warranted, it is recommended to check for the potential variations of the LF/HF ratio before concluding that RR variability indices expressed in absolute units indicate modifications of the autonomic control.

Concurrent Assessment of RR and QT Variability

The difficulty in the assessment of the sympathetic modulation from RR variability is a direct consequence of the vagal nature of the spontaneous fluctuations of RR (Eckberg, 1997), especially when the magnitude of the RR changes is assessed in absolute units (Montano et al., 1994). This observation, in association with the clinical importance of the non-invasive inference of cardiac sympathetic modulation, has led to search for possible alternatives, still obtained from the ECG, to the sole analysis of RR variability.

An important one, in our opinion, is the study of the QT interval variability (Malik, 2008; Berger, 2009; Baumert et al., 2016). Its interest lies in the fact that the amplitude of the QT changes has been related to the magnitude of sympathetic control. Indeed, the higher the sympathetic drive and its variations about its mean value such as during an orthostatic challenge, mental stress, or advanced age, the greater the magnitude of the QT variations in healthy individuals (Negoescu et al., 1997; Porta et al., 1998a, 2010, 2011; Yeragani et al., 2000a; Piccirillo et al., 2001, 2006; Boettger et al., 2010; Baumert et al., 2016; El-Hamad et al., 2019). This link holds even in pathological conditions characterized by a high sympathetic drive (Berger et al., 1997; Yeragani et al., 2000b; Bär et al., 2007; Baumert et al., 2008, 2011) and provides new clues for stratifying the risk of arrhythmic events (Atiga et al., 1998; Piccirillo et al., 2007; Segerson et al., 2008; Chen et al., 2011; Dobson et al., 2011; Oosterhoff et al., 2011; Tereshchenko et al., 2012; Porta et al., 2015).

These observations suggested a possible strategy to separately quantify vagal and sympathetic modulations in humans *via* the concomitant analysis of RR and QT variabilities (Porta et al., 2015). Vagal modulation is inferred from the respiratory sinus arrhythmia, namely the portion of the RR variability in the HF (from 0.15 to 0.5 Hz) band (Hirsch and Bishop, 1981; Pomeranz et al., 1985). Sympathetic modulation is inferred from the power of the QT variability in the LF (from 0.04 to 0.15 Hz) band (Porta et al., 2011; Baumert et al., 2016). This choice is more robust than the mere exploitation of the QT variance because it prevents the bias produced by non-autonomic influences such as cardiac axis movements leading to periodical artifacts which would affect the QT measurement at the respiratory rate (Lombardi et al., 1996; Porta et al., 1998b). The interpretation of QT variability markers is made more complex by the QT-RR relation (Bazett, 1920), which mirrors on the surface ECG the adaptation of action potential duration to the cycle length observed at the cellular level (Conrath and Opthof, 2006), and by the influences of the autonomic nervous system on the QT-RR relation (Zaza et al., 1991; Porta et al., 1998a; Magnano et al., 2002). Modeling approaches can describe the dynamic dependence of QT on previous RR variations (Zaza et al., 1991; Porta et al., 1998a, 2010) and even account for confounding factors such as respiration (Porta et al., 2017). Alternative approaches excluding the influences of cardiac neural control directed to the sinus node on the regulation of the QT dynamics and preventing the need of hypothesizing any *a priori* defined, and arbitrary, QT-RR relation (Pueyo et al., 2004) are based on gating the QT variability analysis at similar RR mean (Browne et al., 1983) or on the normalization of QT variability markers to the magnitude of RR changes (Berger et al., 1997; Baumert et al., 2016).

Complexity of the Cardiac Autonomic Control

Complexity analysis is an additional approach for the assessment of cardiac control with an inherent normalization given that it is fully independent of the amplitude of spontaneous RR and QT changes (Pincus and Goldberger, 1994; Porta et al., 2009). Under normal conditions, the simultaneous action of multiple regulatory mechanisms operating with slightly different frequencies within the LF and HF bands produces irregular changes of RR and QT intervals. Disease and aging impair the sinus node responsiveness and decrease the level of irregularity of the RR and QT beat-to-beat dynamics (Goldberger, 1996). Complexity analyses of RR and QT variabilities provide non-redundant information. Indeed, the larger irregularity of the QT variability compared to that of the RR variability points to the greater complexity of the neural control directed to the ventricles than that to the sinus node (Inoue and Zipes, 1987; Lewis and Short, 2007; Baumert et al., 2012; Bari et al., 2014a). The decreased complexity of the RR variability during vagal withdrawal and sympathetic activation induced by orthostatic challenge (Porta et al., 2007; Turianikova et al., 2011; Baumert et al., 2014)

is interpreted as a consequence of the reduction of the respiratory sinus arrhythmia and of the increase of a dominant LF component limiting the spectral content of the RR variability series (Porta et al., 2012). Therefore, complexity indices derived from RR variability are mainly under vagal control (Porta et al., 2012). Indeed, low-pass filtering approach canceling respiratory sinus arrhythmia from the RR variability prevented the increase of RR variability complexity during nighttime and under β-blockers (Bari et al., 2014a). At difference with the complexity of RR variability, the complexity of the QT variability in healthy individuals during orthostatic challenge and in pathological populations featuring a dominant sympathetic drive remains high (Baumert et al., 2014; Li et al., 2019) or even increases (Sosnowski et al., 2001; Nahshoni et al., 2004; Porta et al., 2010; Li et al., 2015) compared to basal condition or control subjects. Senescence in a healthy population is accompanied by an increase of QT variability complexity (Boettger et al., 2010). The dynamics of QT variability become more irregular during sympathetic activation due to the prevailing action of inputs driving QT independently of RR changes (Porta et al., 2010). The decrease of the T-wave amplitude with sympathetic activation is likely to play a role in increasing the beat-to-beat irregularity of QT by making the process of delineation of the T-wave offset more difficult (Baumert et al., 2016). Therefore, the complexity of the QT variability could largely represent the sympathetic control directed to the ventricles, largely unrelated to the cardiac autonomic regulation impinging on the sinus node. We suggested that a limited complexity of the QT variability might be protective against arrhythmic risk (Bari et al., 2014a,b).

RISK STRATIFICATION

Effective risk stratification for patients who might develop life-threatening ventricular arrhythmia and sudden cardiac death is one of the main unsolved areas in clinical cardiology. Arrhythmic risk represents the sum of several different risk-augmenting processes and factors. Understanding the relation between changes in autonomic activity and cardiac electrophysiological properties has led to the view that the autonomic nervous system modulates interactions between triggering factors and the underlying electrophysiologic substrate. This points to a significant potential prognostic value of markers of autonomic activity.

Since the 1990s, the analysis of BRS has been considered as a tool that might help identifying "high-risk" patients. A multicenter study on more than 1,200 post-infarction patients demonstrated the incremental prognostic value provided by an impaired BRS when combined to left ventricular ejection function and to the potential trigger of non-sustained ventricular tachycardia (La Rovere et al., 1998, 2001). Specifically, a depressed BRS, a reduced left ventricular ejection fraction, and the presence of non-sustained ventricular tachycardia were all independent predictors of mortality, but depressed BRS almost doubled the risk of death provided by the other two markers. Moreover, among patients with either reduced or preserved left ventricular function but without signs of electrical instability, mortality differed significantly according to the presence or absence of preserved autonomic function (La Rovere et al., 2001; De Ferrari et al., 2007).

The role of baroreflex-mediated responses in the control of hemodynamic stability is particularly relevant during the course of a sustained ventricular rhythm. Inadequate baroreflex-mediated sympatho-excitation during a sustained ventricular tachycardia in post-infarction patients was the leading cause of an unfavorable hemodynamic profile leading to circulatory collapse (Landolina et al., 1997).

Randomized trials, demonstrating that among post-infarction patients mortality can be effectively reduced by prophylactic implantation of a cardioverter defibrillator, established a paradigm shift in risk stratification through the assessment of left ventricular ejection fraction as the gold standard risk predictor. However, this does not deprive autonomic markers of their clinical value (Wellens et al., 2014). It is now clear that left ventricular ejection fraction measurement has both limited sensitivity and specificity as a tool for arrhythmic risk stratification and that the field of risk stratification should move from the "high-risk ejection fraction" to the broader concept of the "high-risk patients" (Chugh, 2017). This transition implies a novel opportunity for autonomic markers to be re-evaluated in their involvement in the pathogenesis of arrhythmic risk and incorporated in novel prediction models. Moreover, novel ECG-based risk markers that quantify sympathetic activity-associated repolarization instabilities are promising in their ability to guide decisions about the prophylactic implantation of a cardioverter defibrillator (Bauer et al., 2019). The markers tested by Bauer et al. (2019) are framed in an emerging area of biomedical signal processing aiming at monitoring relevant electrocardiographic fiducial points and time intervals under the hypothesis such that their evolution over time might provide information about cardiac control.

In a founder population of long QT syndrome type 1 (LQT1), which avoids the confounding factors due to different mutations and segregates the malignant *KCNQ1*-A341V mutation (Brink et al., 2005; Crotti et al., 2007; Brink and Schwartz, 2009), the characterization of cardiac autonomic control and baroreflex function was found to be useful to improve the risk stratification of arrhythmic events (Schwartz et al., 2008b; Crotti et al., 2012; Bari et al., 2014a,b, 2015; Porta et al., 2015). In this population which is at the highest risk of fatal events in situations of high sympathetic drive (Schwartz et al., 2001), it was found that subjects who did not experience arrhythmic events, namely the asymptomatic mutation-carriers, have a completely different autonomic profile compared to those experiencing syncope or cardiac arrest requiring resuscitation. Indeed, asymptomatic individuals exhibited longer RR (Schwartz et al., 2008b), lower BRS (Schwartz et al., 2008b), higher QT variability in the LF band during daytime (Porta et al., 2015), lower respiratory sinus arrhythmia during nighttime and under β-blockers (Porta et al., 2015), slower heart rate recovery after exercise test (Crotti et al., 2012), and lower QT variability complexity (Bari et al., 2014a,b, 2015). These findings suggested that, besides RR lengthening, the combination of a more reactive sympathetic drive to the ventricles (i.e., adapting more rapidly QT to RR changes and limiting irregularity of QT changes during a

sympathetic stressor) and of a sluggish vagal responsiveness after exercise represents a protective mechanism. Remarkably, non-mutation carriers belonging to the same family line (Brink et al., 2005; Brink and Schwartz, 2009) have an autonomic profile more similar to symptomatic patients than asymptomatic ones, thus suggesting that there are peculiar traits of the autonomic control that might be key for survival because they reduce the severity of the disease (Schwartz et al., 2008b; Porta et al., 2015).

NEUROMODULATION

Vagal Neuromodulation

One relevant aspect of several abnormalities related to the baroreceptors and autonomic nervous system pathophysiology is that they are often correctable by treatment. While β-blockers are the mainstay in the management of autonomic imbalance, device technology and advances in neuromodulatory techniques paved the way to directly target the autonomic nervous system. Baroreflex activation therapy (BAT), providing chronic baroreflex activation through electrical stimulation of the carotid sinus, has been initially developed for the treatment of resistant hypertension. Clinical studies have underlined the potential of BAT to improve blood pressure control and reduce the need of anti-hypertensive therapy at cost of few side effects despite the invasiveness of the procedure (Bolignano and Coppolino, 2018). BAT is currently being evaluated in heart failure with reduced ejection fraction. Initial studies support the hypothesis that baroreflex activation can add significant therapeutic benefit on top of guideline-directed medical therapy in patients with advanced heart failure. A randomized controlled trial (the BeAT-HF trial) is actively recruiting an estimated sample size of 480 patients with New York Heart Association functional class II heart failure but excluding patients actively receiving cardiac resynchronization therapy; its completion is expected by April 2021 (Mann and Abraham, 2019).

Experimental studies in an established conscious canine model of post-MI sudden cardiac death (Schwartz et al., 1984) demonstrated that vagus nerve stimulation (VNS) was effective in preventing ventricular fibrillation induced by acute myocardial ischemia (Vanoli et al., 1991). The initially promising translation of animal studies to the clinical setting of patients with HF and reduced ejection fraction (Schwartz et al., 2008a; De Ferrari et al., 2011) did not show consistent results in randomized trials (Zannad et al., 2015; Gold et al., 2016). In the debate following these studies, several critical issues (patient selection, proper titration of VNS therapy, effective markers for therapy, and pattern of vagal fibers stimulation) have been identified that would require further assessment.

Transcutaneous electrical stimulation of the auricular branch of the vagus nerve located at the tragus, which is effective in stimulating afferent vagal nerve fibers, has been suggested to represent an alternative access path to the same neuronal network without invasiveness and common side effects including hoarseness, sore throat, shortness of breath, and coughing, even though it is likely to lead to a smaller release of ACh compared to direct vagal efferent stimulation. In a study based on spontaneous variability, in young healthy subjects, transcutaneous VNS acutely reduced resting heart rate and the response to orthostatic stress (Tobaldini et al., 2019). Transcutaneous VNS is being studied for a number of pathological conditions including ventricular arrhythmias, heart failure, and myocardial infarction. Experimental and clinical data recently suggested that chronic intermittent VNS lasting 2 h/day for 2 months reduced inducibility of ventricular arrhythmias (Zhu et al., 2019).

Sympathetic Neuromodulation

The fact that acute myocardial ischemia is often associated with life-threatening arrhythmias was recognized from the early days (Harris et al., 1971). When it was shown that acute myocardial ischemia also elicits a powerful excitatory sympathetic reflex within seconds (Malliani et al., 1969), thus increasing the release of norepinephrine at the ventricular level, the link was established. One obvious consequence was the rationale for the use of β-adrenergic blocking agents to prevent cardiac arrhythmias in ischemic heart disease. Another consequence was the concept that if arrhythmias are triggered by an abrupt release of norepinephrine, the section of the nerves mediating this release might have had a protective effect (Schwartz, 2014).

Given the quantitative dominance of the left sided cardiac sympathetic nerves at the ventricular level, the interest went immediately to the potential effects of left cardiac sympathetic denervation (LCSD). Thus, a series of experiments, mostly performed in the 1970s, provided the necessary information. It was shown that LCSD prevents arrhythmias associated with acute myocardial ischemia in normal hearts (Schwartz et al., 1976b) and in hearts with a healed myocardial infarction (Schwartz and Stone, 1980), that it does not impair cardiovascular performance during exercise (Schwartz and Stone, 1979), that it does increase the capability of the coronary bed to dilate (Schwartz and Stone, 1977), and that it does not cause denervation supersensitivity (Schwartz and Stone, 1982). However, the most important effect in terms of clinical relevance is the increase produced by LCSD on the threshold for ventricular fibrillation (Schwartz et al., 1976a). This makes it less likely that a heart will fibrillate and, together with the overall reduction in the norepinephrine release, constitutes the primary rationale for the use of LCSD in several conditions in which the risk for ventricular fibrillation is high.

The evidence for a powerful antifibrillatory effect of LCSD is now firmly established (Schwartz, 2014) and has been observed at clinical level in three different sets of patients: post-MI patients at high risk for sudden death (Schwartz et al., 1992b), long QT syndrome patients (Schwartz et al., 2004), and patients with catecholamine polymorphic ventricular tachycardia (CPVT) syndrome (De Ferrari et al., 2015). Whenever there is a recurrence after LCSD, which is not common for LQTS and CPVT patients, it is reasonable to perform right cardiac sympathetic denervation as well, as we started to do in the 1990s (Schwartz et al., 1991, 2004). There are growing data suggesting that bilateral cardiac sympathetic denervation can be useful in patients with recurrent ventricular tachycardia related to either ischemic heart disease or dilated cardiomyopathy (Vaseghi et al., 2014). Different views exist on the timing for ablating the right cardiac sympathetic nerves; namely, whether together with the left or just in case

of failure of unilateral left cardiac sympathetic denervation. Our view is to follow the time-honored precepts of medicine which suggest to begin by the lowest effective dose and to increase it whenever this fails. An implication is that for a number of patients, unilateral left cardiac sympathetic denervation will be sufficient (Schwartz, 2014).

Overall, it is now clear that cardiac sympathetic denervation can save lives while preserving adequate quality of life (Antiel et al., 2016; Schwartz, 2016) and that there is not always the need to rush toward an implantable cardioverter defibrillator.

Renal Denervation

Renal sympathetic nerve activity plays a crucial role in the control of cardiovascular homeostasis and is involved not only in the pathogenesis of hypertension but also in other cardiovascular processes such as heart failure, and perhaps cardiac arrhythmias. Renal afferent and efferent nerves function in a reflex loop where afferent input from the kidney to the central nervous system is integrated with inputs from other neural reflexes to determine the level of sympathetic outflow to individual organs. Renal denervation (RDN) as a method of modulating sympathetic activity by interrupting afferent and efferent sympathetic nerve signaling appears to be an attractive therapeutic target in patients with cardiovascular disease triggered by sympathetic overactivity such as hypertension, heart failure, and – according to some – even atrial or ventricular arrhythmias. RDN has been initially introduced to reduce blood pressure in subjects with resistant hypertension (Mahfoud et al., 2013). While initial clinical trial results failed to reach a consensus on the efficacy of RDN in this context (Bhatt et al., 2014), three subsequent sham-controlled studies that were carefully designed and rigorously conducted have shown that RDN significantly reduces blood pressure regardless of the use of antihypertensive drugs (Townsend et al., 2017; Azizi et al., 2018; Kandzari et al., 2018). Notably, the use of multi-electrode catheter and more ablations per artery have definitely improved the RDN procedure in the more recent studies that also took into account the distribution of the sympathetic nerves among the renal arteries.

Clinical implications of RDN are well beyond blood pressure control. Interestingly, a recent meta-analysis including 17 studies revealed that RDN improved a number of cardiovascular markers of organ damage including left ventricular mass index, central augmentation index, and carotid-femoral pulse wave velocity independent of blood pressure (Kordalis et al., 2018). Moreover, several clinical RDN studies report beneficial effects on ventricular and supraventricular arrhythmias (Ukena et al., 2012; Pokushalov et al., 2014). In the recently reported ERADICATE-AF trial that randomized 302 patients with paroxysmal atrial fibrillation and hypertension, RDN added to catheter ablation, compared with catheter ablation alone, significantly increased the likelihood of freedom from atrial fibrillation at 12 months (Steinberg et al., 2020). While we report these studies and their claims, we cannot help expressing a certain degree of skepticism on the rationale by which RD should provide protection against life-threatening cardiac arrhythmias. The underlying concept seems to be that reduction or elimination of renal afferent would decrease the efferent sympathetic activity directed to the heart, which is mediated by the stellate ganglia. We find it difficult to conceive how this "reduction" could be greater than that produced by the direct section of these nerves, as it is produced by the cardiac sympathetic denervation performed by removing the lower half of the stellate ganglion/ganglia with the first four thoracic ganglia.

RDN has been reported to exert beneficial effects on cardiac function and remodeling in animal models of heart failure (Sharp et al., 2018), but the results in patients are largely inconsistent due in part to limited power with small sample sizes. In a meta-analysis including two controlled (80 patients) and two uncontrolled studies (21 patients) (Fukuta et al., 2017), 6 months after RDN, there was a greater increase in left ventricular ejection fraction and a greater decrease in left ventricular end-diastolic diameter in the RDN group than in the control group. No serious adverse events such as acute renal artery stenosis and dissection occurred.

CONCLUSIONS

A paper like this one does not really need a traditional conclusion, which would merely be a pale summary of what has been a serious effort to share with the interested reader our experience and our views. Our hope is that more and more young investigators will be attracted by this fascinating field of research, which is endowed with so many areas of clinical relevance.

AUTHOR CONTRIBUTIONS

PS, AP, and MR contributed to the conception and design of research, drafted the manuscript, edited and revised critically the manuscript, and approved the final version of the manuscript.

ACKNOWLEDGMENTS

The authors are grateful to Pinuccia De Tomasi for expert editorial support.

REFERENCES

Akselrod, S., Gordon, D., Ubel, F. A., Shannon, D. C., Berger, A. C., and Cohen, R. J. (1981). Power spectrum analysis of heart rate fluctuation: a quantitative probe of beat-to-beat cardiovascular control. *Science* 213, 220–222. doi: 10.1126/science.6166045

Antiel, R. M., Bos, J. M., Joyce, D. D., Owen, H. J., Roskos, P. L., Moir, C., et al. (2016). Quality of life after videoscopic left cardiac sympathetic denervation in patients with potentially life-threatening cardiac channelopathies/cardiomyopathies. *Heart Rhythm.* 13, 62–69. doi: 10.1016/j.hrthm.2015.09.001

Atiga, W. L., Calkins, H., Lawrence, J. H., Tomaselli, G. F., Smith, J. M., and Berger, R. D. (1998). Beat-to-beat repolarization lability identifies patients

at risk for sudden cardiac death. *J. Cardiovasc. Electrophysiol.* 9, 899–908. doi: 10.1111/j.1540-8167.1998.tb00130.x

Azizi, M., Schmieder, R. E., Mahfoud, F., Weber, M. A., Daemen, J., Davies, J., et al. (2018). Endovascular ultrasound renal denervation to treat hypertension (RADIANCE-HTN SOLO): a multicentre, international, single-blind, randomised, sham-controlled trial. *Lancet* 391, 2335–2345. doi: 10.1016/S0140-6736(18)31082-1

Bär, K.-J., Koschke, M., Boettger, M. K., Berger, S., Kabisch, A., Sauer, H., et al. (2007). Acute psychosis leads to increased QT variability in patients suffering from schizophrenia. *Schizophr. Res.* 95, 115–123. doi: 10.1016/j.schres.2007.05.034

Bari, V., Girardengo, G., Marchi, A., De Maria, B., Brink, P. A., Crotti, L., et al. (2015). A refined multiscale self-entropy approach for the assessment of cardiac control complexity: application to long QT syndrome type 1 patients. *Entropy* 17, 7768–7785. doi: 10.3390/e17117768

Bari, V., Marchi, A., De Maria, B., Girardengo, G., George, A. L., Brink, P. A., et al. (2014a). Low-pass filtering approach via empirical mode decomposition improves short-scale entropy-based complexity estimation of QT interval variability in long QT syndrome type 1 patients. *Entropy* 16, 4839–4854. doi: 10.3390/e16094839

Bari, V., Valencia, J. F., Vallverdú, M., Girardengo, G., Marchi, A., Bassani, T., et al. (2014b). Multiscale complexity analysis of the cardiac control identifies asymptomatic and symptomatic patients in long QT syndrome type 1. *PLoS One* 9:e93808. doi: 10.1371/journal.pone.0093808

Bauer, A., Camm, A. J., Cerutti, S., Guzik, P., Huikuri, H., Lombardi, F., et al. (2017). Reference values of heart rate variability. *Heart Rhythm.* 14, 302–303. doi: 10.1016/j.hrthm.2016.12.015

Bauer, A., Klemm, M., Rizas, K. D., Hamm, W., von Stülpnagel, L., Dommasch, M., et al. (2019). Prediction of mortality benefit based on periodic repolarisation dynamics in patients undergoing prophylactic implantation of a defibrillator: a prospective, controlled, multicentre cohort study. *Lancet* 394, 1344–1351. doi: 10.1016/S0140-6736(19)31996-8

Bauer, A., Morley-Davies, A., Barthel, P., Muller, A., Ulm, K., Malik, M., et al. (2010). Bivariate phase-rectified signal averaging for assessment of spontaneous baroreflex sensitivity: pilot study of the technology. *J. Electrocardiol.* 43, 649–653. doi: 10.1016/j.jelectrocard.2010.05.012

Baumert, M., Czippelova, B., Ganesan, A., Schmidt, M., Zaunseder, S., and Javorka, M. (2014). Entropy analysis of RR and QT interval variability during orthostatic and mental stress in healthy subjects. *Entropy* 16, 6384–6393. doi: 10.3390/e16126384

Baumert, M., Javorka, M., Seeck, A., Faber, R., Sanders, P., and Voss, A. (2012). Multiscale entropy and detrended fluctuation analysis of QT interval and heart rate variability during normal pregnancy. *Comput. Biol. Med.* 42, 347–352. doi: 10.1016/j.compbiomed.2011.03.019

Baumert, M., Lambert, G. W., Dawood, T., Lambert, E. A., Esler, M. D., McGrane, M., et al. (2008). QT interval variability and cardiac norepinephrine spillover in patients with depression and panic disorder. *Am. J. Phys.* 295, H962–H968. doi: 10.1152/ajpheart.00301.2008

Baumert, M., Porta, A., Vos, M. A., Malik, M., Couderc, J.-P., Laguna, P., et al. (2016). QT interval variability in body surface ECG: measurement, physiological basis, and clinical value: position statement and consensus guidance endorsed by the European Heart Rhythm Association jointly with the ESC Working Group on cardiac cellular electrophsiology. *Europace* 18, 925–944. doi: 10.1093/europace/euv405

Baumert, M., Schlaich, M. P., Nalivaiko, E., Lambert, E., Sari, C. I., Kaye, D. M., et al. (2011). Relation between QT interval variability and cardiac sympathetic activity in hypertension. *Am. J. Phys.* 300, H1412–H1427. doi: 10.1152/ajpheart.01184.2010

Bazett, H. C. (1920). An analysis of the time-relations of electrocardiograms. *Heart* 7, 353–370.

Berger, R. D. (2009). QT interval variability is it a measure of autonomic activity? *J. Am. Coll. Cardiol.* 54, 851–852. doi: 10.1016/j.jacc.2009.06.007

Berger, R. D., Kasper, E. K., Baughman, K. L., Marban, E., Calkins, H., and Tomaselli, G. F. (1997). Beat-to-beat QT interval variability: novel evidence for repolarization lability in ischemic and nonischemic dilated cardiomyopathy. *Circulation* 96, 1557–1565. doi: 10.1161/01.CIR.96.5.1557

Bertinieri, G., di Rienzo, M., Cavallazzi, A., Ferrari, A. U., Pedotti, A., and Mancia, G. (1985). A new approach to analysis of the arterial baroreflex. *J. Hypertens.* 3, S79–S81.

Bhatt, D. L., Kandzari, D. E., O'Neill, W. W., D'Agostino, R., Flack, J. M., Katzen, B. T., et al. (2014). A controlled trial of renal denervation for resistant hypertension. *N. Engl. J. Med.* 370, 1393–1401. doi: 10.1056/NEJMoa1402670

Billman, G. E. (2009). Cardiac autonomic neural remodeling and susceptibility to sudden cardiac death: effect of endurance exercise training. *Am. J. Phys.* 297, H1171–H1193. doi: 10.1152/ajpheart.00534.2009

Billman, G. E., Schwartz, P. J., and Stone, H. L. (1982). Baroreceptor reflex control of heart rate: a predictor of sudden cardiac death. *Circulation* 66, 874–880. doi: 10.1161/01.CIR.66.4.874

Boettger, M. K., Schulz, S., Berger, S., Tancer, M., Yeragani, V. K., Voss, A., et al. (2010). Influence of age on linear and nonlinear measures of autonomic cardiovascular modulation. *Ann. Noninvasive Electrocardiol.* 15, 165–174. doi: 10.1111/j.1542-474X.2010.00358.x

Bolignano, D., and Coppolino, G. (2018). Baroreflex stimulation for treating resistant hypertension: ready for the prime-time? *Rev. Cardiovasc. Med.* 19, 89–95. doi: 10.31083/j.rcm.2018.03.3185

Boyett, M., Wang, Y., and D'Souza, A. (2019). CrossTalk opposing view: heart rate variability as a measure of cardiac autonomic responsiveness is fundamentally flawed. *J. Physiol.* 597, 2599–2601. doi: 10.1113/JP277501

Brink, P. A., Crotti, L., Corfield, V., Goosen, A., Durrheim, G., Hedley, P., et al. (2005). Phenotypic variability and unusual clinical severity of congenital long-QT syndrome in a founder population. *Circulation* 112, 2602–2610. doi: 10.1161/CIRCULATIONAHA.105.572453

Brink, P. A., and Schwartz, P. J. (2009). Of founder populations, long QT syndrome, and destiny. *Heart Rhythm.* 6, S25–S33. doi: 10.1016/j.hrthm.2009.08.036

Browne, K. F., Prystowsky, E., Heger, J. J., Chilson, D. A., and Zipes, D. P. (1983). Prolongation of the Q-T interval in man during sleep. *Am. J. Cardiol.* 52, 55–59. doi: 10.1016/0002-9149(83)90068-1

Cao, J. M., Chen, L. S., KenKnight, B. H., Ohara, T., Lee, M. H., Tsai, J., et al. (2000). Nerve sprouting and sudden cardiac death. *Circ. Res.* 86, 816–821. doi: 10.1161/01.RES.86.7.816

Cerati, D., and Schwartz, P. J. (1991). Single cardiac vagal fiber activity, acute myocardial ischemia, and risk for sudden death. *Circ. Res.* 69, 1389–1401. doi: 10.1161/01.RES.69.5.1389

Chen, X., Hu, Y., Fetics, B. J., Berger, R. D., and Trayanova, N. A. (2011). Unstable QT interval dynamics precedes ventricular tachycardia onset in patients with acute myocardial infarction: a novel approach to detect instability in QT interval dynamics from clinical ECG. *Circ. Arrhythm. Electrophysiol.* 4, 858–866. doi: 10.1161/CIRCEP.110.961763

Chugh, S. S. (2017). Sudden cardiac death in 2017: spotlight on prediction and prevention. *Int. J. Cardiol.* 237, 2–5. doi: 10.1016/j.ijcard.2017.03.086

Conrath, C. E., and Opthof, T. (2006). Ventricular repolarization: an overview of (patho)physiology, sympathetic effects and genetic aspects. *Prog. Biophys. Mol. Biol.* 92, 269–307. doi: 10.1016/j.pbiomolbio.2005.05.009

Crotti, L., Spazzolini, C., Porretta, A. P., Dagradi, F., Taravelli, E., Petracci, B., et al. (2012). Vagal reflexes following an exercise stress test: a simple clinical tool for gene-specific risk stratification in the long QT syndrome. *J. Am. Coll. Cardiol.* 60, 2515–2524. doi: 10.1016/j.jacc.2012.08.1009

Crotti, L., Spazzolini, C., Schwartz, P. J., Shimizu, W., Denjoy, I., Schulze-Bahr, E., et al. (2007). The common long-QT syndrome mutation KCNQ1/A341V causes unusually severe clinical manifestations in patients with different ethnic backgrounds: toward a mutation-specific risk stratification. *Circulation* 116, 2366–2375. doi: 10.1161/CIRCULATIONAHA.107.726950

Da Silva, V. J. D., Tobaldini, E., Rocchetti, M., Wu, M. A., Malfatto, G., Montano, N., et al. (2015). Modulation of sympathetic activity and heart rate variability by Ivabradine. *Cardiovasc. Res.* 108, 31–38. doi: 10.1093/cvr/cvv180

De Ferrari, G. M., Crijns, H. J. G. M., Borggrefe, M., Milasinovic, G., Smid, J., Zabel, M., et al. (2011). Chronic vagus nerve stimulation: a new and promising therapeutic approach for chronic heart failure. *Eur. Heart J.* 32, 847–855. doi: 10.1093/eurheartj/ehq391

De Ferrari, G. M., Dusi, V., Spazzolini, C., Bos, J. M., Abrams, D. J., Berul, C. I., et al. (2015). Clinical management of catecholaminergic polymorphic ventricular tachycardia: the role of left cardiac sympathetic denervation. *Circulation* 131, 2185–2193. doi: 10.1161/CIRCULATIONAHA.115.015731

De Ferrari, G. M., Landolina, M., Mantica, M., Manfredini, R., Schwartz, P. J., and Lotto, A. (1995). Baroreflex sensitivity, but not heart rate variability, is

reduced in patients with life-threatening ventricular arrhythmias long after myocardial infarction. *Am. Heart J.* 130, 473–480. doi: 10.1016/0002-8703(95)90354-2

De Ferrari, G. M., Sanzo, A., Bertoletti, A., Specchia, G., Vanoli, E., and Schwartz, P. J. (2007). Baroreflex sensitivity predicts long-term cardiovascular mortality after myocardial infarction even in patients with preserved left ventricular function. *J. Am. Coll. Cardiol.* 50, 2285–2290. doi: 10.1016/j.jacc.2007.08.043

Diaz, T., and Taylor, J. A. (2006). Probing the arterial baroreflex: is there a 'spontaneous' baroreflex? *Clin. Auton. Res.* 16, 256–261. doi: 10.1007/s10286-006-0352-5

Dobson, C. P., La Rovere, M. T., Pinna, G. D., Goldstein, R., Olsen, C., Bernardinangeli, M., et al. (2011). QT variability index on 24-hour Holter independently predicts mortality in patients with heart failure: analysis of Gruppo Italiano per Lo tudio Della Sopravvivenza Nell'Insufficienza Cardiaca (GISSI-HF) trial. *Heart Rhythm.* 8, 1237–1242. doi: 10.1016/j.hrthm.2011.03.055

Dusi, V., De Ferrari, G. M., and Schwartz, P. J. (2020). There are 100 ways by which the sympathetic nervous system can trigger life-threatening arrhythmias. *Eur. Heart J*, ehz950. doi: 10.1093/eurheartj/ehz950 (in press).

Eckberg, D. L. (1997). Sympathovagal balance: a critical appraisal. *Circulation* 96, 3224–3232. doi: 10.1161/01.CIR.96.9.3224

Eckberg, D. L., Drabinsky, M., and Braunwald, E. (1971). Defective cardiac parasympathetic control in patients with heart disease. *N. Engl. J. Med.* 285, 877–883. doi: 10.1056/NEJM197110142851602

Eckberg, D. L., and Sleight, P. (1992). *Human baroreflexes in health and disease*. Oxford: Clarendon Press.

El-Hamad, F., Javorka, M., Czippelova, B., Krohova, J., Turianikova, Z., Porta, A., et al. (2019). Repolarization variability independent of heart rate during sympathetic activation elicited by head-up tilt. *Med. Biol. Eng. Comput.* 57, 1753–1762. doi: 10.1007/s11517-019-01998-9

Floras, J. S., and Ponikowski, P. (2015). The sympathetic/parasympathetic imbalance in heart failure with reduced ejection fraction. *Eur. Heart J.* 36, 1974–1982. doi: 10.1093/eurheartj/ehv087

Fukuta, H., Goto, T., Wakami, K., and Ohte, N. (2017). Effects of catheter-based renal denervation on heart failure with reduced ejection fraction: a systematic review and meta-analysis. *Heart Fail. Rev.* 22, 657–664. doi: 10.1007/s10741-017-9629-0

Gold, M. R., Van Veldhuisen, D. J., Hauptman, P. J., Borggrefe, M., Kubo, S. H., Lieberman, R. A., et al. (2016). Vagus nerve stimulation for the treatment of heart failure: the INOVATE-HF trial. *J. Am. Coll. Cardiol.* 68, 149–158. doi: 10.1016/j.jacc.2016.03.525

Goldberger, A. L. (1996). Non-linear dynamics for clinicians: chaos theory, fractals, and complexity at the bedside. *Lancet* 347, 1312–1314. doi: 10.1016/S0140-6736(96)90948-4

Harris, A. S., Otero, H., and Bocage, A. J. (1971). The induction of arrhythmias by sympathetic activity before and after occlusion of a coronary artery in the canine heart. *J. Electrocardiol.* 4, 34–43. doi: 10.1016/S0022-0736(71)80048-1

Hartupee, J., and Mann, D. L. (2017). Neurohormonal activation in heart failure with reduced ejection fraction. *Nat. Rev. Cardiol.* 14, 30–38. doi: 10.1038/nrcardio.2016.163

Hauptman, P. J., Schwartz, P. J., Gold, M. R., Borggrefe, M., Van Veldhuisen, D. J., Starling, R. C., et al. (2012). Rationale and study design of the increase of vagal tone in heart failure study: INOVATE-HF. *Am. Heart J.* 163, 954–962. doi: 10.1016/j.ahj.2012.03.021

Hirsch, J. A., and Bishop, B. (1981). Respiratory sinus arrhythmia in humans: how breathing pattern modulates heart rate. *Am. J. Phys.* 241, H620–H629. doi: 10.1152/ajpheart.1981.241.4.H620

Inoue, H., and Zipes, D. P. (1987). Changes in atrial and ventricular refractoriness and in atrioventricular nodal conduction produced by combinations of vagal and sympathetic stimulation that result in a constant spontaneous sinus cycle length. *Circ. Res.* 60, 942–951. doi: 10.1161/01.RES.60.6.942

Janse, M. J., Schwartz, P. J., Wilms-Schopman, F., Peters, R. J., and Durrer, D. (1985). Effects of unilateral stellate ganglion stimulation and ablation on electrophysiologic changes induced by acute myocardial ischemia in dogs. *Circulation* 72, 585–595.

Jose, A. D., and Collison, D. (1970). The normal range and determinants of the intrinsic heart rate in man. *Cardiovasc. Res.* 4, 160–167. doi: 10.1093/cvr/4.2.160

Kandzari, D. E., Böhm, M., Mahfoud, F., Townsend, R. R., Weber, M. A., Pocock, S., et al. (2018). Effect of renal denervation on blood pressure in the presence of antihypertensive drugs: 6-month efficacy and safety results from the SPYRAL HTN-ON MED proof-of-concept randomised trial. *Lancet* 391, 2346–2355. doi: 10.1016/S0140-6736(18)30951-6

Kent, K. M., Smith, E. R., Redwood, D. R., and Epstein, S. E. (1973). Electrical stability of acutely ischemic myocardium. Influences of heart rate and vagal stimulation. *Circulation* 47, 291–298. doi: 10.1161/01.CIR.47.2.291

Kleiger, R. E., Miller, J. P., Bigger, J. T., and Moss, A. J. (1987). Decreased heart rate variability and its association with increased mortality after acute myocardial infarction. *Am. J. Cardiol.* 59, 256–262. doi: 10.1016/0002-9149(87)90795-8

Kordalis, A., Tsiachris, D., Pietri, P., Tsioufis, C., and Stefanadis, C. (2018). Regression of organ damage following renal denervation in resistant hypertension: a meta-analysis. *J. Hypertens.* 36, 1614–1621. doi: 10.1097/HJH.0000000000001798

Kunze, D. L. (1972). Reflex discharge patterns of cardiac vagal efferent fibres. *J. Physiol.* 222, 1–15. doi: 10.1113/jphysiol.1972.sp009784

La Rovere, M. T., Bigger, J. T., Marcus, F. I., Mortara, A., and Schwartz, P. J. (1998). Baroreflex sensitivity and heart-rate variability in prediction of total cardiac mortality after myocardial infarction. *Lancet* 351, 478–484. doi: 10.1016/S0140-6736(97)11144-8

La Rovere, M. T., Maestri, R., Pinna, G. D., Sleight, P., and Febo, O. (2011). Clinical and haemodynamic correlates of heart rate turbulence as a non-invasive index of baroreflex sensitivity in chronic heart failure. *Clin. Sci.* 121, 279–284. doi: 10.1042/CS20110063

La Rovere, M. T., Pinna, G. D., Hohnloser, S. H., Marcus, F. I., Mortara, A., Nohara, R., et al. (2001). Baroreflex sensitivity and heart rate variability in the identification of patients at risk for life-threatening arrhythmias: implications for clinical trials. *Circulation* 103, 2072–2077. doi: 10.1161/01.CIR.103.16.2072

La Rovere, M. T., Pinna, G. D., Maestri, R., Mortara, A., Capomolla, S., Febo, O., et al. (2003). Short-term heart rate variability strongly predicts sudden cardiac death in chronic heart failure patients. *Circulation* 107, 565–570. doi: 10.1161/01.CIR.0000047275.25795.17

La Rovere, M. T., Pinna, G. D., and Raczak, G. (2008). Baroreflex sensitivity: measurement and clinical implications. *Ann. Noninvasive Electrocardiol.* 13, 191–207. doi: 10.1111/j.1542-474X.2008.00219.x

Landolina, M., Mantica, M., Pessano, P., Manfredini, R., Foresti, A., Schwartz, P. J., et al. (1997). Impaired baroreflex sensitivity is correlated with hemodynamic deterioration of sustained ventricular tachycardia. *J. Am. Coll. Cardiol.* 29, 568–575.

Levy, M. N., and Schwartz, P. J. (1994). *Vagal control of the heart: Experimental basis and clinical implications*. Armonk, NY: Futura Publishing Co.

Lewis, M. J., and Short, A. L. (2007). Sample entropy of electrocardiographic RR and QT time-series data during rest and exercise. *Physiol. Meas.* 28, 731–744. doi: 10.1088/0967-3334/28/6/011

Li, Y., Li, P., Karmakar, C., and Liu, C.-T. (2015). Distribution entropy for short-term QT interval variability analysis: a comparison between the heart failure and healthy control groups. *Comput. Cardiol.* 42, 1153–1156. doi: 10.1109/CIC.2015.7411120

Li, Y., Li, P., Wang, X., Karmakar, C., Liu, C., and Liu, C. (2019). Variability in patients with coronary artery disease and congestive heart failure: a comparison with healthy control subjects. *Med. Biol. Eng. Comput.* 57, 389–400. doi: 10.1007/s11517-018-1870-8

Lombardi, F., Sandrone, G., Porta, A., Torzillo, D., Terranova, G., Baselli, G., et al. (1996). Spectral analysis of short term R-Tapex interval variability during sinus rhythm and fixed atrial rate. *Eur. Heart J.* 17, 769–778. doi: 10.1093/oxfordjournals.eurheartj.a014945

Magnano, A. R., Holleran, S., Ramakrishnan, R., Reiffel, J. A., and Bloomfield, D. M. (2002). Autonomic nervous system influences on QT interval in normal subjects. *J. Am. Coll. Cardiol.* 39, 1820–1826. doi: 10.1016/s0735-1097(02)01852-1

Mahfoud, F., Lüscher, T. F., Andersson, B., Baumgartner, I., Cifkova, R., Dimario, C., et al. (2013). European Society of Cardiology. Expert consensus document from the European Society of Cardiology on catheter-based renal denervation. *Eur. Heart J.* 34, 2149–2157. doi: 10.1093/eurheartj/eht154

Malik, M. (2008). Beat-to-beat QT variability and cardiac autonomic regulation. *Am. J. Phys.* 295, H923–H925. doi: 10.1152/ajpheart.00709.2008

Malik, M., Hnatkova, K., Huikuri, H. V., Lombardi, F., Schmidt, G., and Zabel, M. (2019a). CrossTalk proposal: heart rate variability is a valid measure of cardiac autonomic responsiveness. *J. Physiol.* 597, 2595–2598. doi: 10.1113/JP277500

Malik, M., Hnatkova, K., Huikuri, H. V., Lombardi, F., Schmidt, G., and Zabel, M. (2019b). Rebuttal from Marek Malik, Katerina Hnatkova, Heikki V. Huikuri, Federico Lombardi, Georg Schmidt and Markus Zabel. *J. Physiol.* 597, 2603–2604. doi: 10.1113/JP277962

Malliani, A., Recordati, G., and Schwartz, P. J. (1973). Nervous activity of afferent cardiac sympathetic fibres with atrial and ventricular endings. *J. Physiol.* 229, 457–469. doi: 10.1113/jphysiol.1973.sp010147

Malliani, A., Schwartz, P. J., and Zanchetti, A. (1969). A sympathetic reflex elicited by experimental coronary occlusion. *Am. J. Phys.* 217, 703–709.

Mann, J. A., and Abraham, W. T. (2019). Cardiac contractility modulation and baroreflex activation therapy in heart failure patients. *Curr. Heart Fail. Rep.* 16, 38–46. doi: 10.1007/s11897-019-0422-3

Milan-Mattos, J. C., Porta, A., Perseguini, N. M., Minatel, V., Rehder-Santos, P., Takahashi, A. C. M., et al. (2018). Influence of age and gender on the phase and strength of the relation between heart period and systolic blood pressure spontaneous fluctuations. *J. Appl. Physiol.* 124, 791–804. doi: 10.1152/japplphysiol.00903.2017

Montano, N., Cogliati, C., Porta, A., Pagani, M., Malliani, A., Narkiewicz, K., et al. (1998). Central vagotonic effects of atropine modulate spectral oscillations of sympathetic nerve activity. *Circulation* 98, 1394–1399. doi: 10.1161/01.CIR.98.14.1394

Montano, N., Gnecchi-Ruscone, T., Porta, A., Lombardi, F., Pagani, M., and Malliani, A. (1994). Power spectrum analysis of heart rate variability to assess the changes in sympathovagal balance during graded orthostatic tilt. *Circulation* 90, 1826–1831. doi: 10.1161/01.CIR.90.4.1826

Mortara, A., La Rovere, M. T., Pinna, G. D., Prpa, A., Maestri, R., Febo, O., et al. (1997). Arterial baroreflex modulation of heart rate in chronic heart failure: clinical and hemodynamic correlates and prognostic implications. *Circulation* 96, 3450–3458. doi: 10.1161/01.CIR.96.10.3450

Nahshoni, E., Strasberg, B., Adler, E., Imbar, S., Sulkes, J., and Weizman, A. (2004). Complexity of the dynamic QT variability and RR variability in patients with acute anterior wall myocardial infarction: a novel technique using a non-linear method. *J. Electrocardiol.* 37, 173–179. doi: 10.1016/j.jelectrocard.2004.04.008

Negoescu, R., Dinca-Panaitescu, S., Filcescu, V., Ionescu, D., and Wolf, S. (1997). Mental stress enhances the sympathetic fraction of QT variability in an RR-independent way. *Integr. Physiol. Behav. Sci.* 32, 220–227. doi: 10.1007/BF02688620

Nollo, G., Faes, L., Porta, A., Antolini, R., and Ravelli, F. (2005). Exploring directionality in spontaneous heart period and systolic pressure variability interactions in humans: implications in the evaluation of baroreflex gain. *Am. J. Phys.* 288, H1777–H1785. doi: 10.1152/ajpheart.00594.2004

Oosterhoff, P., Tereshchenko, L. G., van der Heyden, M. A. G., Ghanem, R. N., Fetics, B. J., Berger, R. D., et al. (2011). Short-term variability of repolarization predicts ventricular tachycardia and sudden cardiac death in patients with structural heart disease: a comparison with QT variability index. *Heart Rhythm.* 8, 1584–1590. doi: 10.1016/j.hrthm.2011.04.033

Opthof, T., de Jonge, B., Schade, B., Jongsma, H. J., and Bouman, L. N. (1984). Cycle length dependence of the chronotropic effects of adrenaline, acetylcholine, Ca2+ and Mg2+ in the Guinea-pig sinoatrial node. *J. Auton. Nerv. Syst.* 11, 349–366.

Pagani, M., Montano, N., Porta, A., Malliani, A., Abboud, F. M., Birkett, C., et al. (1997). Relationship between spectral components of cardiovascular variabilities and direct measures of muscle sympathetic nerve activity in humans. *Circulation* 95, 1441–1448. doi: 10.1161/01.CIR.95.6.1441

Pagani, M., Schwartz, P. J., Banks, R., Lombardi, F., and Malliani, A. (1974). Reflex responses of sympathetic preganglionic neurons initiated by different cardiovascular receptors in spinal animals. *Brain Res.* 68, 215–225. doi: 10.1016/0006-8993(74)90391-6

Paintal, A. S. (1963). "Vagal afferent fibres" in *Ergebnisse Der Physiologie, Biologischen Chemie Und Experimentellen Pharmakologie*, Vol. 52, Springer-Verlag, 74–156.

Piccirillo, G., Cacciafesta, M., Lionetti, M., Nocco, M., Di Giuseppe, V., Moisè, A., et al. (2001). Influence of age, the autonomic nervous system and anxiety on QT-interval variability. *Clin. Sci.* 101, 429–438. doi: 10.1042/cs1010429

Piccirillo, G., Magnanti, M., Matera, S., Di Carlo, S., De Laurentis, T., Torrini, A., et al. (2006). Age and QT variability index during free breathing, controlled breathing and tilt in patients with chronic heart failure and healthy control subjects. *Transl. Res.* 148, 72–78. doi: 10.1016/j.trsl.2006.02.001

Piccirillo, G., Magrì, D., Matera, S., Magnanti, M., Torrini, A., Pasquazzi, E., et al. (2007). QT variability strongly predicts sudden cardiac death in asymptomatic subjects with mild or moderate left ventricular systolic dysfunction: a prospective study. *Eur. Heart J.* 28, 1344–1350. doi: 10.1093/eurheartj/ehl367

Pincus, S. M., and Goldberger, A. L. (1994). Physiological time-series analysis: what does regularity quantify? *Am. J. Phys.* 266, H1643–H1656. doi: 10.1152/ajpheart.1994.266.4.H1643

Pinna, G. D., Maestri, R., and La Rovere, M. T. (2015). Assessment of baroreflex sensitivity from spontaneous oscillations of blood pressure and heart rate: proven clinical value? *Physiol. Meas.* 36, 741–753. doi: 10.1088/0967-ss3334/36/4/741

Pinna, G. D., Maestri, R., Raczak, G., and La Rovere, M. T. (2002). Measuring baroreflex sensitivity from the gain function between arterial pressure and heart period. *Clin. Sci.* 103, 81–88. doi: 10.1042/cs1030081

Pinna, G. D., Porta, A., Maestri, R., De Maria, B., Dalla Vecchia, L. A., and La Rovere, M. T. (2017). Different estimation methods of spontaneous baroreflex sensitivity have different predictive value in heart failure patients. *J. Hypertens.* 35, 1666–1675. doi: 10.1097/HJH.0000000000001377

Pokushalov, E., Romanov, A., Katritsis, D. G., Artyomenko, S., Bayramova, S., Losik, D., et al. (2014). Renal denervation for improving outcomes of catheter ablation in patients with atrial fibrillation and hypertension: early experience. *Heart Rhythm.* 11, 1131–1138. doi: 10.1016/j.hrthm.2014.03.055

Pomeranz, B., Macaulay, R. J., Caudill, M. A., Kutz, I., Adam, D., Gordon, D., et al. (1985). Assessment of autonomic function in humans by heart rate spectral analysis. *Am. J. Phys.* 248, H151–H153. doi: 10.1152/ajpheart.1985.248.1.H151

Porta, A., Bari, V., Badilini, F., Tobaldini, E., Gnecchi-Ruscone, T., and Montano, N. (2011). Frequency domain assessment of the coupling strength between ventricular repolarization duration and heart period during graded head-up tilt. *J. Electrocardiol.* 44, 662–668. doi: 10.1016/j.jelectrocard.2011.08.002

Porta, A., Baselli, G., Caiani, E., Malliani, A., Lombardi, F., and Cerutti, S. (1998a). Quantifying electrocardiogram RT-RR variability interactions. *Med. Biol. Eng. Comput.* 36, 27–34.

Porta, A., Bari, V., De Maria, B., and Baumert, M. (2017). A network physiology approach to the assessment of the link between sinoatrial and ventricular cardiac controls. *Physiol. Meas.* 38, 1472–1489. doi: 10.1088/1361-6579/aa6e95

Porta, A., Baselli, G., Lombardi, F., Cerutti, S., Antolini, R., Del Greco, M., et al. (1998b). Performance assessment of standard algorithms for dynamic R-T interval measurement: comparison between R-Tapex and R-tend approach. *Med. Biol. Eng. Comput.* 36, 35–42.

Porta, A., Baselli, G., Rimoldi, O., Malliani, A., and Pagani, M. (2000). Assessing baroreflex gain from spontaneous variability in conscious dogs: role of causality and respiration. *Am. J. Phys.* 279, H2558–H2567. doi: 10.1152/ajpheart.2000.279.5.H2558

Porta, A., Castiglioni, P., Di Rienzo, M., Bari, V., Bassani, T., Marchi, A., et al. (2012). Short-term complexity indexes of heart period and systolic arterial pressure variabilities provide complementary information. *J. Appl. Physiol.* 113, 1810–1820. doi: 10.1152/japplphysiol.00755.2012

Porta, A., Di Rienzo, M., Wessel, N., and Kurths, J. (2009). Addressing the complexity of cardiovascular regulation. *Phil. Trans. R. Soc. A* 367, 1215–1218. doi: 10.1098/rsta.2008.0292

Porta, A., Girardengo, G., Bari, V., George, A. L., Brink, P. A., Goosen, A., et al. (2015). Autonomic control of heart rate and QT interval variability influences arrhythmic risk in long QT syndrome type 1. *J. Am. Coll. Cardiol.* 65, 367–374. doi: 10.1016/j.jacc.2014.11.015

Porta, A., Gnecchi-Ruscone, T., Tobaldini, E., Guzzetti, S., Furlan, R., and Montano, N. (2007). Progressive decrease of heart period variability entropy-based complexity during graded head-up tilt. *J. Appl. Physiol.* 103, 1143–1149. doi: 10.1152/japplphysiol.00293.2007

Porta, A., Tobaldini, E., Gnecchi-Ruscone, T., and Montano, N. (2010). RT variability unrelated to heart period and respiration progressively increases during graded head-up tilt. *Am. J. Phys.* 298, H1406–H1414. doi: 10.1152/ajpheart.01206.2009

Pueyo, E., Smetana, P., Caminal, P., Bayes de Luna, A., Malik, M., and Laguna, P. (2004). Characterization of QT interval adaptation to RR interval changes

and its use as a risk-stratifier of arrhythmic mortality in amiodarone-treated survivors of acute myocardial infarction. *IEEE Trans. Biomed. Eng.* 51, 1511–1520. doi: 10.1109/TBME.2004.828050

Randall, W. C. (ed.) (1984). "Selective autonomic innervation of the heart" in *Nervous control of cardiovascular function* (New York: Oxford UP), 46–67.

Robbe, H. W., Mulder, L. J., Ruddel, H., Langewitz, W. A., Veldman, J. B., and Mulder, G. (1987). Assessment of baroreceptor reflex sensitivity by means of spectral analysis. *Hypertension* 10, 538–543. doi: 10.1161/01.HYP.10.5.538

Schmidt, G., Malik, M., Barthel, P., Schneider, R., Ulm, K., Rolnitzky, L., et al. (1999). Heart-rate turbulence after ventricular premature beats as a predictor of mortality after acute myocardial infarction. *Lancet* 353, 1390–1396. doi: 10.1016/S0140-6736(98)08428-1

Schwartz, P. J. (1985). Idiopathic long QT syndrome: progress and questions. *Am. Heart J.* 109, 399–411. doi: 10.1016/0002-8703(85)90626-X

Schwartz, P. J. (2014). Cardiac sympathetic denervation to prevent life-threatening arrhythmias. *Nat. Rev. Cardiol.* 11, 346–353. doi: 10.1038/nrcardio.2014.19

Schwartz, P. J. (2016). When the risk is sudden death, does quality of life matter? *Heart Rhythm.* 13, 70–71. doi: 10.1016/j.hrthm.2015.09.020

Schwartz, P. J., Billman, G. E., and Stone, H. L. (1984). Autonomic mechanisms in ventricular fibrillation induced by myocardial ischemia during exercise in dogs with healed myocardial infarction. An experimental preparation for sudden cardiac death. *Circulation* 69, 790–800. doi: 10.1161/01.CIR.69.4.790

Schwartz, P. J., De Ferrari, G. M., Sanzo, A., Landolina, M., Rordorf, R., Raineri, C., et al. (2008a). Long term vagal stimulation in patients with advanced heart failure. First experience in man. *Eur. J. Heart Fail.* 10, 884–891. doi: 10.1016/j.ejheart.2008.07.016

Schwartz, P. J., La Rovere, M. T., De Ferrari, G. M., and Mann, D. L. (2015). Autonomic modulation for the management of patients with chronic heart failure. *Circ. Heart Fail.* 8, 619–628. doi: 10.1161/CIRCHEARTFAILURE.114.001964

Schwartz, P. J., La Rovere, M. T., and Vanoli, E. (1992a). Autonomic nervous system and sudden cardiac death. Experimental basis and clinical observations for post-myocardial infarction risk stratification. *Circulation* 85, I77–I191.

Schwartz, P. J., Locati, E. H., Moss, A. J., Crampton, R. S., Trazzi, R., and Ruberti, U. (1991). Left cardiac sympathetic denervation in the therapy of congenital long QT syndrome: a worldwide report. *Circulation* 84, 503–511. doi: 10.1161/01.cir.84.2.503

Schwartz, P. J., Motolese, M., Pollavini, G., Lotto, A., Ruberti, U., Trazzi, R., et al. (1992b). Prevention of sudden cardiac death after a first myocardial infarction by pharmacologic or surgical antiadrenergic interventions. *J. Cardiovasc. Electrophysiol.* 3, 2–16. doi: 10.1111/j.1540-8167.1992.tb01090.x

Schwartz, P. J., Pagani, M., Lombardi, F., Malliani, A., and Brown, A. M. (1973). A cardiocardiac sympathovagal reflex in the cat. *Circ. Res.* 32, 215–220. doi: 10.1161/01.RES.32.2.215

Schwartz, P. J., Priori, S. G., Cerrone, M., Spazzolini, C., Odero, A., Napolitano, C., et al. (2004). Left cardiac sympathetic denervation in the management of high-risk patients affected by the long-QT syndrome. *Circulation* 109, 1826–1833. doi: 10.1161/01.CIR.0000125523.14403.1E

Schwartz, P. J., Priori, S. G., Spazzolini, C., Moss, A. J., Vincent, G. M., Napolitano, C., et al. (2001). Genotype-phenotype correlation in the long-QT syndrome: gene-specific triggers for life-threatening arrhythmias. *Circulation* 103, 89–95. doi: 10.1161/01.CIR.103.1.89

Schwartz, P. J., Snebold, N. G., and Brown, A. M. (1976a). Effects of unilateral cardiac sympathetic denervation on the ventricular fibrillation threshold. *Am. J. Cardiol.* 37, 1034–1040. doi: 10.1016/0002-9149(76)90420-3

Schwartz, P. J., and Stone, H. L. (1977). Tonic influence of the sympathetic nervous system on myocardial reactive hyperemia and on coronary blood flow distribution in dogs. *Circ. Res.* 41, 51–58. doi: 10.1161/01.RES.41.1.51

Schwartz, P. J., and Stone, H. L. (1979). Effects of unilateral stellectomy upon cardiac performance during exercise in dogs. *Circ. Res.* 44, 637–645. doi: 10.1161/01.RES.44.5.637

Schwartz, P. J., and Stone, H. L. (1980). Left stellectomy in the prevention of ventricular fibrillation caused by acute myocardial ischemia in conscious dogs with anterior myocardial infarction. *Circulation* 62, 1256–1265. doi: 10.1161/01.CIR.62.6.1256

Schwartz, P. J., and Stone, H. L. (1982). Left stellectomy and denervation supersensitivity in conscious dogs. *Am. J. Cardiol.* 49, 1185–1190. doi: 10.1016/0002-9149(82)90043-1

Schwartz, P. J., Stone, H. L., and Brown, A. M. (1976b). Effects of unilateral stellate ganglion blockade on the arrhythmias associated with coronary occlusion. *Am. Heart J.* 92, 589–599. doi: 10.1016/S0002-8703(76)80078-6

Schwartz, P. J., and Vanoli, E. (1981). Cardiac arrhythmias elicited by interaction between acute myocardial ischemia and sympathetic hyperactivity: a new experimental model for the study of antiarrhythmic drugs. *J. Cardiovasc. Pharmacol.* 3, 1251–1259. doi: 10.1097/00005344-198111000-00012

Schwartz, P. J., Vanoli, E., Crotti, L., Spazzolini, C., Ferrandi, C., Goosen, A., et al. (2008b). Neural control of heart rate is an arrhythmia risk modifier in long QT syndrome. *J. Am. Coll. Cardiol.* 51, 920–929. doi: 10.1016/j.jacc.2007.09.069

Schwartz, P. J., Vanoli, E., Stramba-Badiale, M., De Ferrari, G. M., Billman, G. E., and Foreman, R. D., (1988). Autonomic mechanisms and sudden death. New insights from analysis of baroreceptor reflexes in conscious dogs with and without a myocardial infarction. *Circulation* 78, 969–979. doi: 10.1161/01.CIR.78.4.969

Schwartz, P. J., Vanoli, E., Zaza, A., and Zuanetti, G. (1985). The effect of antiarrhythmic drugs on life-threatening arrhythmias induced by the interaction between acute myocardial ischemia and sympathetic hyperactivity. *Am. Heart J.* 109, 937–948. doi: 10.1016/0002-8703(85)90233-9

Segerson, N. M., Litwin, S. E., Daccarett, M., Wall, T. S., Hamdan, M. H., and Lux, R. L. (2008). Scatter in repolarization timing predicts clinical events in post-myocardial infarction patients. *Heart Rhythm.* 5, 208–214. doi: 10.1016/j.hrthm.2007.10.006

Sharp, T. E. 3rd, Polhemus, D. J., Li, Z., Spaletra, P., Jenkins, J. S., Reilly, J. P., et al. (2018). Renal denervation prevents heart failure progression via inhibition of the renin-angiotensin system. *J. Am. Coll. Cardiol.* 72, 2609–2621. doi: 10.1016/j.jacc.2018.08.2186

Shivkumar, K., Ajijola, O. A., Anand, I., Armour, J. A., Chen, P. S., Esler, M., et al. (2016). Clinical neurocardiology defining the value of neuroscience-based cardiovascular therapeutics. *J. Physiol.* 594, 3911–3954. doi: 10.1113/JP271870

Smyth, H. S., Sleight, P., and Pickering, G. W. (1969). Reflex regulation of the arterial pressure during sleep in man. A quantitative method of assessing baroreflex sensitivity. *Circ. Res.* 24, 109–121. doi: 10.1161/01.RES.24.1.109

Sosnowski, M., Czyz, Z., and Tendera, M. (2001). Scatterplots of RR and RT interval variability bring evidence for diverse non-linear dynamics of heart rate and ventricular repolarization duration in coronary heart disease. *Europace* 3, 39–45. doi: 10.1053/eupc.2000.0144

Steinberg, J. S., Shabanov, V., Ponomarev, D., Losik, D., Ivanickiy, E., Kropotkin, E., et al. (2020). Effect of renal denervation and catheter ablation vs catheter ablation alone on atrial fibrillation recurrence among patients with paroxysmal atrial fibrillation and hypertension: the ERADICATE-AF randomized clinical trial. *JAMA* 323, 248–255. doi: 10.1001/jama.2019.21187

Task Force of the European Society of Cardiology and the North American Society of Pacing and Electrophysiology (1996). Heart rate variability. Standards of measurement, physiological interpretation, and clinical use. *Eur. Heart J.* 17, 354–381. doi: 10.1093/oxfordjournals.eurheartj.a014868

Tereshchenko, L. G., Cygankiewicz, I., McNitt, S., Vazquez, R., Bayes-Genis, A., Han, L., et al. (2012). Predictive value of beat-to-beat QT variability index across the continuum of left ventricular dysfunction: competing risks of noncardiac or cardiovascular death and sudden or nonsudden cardiac death. *Circ. Arrhythm. Electrophysiol.* 5, 719–727. doi: 10.1161/CIRCEP.112.970541

Tobaldini, E., Toschi-Dias, E., Appratto de Souza, L., Rabello Casali, K., Vicenzi, M., Sandrone, G., et al. (2019). Cardiac and peripheral autonomic responses to orthostatic stress during transcutaneous vagus nerve stimulation in healthy subjects. *J. Clin. Med.* 8:496. doi: 10.3390/jcm8040496

Townsend, R. R., Mahfoud, F., Kandzari, D. E., Kario, K., Pocock, S., Weber, M. A., et al. (2017). Catheter-based renal denervation in patients with uncontrolled hypertension in the absence of antihypertensive medications (SPYRAL HTN-OFF MED): a randomised, sham-controlled, proof-of-concept trial. *Lancet* 390, 2160–2170. doi: 10.1016/S0140-6736(17)32281-X

Turianikova, Z., Javorka, K., Baumert, M., Calkovska, A., and Javorka, M. (2011). The effect of orthostatic stress on multiscale entropy of heart rate and blood pressure. *Physiol. Meas.* 32, 1425–1437. doi: 10.1088/0967-3334/32/9/006

Ukena, C., Bauer, A., Mahfoud, F., Schreieck, J., Neuberger, H.-R., Eick, C., et al. (2012). Renal sympathetic denervation for treatment of electrical storm:

first-in-man experience. *Clin. Res. Cardiol.* 101, 63–67. doi: 10.1007/s00392-011-0365-5

Vanoli, E., De Ferrari, G. M., Stramba-Badiale, M., Hull, S. S., Foreman, R. D., and Schwartz, P. J. (1991). Vagal stimulation and prevention of sudden death in conscious dogs with a healed myocardial infarction. *Circ. Res.* 68, 1471–1481. doi: 10.1161/01.RES.68.5.1471

Vaseghi, M., Gima, J., Kanaan, C., Ajijola, O. A., Marmureanu, A., Mahajan, A., et al. (2014). Cardiac sympathetic denervation in patients with refractory ventricular arrhythmias or electrical storm: intermediate and long-term follow-up. *Heart Rhythm.* 11, 360–366. doi: 10.1016/j.hrthm.2013.11.028

Wellens, H. J. J., Schwartz, P. J., Lindemans, F. W., Buxton, A. E., Goldberger, J. J., Hohnloser, S. H., et al. (2014). Risk stratification for sudden cardiac death: current status and challenges for the future. *Eur. Heart J.* 35, 1642–1651. doi: 10.1093/eurheartj/ehu176

Westerhof, B. E., Gisolf, J., Stok, W. J., Wesseling, K. H., and Karemaker, J. M. (2004). Time-domain cross-correlation baroreflex sensitivity: performance on the EUROBAVAR data set. *J. Hypertens.* 22, 1371–1380. doi: 10.1097/01.hjh.0000125439.28861.ed

Wurster, R. D. (1984). "Central nervous system regulation of the heart: an overview" in *Nervous control of cardiovascular function*. ed. W. C. Randall (New York: Oxford UP), 307–320.

Yeragani, V. K., Pohl, R., Jampala, V. C., Balon, R., Kay, J., and Igel, G. (2000a). Effect of posture and isoproterenol on beat-to-beat heart rate and QT variability. *Neuropsychobiology* 41, 113–123. doi: 10.1159/000026642

Yeragani, V. K., Pohl, R., Jampala, V. C., Balon, R., Ramesh, C., and Srinivasan, K. (2000b). Increased QT variability in patients with panic disorder and depression. *Psychiatry Res.* 93, 225–235. doi: 10.1016/S0165-1781(00)00119-0

Zannad, F., De Ferrari, G. M., Tuinenburg, A. E., Wright, D., Brugada, J., Butter, C., et al. (2015). Chronic vagal stimulation for the treatment of low ejection fraction heart failure: results of the NEural Cardiac TherApy foR Heart Failure (NECTAR-HF) randomized controlled trial. *Eur. Heart J.* 36, 425–433. doi: 10.1093/eurheartj/ehu345

Zaza, A., and Lombardi, F. (2001). Autonomic indexes based on the analysis of heart rate variability: a view from the sinus node. *Cardiovasc. Res.* 50, 434–442. doi: 10.1016/S0008-6363(01)00240-1

Zaza, A., Malfatto, G., and Schwartz, P. J. (1991). Sympathetic modulation of the relation between ventricular repolarization and cycle length. *Circ. Res.* 68, 1191–1203. doi: 10.1161/01.RES.68.5.1191

Zhu, C., Hanna, P., Rajendran, P. S., and Shivkumar, K. (2019). Neuromodulation for ventricular tachycardia and atrial fibrillation: a clinical scenario-based review. *JACC Clin. Electrophysiol.* 5, 881–896. doi: 10.1016/j.jacep.2019.06.009

Conflict of Interest: The authors declare that the research was conducted in the absence of any commercial or financial relationships that could be construed as a potential conflict of interest.

Advantages of publishing in Frontiers

OPEN ACCESS
Articles are free to read for greatest visibility and readership

FAST PUBLICATION
Around 90 days from submission to decision

HIGH QUALITY PEER-REVIEW
Rigorous, collaborative, and constructive peer-review

TRANSPARENT PEER-REVIEW
Editors and reviewers acknowledged by name on published articles

Frontiers
Avenue du Tribunal-Fédéral 34
1005 Lausanne | Switzerland

Visit us: www.frontiersin.org
Contact us: info@frontiersin.org | +41 21 510 17 00

REPRODUCIBILITY OF RESEARCH
Support open data and methods to enhance research reproducibility

DIGITAL PUBLISHING
Articles designed for optimal readership across devices

FOLLOW US
@frontiersin

IMPACT METRICS
Advanced article metrics track visibility across digital media

EXTENSIVE PROMOTION
Marketing and promotion of impactful research

LOOP RESEARCH NETWORK
Our network increases your article's readership